APPLIED MATERIALS AND METHODS FOR SURFACE MODIFICATION

A Dissertation

Presented to the Faculty of the Graduate School

of Cornell University

In Partial Fulfillment of the Requirements for the Degree of

Doctor of Philosophy

by

Lin Chen

January 2014

APPLIED MATERIALS AND METHODS FOR SURFACE MODIFICATION

Lin Chen, Ph. D.

Cornell University 2014

Surface modification is very important in tailoring materials properties. Various methods and materials have been explored and developed to provide unique properties on different substrates for practical applications. One of the most effective methods is to use surface-grafting procedures to introduce functional coatings on various substrates. Here in this thesis, grafting techniques are applied to grow polymer brushes on substrates with selected surface morphologies, e.g. flat and spherical surfaces. By tailoring the functionalities of the polymers, desirable properties such as antifouling behavior and enhanced solubility can be specifically designed and achieved. These as-modified functional materials can be successfully applied to complex working environments, indicating the methods and materials can be used for additional promising surface modification processes.

The first example is to functionalize reverse osmosis membranes with antifouling polymer brushes using a 'layer-by-layer' mediated method. This specific method not only protects the membrane surface from potential chemical damage, but also amplifies the reaction sites on the surface. Different antifouling polymer brushes were successfully grown on the flat membrane surfaces through both 'grafted to' and 'grafted from' approaches. The membrane exhibits improved antifouling properties against different kinds of bio-foulants with no change of water flux and salt rejection ratios.

The second example is the synthesis of hybrid nanoparticles as potential tracers for enhanced oil recovery and carbon dioxide (CO_2) sequestration. Fluorinated polymers were modified onto different nanoparticle spherical cores through a surface-initiated atomic transfer radical polymerization (SI-ATRP) reaction. Incorporation of fluorescent labels makes the nanoparticles easy to be detected. The as-prepared nanohybrids have diameters around 40 nanometers and the solubility of these nanoparticles in $scCO_2$ has been significantly improved. Further application of the nanopraticles in diffusion tests shows that they can be applied as potential tracers in real geological oil fields.

While surface-grafting techniques are one type of modification method, which in principal is to add coatigs on the substrates, another kind of modification methods is to remove coatings from a substrate using methods such as plasma or chemical etching. In this thesis, new etching processes are also investigated. Supercritical carbon dioxide is used as a processing medium to remove post-etch organic residue on silicon wafers and to etch titanium nitride (TiN) as well. $scCO_2$ compatible quaternary ammonium salts were synthesized and applied with co-solvents to enhance the cleaning efficiency. Strong organic acids and peroxides, together with alcohols as stabilizers, were used to successfully etch TiN from silicon surfaces in both organic solvents and $scCO_2$.

BIOGRAPHICAL SKETCH

Lin Chen was born in Shanghai, China on October 16, 1982 to Yaping Chen and Weiguo Qiu. His childhood was spent in Yangpu District. After finishing primary school, Lin, with his family, moved to Baoshan District, where he finished his secondary and high school education in Wusong High School. Lin enrolled in Fudan University in 2001 and obtained the Bachelor of Science degree in Chemistry, 2005. He stayed in Fudan University and finished his master course and research in Physical Chemistry, 2008. In the Summer of 2008, Lin enrolled in Cornell University, US and joined the research group of Professor Christopher K. Ober. After finishing his PhD degree in the Summer of 2013, Lin started his professional career in 3M's Homecare Division as a research chemist.

To Yaping Chen and Weiguo Qiu, who made it all possible

To Jin Niu, for her love and support

ACKNOWLEDGMENTS

First, I would like to thank my parents, Yaping Chen and Weiguo Qiu, for their lifelong love and support. I would not have achieved any success without them. Second, I would like to thank my Ph.D adviser Professor Christopher Ober, who allowed me to work in his group and always gives me valuable suggestions on both research and social activities. I'm also grateful to Professor Barbara Baird and Professor Geoffrey Coates for being my committee members and Professor Uli Wiesner for being the proxy. KAUST-Cornell research center and Samsung Company are highly appreciated for their financial support.

I would like to thank all the people in the Ober group for their support and help. I would like to thank Dr. Héloïse Thérien-Aubin, who provided tremendous help and guidance on my research at the very first beginning of my Ph.D study. I would like to thank Dr. Yisheng Xu, Dr. Youyong Xu, Dr. Kui Xu and Dr. Hyosan Lee for their assistance in the lab. I would like to thank David Calabrese and Dr. Evan Schwartz for helping me with my thesis writing. I would also like to thank my other lab mates and friends who have helped me in my research and life. Last but not least, I would like to thank Jin Niu, whose love and encouragement accompanied me throughout the difficult time during my final year of graduate school.

TABLE OF CONTENTS

LIST OF FIGURES

LIST OF TABLES

TABLE OF ABBREVIATIONS

AFM	Atomic force microscopy
ATR-FTIR	Attenuated total reflectance-Fourier transform infrared spectroscopy
ATRP	Atom-transfer radical-polymerization
^{13}CNMR	Carbon nuclear magnetic resonance spectroscopy
DLS	Dynamic light scattering
EOR	Enhanced oil recovery
EPS	Extracelluar polymeric substances
GPC	Gel permeation chromatography
HFE	Hydrofluoroether
^{1}HNMR	Proton nuclear magnetic resonance spectroscopy
IPA	Isopropanol
LBL	Layer by layer
NP	Nanoparticle
PEG	Poly(ethylene glycol)
PVP	Polyvinylpyrrolidone
QAS	Quaternary ammonium salt
RAFT	Reverse addition-fragmentation chain transfer
RO	Reverse osmosis
$scCO_2$	Supercritical carbon dioxide
SEM	Scanning electron microscopy
SI-ATRP	Surface initiated atom-transfer radical-polymerization
TEM	Transmission electron microscopy
TGA	Thermogravimetric analysis
TiN	Titanium nitride
UV	Ultraviolet

UV-vis	Ultraviolet-visible
XPS	X-ray photoelectron spectroscopy

CHAPTER ONE:

APPLIED MATERIALS AND METHODS FOR SURFACE MODIFICATION*

*The author would like to suggest readers who are interested in selected references of this chapter to refer to specific publishers' websites for more details.

1.1 Introduction

Surface modification is very important in tailoring materials properties. From cooking to electronics processing, from ocean transportation to device design, surface modification is applied in almost every aspect of our daily life. In order to acquire unique properties and key functions on specific substrates, modification and treatment of surfaces are essential for advanced materials performance. As a specific example, adhesion resistant coatings have been widely applied in improving people's life. Fluoropolymers, commonly known by the Teflon brandname from Dupont Co., are used to coat frying pans for prevention of adhesion. The unique hydrophobicity and non-reactive properties of fluoropolymers make it a good protective coating against water and corrosive materials. Scotchgard, a product from 3M Co., is a coating applied to carpets and cloth for prevention of soiling by oil and water. Fluorochemical structures help to providee both oil and water repellent properties to the substrates. Anti-reflective coatings play very important roles in developing advanced technologies. PureCoat™ lenses are products from Zeiss Co., which contain layers composed of anti-reflective coatings. It is used to modify surfaces of a lens or other optical devices to reduce light reflection, improving the efficiency of the system and the contrast of the images as well. ARC products from Brewer Science Co. are anti-reflective materials applied in photolithographic patterning to reduce the line edge roughness of the patterns. Photoresists, such as the HKT series from AZ Electronic Materials Co., are another important category of surface coating materials in the field of semiconductor photolithography. Usually composed of one type of diblock or triblock copolymers, these materials can be altered with their chemical and physical

functionalities upon ultraviolet (UV) irradiation. With the amplification of photoacid generators and post-exposure development, photoresists can form either positive or negative tone patterns. Subsequent etching processes such as plasma etching transfer a pattern to silicon substrates, constructing the pre-designed circuits for electronic devices. Nowadays, due to the continuously downscaling of the sizes of microelectronics devices, smaller and smaller features within nanometer (nm) scales are required for high-resolution lithographic patterning. Minimum feature sizes have been decreased from micrometers in the 1980's to sub-50 nm in today's semiconductor industry. Sub-30 nm patterning dimensions are expected to be achieved in the near future. Development of new materials as photoresists for advanced patterning technologies such as extreme ultraviolet (EUV) photolithography are highly desired [1].

Methods for surface modification include many different process steps. Spin coating is a commonly used modifying method in the laboratory; film casting is generally used in industrial production lines; plasma treatments are applied in both bench and industrial scales. Generally, the various methods can be divided into two categories. One is simple 'additive' methods, meaning adding materials or films onto substrates. Dip coating, spin and spray coating, chemical and physical vapor deposition, etc. are some representative methods in this category. On the other hand, another kind of modification method is 'substrative', meaning removing materials from the substrates. Mechanical polishing, chemical and plasma etching, post-etch cleaning, etc. fall into this category. Materials that can be applied for surface modification range from from polymeric matrices to metallic films, from small

organic molecules to shaped inorganic nanoparticles. Combinations of these materials are also commonly designed and used.

Herein, research studies will focus on several important applications of surface modification. Different materials and application methods will be discussed, which will provide information of both a fundamental scientific nature and potential practical industrial applications.

1.2 Antifouling Coatings

1.2.1 Background

Fouling by attachment or deposition of microorganisms is a serious problem in many areas affecting our daily life. Medical devices, household sanitation equipment, water purity, marine shipping, etc. are all systems that can be severely contaminated by many kinds of bacteria, for example, causing enormous energy loss and cost increases [2-4]. Due to protein adsorption and fouling, medical implants designed for long-term may instead lead to potential serious implant-related infections [5.] Not only the efficiency of devices is reduced, but harmful side effects such as thrombosis may be caused [6]. In fact, nearly one-half of all nonsocomial infections result from infections from medical implants [2]. Removal of the implant is often required when serious infections are caused by bacteria resistant to multiple antibiotics. The problem becomes even more dangerous when in site infections occur in the brain or cerebrospinal fluid, since many antibiotics can be blocked by the blood-brain barrier, weakening the therapeutic effect. Marine biological fouling is another serious problem

and is defined as the undesirable accumulation of microorganisms, plants, and animals on artificial surfaces immersed in sea water [7]. Growth of marine bacteria on the surface of boats and ships serves as the first step in fouling and can cause many adverse side effects such as high frictional resistance, deterioration of corrosion protective coatings, increase of dry-docking cleaning frequencies, etc. These effects can add up 40% more on fuel consumption and 77% on overall voyage costs [8, 9]. Plus, ships may also bring alien species to water bodies where they have never been naturally present, causing unexpected environmental issues [10]. Another important area that is affected much by fouling is water filtration systems. Membranes used in all kinds of filtration processes from microfiltration to reverse osmosis desalination can be seriously fouled by various kinds of biological substances. Direct deposition of microbial colonies such as P. putida and S. cerevisiae has been observed on reverse osmosis and nanofiltration membranes [11, 12]. The foulants will adhere to the pores and surfaces of membranes, building up additional barrier layers, clogging the pores and blocking the surfaces, reducing the water flux and membrane performance, increasing the operational cost and shortening the membrane lifetime. Biofouling films, which have been called the Achilles heel of membrane processes, are estimated to account for 50-60% of total organic carbons of all membrane fouling [13-15].

Nearly 4000 species of microorganisms have been identified as potential foulant sources [16]. Detailed mechanisms of biofouling are varied for different fouling species, which is still an important research field of interest [17-19]. However, a general process with four stages can be assigned [7]. The first is so-called ‘conditioning film’ stage. Small organic molecules such as proteins and polysaccharides are rapidly accumulated

on the substrate. Physical interactions such as hydrophobic and electrostatic interactions are the driving forces, which could happen within minutes [20, 21]. Within the next 1-24 hours, bacteria and single cell diatoms such as *Vibio alginofyticus* and *Amphiprora paludosa* etc. can settle down rapidly on the conditioning film on the substrates. These 'primary colonizers' are first 'absorbed' physically and reversibly and afterwards 'adhered' irreversibly, forming a microbial film [21, 22]. This stage of bacteria deposition not only provides the microorganisms a better protection from potential dangers from predators or toxins, but also a better environment for easy capture of nutrients and energy from other microorganisms [23]. The biofilm containing both organic substances and bacteria is made of so-called 'extracellular polymeric substances' (EPS). Due to the existence of EPS, more particles and microorganisms are likely to be trapped. Spores of macroalgae such as *Ulothrix zonata* and marine fungi and protozoa, e.g. *Vaginicola sp.*, can be attracted onto a surface through sensory stimuli, which will form a more complex biological community than simple microbial biofilms [22]. The community will consist of primary producers, grazers and decomposers. This third stage usually takes about one week. The final stage (2-3 weeks) involves settlement and growth of larger larvae of macrofoulers such as *Crustacea* and *Bryozoa* etc. These macroalgae are typically with fast rapid growth rates, low degree of substrate preferences and high adaptability to different environments [24].

Depending on the fouling mechanisms, a variety of parameters are considered to have impacts on the interactions between microorganisms and substrates, affecting the growth of biofilms. Several important factors include surface hydrophilicity, surface

charge and surface roughness. Hydrophilicity of substrate surfaces is believed to be one of the key factors affecting adhesion of proteins and bacteria. A thin layer of absorbed water molecules on top of the hydrophilic surface helps to prevent hydrophobic proteins from attachment. It is generally assumed that the more hydrophilic is the surface, the weaker the driving forces for attachment will be for most of the hydrophobic bioorganic substances. In membrane fouling cases, direct correlation between surface hydrophilicity and relative water flux is obtained [25]. Based on this assumption, much effort has been made on hydrophilization of substrate surfaces to reduce protein and cell adhesion. Studies show that hydrophobic surfaces with low surface energy can also be used as fouling release coatings, which will be discussed in detail in Section 1.2.4. Surface charge is another factor affecting the fouling process. Since most proteins and cellular components are negatively charged, in some cases, simple treatment to introduce negatively charged functional groups on a surface can prevent biofouling problems [26-28]. Attempts were also made to develop antifouling positively charged surfaces, which behave as barriers and repulsive layers against positively charged proteins [29, 30]. Materials containing both negatively and positively charged moieties have been recently found to be good antifouling reagents as well [31-33]. The effect of surface roughness on fouling is controversial. Studies on different substrates under different testing conditions show both positive and negative results [34-37]. It is believed that during the very first stage of fouling, particles are in direct contact with substrates; hence the interaction between organic particles and substrate surfaces are primary driving forces for fouling interactions. After the EPS is formed, the interactions between absorbed organic substances become dominant.

Therefore, it is still unclear what effect of surface roughness has on overall fouling performance [13]. However, it is a common belief that the smoother the surface is, the smaller the surface area, and as a result the less adsorption of organic particles can occur. Other factors that can affect biofouling includes specific chemical groups on the surface, the structure of adsorbed water, salinity, pH etc. [38-40]

In order to reduce and prevent fouling, a variety of materials have been synthesized and developed. According to proposed working mechanisms, they can be categorized into three different kinds: antimicrobial, fouling resistant and fouling release coatings.

1.2.2 Antimicrobial Coatings

Antimicrobial agents are generally defined as materials that are capable of killing bacteria or microorganisms. Also known as biocides, these materials are widely used in sterilization of water and soil, drug delivery and food preservation etc. [41] One main category of antimicrobial materials is polymeric biocides. Polymers that have antimicrobial activities usually contain chemical functionalities such as quaternary ammonium and phosphonium salts as side chains. These materials can adsorb onto a bacterial cell surface, diffuse through the cell wall, adsorb and disrupt the cell membrane, leak lethal cationic components and kill the cell [42]. Antimicrobial polymers have promising applications in the area of health care and hygienic medical care. Polymeric coatings have been applied to the surface of surgical gowns and shower walls to minimize biofouling problems and release the pathogenic bacteria into streams of flowing fluids [43]. The advantage of using polymeric antimicrobial agents is

that they are nonvolatile and chemically stable, which can reduce the potential loss of efficacy due to issues of volatilization and biological decomposition [44-46]. Basic requirements for antimicrobial polymers have been suggested by Kenawy et al. [2] Ideal polymeric biocides should have the following characteristics: easily synthesized and incorporated at low cost; long-term thermal and chemical stability; non-toxic or irritating to human bodies; can be regenerated upon loss of activity; biocidal to a broad range of bacteria species in brief times of contact. Reddy et al. [47] synthesized copolymers with 4-acrylamido-N-(5-methyl-3-isoxazolyl)benzenesulfonamide (AMBS), 4-methacrylamido-N-(5-methyl-3-isoxazolyl)benzenesulfonamide (MMBS) and N-[4-sulfamido-N-(5-methyl-3-isoxazolyl)phenyl]maleimide (SMPM), which were found to have antifungal functions against several fungi such as *A. niger and C. albicans*. Endo et al. [48] synthesized and investigated the antibacterial effect of polymeric sulfonium salts. The polymers exhibited high antimicrobial activities against Gram-positive bacteria. Patel et al. [49] developed a series homo- and copolymers from 2,4-dichlorophenyl acrylate and evaluated their antibacterial activities against bacterial strains, fungi and yeasts.

Factors that can affect the antimicrobial activities of polymeric biocides include molecular weight, counterion and spacer length. Kanazawa and co-workers found that the antibacterial properties of poly(tribuyl 4-vinylbenzyl phosphonium chloride) against *S. aureus* increased with the increase of molecular weight [50]. Ikeda et al. [51] studied the antimicrobial activities of homopolymers of polyacrylates and polymethacrylates with biguanide chemical functionalities as side chains. They found there was a working window for the polymers to behave effectively against *S. aureus*.

Polymers with a molecular weight between 5 x 10^4 and 1.2 x 10^5 Da were found to work best. However, investigations also showed little dependence on molecular weight as for the biocidal activities against several other microorganisms such as *B. subtilis* and *A. aerogenes*. Chen et al. [52] synthesized quaternary ammonium dendrimers as antimicrobial agents against *E. coli*. It was observed that the activities of the dendrimers were strongly dependent on the anions. Biocides with bromide anions appeared to behave better than those with chloride anions. However, Panarin et al. [53] showed that no effect for the counter anions was found on the antibacterial activities of the as-synthesized homopolymers of vinylamine and methyl methacrylate with pendent quaternary ammonium salts. Whether the counterion has an effect and how it affects the antimicrobial properties of polymeric biocides is still unclear. Spacer length, however, is believed to have an impact on antimicrobial activities. With a change of spacer length, both conformation and charge density can be changed in the polymeric matrix, resulting in different interactions between the biocidal agents and the cell membrane [54]. Sawada prepared unique perfluoro-propylated and perfluoro-oxaalkylated end-capped 2-(3-acrylamidopropyldimethylammonio) ethanoate (APDMAE) polymers. [55] In tests against *S. aureus* and *P. aeruginosa*, the oxaalkylated polymer was found to be more biocidally active than the propylated polymer, probably due to its longer alkyl chains. Nonaka et al. [56] synthesized copolymers from methacryloylethyl trialkyl phosphonium chlorides and *N*-isopropylacrylamide. Investigations on the antimicrobial activities of the copolymers against *E. coli* showed that activities increased with an increase of alkyl chain length in the phosphonium groups. While the impact of spacer length has been widely

recognized, debate still exists on how the alkly chain length makes an effect on antimicrobial activities of polymeric materials.

Immobilizations of antimicrobial polymers on different substrates can find various applications in different areas. Antimicrobial polyamide fibers were obtained by first graft polymerization of the acrylic acid and then modification with penicillin. The as-synthesized yarn exhibited strong biocidal activities against both Gram-positive bacteria e.g. *S. aureus* and Gram-negative bacteria such as *E. coli* [57]. Ion-exchange fibers modified with methacryloyloxyethyl trimethyl ammonium chloride showed high antibacterial activities against several microorganism species [58]. Polypropylene nonwoven grafted with 4-vinylpyridine and quaternized with halohydrocarbons was found to behave well in removal of *E. coli* [59]. Quaternary ammonium derivatives of chitosans have been widely applied in hair products as film formers, conditioners and shampoos [60].

In contrast to polymeric biocides, another more traditional and more developed category of antimicrobial materials is chemical complexes based on heavy metal ions. Ever since the times of ancient Greece, silver (Ag) has been known for its antimicrobial activities. [61] Silver cations have been applied to kill bacteria for many, many years. $AgNO_3$ can show antimicrobial activities at a concentration as low as 3 μM [62]. Due to the discovery and development of antibiotics in the middle of the 20th century, using silver as antimicrobial material was abandoned. [63] However, with the rapid increase of bacteria resistance against conventional antibiotics, new silver-based materials, especially silver nanoparticles (AgNPs) have attracted considerable research

interest since the beginning of the millennium [64]. Traditional bulk silver compounds, because of their large particle sizes and aggregation morphologies, are non-competitors against the new innovative AgNPs [65]. Silver particles with sizes within nanoscales have shown great antimicrobial activities against a broad range of bacteria, fungi and viruses. Lok et al. [66] synthesized spherical AgNPs with a diameter about 9.3 nm and used it against *E. coli* cells. Sadhasivam et al. [67] prepared AgNPs through a biosynthetic approach by *Streptomyces hygroscopicus*. The 20-30 nm large particles showed good antimicrobial activities against a series of pathogenic microorganisms such as *B. subtilis* and *E. faecalis*. Sun et al. [68] fabricated AgNPs in Hepes buffer and the particles exhibited potent cytoprotective and post-infected antimicrobial activities toward Hut/CCR5 cells. Lara et al. [69] coated commercial AgNPs (30-50 nm) with polyvinylpyrrolidone and studied its antiviral actions against HIV-1. It is generally believed that the greater antimicrobial effect can be achieved with smaller particle sizes since more available surface areas per unit mass allow higher silver release and easier interactions with the bacteria [70, 71].

It has been reported that silver biocidal materials exhibit multidirectional activities in killing cells and bacteria. Research has been done in order to elucidate a mode of action [72-74]. Although a complete understanding of the antimicrobial mechanisms of AgNPs against bacteria has not been reached, several stages and interactions between AgNPs and cell walls and membranes have been classified. The attack and crossing of the cell plasma membrane is the first important step for successful antimicrobial performances. Direct contact of Ag (I) with bacterial cell walls can cause a change of wall morphology and detachment of plasma membranes, resulting in leakage of the

cell interior [75, 76]. The diffusion of silver ions into the cell and interactions with DNA and enzymes is the next stage. A 60% of silver ion transport and uptake inside the cell was determined by Holt et al [77]. Arakawa et al. [78] identified preferential binding sites of Ag (I) in DNA on a molecular level. It is found that once silver ions penetrate into the cell, they will not only interact with DNA, but enzymes as well. Li et al [72] observed that the activity of certain enzymes in *S. aureus* cells decreased with increasing concentrations of AgNPs. Similar proportional correlations can also be found in other bacteria [79, 80]. Amino acid groups in enzymes have been proven both theoretically and experimentally to be good binding sites for silver ions [81]. Ag (I) can interfere with enzymes by forming complexes with amino acid groups in the enzyme, leading to the replacement of the native bounded metal cations such as Cu [82] etc. This binding process is thought to be essential to inactivate enzymes. Kim et al. [83] observed that AgNPs were more active and effective biocides once the silver ions formed complexes with cysteine. Xu et al. [84] showed that an iron-sulfur cluster, which is an important cofactor involved in many enzymatic reactions, was destroyed by the presence of Ag (I) due to the binding of silver to cysteine. Interactions between silver ions and DNA and enzymes will result in the generation of reactive oxygen species (ROS), which is catastrophic to the bacteria. The ROS, generally hydrogen peroxide, superoxide radical anion and hydroxyl radicals, are known to attack lipids, DNA, protein, etc., causing severe consequences, e.g. malfunction of DAN replication [85, 86]. By studying the antimicrobial behavior of AgNPs against *S. epidermidis*, Gordon et al. [87] suggested an enhanced ROS production as a result of binding silver ions with enzymes in the respiratory chain. Inoue et al. [88] used silver loaded zeolite to prove that

the participation of ROS in the silver ions action mode. They found that the presence of oxygen is essential for the zeolite to be biocidal active and using ROS inhibitors could deactivate the zeolite drastically, which suggest that formation of ROS is one of the key factors for antimicrobial activity of silver. The general working mechanisms discussed above can also be found in other metal-complex antimicrobial materials.

Triorganotin and its derivatives were extensively used as antifouling paints on ocean going boats and ships since the 1950s [89]. The high-toxicity to a broad range of marine microorganism species, no galvanic corrosion, and colorless characteristics make these tin-based organic materials good additives in matrix paints as releasing biocides [90]. One representative material of this matrix-biocide combined coatings is tributyltin (TBT) self-polishing copolymer paints. Montermoso *et al.* first studied possible antimicrobial applications of TBT acrylate esters in 1958 [89]. A patent about the use of copolymers of TBT acrylate and methyl methacrylate was issued to James in 1964 [91]. In 1974, TBT self-polishing copolymer technology was patented by Milne et al. and [92] revolutionized antifouling paints and the shipping industries. TBT self-polishing materials are usually polymers with acrylic or methacrylate backbones and tributyltin side groups bound by an ester linkage [93]. Upon immersion of the paint in sea water, the carboxyl-TBT ester bonds, which are susceptible to hydrolytic decomposition under alkaline conditions, will be hydrolyzed in a slow and controlled manner, releasing TBT biocidal moieties. Self-polishing effects occur when the partially reacted polymers are eroded and form a less reacted paint surface. Balanced dissolution rate and erosion rate are reached, resulting in a steady value of the leached layer thickness [94-96]. Unlike other coatings, TBT-based paints show antimicrobial

activities even under static conditions [93]. Advantages of using the TBT self-polishing materials are: (i) the polymer chemistry can be modified to meet customized polishing and biocide releasing rates to maximize the effective lifetime of the paint [93]; (ii) binding positions of the biocides can be carefully selected and controlled by optimizing the polymerization conditions, allowing flexible design of antimicrobial coatings for different ships with specific activities [7]. Other unique properties of this paint include short drying times, high durability and high mechanical strength, etc. [90]

Although TBT self-polishing materials have been the most successful anti-biofouling coatings, their adverse impact on the environment is also drastic. It has been shown that TBT moieties can cause defective shell growth and malformations in many species even at extremely low concentrations [97, 98]. Accumulations of TBT in mammals and debilitation of immunological defenses in fish were also reported [99]. After the International Convention in 2001, the applications of TBT-based antifouling coatings were required to be banned from 1 January 2003 and no presence of such paints on vessels from 2008 onward [100].

A series of self-polishing coatings replacing TBT with different metal complexes were then developed. International Marine Coatings Co. patented several products, including Intersmooth Ecoloflex SPC, as acrylic based self-polishing materials with copper salts as released biocides [100]. Early reports showed a long-term antimicrobial activity up to three years for the copper-acrylate coatings [101, 102], which has been further improved to 5 years [103, 104]. Open sources of relative performance of the antifouling coatings are available on International's website. Exion, a main product

from Kansai Paint Co., is a self-polishing coating containing pendent zinc ions as releasing biocides. It is proposed that ion exchange procedures between zinc and sodium ions from the same polymeric chains are necessary for polishing of the paint [105]. Factors such as the content of zinc acrylate and the ratios of acrylate and methacrylate can affect the binding reactions and hydrophobicity of the copolymer, resulting in different antifouling reactivity [106].

Although new coatings containing different metal ions as antimicrobial biocides have been developed and commercialized, environmental concerns still exist. It has been pointed out that by reaction with some of currently used booster biocides, e.g. thiocarbamates, copper-based lipophilic complexes may enhance the bioaccumulation of copper [107]. High concentrations of copper in waters and oysters in France and Sweden as a result of copper release from antifouling coatings have already been reported [108]. Unexpected lethal effects could be caused in biological species if the copper concentration exceeds the Environmental Quality Standards.

In spite of their superior abilities for killing bacteria and microorganisms, antimicrobial materials also have disadvantages: (i) the remains of bacteria killed by antimicrobial agents can adhere to the surface, not only affecting further antifouling efficiency, especially for those self-polishing coatings, but also serve as food and nutrients for new incoming bacteria, causing a fresh cycle of biofilm deposition on the substrate; (ii) cheap commercial antimicrobial coatings usually contain strong toxic biocides such as metal ions. These biocides are so strong that they not only kill the bacteria, but also have harmful effects on other living species. Moreover,

decomposition of these highly toxic materials is slow or even impossible under natural conditions, which may result ultimately in bioaccumulation in mammalian bodies and serious environmental problems in a long term; (iii) non-metallic based antimicrobial agents such as organic booster biocides or quaternary ammonium polymeric materials are usually not as effective as metal-based biocides with respect to biocidal efficacy, long-term stability, ease of preparation and application, etc. Furthermore the environmental profiles of these materials are still under question. Therefore, development of new antifouling materials working on totally different mechanisms is highly desired.

1.2.3 Fouling Resistant Coatings

Fouling resistant coatings are generally defined as materials that can prevent bacteria from binding to the surface. Unlike antimicrobial coatings that release biocides to kill the bacteria, fouling resistant agents contain no toxic substances. They reduce the bacterial attachment on the substrate by reducing non-specific interactions between the coatings and microorganisms through changes of surface hydrophobicity, structural conformations and biomimetic working mechanisms. Since they are non-toxic and environmentally benign, these materials have been rapidly developed as promising antifouling coatings during the last few decades.

The most commonly used fouling resistant materials are polymeric derivatives of poly(ethylene glycol) (PEG), also known as poly(ethylene oxide) (PEO),. The protein and bacterial resistant properties of PEG have been widely reported. Lee et al. [109] prepared PEO-containing block copolymer surfactants, which were used as coatings

on low density polyethylene hydrophobic surfaces. Adsorption of human albumin was significantly decreased as compared to the untreated surface. Kevin et al. [110] modified the gold surface with a series of self-assembled organic monolayers (SAMs) including hydrophobic and hydrophilic alkanethiols. They found that the hexa(ethylene glycol)-terminated SAMs are the most effective in resisting adsorption of different kinds of proteins such as ribounuclease, pyruvate kinase, fibrinogen, etc. Park et al. [111] reported that after modification by PEG, polyurethane surfaces showed reduced adhesion of *S. epidermidis* and *E. coli* bacteria. Kingshott et al. [112] coated poly(ethylenimine) with PEG, which was then physically adsorbed onto a stainless-steel substrate and also covalently immobilized onto a carboxylated poly(ethylene terephthalate) surface. Adsorption tests against Gram-negative bacteria (*Pseudomonas* sp.) showed that no cell adhesion reduction was observed on the as-modified stainless steel surface, while the poly(ethylene terephthalate) surface after modification showed reduced levels of adhesion by between 2 and 4 orders of magnitude.

Although it is still not clear about the detailed mechanisms and factors that can affect the PEG-based antifouling system, theoretical models and experimental research have been extensively carried out to understand the protein resistance conferred to a surface by attaching PEG to it [113]. Jeon et al. [114, 115] studied and modeled the PEG surfaces with low protein adsorption. By assuming that proteins are finite spherical particles, they proposed that proteins approaching a surface could lead to compression of the PEG chains, resulting in repulsive elastic forces. Meanwhile a thermodynamically unfavorable osmotic penalty was created when water molecules that were stressed out from the hydratation of polymer chains were compressed. These

repulsive forces, which could be affected by molecular weight, chain length and grafting densities of the polymers, were suggested to be main reasons for PEG antifouling properties. Prime and co-workers, instead focusing on long-chain PEG polymers, developed antifouling coatings based on SAMs [110]. Their work indicated that SAM PEGs with shorter chain lengths could also be used as protein resistant coatings probably because their grafting densities, i.e. number of chains per unit surface area, are larger than that of the long-chain coating. Szleifer et al. [116] used single-chain mean field theory to investigate the interaction between proteins and SAM PEGs. Taking into account the forces between proteins and polymer-modified substrate averaged over all possible chain conformations, they suggested that the density of PEG molecules in the region close to the substrate was a key parameter in determining reduction of protein adhesion. Grunze *et al*. [117, 118] studied fouling resistant behavior of methoxy-teminated oligo (ethylene glycol) SAMs and found the antifouling properties were strongly dependent on the conformation of the polymer chains. Monte Carlo simulations indicated that SAMs with helical molecular structures would interact more with water than *trans* SAMs, being more favorable to the antifouling performance of the PEG coating. Efremova *et al*. [119] characterized the molecular weight and temperature effects on PEG coatings against Streptavidin. Results showed that two different states of grafted PEG chains existed: a protein-repulsive state and a protein-attractive state. The critical load to induce the protein-attractive form and the relaxation time back to the protein-resistant state depended strongly on the molecular weight of polymer chains and testing temperatures.

PEG polymeric antifouling materials have already been applied in modification of water filtration membranes, marine ship coatings, biosensors etc. Saglea et al. [120] coated reverse osmosis membranes with PEG layers to observe its desalination properties and fouling resistance. Shi et al. [121] synthesized PEGylated polyethersulfone and studied its application in an antifouling ultrafiltration membrane. Gudipati et al. [122] prepared a hyperbranched fluoropolymer-PEG composite and evaluated its antifouling properties against alga *Ulva* as a marine coating. Emmenegger et al. [123] modified the gold surface of surface plasmon resonance (SPR) sensors with PEG polymer chains to reduce nonspecific adsorption from human blood plasma and from single-protein solutions of human serum albumin, immunoglobulin G, fibrinogen, and lysozyme.

Polymeric compounds with zwitterionic sidechains, e.g. carboxybetaine and sulfobetaine, are traditionally used in textile and medical industries as blood compatible substances [124]. Due to the dipolar internal salt structures of zwitterionic groups, these materials can have some unique properties such as high chain rigidity, antipolyelectrolyte behavior and regular molecular conformation. Recently, these kinds of materials have emerged as good fouling resistant coatings. Jiang et al. [125] first applied zwitterionic polymers as antifouling agents. Two polymers, poly(sulfobetaine methacrylate) (polySBMA) and poly(carboxybetaine methacrylate) (polyCBMA) were grafted from pre-treated glass slides. Reduction of adsorption of fibrinogen on the as-modified surface was observed. Bovine aortic endothelial cells could only attach and spread in areas with no modification, indicating good fouling resistance for the zwitterionic polymer. Chang et al. [126] modified gold surfaces with polySBMA and

tested the antifouling behavior against three model proteins under a wide range of various testing conditions. They demonstrated that these well-packed polymer bushes effectively reduced plasma protein adsorption and no adhesion and activation of platelets were observed on the surface. Chiang et al. [127] prepared poly(vinylidene fluoride) ultrafiltration membranes grafted with polySBMA. No bovine serum albumin (BSA) could be observed if the grafting density exceeded 0.4 mg/cm^2. Adsorption of γ-globulin was also greatly reduced. Fundamental studies on the molecular level indicate that charge balance, minimized dipole and close packing density are some key parameters that can affect antifouling properties of zwitterionic polymers. In the case of polyphosphonate-betains (PB), low adsorption of fibrinogen and BSA could only be obtained when ratio of positive to negative charge reached 1:1, maintaining charge neutrality. Thickness measurements of PB-SAMs indicated that the zwitterionc groups were in an antiparallel orientation through charge and dipole interaction. Molecular dynamic simulation revealed that a 2-D crystalline structure similar to packing configuration as zwitterionic groups of membrane lipids was formed. [128-130] In addition to traditional zwitterionic polymers, another group of polymers that are formed by a pair of separate monomers with two opposite charge moieties have been developed. Bernards et al. [131] modified gold-coated surfaces with polymer brushes composed of varying mixtures of positively and negatively charged monomers. Different charge ratios could be obtained by changing grafting conditions and it was found that antifouling properties were maximized only when the coating was formed as a statistical copolymer from the two charged components.

Biomimetic fouling resistant materials comprise another important category of materials whose antifouling properties come from mimicking natural fouling-defense system. Many species in nature have evolved defensive mechanisms against the settlement and growth of fouling organisms [132]. Gorgonian coral, *P. acerose*, was one of the first studied models due to its good fouling resistant properties. It has multiple defence strategies against fouling [133]. The surface roughness of this species is of 2-4 μm and the surface free energy is only 20-30 mN/m, low for bioadhesiveness [134]. It can also produce secondary metabolites and sulphated polysaccharide mucus to prevent diatom attachment [135]. Another aspect naturally present in antifouling organisms are skins such as the skin of sharks and killer whales. Studies show that the clean surface of *Globicephala melas*, a pilot whale, is attributed to the nano-ridge pores on the skin surface [136]. The nano-ridge pores (0.1-1.2 μm^2) are smaller than most fouling organisms, providing no contact points for cell adhesion. The whale skin also contains a zymogel, which can hydrolyze the adhesives of settling bacteria, preventing bio-attachment through enzymatic digestion [137]. Shark skin is a more recent focus as antifouling biomimetic technology. It is believed that the special microtopographical ridge patterns are the key factors protecting the skin from adhesion of microorganisms [138]. Other biomimetic models include dogfish egg-case, echinoderms, algae etc [132]. By inspiration and mimicry of natural species, a variety of antifouling coatings have been developed. Cao et al. [139] constructed a layer-by-layer film composed of poly(acrylic acid) and poly(ethylenimine) by spray coating to mimic the surface morphology of *G. melas*. It is shown that although surfaces with different ranges of roughness features and chemistry were obtained, the best antifouling results against green alga Ulva came

from samples with surface characteristics similar to that of *G. melas*. Based on the concept that proteins in the bloodstream do not adsorb irreversibly onto the surface of the cell, materials mimicking the cell membranes have been proposed. Ye et al. [140] blended a cellulose acetate membrane with poly(2-methacryloyloxyethyl phosphorvicholine (MPC)-co-n-butyl methacrylate (BMA)) (PMB30) as a blood purification membrane. Antifouling tests showed that the amount of proteins adsorbed on the blend membranes decreased, and adhesion and activation of platelets on the membrane were reduced. Huang et al. [141] improved the antifouling properties and biocompatibility for polyacrylonitrile-based asymmetric membranes, in which phospholipid moieties were directly anchored on the poly(acrylonitrile-co-2-hydroxyethyl methacrylate) (PANCHEMA) membrane surface. They found that increasing the content of phospholipid moieties on the membrane surface could enhance the hydrophilicity and biocompatibility of the membrane and meanwhile reduce the macrophage adhesion. Statz et al. [142] immobilized peptidomimetic polymers consisting of poly-N-substituted glycine oligomers (polypeptoids) conjugated to polypeptides onto the surface of titanium dioxide and investigated the side chain effect on the antifouling properties of the coating. Reduced adsorption of a series of proteins such as lysozyme, fibrinogen and serum was observed on all polypeptoid-modified surfaces. Long-term *in vitro* 3T3 fibroblast cell attachment studies showed that polypeptoid with a methoxyethyl side chain exhibited superior long-term fouling resistance compared to hydroxyethyl and hydroxypropyl side chains during the six week testing period. In addition, attachment of both gram-positive and gram-negative bacteria for up to four days under continuous-flow conditions was

significantly reduced on the polypeptoid-modified surfaces. Finally, antifouling films mimicking the placoid micron-scale patterns of the shark skin have already been commercialized by fabrication of polydimethylsiloxane elastomer through photolithography [143].

In general, as for the environmental impact, fouling resistant materials are more friendly and promising than antimicrobial compounds. However, unlike antimicrobial biocides, which kill bacteria almost with no exceptions, most fouling resistant coatings are only effective to certain kinds of microorganisms, limiting their applications in real biologically complicated environments such as sea water. Therefore, another kind of antifouling material, i.e. fouling release coatings, has been attracting more and more attention.

1.2.4 Fouling Release Coatings

Fouling release materials are special antifouling agents well known for their self-cleaning properties. Unlike antimicrobial or fouling resistant coatings, fouling release coatings usually allow cell attachment at first place, while the adhered bacteria can be easily removed by hydrodynamic stress during ship navigations or a simple mechanical flushing cleaning. Due to the low surface energy, non-sticky properties and easy access and fabrications of these materials, fouling release coatings have become more and more popular as alternatives to antimicrobial and fouling resistant agents [144].

Silicone-based compounds are one of the two main fouling release coating materials. The first use of cross-linked silicones in marine coatings can be traced back

to 1961. [145] Robbart found that the settlement of barnacles could be reduced on a surface coated with silicone resin. In 1970s, silicone rubber was developed for antifouling coatings. Kroyer found that silicone rubber showed less fouling compared to a silicone resin [146]; Mueller et al. [147] reported applications of cured silicone rubber as drag reducing antifouling coatings for vessels; Milne [148] first patented the enhancement of antifouling properties of coated panels by using silicone oil, i.e. poly(methylphenylsiloxane) within a cured silicone rubber. Current interest in polydimethylsiloxane (PDMS)-based materials is focused not only on fundamental scientific research but on factors that can affect the fouling release behavior of this silicone-based coatings. The elastic modulus is believed to play an important role in the fouling release mechanism. Generally, low elastic modulus results in low bioadhesion. Chaudhury et al. [149] showed that 80% of the attached green alga *Ulva linza* was from PDMS model coatings. A sporeling will release at moduli ranging from 0.2 and 0.8 MPa whereas almost no release was observed for a modulus as high as 9.4 MPa. Kim et al. [150] reported that better release of pseudobarnacles from platinum-cured silicones was obtained as the coating modulus decreased from 1.3 to 0.08 MPa. Thickness of silicone coatings is another important parameter influencing removal behavior. Chaudhury et al. [149] observed that the release of sporelings was particularly improved for the 430-μm-thick coatings compared to that of thinner coatings (16 and 100 μm). Wendt et al. [151] demonstrated that the critical removal stress of live barnacle *A. amphitrite* from silicone coatings decreased from 0.093 to 0.055 MPa when the film thickness increased from 0.1 to 2 mm. In addition to laboratory research, commercial fouling release products based on silicone have already been

made. Sylgard184 is an unfilled, clear two-part PDMS-based formulation developed by Dow Corning, which contains an α,ω-vinyl terminated PDMS polymer, a poly(dimethylsiloxane-co-hydrogenomethylsiloxane) copolymer, a vinyl resin additive, and a platinum-based catalyst.[152] SilasticT-2, another commercial PDMS elastomer product from Dow Corning, is often used as a standard reference due to its fouling release efficiency against barnacles and *Ulva* alga. [153] RTV11 is a representative condensation-cured silicone elastomer from General Electric. This formulated product contains 60−80 wt % of hydroxy-terminated PDMS, 32 wt % of $CaCO_3$ filler, 1.9−2.1 wt % of ethyl silicate 40 cross-linker, and dibutyltin dilaurate catalyst. [154] These PDMS-based fouling release materials are all characterized by a high water contact angle, a low critical surface energy, and low elastic modulus values. Silicone modified hybrid coatings have also been explored. Incorporation of multiwalled carbon nanotubes in PDMS matrices was investigated by Beigbeder et al. [155] They found that addition of carbon nanotubes could reduce the hydrophobicity of PDMS and only small amount of nanotubes (0.05 wt %) could not only improve the release of Ulva zoospores and sporelings, but also reduce the critical removal stress of adult *A. amphitrite* barnacles by more than half. Majumdar et al. [156] synthesized cross-linked PDMS−polyurethane thick coatings with microtopographical surface domains composed primarily of PDMS surrounded by a polyurethane matrix. Improved water immersion stability was shown for this surface coating due to the cross-linking and the presence of the microdomains was helpful to decrease the adhesive strength of *A. amphitrite* barnacles. Hydrogel modified silicones were developed by the Hempel Company. [157] The increase of hydrophilicity of the coating helped to delay the

settlement of diatom slime and segregation of hydrogel at the surface led to a lower hull skin friction over longer periods of time.

Another category of commonly used fouling release coatings is fluorine-based materials. The low critical surface tension and nonpolar stable surface properties make fluorine-based materials good candidates as fouling release agents. The first use of fluoropolymer in an antifouling coating was patented by Berque in 1973 [158] by application of poly(tetrafluoroethylene) (PTFE) or fluorinated ethylene−propylene copolymers as protective coatings for ship hulls. Griffith et al. [159] coated a tugboat with PTFE-filled fluorinated polyurethane paint and regularly inspected and cleaned the boat over a period of 13 years. In the 1990s, perfluoroalkyl polymers, due to their better solvent solubility than PTFE, attracted much intention. Tsibouklis et al. [160] synthesized poly(perfluoro(meth)acrylate) polymers to construct smooth film structures. These fluorinated films showed low settlement of bacteria *Pseudomonas*, alga *Ulva*, and barnacle A. *Amphitrite* due to the preferential chain segregation to the surface and a low surface energy. Schmidt et al. [161] prepared a series of coatings by cross-linking a copolymer of 1H,1H,2H,2H-heptadecafluorodecyl acrylate and acrylic acid with a copolymer of poly(2-isopropenyl-2-oxazoline) and methyl methacrylate in different molar ratios. These materials showed improved fouling release properties due to the higher resistance to surface rearrangement and lower water contact angle hysteresis. Perfluoropolyether polymers were also investigated as alternatives. Brady [162] prepared fluorinated polyurethane elastomers by cross-linking of a poly(perfluoro(oxymethylene-*ran*-oxyethylene)dimethylol)-terminated oligomer (PFPE diol) with a diisocyanate component to control the fluorine content, surface

energy and elastic modulus, respectively. DeSimone et al. [163] developed cross-linkable random PFPE graft terpolymers containing various alkyl (meth)acrylate monomers with glycidyl methacrylate as the curable monomer, which showed reduction of accumulation of alga Ulva in comparison to PDMS and also facilitated fouling release characteristics under suitable hydrodynamic conditions. Although different efforts have been made to construct better fouling release coatings with fluoropolymers, commercialization of such materials has not yet been successful.

Fouling release materials are good antifouling coatings against adherence of most macrofouling organism when the coated surface is submitted to mechanical shear stresses. However, due to the high hydrophobicity of these materials, they are vulnerable to slime layers composed of bacteria and diatoms especially under static conditions. Also, their long term stability and impact on the environment are as yet undetermined.

1.2.5 Methods for Coatings of Antifouling Materials

A variety of methods have been developed and applied not only to prepare single antimicrobial, fouling resistant or fouling release coatings, but also to construct more complex and combined structures of materials working against different antifouling mechanisms.

Depending on how polymer films or brushes are immobilized on a substrate, the author would like to define two categories of modification methods. 'Modified from' methods include all methods that help to add antifouling coatings from a substrate,

while ‘modified to’ methods refer to all methods that add antifouling coatings to a substrate.

One of the most commonly used ‘modified from’ methods is to graft polymer brushes from a variety of substrates by using surface-initiated controlled radical polymerization such as surface initiated atom transfer radical polymerization (SI-ATRP), surface initiated reversible-addition fragmentation chain transfer polymerization (SI-RAFT) and surface-initated nitroxide-mediated polymerization (SI-NMP). A monolayer containing chemical functional groups serving as initiator of polymerization is necessary for these methods, e.g. tertiary bromide groups from SI-ATRP and dithioesters for RAFT. Once the surface is modified with an initiation layer, controlled living polymerization reactions can be used to grow all kinds of polymer brushes from the surface [164]. Russell et al. [165] used SI-ATRP to graft poly(2-(dimethylaminoethyl methacrylate)) brushes on different substrates such as filter paper, glass slides, and silicon wafers. Subsequent quaternization of these brushes with ethyl bromide resulted in quaternary ammonium-modified surfaces with substantial antimicrobial activity against *E. coli or B. subtilis*. Ramstedt et al. [166] modified silicon surface with poly(3-sulfopropylmethacrylate) brushes via SI-ATRP and loaded the brushes with silver ions. The polymer brush coating was behaving as a reservoir for biocidal silver ions, and was found to effectively inhibit the growth of both Gram positive and Gram negative bacteria. Ignatova et al. [167] copolymerized 2-(tert-butylamino)- ethyl methacrylate (TBAEMA) with either monomethyl ether of poly(ethylene oxide) methacrylate (PEOMA) or acrylic acid (AA) or styrene on stainless steel. It was found that proteins (e.g., fibrinogen) were less adsorbed when

brushes contained neutral hydrophilic (PEOMA) co-units rather than negatively charged groups (PAA salt). Compared to a bare stainless steel surface, brushes of poly(TBAEMA-co-PEOMA) and poly(TBAEMA-co-AA) decreased bacterial adhesion by 3 to 4 orders of magnitude against the Gram-positive bacteria *S. aureus*. The main advantage of using SI living polymerization technique to modify the surface is that well controlled grafting density, polymer composition and film thickness can be obtained by manipulating reaction conditions. Ma et al. [168] found that grafted poly(oligo(ethylene glycol) methyl methacrylate) brushes with a thickness of 4 nm were effective in prevention of nonspecific adsorption of fibronectin. They further proposed that poly(poly(ethylene glycol) methacrylate) (PPEGMA) brushes with a thickness of only 1.4 nm were sufficient to significantly reduced nonspecific protein adsorption. [169] PPEGMA brushes prepared by Singh et al. [170] were good fouling resistant coatings against adsorption of smaller molecules such as the GRGDS peptide with a thickness about 10 nm. Fan et al. [171] modified titanium surfaces poly(oligo(ethylene glycol) methyl ether methacrylate) brushes containing side chains with 4, 9, and 23 ethylene oxide (EO) units and investigated their antifouling properties. The short-term results showed that all the three poly(MPEGMA)s reduced cell adhesion for three weeks compared to bare titanium, while for a longer time, they were completely covered with cells in 7, 10, and 11 weeks, respectively. Bozukova et al. [172] modified the surface of poly(2-hydroxyethyl methacrylate-co-methyl methacrylate) hydrogels by grafting of a brush of poly(oligoethylene glycol methyl ether acrylate) and found that the nonspecific protein adsorption decreased and the cell repellency was enhanced with the increase of the brush chain length. Poly(2-

methacryloyloxyethyl phosphorylcholine) (poly(MPC)) brushes with graft density 0.06–0.39 chains/nm2 and chain length 5–200 monomer units were prepared from silicon wafer surfaces by Feng et al. [173] It was shown that the adsorption of fibrinogen adsorption was strongly dependent on both graft density and chain length. Protein adsorption decreased significantly with increasing graft density and/or chain length of poly(MPC) and reached a level of <10 ng/cm^2 at graft density >0.29 chains/nm^2 and chain length >100 units, compared to ca. 570 ng/cm^2 for the unmodified samples. Tugulu et al. [174] found that PPEGMA brushes detached rapidly from glass or silicon substrates at high chain densities, resulting in an increase in nonspecific protein adsorption. By appropriate decrease of the grafting density, the stability of the brushes in a cell culture medium could be improved from less than 1 to more than 7 days, without compromising the nonfouling properties. Although 'modified from' methods have been extensively used in fundamental research, their applications as commercial coating technologies are limited due to the complicated polymerization reactions and various catalysts they need.

Compared to 'modified from' methods, 'modified to' methods are suitable for both laboratory studies and industrial applications. Solution (spray/spin) coating is one of the most widely used methods to add antifouling coatings onto a surface. Cho et al. [175] first synthesized fluorine-free, amphiphilic, nonionic surface active block copolymers (SABCs) through chemical modification of a polystyrene-block-poly(ethylene-ran-butylene)-block-polyisoprene triblock copolymer precursor with selected amphiphilic hydrophobic aliphatic groups combined with a hydrophilic poly(ethylene glycol) (PEG) group-containing moiety. The material was then spin-coated on silicon wafers

and spray-coated on glass slides for antifouling tests. Good fouling-release properties were demonstrated against *Ulva* and *Navicula*. Cao et al. [139] constructed a layer-by-layer film composed of poly(acrylic acid) and poly(ethylenimine) by spray coating to mimic the surface morphology of *G. melas*. Dimitriou et al. [176] investigated the effects of spray coating and spin coating in preparation block copolymer films composed of amphiphilic block copolymers with polystyrene-block-poly(ethylene-*ran*-butylene)-block-polyisoprene backbones and poly(ethylene glycol) monomethyl ether and 10-perfluorodecyl-1-decanol side chains. It was demonstrated that surface compositions of the coatings are different by using different coating methods, which may potentially affect antifouling properties. Dip coating, e.g. layer-by-layer assembly, has also been used an alternative to spin/spray coating methods. Ishigami et al. [177] adopted a layer-by-layer method to deposit poly(sodium 4-styrenesulfonate) (PSS) and poly(allylamine hydrochloride) (PAH) on reverse osmosis membrane. Due to the high hydrophilicity, the polyelectrolyte film was demonstrated to have good fouling resistance against BSA proteins. Yang et al. [178] used a "click" chemistry-enabled layer-by-layer method to construct a coating composed of both fouling-resistant poly(ethylene glycol) methyl ether methacrylate-based polymer chains and antimicrobial 2-(methacryloyloxy)ethyl trimethyl ammonium chloride-based polymer chains. The polymer multilayer coatings were resistant to bacterial adhesion and are bactericidal to marine Gram-negative *Pseudomonas sp*. Antifouling coatings can also be modified on the substrate by chemical vapor depositions. Yang et al. [179] prepared antifouling thin films of poly[N,N-dimethyl-N-methacryloxyethyl-N-(3-sulfopropyl)-co-2-(dimethylamino)ethyl methacrylate-co-ethylene glycol dimethacrylate] (PDDE)

via an all-dry-initiated chemical vapor deposition (iCVD) technique and the coated surfaces exhibited very low absorption of various foulants such as bovine serum albumin (BSA), humic acid (HA), and sodium alginate (SA). Bhatt et al. [180] modified Thermanox, Si wafer, and quartz crystal microbalance (QCM) substrates with copolymer coatings via plasma enhanced chemical vapor deposition of 1H,1H,2H,2H-perfluorodecyl acrylate and diethylene glycol vinyl ether. The as-modified amphiphilic surfaces with low surface energies showed no adhesion with respect to BSA and lysozyme. UV-assisted graft polymerization is a technique widely used in membrane modification. Pieracci et al. [181] photochemically modified poly(ether sulfone) (PES) ultrafiltration membranes with the monomer N-vinyl-2-pyrrolidinone (NVP) to increase surface wettability and decrease adsorptive fouling. A substantial decrease in the irreversible adsorptive fouling of BSA was measured. Ulbricht et al. [182] modified the surface of polyacrylonitrile ultrafiltration membranes with UV irradiation-initiated graft polymerizations of monomers from water solution. Results of adsorption experiments with *γ-globulins*, BSA and *cytochrome C* showed that membranes modified with PEGMA behaved the best. Other 'modified to' include blending, plasma treatment, etc. [183-186]

In summary, a variety of methods and materials can be applied to surface modification for antifouling purposes. Both fundamental research and practical applications are expected to develop coatings with improved antifouling properties and environmental compatibilities. Detailed applications of antifouling coatings on reverse osmosis membranes are explored and discussed in Chapter II and Chapter III.

1.3 Hybrid Materials

1.3.1 Background

Hybrid materials compose one large category of materials that are not only one of the most popular focuses of scientific research, but also one of the most important commercial products applied in our daily life. A broad and general definition of hybrid materials is given as nanocomposites with intimately mixed organic and inorganic components. [187] They are either homogeneous systems derived from monomers and miscible organic and inorganic components, or heterogeneous systems where at least one of the components' domains has a dimension ranging from some Å to several nanometers. [188] Although the concept of 'hybrid materials' was not mentioned until the 1980's, the application of composite materials in human life has occurred for thousands of years. The first use of hybrids might be traced back to pigments and paintings in ancient countries. Maya blue, frequently used in ancient Maya fresco paintings, is a quite old man-made hybrid material composed of molecules of the natural blue indigo encapsulated within the channels of a clay mineral known as palygorskite. This old pigment has remarkable stability and resistance against biodegradation, acids, alkalis and organic solvents. [189, 190] Adobe, used by ancient Greeks to make bricks and walls in arid regions throughout history, is a mixture of clay and straw that serves as an effective structural composite material. [191] In the 1950's, with the development of sol-gel processes, successful commercial hybrid organic–inorganic materials have been part of manufacturing technology. [192] Typical zinc-rich and silicate-based hybrid resins, due to their high performance and multiple functions, are widely used in optical, automotive and electrical industries as

protective coatings. [193-195] In 1980's, further development of soft inorganic chemistry processes facilitated the establishment of modern hybrid materials, which are focused on molecular interactions between organic and inorganic components, reduced domain sizes ranging in 1-100nm and more versatile functions in advanced science and technology. [196]

Based on the interaction between the two distinctive components, Sanchez et al. divided hybrid materials into two classes. In class I, organic and inorganic components are embedded through weak bonds such as hydrogen, van der Waals or ionic bonds, providing the cohesion to the whole structure. In class II materials, the two phases are linked together through strong chemical bonds such as covalent or iono-covalent bonds. [187] Class I hybrid materials are usually obtained by incorporation of organic molecules and bio-additives into metal oxide networks and matrices through mixing or entrapment during the preparation processes. Photochromic hybrids with elaborated optical properties are representatives of this class. TV screens are coated with dye-containing hybrid coatings made of indigo dye embedded in a silica/zirconia matrix. [197] UV-pearls', made by encapsulation of active organic UV filters in silica micro-capsules, has been used in suitable cosmetic vehicles to achieve high sun protection factors. [187] Bioactive hybrid materials are also typical class I hybrids widely applied in the field of biotechnology. Enzymes, antibodies or microorganisms are immobilized or trapped within glass or ceramics through sol-gel processes. Hybrid biosensors based on glucose oxidase have been explored to detect glucose in fruit juice, CocaCola and human blood. [198] Bio-hybrids using using *Leishmania donovani infantum* promastigotes as antigens trapped within silica gel were developed and applied in

detection of specific antibodies in the serum of human and dog. [199] Biogel transplants prepared by encapsulation of swine hepatocytes and rat liver in a silica film have already been used as a bridge to liver transplantation in patients with fulminant hepatic failure. [200] Unlike class I materials that are based on weak physical interactions, class II hybrid composites require more complicated and versatile designed strategies to build strong chemical or ionic bonding between organic and inorganic components. Zinc based hybrid paints with protective functions were and are still being used as corrosion-resistant primers and high-temperature coatings for steel. [201] Dye-sensitized solar cells, with a hybrid structure of anchoring organic dye sensitizer onto the surface of a wide band gap oxide semiconductor, appears to be promising technique for photovoltaic devices. [202] Nanocomposite membranes prepared by incorporation of oxide particles in sulfonated-polymer matrices are found to be good competitors for commercial Nafion proton exchange membranes used in fuel cell systems. [203]

Taking advantage of unique compositional structures, hybrid materials usually exhibit improved properties that can be fine tuned by optimizations of selected organic and inorganic phases, promoting new potential applications for the resulting composite materials. [204] Lanthanide-based luminescent materials have been extensively synthesized and investigated by using different lanthanide complexes imbedded in different matrices. Binnemans et al. [205] coupled luminescent $[Ln(tta)_3(phen)]$ complexes to a Merrifield resin, which is the standard solid support for solid-state organic synthesis and consists of polystyrene cross-linked by divinyl benzene. Strong red luminescence was detected for the Eu^{3+} complex, whereas near-infrared luminescence could be obtained for complexes where Ln - Sm, Nd, Er, or Yb. Wang *et*

al. [206] used free radical copolymerization of styrene and methylacrylic acid in the presence of a europium(III) or terbium(III) complex such as $[Eu(tta)_3(phen)]$, $[Eu(dmb)_3(phen)]$, $[Tb(phen)_2Cl_3] \cdot 2H_2O$, and $[Tb(sal)_3]$ to prepare luminescent resins. It was found that the emission lines of Eu^{3+} and Tb^{3+} were narrower and more intense in the resin and the decay times were longer after incorporation in the matrix. Loading different luminescent nanoparticles in poly(ethylene oxide), poly(methyl methacrylate) and poly(phenylene vinylene) was also tried. [207-209] These hybrids were found to have both good processability good mechanical properties from polymer matrices and high luminescence efficiency and long-term chemical stability from inorganic nanoparticles. Polymer–clay nanocomposites are of great importance in the industrial market due to their improved properties of strength, modulus, and toughness, etc. Inagaki et al. [210] from Toyota Company first reported the synthesis of a clay–nylon nanocomposite through the *in situ* polymerization method. Structural applications in vehicles demonstrated a doubling in tensile modulus and strength without sacrificing impact resistance with a 2 vol% loading of silicate clays. Nanocor and Mitsubishi Gas Chemical Company developed the MXD6 high barrier semi-aromatic nylons in nanocomposite form, featuring oxygen and carbon dioxide barrier properties that were previously unachievable. [187] Silicate–polymer nanocomposites have also been developed as fireproof hybrid materials due to the low loading of clays and high heat-distortion temperature. [211] Other hybrid-based materials include hybrid organic−inorganic polyoxometalate compounds [212] and polylactide-based bio-nanocomposites etc. [213]

Herein, further detailed discussion of hybrid materials will be focused on several important nanocomposite systems.

1.3.2 Silica Based Materials

Due to its unique physical and chemical properties such as thermal stability, chemical stability, strong mechanical strength, easy access and modification, silica has been extensively explored and studied not only as a superior component for preparation of innovative hybrid materials, but also as ideal model systems for fundamental scientific research. Generally, silica can be used both as a filler and a network former. As a filler, silica nanoparticles are usually incorporated into polymer matrices either in the form of a core-shell structure or as pendent groups on the side chains, while as a former, silica network matrices are constructed, which will be subsequently modified with either organic functionalities or inorganic nanoparticles.

Silsesquioxanes are probably the most prominent representatives of cluster-like inorganic components. Octafunctionalized cages such as the anionic oxyfunctionalized system $(SiO_{2.5})_8^{8-}$ or the octahydrido species $(HSiO_{1.5})_8$ are obtained in reasonable yields and have been used as precursors for multifunctionalized crosslinking agents. [214] polyhedral oligomeric silsesquioxanes (POSS, $R_8Si_8O_{12}$) are typical cube cages developed in hybrid composites. Polymers modified with these inorganic building blocks have improved properties of thermal, oxidative and dimensional stabilities. Lichtenhan et al. [215] synthesized POSS with methacrylic monomers by corner capping the trisilanol cages $R_7Si_7O_9(OH)_3$ (R = *c*-C_6H_{11}, *c*-C_5H_9) with methacrylate containing trichlorosilanes. Homo- and copolymers of these systems showed no thermal

transitions below their decomposition temperatures. Studies by Lee et al. [216] on epoxy resins embedding monofunctional POSS-epoxy macromers showed that the glass transition temperature, Tg, increased with increasing weight fraction of the monofunctional POSS-epoxy. Experiments performed under identical thermodynamic states revealed that the molecular level reinforcement provided by the POSS cages also retarded the physical aging process in the glassy state. Fu et al. [217] investigated mechanical properties of POSS modified polyurethane and found an increase of the tensile modulus as compared to unmodified polyurethane. Further wide-angle X ray diffraction (WAXD), small-angle X-ray scattering (SAXS) and transmission electron microscopy (TEM) characterizations revealed that POSS molecules formed nanoscale crystals in the hard domain and a preferred orientation of deformed hard domains perpendicular to the stretching direction was observed. Haddad et al. [218] synthesized and characterized a series of linear thermoplastic hybrid materials containing an organic polystyrene backbone and large inorganic silsesquioxane groups pendent to the polymer backbone. Preliminary results indicated that the pendent inorganic groups drastically modified the thermal properties of the polystyrene and that interchain and/or intrachain POSS-POSS interactions result in variations in solubility and thermal properties. In addition to small silsesquioxanes cube clusters, nanometer- and micrometer-sized silica particles have also been modified with different polymers. Laibal et al. [219] developed a multistep synthesis to grow polymers from the silica particle. Pyrogenic amorphous silica was first surface-modified with diazo groups, which served as initiating sites for subsequent polymerizations of polystyrene. The coverage of diazo groups on silica surfaces ranged from 0.03 to 0.1 groups per 100 $Å^2$

and a linear dependence between the monomer and initiator concentration and the polymer coverage was observed. Huang et al. [220] used ATRP reaction to grow poly(acrylic acid) from the surface of a silica gel with a particle diameter of 5 mm and a pore size of 86 nm. The polymer film thickness was calculated to be 10 pm. Applications of the modified silica as a solid phase in size-exclusion chromatography revealed a very good separation behavior for a mixture of proteins and much faster elution times. Homopolymers, diblock-, and branched triblock copolymers could also be grown on silica particles and POSS as well. [221, 222]

Another very important application of silica in hybrid materials is to construct a mesoporous structured silica network and tailor modify it with functional organic molecules or inorganic particles. In the presence of structure-directing agents (SDAs), inorganic silica precursors such as tetraethylorthosilica (TEOS) or tetramethylorthosilica (TMOS) can be condensed or self-assembled into well-ordered structures with high porosity and large specific surface area. [223] Incorporation of organic molecules or embedding inorganic particles can be achieved by post synthetic functionalization. This process is carried out primarily by reaction of organosilanes of the type $(R'O)_3SiR$, or less frequently chlorosilanes $ClSiR_3$ or silazanes $HN(SiR_3)_3$, with the free silanol groups of the pore surfaces. Ma et al. [224] successfully constructed a photochemically controlled hybrid silica system for compound uptake and release. Coumarin was first anchored on the pore openings of MCM-41 silica phases. Active compounds such as cholestane derivatives were then inserted into the pores. By irradiation of the samples with UV light of different wavelengths, sealing and cleavage of the coumarin dimers could be achieved, allowing encapsulation and release of the

enclosed active compounds. Radu et al. [225] synthesized a poly(lactic acid) coated MCM-41-type mesoporous silica nanosphere hybrid material and utilize it as a fluorescence sensor system for detection of amino-containing neurotransmitter. The PLA layer was working as a gatekeeper and the sensor showed a unique "sieving" effect on several structurally simple neurotransmitters, i.e., dopamine, tyrosine, and glutamic acid, which regulates the rates of diffusion of the amino acid-based neurotransmitters into the sensor mesopores of the material. Lei et al. [226] modified mesoporous silica with carboxylethyl- or aminopropyl- functionalities to entrape the enzyme organophosphorus hydrolase (OPH). The hybrid system yielded larger amounts of protein loading and much higher specific activity of the enzyme compared to the unfunctionalized mesoporous silica and normal porous silica with the same pore size. The entrapped OPH in the organically functionalized nanopores showed an exceptional high immobilization efficiency of more than 200% and enhanced stability far exceeding that of the free enzyme in solution. Another approach to obtain mesoporous silica hybrids is co-condensation, or one-pot synthesis. It method is achieved by the co-condensation of TEOS or TMOS with terminal $(R'O)_3SiR$ in the presence of SDAs, leading to materials with organic residues anchored covalently to the pore walls. [223] Macquarrie et al. [227] prepared a series of aminopropyl-substituted micelle templated silicas by a one-step co-condensation route using dodecylamine as template. The effect of solvent composition on the material properties, reactivity and catalytic activity was investigated in detail. Stucky et al. [228] developed a simple procedure to synthesize functionalized mesoporous materials with sulfonic groups involving the co-condensation of tetraethoxysilane and

mercaptopropyltrimethoxysilane in the presence of block copolymers and hydrogen peroxide under acidic conditions. The modified SBA-15 materials show hexagonal mesoscopic order and pore sizes up to 60 Å, with acid exchange capacities ranging from 1 to 2 mequiv of H^+/g of SiO_2, surface areas up to 800 m^2/g, and excellent thermal and hydrothermal stabilities. Jia et al. [229] synthesized a novel mesoporous MCM-41-type of hybrid material by co-condensation of tetraethyl orthosilicate and the chelate ligand (3-trimethoxysilylpropyl)[3-(2-pyridyl)-1-pyrazolyl]acetamide in the presence of cetyltrimethylammonium bromide as template. By a ligand exchange reaction, oxodiperoxomolybdenum species $MoO(O_2)_2$ could be introduced. All the molybdenum-containing solid epoxidation catalysts showed high activity for the liquid-phase epoxidation of cyclooctene with tBuOOH and stability against leaching of active molybdenum species. Other organic moieties such as thiol, cyano, vinyl etc. could be modified onto the silica network by one-pot synthesis. [230-232]

Different applications have been explored and developed by using silica-based hybrid materials. Kim et al. [233] synthesized spherical periodic mesoporous organosilica particles with diameters between 1.5 and 2.5 mm and bridged by ethane. Separation tests of the material as a packing agent in a micro-HPLC showed that good separation could be obtained for a mixture of eight substances of medium to high hydrophobicity. Zhang et al. [234] modified mesoporous silica with a bridged tetrasulfide moiety ($(EtO)_3Si(CH_2)_3S\text{-}S\text{-}S\text{-}S(CH_2)_3Si(OEt)_3$) and applied it as an effective absorbent for Hg^{2+} ions. Large degrees of adsorption and selective removal of mercury ions from aqueous solutions that contained the competitive cations such as Pb^{2+}, Cd^{2+}, Zn^{2+} etc. were achieved. Fukuoka et al. [235] incorporated pure Pt, Rh, and Pt/Rh and Pt/Pd

mixtures into ethane bridged 2D hexagonal silica mesostructures. The as-prepared nanowires prepared exhibit bead-chain-like morphologies and the magnetic susceptibilities at temperatures below 90^{o}C of the Pt/Rh and Pt/Pd hybrid nanowires were two and three times of the sum of the values for the two individual component metals. Other applications of mesoporous silica hybrids include acid/base catalysis, low-k thin films etc. [236-238]

1.3.3 Polyvinylpyrrolidone (PVP) Based Materials

Polyvinylpyrrolidone (PVP), also called polyvidone or povidone, is a typical type of polymer that has been widely investigated and developed as matrix in hybrid materials. Based on its unique properties such as water solubility, high polarity, easy synthesis with fine-tuned molecular weight, relatively high Tg, etc., PVP-based hybrids have been applied in a variety of practical applications such as drug delivery, metal nanowire processing, etc.

Probably the most prominent function of PVP as polymeric matrices in hybrid nanocomposites is its application in drug delivery systems. The high water solubility of PVP makes it a good drug carrier entrapping poorly water-soluble drugs in a solid solution drug delivery system. [239] Tachibani et al. [240] first developed a solvent method to prepare amorphous solid solution. By dissolving both the drug and the carrier in a common solvent and then evaporating the solvent under vacuum, a solid solution of the highly lipophilic b-carotene in PVP was produced. Mayersohn et al. [241] used this method to incorporate griseofulvin in PVP and the release rate of griseofulvin from the solid dispersion was 5 to 11 times higher than that of micronized drug. The molecular

weight of PVP is believed to be one of the most important factors affecting the dissolution rate of the dispersed drug from the solid dispersion. It has been stated that the aqueous solubility of the PVPs becomes poorer and viscosity becomes higher with increasing chain length molecular weight. [242] Hilton et al. [243] found that the dissolution rate of indomethacin decreased when molecular weight of PVP increased from 2500 to 1000000. They attributed the slower rate to the higher viscosity generated by PVP with higher molecular weight in the diffusion boundary layer adjacent to the dissolving surface of the dispersion. Other drugs such as for sulphathiazole and phenytoin were also found to have slower release rates when embedded in PVPs of higher molecular weight. [244, 245] While previous studies were concerned about fundamental applications of PVP in drug delivery, recent research is focused on developing more innovative and complicated hybrid systems. Risbud et al. [246] develop a pH-sensitive chitosan / poly(vinyl pyrrolidone) (PVP) based controlled drug release system. The hydrogels were synthesized by crosslinking chitosan and PVP blend with glutaraldehyde to form a semi-interpenetrating polymer network. Membranes after freeze-drying showed superior drug-release properties, releasing 73% of the amoxicillin in 3 h at pH 1.0. Shan et al. [247] constructed a novel polyvinylpyrrolidone-protected graphene/polyethylenimine-functionalized ionic liquid/glucose oxidase electrochemical biosensor, which achieved the direct electron transfer of glucose oxidase, maintained its bioactivity and showed potential application for the fabrication of novel glucose biosensors with linear glucose response up to 14 mM. Block copolymer matrices based on PVP are another popular research topic. Chun et al. [248] developed a new mucoadhesive drug carrier with poly(acrylic acid) (PAA)/PVP

interpolymer complexes. The adhesive forces of the PVP/PAA interpolymer complexes were found to be higher and the release rate of ketoprofen could be controlled by changing the mole ratios of PVP and PAA. Lele et al. [249] used free radical polymerization to prepare poly(N-vinyl-2-pyrrolidone)-block-poly(ε-caprolactone)-block-poly(N-vinyl-2-pyrrolidone) (PVP-b-PCL-b-PVP),amphiphilic triblock copolymers, which self-assembled in aqueous solution to form supramolecular aggregates of 30-200 nm size. The triblock copolymer micelles were loaded by a dialysis procedure with 1-4% (w/w) of two model poorly water-soluble drugs, i.e., doxorubicin and amphotericin B and found to be useful nanocarriers for the solubilization and transport of hydrophobic drugs. Other PVP-based copolymers, e.g. PVP-block-poly(D,L-lactide), PVP-block-poly (ethylene oxide) etc. have also been prepared. [250, 251]

PVP, due to its high polarity, has also been extensively used in stabilizing, controlling and constructing metal nanoparticles and nanowires. The use of PVP as a capping agent has proved to be a key role in preparation of shape-controlled nanoparticles. Xia et al. [252] first reported the synthesis of monodispersed silver nanocubes in large quantities by reducing silver nitrate with ethylene glycol in the presence of PVP. It is suggested that the selective interaction between PVP and various crystallographic planes of silver could greatly reduce the growth rate along the one facet direction and/or enhance the growth rate along the other direction, and therefore, by tuning the molar ratio between the repeating unit of PVP and $AgNO_3$, the morphology and dimensions of the product could be changed. Chou et al. [253] tested PVP of three different molecular weights (MW = 8000, 29,000, 55,000) to investigate

their ability to stabilize silver colloids obtained from chemical reduction by formaldehyde. The results indicated that their effects against agglomeration would depend to a great extent on the alkaline used for the promotion of reduction reaction at ambient temperature. When strong base e.g. NaOH was used, the reaction rate was very fast and only PVP with large molecular weight could produce silver colloids of sizes around 20 nm. While PVP with low molecular weight was strong enough to protect silver colloids against agglomeration when weak base was used. Teranishi et al. [254] obtained monodispersed Pd nanoparticles by a one-step reduction reaction of $[PdCl_4]^{2-}$ ions in alcohols with PVP as the protective polymer. The mean diameter of Pd nanoparticles could be controlled from 17 to 30 Å by changing the amount of PVP and the kind and/or the concentration of alcohol in the solvent. Detailed studies indicated that although increasing the amount of protective polymer made the size of Pd nanoparticles smaller, the particle size appeared to have a lower limit determined by the kind of alcohol. Narayanan et al. [255] used PVP-Pd nanoparticles to catalyze the Suzuki reaction between phenylboronic acid and iodobenzene. By investigating the effect of catalysis, recycling, and the different individual chemicals on the stability and catalytic activity of the nanoparticles during the reaction, they found that addition of excess PVP stabilizer to the reaction mixture could lead to the stability of the nanoparticle surface and size, perhaps due to the inhibition of the Ostwald ripening process while the catalytic efficiency of the nanoparticles decreased, possibly due to capping of the nanoparticle surface. Santos et al. [256] used PVP to complex and stabilize silver and gold nanoparticles formed through the reduction of Ag^+ or $AuCl^{4-}$ ions with N,N-dimethylformamide. The use of PVP with different polymer chain

lengths resulted in particles with similar sizes but a different degree of stability. In addition to metal complexes, PVP have also been to modify and stabilize other functional inorganic particles. Graf et al. [257] developed a general method to coat colloids with silica. PVP was used as adsorbent to various colloidal particles such as small gold and silver colloids, boehmite rods, gibbsite platelets, and charged polystyrene. The PVP-stabilized particles were then transferred to a solution of ammonia in ethanol and directly coated with smooth and homogeneous silica shells of variable thickness. The length of PVP was found to have strong influence on the stability of the colloids and the homogeneity and smoothness of the initial silica coating. Guo et al. [258] reported the preparation of highly monodisperse zinc oxide nanoparticles using PVP as the capping agents. Distinct excitonic features of the optical absorption, enhanced near-band-edge ultraviolet photoluminescence and significantly reduced defect-related green emission were observed due to the nearly perfect surface passivation of the PVP-modified ZnO nanocomposite. Other PVP-based hybrid materials include single-walled carbon nanotubes with enhanced aqueous stability, metal-organic frameworks with luminescence sensing etc. [259, 260]

1.3.4 Other Hybrid Materials

In addition to silica and PVP-based hybrid systems, some other hybrid materials worth mentioning are discussed in this section.

Gold, due to its superior inert character and its optical properties, is always on the focus of scientific research. Hybrid materials based on gold have been developed and applied in various areas such as catalysis, biology and nanotechnology etc. Robert et al.

[261] reported a highly selective, colorimetric polynucleotide detection method based on mercaptoalkyloligonucleotide-modified gold nanoparticle probes. Introduction of a single-stranded target oligonucleotide (30 bases) into a solution containing the appropriate probes resulted in the formation of a polymeric network of nanoparticles with a concomitant red-to-pinkish/purple color change. Hybridization was carried out by freezing and thawing of the solutions and ransfer of the hybridization mixture to a reverse-phase silica plate resulted in a blue color upon drying that could be detected visually. The unoptimized system can detect about 10 femtomoles of an oligonucleotide. Maxwell et al. [262] prepared colloidal gold nanocrystals for a new class of nanobiosensors capable of recognizing and detecting specific DNA sequences and single-base mutations in a homogeneous format. The hybrid material contained a core of 2.5-nm gold nanoparticles, which functioned as both a nano-scaffold and a nano-quencher. Oligonucleotide molecules labeled with a thiol group at one end and a fluorophore at the other were then attached to the core. Upon binding of target molecules, the biosensor exhibited a conformational change, which restored the fluorescence of the quenched fluorophore. In comparison with traditional organic quencher, these hybrid bio/inorganic nanoparticles had unique structural and optical properties for new applications in biosensing and molecular engineering. Yu et al. [263] prepared polyelectrolyte (PE)/gold nanoparticle hybrid films by infiltrating 4-(dimethylamino)pyridine-stabilized gold nanoparticles (DMAP−AuNP) into PE multilayers preassembled on indium tin oxide (ITO) electrodes. This composite film was used as an efficient electrochemical sensor, which showed high electrocatalytic activity to the oxidation of nitric oxide (NO) in the presence of gold. Grohn et al. [264]

used charged poly(amidoamine) (PAMAM) dendrimers to create gold colloids upon reduction of a gold salt precursor in aqueous solution. Characterization showed that dendrimers of generation 6−9 could template one gold colloid particle per dendrimer molecule, while for generation 10, multiple smaller gold particles per dendrimer were observed. Gibson et al. [265] covalently functionalized 2 nm gold nanoparticles with a chemotherapeutic drug, paclitaxel. The reaction was carried out under mild esterification conditions and yielded the product with a high molecular weight and low polydispersity index The content of the covalently attached organic shell was as nearly 67% by weight, which corresponded to 70 molecules of paclitaxel per nanoparticle thereby indicating a high grafting density. This approach provided a new alternative method to design innovative nanosized drug-delivery systems. Other gold-based hybrid materials include gold-functionalized carbon nanotubes, high ordered self-assembled gold nanorods etc. [266, 267.]

Magnetic hybrid nanocomposites, mainly based on Fe_3O_4 or γ-Fe_2O_3, are of specific interest in various fields of biology and medicine. These nanoparticles are usually constructed in a “core/shell” configuration in which biological species, such as cells, nucleic acids, and proteins, are bound to the magnetic “core” through organic linkers. Since these nanomaterials have unique properties such as well-controlled size, ability to be manipulated externally, and enhancement of contrast in magnetic resonance imaging (MRI), they have been applied in magnetic targeting of drugs, genes, and radiopharmaceuticals), diagnostics, immunoassays, RNA and DNA purification, gene cloning, and cell separation and purification, etc. [268] Dyal et al. [269] immobilized *Candida rugosa* lipase on γ-Fe_2O_3 magnetic nanoparticles by reacting the

enzyme amine group with a nanoparticle surface acetyl, or amine groups. A particle size of 20 ± 10 nm after deconvolution was characterized. Further investigation of the stability and enzymatic activity of the immobilized lipase showed that the covalently immobilized enzyme was stabile and reactive over 30 days. Liao et al. [270] prepared a novel magnetic nano-adsorbent by covalently binding polyacrylic acid (PAA) on Fe_3O_4 superparamagnetic nanoparticles (13.2 nm) via carbodiimide activation. The hybrid nanocomposite showed a high ionic exchange capacity of 1.64 meq g^{-1} and was applied for the recovery of lysozyme. Perez et al. [271] synthesized monodisperse magnetic nanoparticles by conjugation with virus-surface-specific antibodies in the presence of specific viral particles. The supramolecular structures showed enhanced magnetic properties and highly sensitive and selective detection of a virus in complex biological media. Detection of adenovirus-5 and herpes simplex virus-1 was done at concentrations of 5 viral particles/10 μL without the need of extensive sample preparation. Eugenii et al. [272] modified Fe_3O_4 with relay such as naphthoquinone, pyrroloquinoline quinone, microperoxidase etc. The hybrid material was used as magnetic switching of redox reactions and bioelectrocatalytic transformations by an external magnet upon the attraction of the magnetic particles to an electrode or their retraction from the electrode, respectively. Bioelectrocatalytic oxidation of glucose in the presence of glucose oxidase, reduction of nitrate (NO_3^-) in the presence of nitrate reductase and oxidation of lactate in the presence of lactate dehydrogenase were achieved respectively. Other design, synthesis and biological applications of magnetic nanohybrids have been discussed. [268, 273]

Although it has not attracted much research interest and is still in its very initial stage of development, fluoropolymer-based hybrid composites are promising materials that can find potential applications in protective coatings, fuel cell membranes, oil exploration etc. Qu et al. [274] used emulsion polymerization to prepare composite particles with core/shell structure with silica seed and hydrophobic fluoro-copolymer as corona. Morphology of the hybrid composites strongly depended on the amount of the silica seeds, concentration of reactive surfactant, as well as the addition of polymers. One advantage of this process was that there was only one silica bead for each composite particle. The stable core–shell structural hybrid latex was suggested to be useful for preparing high performance hydrophobic coating. Niepceron et al. [275] developed a novel route to obtain low-cost proton-exchange membranes. Silica particles were first grafted with poly(sodium 4-styrenesulfonate) by atom transfer radical polymerization. The *as-modified* particles were then loaded into an inert polymer matrix of poly(vinylidene fluoride-co-hexafluoropropylene) by solvent casting. Membranes with loadings ranging from 30 to 60 wt.% exhibited proton conductivities from 15 to 95 mS/cm at room temperature in water and composite membranes with a loading of 50 wt.% exhibited power densities above 1 W/cm^2 at 70 °C in single-cell fuel cell tests with non-hydrated gas feeds. Sung et al. [276] modified titanium oxide layers with an ultra thin (~30 nm) fluoropolymer Cytop® layer and utilized the composite film as a gate dielectric for achieving low voltage driven transistors and complementary inverters. High capacitance bi-layer dielectrics (k ~ 20) were measured. The fluoropolymer was helpful in reducing the leakage in the dielectric films and also enhanced the organic transistor performance. Bescher et al.

prepared a fluorinated copolymer/metal oxide hybrid by refluxing a high hydroxyl content fluorinated copolymer with tetraethoxysilane. The resulting organic-inorganic hybrids exhibited a continuous variation in hardness, hydrophobicity, and abrasion resistance, intermediary between the properties of the pure polymer and that of a silica gel. Nd^{3+}-doped fluoropolymers could be obtained if Nd(III) alkoxide was used. Recently, our group has developed hybrid nanoparticles with silica and iron oxide as cores and fluoropolymer as shell. These materials could be well dispersed in supercritical carbon dioxide and processed potential applications in enhanced oil recovery and carbon dioxide sequestration (see Chapter IV).

1.3.5 Methods for Preparation of Hybrid Materials

A variety of methods have been developed and applied to prepare hybrid materials with specific structural and property design. In this section, some of the most used preparation methods will be discussed.

Among all the methods applied in preparation of hybrid composites, sol-gel processes are probably the most popular and widely used method. The 'sol-gel' processes are a method of forming dispersed inorganic materials in solvents through the growth of metal-oxo polymers. [277] It usually involves water, solvents, metal precursors and sometimes catalysts. The first step in sol-gel synthesis is the hydroxylation of the metal alkoxide precursors by hydrolysis of the alkoxy groups. The as-generated reactive hydroxy groups then undergo polycondensation reactions *via* either oxolation mechanism through formation of an oxygen bridge or olation mechanism thought the formation of a hydroxo bridge. Rearrangements then occur for

the as-produced metal-oxo based oligomers and polymers and when these structures reach macroscopic size, a gel is obtained. This procedure going from colloidal 'sols' and to 'gels' can be well controlled by tailoring the reactivity of the metal alkoxide, the hydrolysis ratio, the solvent, the reaction temperature, the use of complexing agents or catalysts, etc. [277] Incorporation of organic components in 'sol-gel' processes can thus help to obtain hybrid materials in the form of thin films or solid powders with fine-tuned structures and properties. Sanchez et al. [278] prepared homogeneous nanoporous dye-sensitized TiO_2 films by the sol–gel methodology. Applications of the film in solid-state solar cells achieved a high solar-conversion efficiency associated with excellent stability under light and air exposure. The efficiency of the solar cells could be optimized by control of the architecture, porosity, and layer thickness of the hybrid film. Ferrer et al. [279] embedded highly fluorescent Nile Red (NR) nanoparticles in a glass by using sol−gel processes. Averaged dimensions of the nanoparticles were below 36 nm due to the confined crystallite growth within the porous hybrid matrix. The conformation adopted by single NR molecules and the aggregates could be controlled during the synthetic procedure. A significant increase of the fluorescence emission intensity was observed. Tajima et al. [280] incorporated a rhodamine B derivative in a silicate and charged oligo(p-phenylene vinylene) amphiphiles network. The hybrid film is better ordered compared to disordered polymer films. Optical property measurements showed enhanced emission from rhodamine B and also fluorescence quenching from OPV segments, indicating that the ordered and nanostructured environment resulted in highly efficient energy transfer among organic components in these hybrid films. The sol-gel method has also been widely used in

preparing periodic mesoporous hybrid materials. Ozin et al. [281] synthesized a periodic mesoporous organosilicate with bridge-bonded ethene groups directly integrated into the silica framework. A stable and periodic mesoporous ethene silica with high surface area and ethene groups were obtained after solvent extraction and ion-exchange of the surfactant templates. The sol-gel based method allowed incorporation of a variety of bridging organic and organometallic species in the silica network, raise the prospect to generate new materials with interesting chemical, mechanical electronic, optical and magnetic properties. Inagaki et al. [282] synthesized novel organic−inorganic silica-based hybrid mesoporous materials with organic and inorganic oxide moieties homogeneously distributed at the molecular level in the framework, forming a covalently bonded network. The highly ordered mesoporous structures showed two- and three-dimensional hexagonal symmetries and well-defined external morphologies. A uniform pore-size distribution with pore diameters of 31 and 27 Å, and high surface areas of 750 and 1170 m^2/g were measured. Ding et al. [283] incorporated titania and quinacridone molecules into the inner pore wall of mesoporous SBA-15 silica and the resulting hybrid material that still kept the original hexagonal structure of SBA-15 showed enhanced photocatalytic efficiency of decomposing indigo carmine than anatase TiO_2 and Ti-modified SBA-15 by using visible light irradiation. Kim et al. [284] developed a simple route to fabricate highly ordered organic–inorganic hybrid nanostructures, using polystyrene-block-poly(ethylene oxide) diblock copolymer (PS-b-PEO) thin films coupled with sol–gel chemistry. Hexagonally packed arrays of titania nanodomains were produced from solutions containing a titania precursor and PS-b-PEO, where the precursor was selectively incorporated into the PEO domain. A

highly dense array of hexagonally packed titania dots was obtained after the polymer template was removed by UV treatment. The size of the dots and the lattice spacing of the array could be fine-tuned by simply controlling the relative amount of sol–gel precursor to polymer component. Other hybrid materials prepared by sol-gel chemistry included hierarchically ordered networks of crystalline ZrO_2 tubes, Gallium nitride-functionalized rare earth organic/inorganic mesoporous nanocomposites etc. [285, 286]

Similar to the modification methods mentioned in section 1.2.5, these grafting approaches can also be used to covalently bind organic components to the inorganic particles to prepare hybrid materials. Ohno et al. [287] prepared monodisperse silica particles of diameter between 100 and 1500 nm were by surface modification of silica with poly(methyl methacrylate) using atom transfer radical polymerization (ATRP). Well-defined polymer of a target molecular weight up to 480K and a graft density as high as 0.65 chains/nm^2 was grafted. These hybrid particles were found to exceptionally well dispersed in organic solvents. Kong et al. [288] used *in situ* ATRP processes to construct a core−shell hybrid nanostructure with a hard backbone of multiwalled carbon nanotube and a soft shell of brushlike polystyrene. The molecular weight of PS was well controlled, as was the thickness of the shell layer. Further copolymerization of *tert*-butyl acrylate with the hybrid nanotubes was successful, illustrating the possibility to modify carbon nanotubes with block copolymer, which may have potential applications for the design, fabrication, and application of more functional carbon nanotube-related hybrid nanomaterials. Farmer *et al.* [289] grafted poly (methyl methacrylate) from CdS/SiO_2 nanoparticles, which were then cast into films. The as-prepared film retained the photoluminescence of the precursor CdS

nanoparticles and showed even dispersal of the CdS/SiO_2 cores throughout the polymer matrix. Structures and compositions of the hybrid nanoparticles could be altered to introduce new properties to the material i.e., the luminescence of the inorganic core or the conductivity of the polymer arms. Instead of using ATRP, Li *et al.* [290] applied reversible addition−fragmentation chain transfer polymerization (RAFT) to grow polystyrene and poly(n-butyl acrylate) from silica nanoparticles. The molecular weights of grafted polymers were found to increase linearly with conversions and well-defined block copolymers attached to silica nanoparticles were also prepared. Boyer et al. [291] synthesized a series of thermosensitive copoly(oligoethylene oxide) acrylates using RAFT polymerization. These copolymers were then grafted onto gold nanoparticle surfaces yielding thermosensitive hybrid nanoparticles. The thermoresponsive properties of these hybrid nanoparticles were evaluated in solution using dynamic light scattering and UV−vis spectroscopy. In addition, the susceptibility of these GNPs to protein fouling was found to be significantly reduced by the copolymer stabilizing layer. Kim et al. [292] developed a new class of hybrid nanoparticles with a small gold core (60 nm in diameter) and a biocompatible hydrogel polymer shell varying from 20 to 90 nm in thick. The hydrogel shell could be thermally activated by exposure to light via exploitation of the strong plasmon absorption of the gold nanoparticle core, the responses of which to external stimuli were completely consistent with the targeted drug-delivery objectives.

In addition to the methods mentioned above, other synthetic procedures such as layer-by layer methods, condensation, hydrothermal synthesis etc. have also been developed to prepare various functional hybrid materials. [187, 223, 293]

In conclusion, hybrid materials with both organic and inorganic components are an important category of materials of fundamental research interest and practical commercial applications. A variety of surface modification techniques have been explored, developed and applied to prepare hybrid materials with specific structural design and versatile chemical and physical functions. Detailed examples of synthesis, characterizations and applications of hybrid materials are exhibited and discussed in Chapter IV.

1.4 Applied Materials and Techniques for Microelectronic Processing and Devices

1.4.1 Background

In today's era of information technology, the industry of microelectronics is going through rapid development and progress. As the foundation of computer science, mobile technology, multimedia engineering, etc., microelectronics play an essential role in constructing a network and social society in which better life is anticipated. Generally defined as 'the design, manufacture and use of microchips and microcircuits', microelectronics are mainly focused on developing and producing smaller devices under micrometer scale as building blocks for larger electronic equipment. Transistors, capacitors, inductors, resistors, diodes and insulators and conductors can all be found in microelectronic devices, which are then engineered and integrated to microelectromechanical systems (MEMS) consisting integrated circuits and analog circuits etc. With the improvement of science and technology, the

dimensional scale of microelectronic components continues to decrease. In 1965, Gordon E. Moore, the co-funder of Intel Co., described 'Moore's law' as 'over the history of computing hardware, the number of transistors on integrated circuits doubles approximately every two years'. [294] The prediction appears to be true since the minimum feature sizes of transistor have decreased from 10 micrometers to the 28-22 nm range through the past half a century years. Continual downscaling from microelectronics to nanoeletronics has to a large extent increased the computing speed of microprocessors, the data storage of random-access memory (RAM) and the reading and writing speed of hard disks. Television displays with higher resolution, portable tablets with smaller size, smart phones with more functions etc. are all results of development of microelectronics.

Fabrication of microelectronics include several processing steps. Lithographic patterning plays a key role in determination of the design and feature size of microelectronics. Normally, a photosensitive material, called as photoresist, is coated on the substrate. By exposure to a radiation source under the cover of a photomask in which patterns are pre-designed, physical or chemical properties of the exposed areas of the photoresist will change. Post-exposure development such as baking and washing removes either the exposed part or the unexposed part, transferring the pattern from the mask to the photoresist. Depending on the radiation sources and photoresists used, several traditional techniques such as photolithography have been established and applied in microelectronic industry for a long time. New innovative lithographic patterning processes e.g. nanoimprint lithography, scanning probe lithography etc. have also been developed especially for fabrication of nanoelectronics.

Etching is another important step through which patterns are transferred from photoresists to the substrate beneath. There are two basic categories of etching processes, i.e. wet etching and dry etching. In wet etching, a substrate is soaked into a solution in which the etching rate of the target material is considerably higher than the mask material, thus selective removal and pattern transfer is achieved. For instance, buffered hydrofluoric acid is commonly used to etch silicon dioxide over a silicon substrate. Another etching process is dry etching, which is done in a dry completely dry environment with no solvent used. Plasma etching is probably the most popular dry etching method. Gas molecule ions produced by plasma will react with the surface of the substrate, etch away the mask materials due to the difference of the etching rates and transfer the pattern eventually. Other microelectronics processes include vapor deposition, post-etch cleaning etc.

Materials applied in microelectronics processing vary from metal oxide to polymer films. Silicon is the most used substrate for integrated circuits productions. Its unique properties such as easy to scale, cheap accessibility and stable electronic incorporation make silicon superior to other materials as the substrate for a wide variety of MEMS applications. Polymer films are usually used as photoresists. Easy processibility and versatile physical and chemical functionalities make polymer films excellent photoresists for patterning and etching. They can be used either as a positive tone resist or a negative tone resist. Ceramics such as the nitrides of silicon, aluminum and titanium have been increasingly applied in microelectronics fabrications. For instance, titanium nitride (TiN), due to its high electron conductivity and thermal stability, has been used as a diffusion barrier in aluminum and copper metallization and a low

resistive, metallic material for gate electrodes in complementary metal–oxide–semiconductor (CMOS) technology.

Here in this section, several key and innovative techniques applied in microelectronics will be discussed and reviewed with the materials used as well.

1.4.2 Photolithography

Photolithography, also termed as optical lithography or UV lithography, is up to now the most developed and industrialized lithographic technique for pattern fabrications. General process of photolithography is similar to what has been described above. Since its first application in 1955 in making patterns on printed circuit boards to produce much finer, more intricate designs on silicon wafers [295], photolithography has been playing a key role in improving and decreasing the feature size of microelectronics. Because the minimum feature size that a projection system can print is proportional to the wavelength of the light source, efforts have been made to apply ultraviolet light radiation with shorter wavelength. Historically, photolithography used Hg lamps in lithography to produce near ultraviolet (NUV) spectral lines at 436 nm, 405 nm and 365 nm from the early 1960s through the mid-1980s, while nowadays deep ultraviolet (DUV) light sources with 248-nm and 193-nm wavelength are widely used in fabrication and manufacturing production lines. The feature size has been reduced below 50 nm. Recently, extreme ultraviolet (EUV) technique with 13.5 nm wavelength has been developed and is expected to be the next generation of photolithography [296].

In addition to optical design and tool setup, materials such as photoresists that are able to work efficiently for pattern fabrications under different wavelengths is another important component for advanced photolithography. Photoresists, depending on their photosensitivity, can be divided into two classes: nonchemically amplified photoresists and chemically amplified photoresists. The former refers to resists that can go property changes upon exposure of light without chemical additives. The latter are resists that do not change properties by light radiation, but with additives such as photochemical acid generators, the resists do change properties during post-exposure development and therefore creating patterns. However, in spite of sensitivity, photoresists are more commonly divided as positive-tone and negative-tone, depending on their patterning mechanism in optical lithography patterning. Upon exposure, the properties of the exposed areas will change, differing from the unexposed areas. For positive-tone resists, patterns are made after the exposed areas are removed through post-exposure development processes, while for negative-tone resists, the unexposed areas are removed instead. The resist system which had been used exclusively in the NUV technology for many years was the diazonaphthoquinone (DNQ)/novolac resist. This type of photoresist originally developed for printing by Suss et al. [297] consists of a novolac resin and a photoactive compound (PAC), diazonaphthoquinone. The novolac resin is soluble in aqueous base in which DNQ is insoluble. Upon UV exposure, a photochemical reaction occurs when DNQ is transformed to a base-soluble indenecarboxylic acid. Therefore, the exposed areas of the resist film dissolve much faster than the unexposed regions in an aqueous base developer, resulting in positive-tone patterns. The DNQ/novolac resists failed when

technology shifted from NUV to DUV, pursuing higher resolution and smaller features. The novolac resin strongly absorbs in the 250 nm region and the DNQ exhibits a significant residual absorption in the DUV region, thus limiting penetration of the light to the surface of the resist film. Attempts at using one-component, nonchemically amplified resist systems such as polymethacrylate-based films were not successful due to the low sensitivities of these materials in DUV region. [298] In 1982, Ito et al. [299] first proposed the concept of chemical amplification by introducing photoacid generators (PAG) as additives in photoresist matrices. Exposure of a PAG to UV radiation will produce strong acid, which will further catalyze a series of chemical reactions during post-exposure baking (PEB) procedures, thus changing the dissolution properties of the exposed resists areas, and creating successful patterns. A variety of PAGs either with ionic or non-ionic chemical structures have been synthesized. Crivello et al. first developed diaryliodonium, triarylsulfonium, triarylelenonium, dialkylphenacylsulfonium, and dialkyl(4-hydroxyphenyl)-sulfonium salts as photoinitiators to carry out long-wavelength light-based cationic polymerization of epoxies and other monomers. These ionic triarylsulfonium salts are thermally stable, producing strong acids and are typically sensitive to deep UV, e-beam, and X-ray irradiation. They can also be used for NUV use by incorporating a chromophore in the structure or by adding a sensitizing molecule. [300-302] Diaryliodonium sulfonates such as di(tertbutylphenyl) iodonium perfluorobutanesulfonate (nonaflate) (DTBPIONf) and perfluorooctanesulfonate are heavily used in resist formulation. [298] Non-ionic PAGs such as β-ketosulfone and organohalides such as tetrabromobisphenol A and 4,6-bis(trichloromethyl)-1,3,5-

triazine were also synthesized and applied to DUV photolithography. [303, 304] Because of the health hazard associated with fluorinated sulfonates, a new class of ionic acid generators based on imides and methides chemical structures has been proposed by 3M. [305] As for photoresist matrices, different polymer systems have been developed for different chemical amplification mechanisms. Poly(4-tertbutoxycarbonyloxystyrene) (PBOCST), developed by IBM, is poly(4-hydroxystyrene) (PHOST) protected with an acid-labile tert-butoxycarbonyl (tBOC) group. [299] Hydrophobic PBOCST is converted to PHOST through reaction with a PAG upon PEB at about 100 °C for a few minutes. The polarity and solubility change can be used for dual tone patterning. Polar solvents such as alcohols and aqueous bases dissolve the polar PHOST in the exposed areas producing positive-tone patterns, while nonpolar solvents such as anisole only dissolves unexposed PBOCST areas, making negative-tone patterns. Poly(hydroxyphenyl methacrylate)s, poly(N-hydroxyphenyl methacrylamide)s and related copolymers modified with the tBOC groups have also been reported. [306] Poly(4-vinylbenzoate)s are typical materials for 193 nm photoresists systems. [307] The polyester is converted to polyacid by reaction with a PAG. This polarity change from a nonpolar to a polar state also allows dual tone patterning. Poly(meth)acrylates are another photoresist system working on a similar mechanism. [308] Poly[4-(1-phenoxyethoxy)styrene] is PHOST protected with acetal groups. The acetal polymer is converted to phenolic polymer through acid-catalyzed hydrolysis. [309] ESCAP is a copolymer photoresist developed by IBM. [310] The random copolymer is composed of 4-hydroxystyrene and tert-butyl acrylate (TBA), which is converted to a copolymer of the hydroxystyrene with acrylic acid through photochemically-induced

acid-catalyzed deprotection reactions. The conversion of the tert-butyl ester to carboxylic acid provides an extremely fast dissolution rate in the exposed regions and large developer selectivity. A terpolymer of tert-butyl methacrylate (TBMA), methyl methacrylate (MMA), and methacrylic acid (MAA) containing 1 wt% of di(tert-butylphenyl)iodonium trifluoromethanesulfonate (triflate) was explored as a photoresist for 193 nm exposures when developed with a dilute aqueous base solution. [311] Incorporation of adamantylmethyl methacrylate into the methacrylate terpolymer resist can improve dry etch resistance of this system. [312] Recent development of a family of phenolic molecular glasses with variable size and branch architecture has been reported as chemically amplified positive tone photoresists for EUV lithography. [313] Furthermore, inorganic particles with high etch resistance such as hafnium oxide and zirconium oxide have been prepared and applied as promising negative tone photoresists for DUV and EUV photolithography. [314] Although some of the new photoresist systems are still in the very first stages of development, efforts have been made to commercialize and industrialize these materials with the rapid growth and increasing desire for advanced photolithography.

1.4.3 $scCO_2$ Processing

Supercritical carbon dioxide ($scCO_2$), commonly treated as a 'greener' substitute solvent for hydrocarbons, has attracted more and more attention in the microelectronics industry. Compared to traditional processing media, $scCO_2$ has several advantages: i) a non-flammable and non-toxic solvent that is environmentally benign; ii) possessing both liquid and gas properties. The liquid properties help to facilitate mass dissolution and transportation, while the gas properties introduce no

surface tension and capillary force, which prevent collapse between patterns with high aspect ratios and small feature sizes; and iii) relatively low critical point (31^{o}C, 1040 psi.) compared to other supercritical fluids. The easy access and processibility makes $scCO_2$ an ideal candidate as a medium for microelectronics fabrication.

Emerging as a new and promising technique only decades ago, $scCO_2$ has already been explored for a variety of applications in microelectronics processing. [315] Wang et al. [316] first used $scCO_2$ to dry-clean chip resistors. Experimental results showed that $scCO_2$ exhibited a superior cleaning ability and is a promising alternative to the traditional deionized aqueous-based rinsing media. Moreover, a higher pressure and temperature were found to facilitate the dry cleaning process. Goldfarb et al. [317] first developed $scCO_2$ cleaning process to eliminate the capillary forces during normal drying of photoresist materials. Combined with n-hexane as a co-solvent, scCO2 successfully dried aqueous-based photoresist without pattern collapse due to the nearly zero surface tension forces. Non-distorted resist lines were observed with aspect ratios of at least 6.8. Ota et al. [318] used a novel supercritical CO_2-pulse cleaning process to remove contamination in high aspect ratio trenches and microholes of highly integrated semiconductor devices. Periodic pressure swing of supercritical fluid between subcritical and supercritical conditions was conducted for removing particles in microholes of fabricated model structures. The supercritical CO_2-pulse was efficient in removal of more than 50 nm fine particles from the deep microholes with no destruction of high aspect ratio model structures. Hoggan et al. [319] synthesized random copolymers of 1,1-dihydroperfluorooctylmethacrylate and 2-tetrahyrdopyranyl methacrylate, which are photoresist soluble in $scCO_2$. Along with specially designed

CO_2-soluble photoacid generators, these resists were spun cast, developed, and stripped all carried out in only liquid and $scCO_2$. Successful patterning using both 248 and 193-nm radiation provided the potential of this new photoresist platform for use as a sustainable technology for the microelectronics industry. Felix et al. [320] synthesized a series of calix[4] resorcinarene derivatives as ultra-high-resolution lithography resists in $scCO_2$. The compounds showed high glass-transition temperatures, excellent solubility in $scCO_2$, and patterning of space features as small as 70 nm. In addition to cleaning and photoresist developing, $scCO_2$ has been developed for other microelectronics applications. Vapor deposition of metal and metal oxide films in $scCO_2$ has been widely studied. Blackburn et al. [321] deposited high-purity palladium films onto Si wafers and polyimide by the reduction of organopalladium compounds in $scCO_2$. Continuous and reflective films of 100−200 nm thicknesses were obtained by hydrogenolysis of π-2-methylallyl(cyclopentadienyl) palladium(II) in $scCO_2$ at 60 °C for less than 2 min. Deposition of thin films on patterned silicon wafers yielded feature sizes as small as 0.1 μm wide by 1.0 μm deep. Cabanas et al. [322] deposited copper films onto planar and etched silicon substrates by the hydrogen-assisted reduction of a series of copper complexes in $scCO_2$. High purity films with exceptional step coverage in features as narrow as 100 nm with an aspect ratio of eight were obtained by reduction of Cu(I)(hfac)(2-butyne) at 225 °C and 200 bar. Zhao et al. [323] studied deposition of silver films in $scCO_2$ using H_2 and acetone as reducing agents for (1,5-cyclooctadiene) (hexafluoroacetylacetonato)silver(I). Continuous films were deposited on Ru substrates by acetone-assisted reduction of 0.006–0.03 mol% precursor in the temperature range of 150–250 °C. while H_2 reduction did not yield

continuous Ag films. A 50 nm-thick film with shiny surface was deposited in optimized conditions. Gougousi et al. [234] demonstrated a universal method for deposition of metal oxide thin films, including Al_2O_3, ZrO_2, MnO_x, and RuO_x in liquid and $scCO_2$. A cyclic deposition process is presented where reactants were introduced sequentially to control surface adsorption and byproduct removal steps. Reactions were done at pressures ranging from 1600 to 3600 psi at 80−200 °C The as-deposited Al_2O_3 films showed good dielectric properties after post-deposition anneal. In opposition to deposition, etching of metal and metal oxide has also been investigated in $scCO_2$. Bessel et al. [325] explored the possibility to etch copper in $scCO_2$ with proper additives. Using ethyl peroxydicarbonate as the oxidation agent and a β-diketone as the chelating agent, they successfully dissolved copper films in $scCO_2$ after 20 h reaction at 40 °C and 214 bar. Shan et al. [326] investigated etching of cuprous oxide films (Cu_2O) in $scCO_2$ using solutions of β-diketones. Reaction temperatures ranged between 80 and 150 °C and pressures between 20 and 27.5 MPa. The films and etched substrates were analyzed by X-ray photoelectron spectroscopy depth profiling, field emission scanning electron microscopy and spectroscopic ellipsometry. Each of the etching agents was effective. Using 2,2,7-trimethyl-3,5-octanedione as the chelating agent, an etch rate of 1.5 nm/min was measured at 150 °C. Etching rates of greater than 10.0 nm/min were expected to be obtained at 200 °C. Jones et al. [327] used hydrofluoric acid (HF) and HF/pyridine as co-solvents in $scCO_2$ for silicon dioxide film etching on single crystal silicon. Etching rates varied from 0.5 nm/min to 2 nm/min with different concentrations of HF and different processing time. Other $scCO_2$ processing in microelectronics fabrications includes making ordered porous

ultralow dielectric constant thin films, direct patterning of dielectrics, silylation of native oxide silicon surfaces etc. [315, 328]

1.4.4 Inkjet Printing

Borrowed from the idea of printing text and images onto paper or transparencies, a variety of scientific and industrial patterning applications based on inkjet printing techniques has been explored and developed. As a result of its precise control, mask-less and cost saving process, inkjet printing has been applied to 'direct write' materials for construction of organic electronics, nanotechnology and tissue engineering with complex patterns. [329] Although there are two commonly used modes for inkjet printing, i.e. continuous-mode and drop-on-demand (DOD) mode, the latter is widely applied in microelectronics fabrications due to its smaller drop size and higher placement accuracy. In a DOD mode, ink droplets are ejected from a reservoir through a nozzle by an acoustic pulse, which is generated either thermally or piezoelectrically. The size and shape of the ejected droplet depends strongly on the physical properties of the ink composition, i.e. the solute and the solvent materials. Fromm proposed a Z number to provide a dimensionless analysis of the mechanics of drop formation in DOD print, which is directly related to the viscosity, density and surface tension of the ink. [330]

As a versatile and practical technique, inkjet printing can be used to print different materials such as polymers and metals for different applications such as thin film transistors (TFT) and electronic wires. Sirringhaus et al. [331] demonstrated direct inkjet printing of complete transistor circuits, including via-hole interconnections based on solution-processed polymer conductors, insulators, and self-organizing

semiconductors. Channel length ranged from micrometer to sub-100 nm. High-resolution definition of practical channel lengths of 5 micrometers, high mobilities of 0.02 square centimeters per volt second and on-off current switching ratios of 10^5 were achieved by the use of substrate surface energy patterning to direct the flow of water-based conducting polymer (PEDOT/PSS) inkjet droplets. They further developed a more cost-effective method without any high-resolution lithography. [332] Self-aligned electrodes with sub-100 nm nanoscale gaps were prepared through hydrophobic treatment of the first printed set of PEDOT/PSS electrodes. Additive printing of organic semiconductor and gate electrode such as poly(9,9-dioctylfluorene-co-bithiophene) (F8T2) resulted in transistors with mobility values of 0.002 $cm^2\ V^{-1}\ s^{-1}$. Paul et al. [333] fabricated organic thin-film transistors by acoustic inkjet printing of solution-processable semiconductors consisting of either poly(9,9'-dioctyl-fluorene-co-bithiophene) or a regioregular poly(thiophene) onto patterned gold source-drain contacts. Channel length was controlled from 40 to 400 μm through digital lithography. The regioregular poly(thiophene) exhibited a mobility of 0.1 $cm^2\ V^{-1}\ s^{-1}$, on-off current ratios of ~10^6 and low threshold voltage. Lee et al. [334] prepared a water-based conducting ink, composed of silver colloids with diameter around 50 nm dispersed in a water and diethylene glycol cosolvent system. The 25 wt% silver ink had a viscosity of about 7.4 cP and surface tension of 33.5 dyn cm^{-1} at 20 ◦C, which was successfully inkjet printed onto ordinary glass substrates using an ordinary commercial Epson R210 printer. After sintering at 260 ◦C for 3min, these lines exhibited a resistivity of $1.6 \times 10^{-5}\ \Omega$ cm, which could serve as conducting lines for electronic applications. Lee et al. [335] synthesized copper nanoparticles through a facile chemical reduction of

copper sulfate with sodium hypophosphite in ethylene glycol within the presence of a polymer surfactant (PVP), which was included to prevent aggregation and give dispersion stability to the resulting colloidal nanoparticles. The size of the copper nanoparticles could be controlled between 30 and 65 nm, and the nanocopper inks were inkjet printed onto polyimide substrates to form metallic copper traces with low electrical resistivities (≥3.6 μΩ cm, or ≥2.2 times the resistivity of bulk copper). Redinger et al. [336] used an all ink-jet-deposited process to deposit gold nanocrystals, creating conductive lines with sheet resistance as low as 23 mΩ per square. Optimal printing conditions were found for polyimide dielectric layers and films as thin as 340 nm were produced, providing potential applications as spiral inductors, interconnect, and parallel plate capacitors.

In addition to TFT fabrication and metallic wire deposition, inkjet printing has been used in other various applications. Tekin et al. [337] used inkjet printing to prepare six alkoxy-substituted poly(*p*-phenylene ethynylene)-*alt*-poly(*p*-phenylenevinylene) (PPE–PPVs) films as potential organic light emitting diodes. The influence on the emission color of π-conjugated polymers by varying side chain, film thickness and thermal treatment were investigated. Characterizations of the optical properties of the printed films showed that the emission colors of the investigated polymers strongly depended on the inter-chain interactions which were increased with increasing film thickness and influenced by the side chains. Moreover, upon annealing at 70 °C, white emission was observed from the printed films. Hoth et al. [338] showed that inkjet printing technology could be used for the fabrication of high-efficiency organic photovoltaics. Selection of a blend of P3HT and PCBM in o-dichlorobenzene and

mesitylene, an ultrasmooth inkjet printed active layer with intimate morphology and interfaces was obtained. The as-fabricated solar cell showed device power-conversion-efficiency of 3%. Voit et al. [339] synthesized and stabilized iron oxide nanoparticles of 65–80nm with dextran or polystyrene coating in dipropylene glycol, which were subsequently inkjet printed onto glass, plastic, and paper substrates. Superconducting quantum interference device magnetometery measurements showed a coercivity of about15 Oe of the nanoparticles at room temperature, which could be applied as possible magnetic data storage media. Borberl et al. [340] inkjet printed a dispersion solution of HgTe in chlorobenzene (2 wt %) on glass as photodetector. demonstrated a highly sensitive photodetector. A detectivity of D = 3.9 x10^{10} cm $Hz^{1/2}$ W^{-1} at 1.4 mm wavelength was measured. The sensitivity increased linearly with the bias voltage, reaching 600 mA W^{-1} at 70V. Roth et al. [341] used high-throughput inkjet printing to control cellular attachment and proliferation by precise, automated deposition of collagen. Viable cellular patterns with a resolution of 350 μm were obtained, indicating potential applications of inkjet printing for tissue engineering and colony patterning.

1.4.5 Holographic Data Storage

As a practical application of holography, holographic data storage is an optical technology that can produce recordable disks with large capacity, short excess time and extremely fast transfer rates. [342] Holographic data storage system (HDSS) is one of the most promising candidates for next generation optical storage system. Fundamental working mechanism of HDSS is similar to holography. A light source, typically lasers of wavelength within visible region, generates a beam, which will be

split into a signal beam and a reference beam. The signal beam is impressed with data by a spatial light modulator or page composer, which then interfere with the reference beam on the storage material, i.e. the recording medium. Local electric field of the recording medium is changed in response to the light exposure and interference, resulting in the change of refractive index of the material due to the electro-optic effect. Data information is stored in the index gratings and can be read out by a reconstruction beam of which the optical properties are the same as those of the reference beam. Since index gratings occur throughout the volume of the recording medium, data storage capacity is superiorly increased.

The performance of HDSS depends largely on the quality and physical properties of the recording material. Lawrence et al. [343] proposed several criteria for an ideal holographic recording material: 1) a high resolution and a flat spatial frequency response to ensure the desired interference pattern to be completely stored; 2) a linear relationship between exposure and the amplitude of the reconstructed beam to ensure the fidelity of data recovery; 3) large dynamic range for a sufficient modulation with good signal to noise ratio to be formed during recording; 4) of high optical quality and lossless for high optical efficiencies; 5) environmentally stable for long storage time; 6) light sensitive enough to react to a low energy exposure. Hesselink et al. [344] listed typical material parameters for optimized holographic performances: thickness >0.5 mm; sensitivity > 500 cm/J; dynamic range > 5.0; shrinkage < 0.05% (for 500 μm; scatter < 10^{-5} $srad^{-1}$. Although until now, no single material meeting all the requirements has yet been developed, a variety of materials have been explored and applied as optimal recording medium, based on which HDSS can either be a read-

write reversible storage system or a write-once-read-many (WORM) system. The former is usually built upon photorefractive materials, which change refractive indices due to the change of the electron status, while the latter is usually composed of photopolymers, which change indices due to the polymerization reactions under light exposure.

Photorefractive materials are usually thick inorganic crystals. A typical photorefractive crystal is ion-doped lithium niobate ($LiNbO_3$) developed by Psaltis et al. [345] By varying the reference beam angle, hundreds of holograms can be superimposed in a single location of the crystal. Data is retrieved by a single reference beam. The advantages of using such materials are that access times are very short, less than 100 μs, and extreme fast data retrieving rates, > 10 Gb/s, storage capacity is around tens of gigabytes and they are rewritable. However, light sensitivity of these crystals is relatively low since one photon can only lead to one photorefractive event, i.e. a local refractive index change. Moreover, a fixing process is required for permanent storage and multiple reads. [344] Other photorefractive crystals include Cu-doped $LiNbO_3$, $KTa_xNb_{1-x}O_3$ and $LiTaO_3$ have also been prepared and applied. [346-348] Another important category of photorefractive recording media is organic photorefractives. Unlike photoactive crystals with only one component, this kind of materials usually contains several key components. A sensitizer is included to increase photogeneration efficiency; a photoductor for transport of photogenerated electrons; a chromophore to provide refractive index change and a plasticizer to lower the T_g for enhanced orientation. [349] Typical materials for organic photorefractive systems are polymer composites, amorphous glasses, polymer-dispersed liquid crystals and hybrid

composites etc. Wright et al. [350] prepared a nonlinear optical chromophore containing a 2-dicyanomethylen- 3-cyano-2,5-dihydrofuran acceptor groups, which was then doped into a plasticized composite of poly(*n*-vinylcarbazole). Large gain coefficients, high photorefractive speed and low sample absorption were observed. Bai et al. [351] investigated photorefractive composites composed of poly(N-vinyl carbazole) (PVK)/liquid crystal/C_{60} with PVK of different molecular weight (MW). The influence of MW on the photorefractivity showed that a higher MW resulted in a larger two-beam coupling coefficient and a larger effective electric–optical coefficient. Ostroverkhova et al. [352] prepared monolithic photorefractive glasses based on new nonlinear optical chromophores containing a 2-dicyanomethylene-3-cyano-2,5-dihydrofuran (DCDHF) acceptor group. Large net gain coefficients are observed in both red and infrared wavelength regions. Winiarz et al. [353] reported a photorefractive medium consisting of a hole-transporting polymer composite matrix (PMMA), electro-optically active liquid crystals (TL202), and cadmium sulfide quantum dots as photosensitizers. The material exhibited greater than 90% internal diffraction efficiency and a net two-beam coupling gain of 22.5 cm^{-1} with a response time of <1 min. Schmidt et al. [354] synthesized a block copolymer with block copolymer consisting of 77.5 wt% polystyrene and a random distribution of 8.4 wt% azobenzene side chains, 12.3 wt% three-ring mesogenic side chains, and 1.8 wt% hydroxyethyl methacrylate. This material was found to be a suitable recording medium for rewritable HDSS with a thickness in the millimeter range. More than 1000 erase–rewrite cycles without a measurable change in the material were obtained. Wang et al. [355] doped a low-*Tg* photorefractive polymer composite, poly(*N*-vinylcarbazole):2,4,7-trinitro-9-

fluorenone:4-(dicyanovinyl-*N*,*N*-diethylaniline) with Au nanoparticles, which exhibited an effective enhancement on the photorefractivity. At an applied electric field of 118 V/μm, two-beam coupling coefficient as high as 206 cm^{-1} was obtained in the sample doped with Au particles, while only 152 cm^{-1} in the sample without Au particles. It was suggested that the enhancement on the photorefractivity was due to the increment of the density of the effective trap center by doping Au particles. However, organic photorefractive materials also suffer the same disadvantages as inorganic photorefractive crystals in terms of sensitivity and long term stability.

Photopolymer is the other material system used as HDSS recording media. It usually contains monomers, photoinitiators and chemically inactive binders. Photopolymerization occurs upon light exposure, resulting in monomer gradients between regions of high intensity and low intensity. Monomers then diffuse from unexposed areas to exposed areas, while binders move the opposite way. The molar refractive change, monomer density change and partial segregation of monomer and binder thus lead to the establishment of index grating in the material. [344] Photopolymers were first used as a holographic recording material by Close in 1969. [356] Using a mixture of monomer and photocatalyst, the system was successfully applied to record hologram with good resolution and diffraction efficiencies of up to 45%. Sugawara [357] et al. developed a system consisting of an acrylamide monomer, a N,N methylene bisacrylamide crosslinker, a methylene blue sensitizer and a photoinitiator. Diffraction efficiencies of 65% with exposure energies of 50 mJ/cm^2 and resolution of 550 lines/mm were achieved. Zhao et al. [358] proposed a new hybrid material containing acrylamide and acrylic acid as monomers, methylene blue as the

dye, material triethanolamine (TEA) and p-toluenesulfonic acid as sensitizers and gelatin as a binder. The maximum diffraction efficiency was greater than 80% with exposure energy of only 2 mJ/cm^2. Resolution was of 4000 lines/mm. Since one photon event can trigger 100 ~ 1000 polymerization events, sensitivity of photopolymer systems are much higher than that of photorefractive systems, at least one to two orders. [344] However, due to relatively small layer thickness, this thin system is not able to superimpose hundreds of holograms and therefore has to be applied in a shifting multiplexing mode. Shrinkage and scatter limits are some other disadvantage of photopolymer based recording media, which might be improved by proper choice of material chemistry, such as incorporation of inorganic nanoparticles in photopolymer films etc. [359, 360]

In this section, various materials and techniques for microelectronic processing and applications were discussed. Detailed studies and researches are investigated in Chapter V.

1.5 Conclusion

Surface modification has been applied and used in almost every aspect of our life. Extensive research and technologies have been explored and developed for successful modification of various surfaces with all kinds of materials. In this chapter, several important applications of surface modification were discussed, including antifouling coating materials for sea boating and water purifications, hybrid composites with both organic and inorganic components and microelectronics processes such as surface patterning and cleaning etc. Materials

such as polymer brushes, inorganic nanoparticles and metal deposition films were explored. Methods such as surface-initiating control living polymerization, sol-gel precipitation and a variety processing techniques were explained. Specific research focused on each application will be investigated and discussed in details in the next several chapters.

The following two chapters (Chapter II and III) focus on modification of polymer surfaces with antifouling polymer brushes. In Chapter II, a layer-by-layer mediated method is adopted to grow fouling resistant polymer brushes containing, for example, poly(ethylene glycol) through either a 'grafted to' or a 'grafted from' approach. Concepts are borrowed from a larger program in biofouling resistance at Cornell. Membrane performance tests show that the antifouling properties of the membrane are improved with no loss of water flux or change of salt rejection ratio. In Chapter III, monomers with functional groups are first synthesized and then used to fabricate homemade polymeric membranes. Polymer brushes are then grafted from the surface and functionalized with different side chains such as perfluorinated chains to fine-tune the antifouling properties of the membranes with either fouling-resistant or fouling-release surfaces.

Chapter IV describes the preparation of supercritical carbon dioxide ($scCO_2$) dispersible nanoparticles as prospective tracers for subsurface mapping technologies. A particle core, i.e. silicon dioxide or iron oxide, is modified with a fluoropolymer corona through a surface initiated atom transfer radical polymerization (ATRP) reaction. The as-prepared nanoparticle has a diameter of 40 nanometers with good

solubility in $scCO_2$. Incorporation of a small amount of fluorescent label improves the detectability of the particle at low concentrations. Experimental results of the diffusion measurements of the nanoparticles match well with predictive curves, indicating the nanoparticles can be used as tracers in a dual-trace system used for further field mapping technologies.

Chapter V explores the application of $scCO_2$ in microelectronics processing. The first part of the chapter describes the synthesis of a quaternary ammonium salt as an additive in $scCO_2$ cleaning processes. Together with co-solvents, the organic residue remaining on the silicon substrate after etching processes can be removed in $scCO_2$ under relatively low pressure and temperature. The second part of the chapter investigates the possibility of titanium nitride (TiN) etching in $scCO_2$. Strong organic acids and oxidants are mixed in alcohols, which serve not only as solvents but also as stabilizers. Wet etching of TiN in alcohols was successfully achieved with an etching rate of more than 1 nanometer/minute. Drying etching of TiN in $scCO_2$, although not as efficient as wet etching, results in promising etching processes, which can be further, optimized and applied.

The appendix discusses the characterization of poly(vinyl pyrrolidone)-coated copper (PVP-Cu) nanoparticles for inkjet printing. Different batches of commercial PVP-Cu particle samples are characterized with a variety of characterization methods including X-ray photoelectron spectroscopy, thermogravimetric analysis, etc. The intermolecular and intramolecular interactions of the particles and their impact on the particle behavior are clarified.

REFERENCES

(1) Black C. T. *ACS Nano* **2007**, *1*, 147.

(2) Kenawy, E.-R.; Worley, S. D.; Broughton, R. *Biomacromolecules* **2007**, *8*, 1359.

(3) Patel, M. B.; Patel, S. A.; Ray, A.; Patel, R. M. *J. Appl. Polym. Sci*. **2003**, *89*, 895.

(4) Park, E.-S.; Lee, H.-J.; Park, H.-Y.; Kim, M.-N.; Chung, K.-H.; Yoon, J.-S. *J. Appl. Polym. Sci.* **2001**, *80*, 728.

(5) Bowersock, T. L.; Woodyard, L.; Hamilton A. J.; Deford, J. A. *J. Controlled Release* **1994**, *31*, 237-243.

(6) Amiji, M.; Park, K. *J. Biomater. Sci. Polym. Ed.* **1993**, *4*, 217.

(7) Yebra, D. M.; Kiil, S.; Dam-Johansen, K. *Prog. Org. Coat.* **2004**, *50*, 75.

(8) Champ, M. A. *Sci. Total Environ.* **2000**, *258*, 21.

(9) Abbott, A.; Abel, P. D.; Milne, A. A. *Sci. Total Environ.* **2000**, *258*, 5.

(10) Reise, K. Gollasch, S. Wolff, W. J. *Helgolander Meeresunters* **1999**, *52*, 219.

(11) Subramani, A.; Hoek, E. M. V. *J. Membrane Sci.* **2008**, *319*, 111.

(12) Hoek, E. M. V.; Allred, J.; Knoell, T.; Jeong, B.-H. *J. Membrane Sci.* **2008**, *314*, 33.

(13) Rana, D.; Matsuura T. *Chem. Rev.* **2010**, *110*, 2448.

(14) Ulbricht, M. *Polymer* **2006**, *47*, 2217.

(15) Pontie, M.; Rapenne, S.; Thekkedath, A.; Duchesne, J.; Jacquemet, V.; Leparc, J.; Suty, H. *Desalination* **2005**, *181*, 75.

(16) Anderson, C. D.; Hunter, J. E. NAV2000 Conference Proceedings, Venice, September 2000.

(17) Koehler, J. A.; Ulbricht, M.; Belfort, G. *Langmuir* **1997**, *13*, 4162.

(18) Koehler, J. A.; Ulbricht, M.; Belfort, G. *Langmuir* **2000**, *16*, 10419.

(19) Susanto, H.; Ulbricht, M. *J. Membrane Sci.* **2005**, *266*, 132.

(20) Callows, M. E.; Fletcher, R. L. *Int. Biodeter. Biodegr.* **1994**, *34*, 333.

(21) Abarzua, S.; Jakubowsky, S. *Mar. Ecol. Prog. Ser.* **1995**, *123*, 301.

(22) Clare, M. E.; Rittschof, D.; Gerhart, D. J.; Maki, J. S. *Invertebr. Reprod. Dev.* **1992**, *22*, 67.

(23) Flemming, H. C.; Grebe, T.; Schaule, G. *Water Sci. Technol.* **1996**, *34*, 517.

(24) Davies, A. NERC News 1995.

(25) Nabe, A.; Staude, E.; Belfort, G. *J. Membrane Sci.* **1997**, *133*, 57.

(26) Guiver, M. D.; Black, P.; Tam, C. M.; Deslandes, Y. *J. Appl. Polym. Sci* **1993**, *48*, 1597.

(27) Freger, V.; Gilron, J.; Belfer, S. *J. Membrane Sci.* **2002**, *209*, 283.

(28) Ulbricht, M.; Belfort, G. *J. Membrane Sci.* **1996**, *111*, 193.

(29) Ulbricht, M.; Richau, K.; Kamusewitz, H. *Colloids Surf., A* **1998**, *138*, 353.

(30) Kato, K.; Sanao, S.; Ikada, Y. *Colloids Surf., B* **1995**, *4*, 221.

(31) Zhang, Z.; Chen, S. F.; Jiang, S. Y. *Biomacromolecules* **2006**, *7*, 3315.

(32) Yang, W.; Chen, S. F.; Cheng, G.; Vaisocherova, H.; Xue, H.; Li, W.; Zhang, J. L.; Jiang, S. Y. *Langmuir* **2008**, *24*, 9211.

(33) Cho, W. K.; Kong, B. Y.; Choi, I. S. *Langmuir* **2007**, *23*, 5678.

(34) Elimelech, M.; Zhu, X.; Childress, A. E.; Hong, S. *J. Membrane Sci.* **1997**, *127*, 101.

(35) Hirose, M.; Ito, H.; Kamiyama, Y. *J. Membrane Sci.* **1996**, *121*, 209.

(36) Reidl, K.; Girard, B.; Lencki, R. W. *J. Membrane Sci.* **1998**, *139*, 155.

(37) Li, Y. S.; Yan, L.; Xiang, C. B.; Hong, L. J. *Desalination* **2006**, *196*, 76.

(38) Tsukagoshi, T.; Kondo, Y.; Yoshino, N. *Colloids Surf., B* **2007**, *54*, 94.

(39) Chandler, K. A. Marine and Offshore Corrosion. Butterworths, London, 1985.

(40) Capurro, L. R. A. Griffith, D. E. Oneanography for Practising Engineers, Barnes & Noble, Inc., New York, 1970.

(41) Kenawy, E.-R.; Abdel-Hay, F. I,; El-Shanshoury, A. E.-R.; El-Hewehy, M. H. *J. Polym. Sci., Part A: Polym. Chem.* **2002**, *40*, 2384.

(42) Ikeda, T.; Yamaguchi, H.; Tazuke, S. *Antimicrob. Agents Chemother.* **1984**, *26*, 139.

(43) Worley, S. D.; Sun, G. *Trends Polym. Sci.* **1996**, *4*, 364.

(44) Acharya, V.; Prabha, C. R.; Narayanamurthy, C. *Biomaterials* **2004**, *25*, 4555.

(45) Jiang, H.; Manolache, S.; Lee Wong, A. C.; Denes, F. S. *J. Appl. Polym. Sci.* **2004**, *93*, 1411.

(46) Baveja, J. K.; Li, G.; Nordon, R. E.; Hume, E. B. H.; Kumar, N.; Wilcox, M. D. P.; Poole-Warren, L. A. *Biomaterials* **2004**, *25*, 5013.

(47) Thamizharasi, S.; Vasantha, J.; Reddy, B. S. R. *Eur. Polym. J.* **2002**, *38*, 551.

(48) Kanazawa, A.; Ikeda, T.; Endo, T. *J. Polym. Sci., Part A: Polym. Chem.* **1993**, *31*, 2873.

(49) Patel, M. B.; Patel, S. A.; Ray, A.; Patel, R. M. *J. Appl. Polym. Sci*. **2003**, *89*, 895.

(50) Kanazawa, A.; Ikeda, T.; Endo, T. *J. Polym. Sci., Part A: Polym. Chem.* **1993**, *31*, 1441.

(51) Ikeda, T.; Tazuke, S. *Polym. Prepr. (Am. Chem. Soc., Div. Polym. Chem.)* **1985**, *26*, 226.

(52) Chen, C. Z.; Beck-Tan, N. C.; Dhurjati, P.; Van Dyk, T. K.; LaRossa, R. A; Cooper, S. L. *Biomacromolecules* **2000**, *1*, 473.

(53) Panarin, E. F.; Solovaskii, M. V.; Zaikina, N. A.; Afinogenov, G. E. *Makromol. Chem. Suppl.* **1985**, *9*, 25.

(54) Ikeda, T.; Hirayama, H.; Suzuki, K.; Yamaguchi, H.; Tazuke, S. *Makromol. Chem.* **1986**, *187*, 333.

(55) Sawada, H.; Umedo, M.; Kawase, T.; Tomita, T.; Baba, M. *Eur. Polym. J.* **1999**, *35*, 1611.

(56) Nonaka, T.; Hua, L.; Ogata, T.; Kurihara, S. *J. Appl. Polym. Sci.* **2003**, *87*, 386.

(57) Buchenska, J. *J. Appl. Polym. Sci.* **1996**, *61*, 567.

(58) Nonaka, T.; Noda, E.; Kurihara, S. *J. Appl. Polym. Sci.* **2000**, *77*, 1077.

(59) Tan, S.; Li, G.; Shen, J.; Liu, Y.; Zong, M. *J. Appl. Polym. Sci.* **2000**, *77*, 1869.

(60) Daly, W. H.; Guerrini, M. M.; Culberson, D.; Macossay, J. In *Science and Technology of Polymers and Ad*V*anced Materials*; Prasad, P. N., James, E., Kandil, S., Kafafi, Z., Eds.; Plenum Press: New York, 998; p 493.

(61) Panacek, A,; Kvitek, L.; Prucek, R.; Kolar, M.; Vecerova, R.; Pizurova, N.; Sharma, V. K.; Nevecna, T.; Zboril, R. *J. Phys. Chem. B* **2006,** *110,* 16248.

(62) Lok, C.-N.; Ho, C.-M.; Chen, R.; He, Q.-Y.; Yu, W.-Y.; Sun, H.; Tam, P. K.-H.; Chiu, J.-F.; Che, C.-M. *J. Biol. Inorg. Chem.* **2007**, *12*, 527.

(63) Chopra, I. J. *Antimicrob. Chemother.* **2007**, *59*, 587.

(64) Morones, J. R.; Elechiguerra, J. L.; Camacho, A.; Holt, K.; Kouri, J. B.; Ramírez, J. T.; Yacaman, M. J. *Nanotechnology* **2005**, *16*, 2346.

(65) Samberg, M. E.; Orndorff, P. E.; Monteiro-Riviere, N. A. *Nanotoxicology* **2011**, *5*, 244.

(66) Lok, C.-N.; Ho, C.-M.; Chen, R.; He, Q.-Y.; Yu, W.-Y.; Sun, H.; Tam, P. K.-H.; Chiu, J.-F.; Che, C.-M. *J. Proteome Res.* **2006**, *5*, 916.

(67) Sadhasivam, S.; Shanmugam, P.; Yun, K. *Colloids Surf., B* **2010**, *81*, 358.

(68) Sun, R. W.-Y.; Chen, R.; Chung, N. P.-Y.; Ho, C.-M.; Lin, C.-L. S.; Che, C.-M. *Chem. Commun.* **2005**, *40*, 5059.

(69) Lara, H. H.; Ayala-Nunnez, N. V.; Ixtepan-Turrent, L.; Rodriguez-Padilla, C. *J. Nanobiotechnol.* **2010**, *8*, 1.

(70) Baker, C.; Pradhan, A.; Pakstis, L.; Pochan, D. J.; Shah, S. I. *J. Nanosci. Nanotechnol.* **2005**, *5,* 244.

(71) Thakkar, K. N.; Mhatre, S. S.; Parikh, R. Y. *Nanomedicine* **2010**, *6*, 257.

(72) Li, W.-R.; Xie, X.-B.; Shi, Q.-S.; Duan, S.-S.; Ouyang, Y.-S.; Chen, Y.-B. *BioMetals* **2011**, *24*, 135.

(73) Kim, J. S.; Kuk, E.; Yu, K. N.; Kim, J.-H.; Park, S. J.; Lee, H. J.; Kim, S. H.; Park, Y. K.; Park, Y. H.; Hwang, C.-Y.; Kim, Y.-K.; Lee, Y.- S.; Jeong, D. H.; Cho, M.-H. *Nanomedicine* **2007**, *3*, 95.

(74) Marambio-Jones, C.; Hoek, E. M. V. *J. Nanopart. Res.* **2010**, *12*, 1531.

(75) Feng, Q. L.; Wu, J.; Chen, G. Q.; Cui, G. Q.; Kim, T. N.; Kim, J. O. *J. Biomed. Mater. Res.* **2000**, *52*, 662.

(76) Jung, W. K.; Koo, H. C.; Kim, K. W.; Shin, S.; Kim, S. H.; Park, Y. H. *Appl. Environ. Microbiol.* **2008**, *74*, 2171.

(77) Holt, K. B.; Bard, A. J. *Biochemistry* **2005**, *44*, 13214.

(78) Arakawa, H.; Neault, J. F.; Tajmir-Riahi, H. A. *Biophys. J.* **2001**, *81*, 1580.

(79) Li, W.-R.; Xie, X.-B.; Shi, Q.-S.; Zeng, H.-Y.; Ouyang, Y.-S.; Chen, Y.-B. *Appl. Microbiol. Biotechnol.* **2010**, *85*, 1115.

(80) AshaRani, P. V.; Low Kah Mun, G.; Hande, M. P.; Valiyaveettil, S. *ACS Nano* **2009**, *3*, 279.

(81) Eckhardt, S.; Brunetto, P. S.; Gagnon, J.; Priebe, M.; Giese, B.; Fromm, K. M. *Chem. Rev.* Web Publication Date: March 15, 2013. **DOI:** 10.1021/cr300288v.

(82) Binder, B. M. *Plant Sci.* **2008**, *175*, 8.

(83) Kim, J. Y.; Lee, C.; Cho, M.; Yoon, *J. Water Res.* **2008**, *42*, 356.

(84) Xu, F. F.; Imlay, J. A. *Appl. Environ. Microbiol.* **2012**, *78*, 3614.

(85) Park, H.-J.; Kim, J. Y.; Kim, J.; Lee, J.-H.; Hahn, J.-S.; Gu, M. B.; Yoon, *J. Water Res.* **2009**, *43*, 1027.

(86) Cabiscol, E.; Tamarit, J.; Ros, J. *Int. Microbiol.* **2000**, *3,* 3.

(87) Gordon, O.; Vig Slenters, T.; Brunetto, P. S.; Villaruz, A. E.; Sturdevant, D. E.; Otto, M.; Landmann, R.; Fromm, K. M. *Antimicrob. Agents Chemother.* **2010**, *54*, 4208.

(88) Inoue, Y.; Hoshino, M.; Takahashi, H.; Noguchi, T.; Murata, T.; Kanzaki, Y.; Hamashima, H.; Sasatsu, M. *J. Inorg. Biochem.* **2002**, *92*, 37.

(89) Gitlitz, M. H. *J. Coat. Technol.* **1981**, *53*, 46.

(90) Omae, I. *Appl. Organometall. Chem.* **2003**, *17*, 81.

(91) Ghiya, S. N. *Paintindia* **1987**, 19.

(92) Milne, A.; Hails, G. Patent GB 1 457 590, **1977**.

(93) Anderson, C. D. CDA, UK, Cda.swsconf, **1995**, pp. 1–12.

(94) Kiil, S.; Weinell, C. E.; Pedersen, M. S.; Dam-Johansen, K.; Codolar, A. S. *J. Coat. Technol.* **2002**, *74*, 45.

(95) Kiil, S.; Weinell, C. E.; Pedersen, M. S.; Dam-Johansen, K. *Ind. Eng. Chem. Res.* **2001**, *40*, 3906.

(96) Kiil, S.; Weinell, C. E.; Pedersen, M. S.; Dam-Johansen, K. *Ind. Eng. Chem. Res.* **2002**, *80*, 45.

(97) Swain, G. Proceedings of the International Symposium on Sea water Drag Reduction, The Naval Undersea Warfare Center, Newport, **1998**, pp. 155–161.

(98) Evans, S. M.; Leksono, T.; McKinnel, P. D. *Mar. Pollut. Bull.* **1995**, *30*, 14.

(99) Champ, M. A. *Sci. Total Environ.* **2000**, *258*, 21.

(100) Champ, M. A. Published in the Proceedings of the 24th UJNR (US/Japan) Marine Facilities Panel Meeting in Hawaii, November 7–8, **2001**.

(101) Hunter, J. E.; Cain, P. IMAS'96, Paper 16, **1996**.

(102) Shilton, C.; *Paints Varnishes* **1997**, *9*, 10.

(103) Anderson, C. D.; Hunter, J. E. NAV2000 Conference Proceedings, Venice, September **2000**.

(104) Anderson, C.D. IBC UK, IBC UK Conferences Limited, United Kingdom, **1998**, pp. 1–12.

(105) Anon. Paint Ink Int. **1999**.

(106) Yonehara, Y.; Yamashita, H.; Kawamura, C.; Itoh, K. *Prog. Org. Coat.* **2001**, *42*, 150.

(107) Voulvoulis, N.; Scrimshaw, M. D.; Lester, J. N. *Appl. Organometall. Chem.* **1999**, *13*, 135.

(108) Evans, S. M.; Birhenough, A. C.; Brancato, M. S. *Mar. Pollut. Bull.* **2000**, *40*, 204.

(109) Lee, J. H.; Kopecek, J.; Andrade, J. D. *J. Biomed. Mater. Res.* **1989**, *23*, 351.

(110) Prime, K.; Whitesides, G. *Science* **1991**, *252*, 1164.

(111) Park, H. D.; Kim, Y. S.; Han, D. K.; Kim, Y. H.; Lee, E. H. B.; Suh, H.; Choi, K. S. *Biomaterials* **1998**, *19*, 851.

(112) Kingshott, P.; Wei, J.; Bagge-Ravn, D.; Gadegaard, N.; Gram, L. *Langmuir* **2003**, 19, 6912.

(113) Banerjee, I.; Pangule, R. C.; Kane, R. S. *Adv. Mater.* **2011**, *23*, 690.

(114) Jeon, S. I.; Lee, J. H.; Andrade, J. D.; Degennes, P. G. *J. Colloid Interface Sci.* **1991**, *142*, 149.

(115) Jeon, S. I.; Andrade, J. D. *J. Colloid Interface Sci.* **1991**, *142*, 159.

(116) Szleifer, I. *Biophys. J.* **1997**, *72*, 595.

(117) Wang, R. L. C.; Kreuzer, H. J.; Grunze, M. *J. Phys. Chem. B* **1997**, *101*, 9767.

(118) Wang, R. L. C.; Kreuzer, H. J.; Grunze, M. *Phys. Chem. Chem. Phys.* **2000**, *2*, 3613.

(119) Efremova, N. V.; Sheth, S. R.; Leckband, D. E. *Langmuir* **2001,** *17,* 7628.

(120) Saglea, A. C.; VanWagnera, E. M.; Jua, H.; McCloskeya, B. D.; Freemana, B. D.; Sharmab, M. M. *J. Membrane. Sci.* **2009**, *340*, 92.

(121) Shi, Q.; Su, Y. L.; Zhu, S. P.; Li, C.; Zhao, Y. Y.; Jiang, Z. Y. *J. Membrane. Sci.* **2007**, *303*, 204.

(122) Gudipati, C. S.; Finlay, J. A.; Callow, J. A.; Callow, M. E.; Wooley, K. L. *Langmuir* **2005,** *21,* 3044.

(123) Emmenegger, C. R.; Brynda, E.; Reidel, T.; Sedlakova, Z.; Houska, M.; Alles, A. B. *Langmuir* **2009,** *25,* 6328.

(124) Yuan, J.; Zhang, J.; Zang, X.; Shen, J.; Lin, S. *Colloids Surf. B* **2003**, *30*, 147.

(125) Zhang, Z.; Chao, T.; Chen, S.; Jiang, S. *Langmuir* **2006,** *22,* 10072.

(126) Chang, Y.; Liao, S.-C.; Higuchi, A.; Ruaan R.-C.; Chu, C.-W.; Chen, W.-Y. *Langmuir*, **2008**, *24*, 5453.

(127) Chiang, Y. C.; Chang, Y.; Higuchi, A.; Chen, W.-Y.; Ruaan R.-C. *J. Membrane. Sci.* **2009**, *339*, 151.

(128) Zheng, J.; He, Y.; Chen, S.; Li, L.; Bernards, M. T.; Jiang, S. *J. Chem. Phys.* **2006**, *125*, 174714.

(129) He, Y.; Hower, J.; Chen, S.; Bernards, M. T.; Chang, Y.; Jiang, S. *Langmuir* **2008**, *24*, 10358.

(130) Chen, S.; Zheng, J.; Li, L.; Jiang, S. *J. Am. Chem. Soc.* **2005**, *127*, 14473.

(131) Bernards, M. T.; Cheng, G.; Zhang, Z.; Chen, S.; Jiang, S. *Macromolecules* **2008**, *41*, 4216.

(132) Scardinoa, A. J.; de Nysb, R. *Biofouling* **2011**, *27*, 73.

(133) Vrolijk, N. H.; Targett, N. M.; Baier, R. E.; Meyer, A. E. *Biofouling*, **1990**, *2*, 39.

(134) Baier, R. E. *Science* **1968**, *162*, 1360.

(135) Tinto, W. F.; John, L.; Reynolds, W. F.; McLean, S. *Tetrahedron* **1991**, *47*, 8679.

(136) Baum, C.; Meyer, W.; Stelzer, R.; Fleischer L.-G.; Siebers, D. *Mar. Biol.* **2002**, *140*, 653.

(137) Baum, C.; Meyer, C.; Roessner, D.; Siebers, D.; Fleischer. L.-G. *Comp. Biochem. Physiol. A* **2001**, *130*, 835.

(138) Bechert, D. W.; Bruse, M.; Hage, W. *Exp. Fluids* **2000**, *28*, 403.

(139) Cao, X.; Pettitt, M. E.; Wode, F.; Sancet, M. P. A.; Fu, J.; Ji, J.; Callow, M. E.; Callow, J. A.; Rosenhahn, A.; Grunze, M. *Adv. Funct. Mater.* **2010**, *20*, 1984.

(140) Ye, S. H.; Watanabe, J.; Iwasaki, Y.; Ishihara, K. *Biomaterials* **2003**, *24*, 4143.

(141) Huang, X. J.; Xu, Z. K.; Huang, X. D.; Wang, Z. G.; Yao, K. *Polymer* **2006**, *47*, 3141.

(142) Statz, A. R.; Barron, A. E.; Messersmith, P. B. *Soft Matter* **2008**, *1*, 131.

(143) Hoipkemeier-Wilson, L.; Schumacher, J. F.; Finlay, J. A.; Perry, R.; Callow, M. E.; Callow, J. A.; Brennan, A. B. Polym. Pre. **2005**, *46*, 1312.

(144) Lejas, M.; Margaillan, A.; Bressy, C. *Chem. Rev.* **2012**, *112*, 4347.

(145) Robbart, E. Ship hull coated with anti-fouling silicone resin and method of coating. US2986474, **1961**.

(146) Kroyer, K. K. K. Marine structure having a surface coating for the prevention of accumulation of marine organisms. GB1307001, **1973**.

(147) Mueller, W. J.; Nowacki, L. J. Ship's hull coated with antifouling silicone rubber. US3702778, **1972**.

(148) Milne, A. Anti-fouling marine compositions. US4025693, **1977**.

(149) Chaudhury, M. K.; Finlay, J. A.; Chung, J. Y.; Callow, M. E.; Callow, J. A. *Biofouling* **2005**, *21*, 41.

(150) Kim, J.; Chisholm, B. J.; Bahr, J. *Biofouling* **2007**, *23*, 113.

(151) Wendt, D.; Kowalke, G.; Kim, J.; Singer, I. *Biofouling* **2006**, *22*, 1.

(152) Beigbeder, A.; Jeusette, M.; Mincheva, R.; Claes, M.; Brocorens, P.; Lazzaroni, R.; Dubois, P. J. Nanostruct. Polym. Nanocompos. **2009**, *5*, 37.

(153) Sommer, S.; Ekin, A.; Webster, D. C.; Stafslien, S. J.; Daniels, J.; VanderWal, L. J.; Thompson, S. E. M.; Callow, M. E.; Callow, J. A. *Biofouling* **2010**, *26*, 961.

(154) Bullock, S.; Johnston, E. E.; Willson, T.; Gatenholm, P.; Wynne, K. J. *J. Colloid Interface Sci.* **1999**, *210*, 18.

(155) Beigbeder, A.; Mincheva, R.; Pettitt, M. E.; Callow, M. E.; Callow, J. A.; Claes, M.; Dubois, P. *J. Nanosci. Nanotechnol.* **2010**, *10*, 2972.

(156) Majumdar, P.; Stafslien, S.; Daniels, J.; Webster, D. C. *J. Coat. Technol. Res.* **2007**, *4*, 131.

(157) Thorlaksen, P.; Yebra, D. M.; Catala, P. *Gallois Mag.* **2010**, *5*, 218.

(158) Berque, T. Coating for undersea protection. FR2157074, **1973**.

(159) Griffith, J. R.; Bultman, J. D. *Ind. Eng. Chem. Prod. Res. Dev.* **1978**, *17*, 8.

(160) Tsibouklis, J.; Nevell, T. G.; Graham, P.; Stone, M. 32nd WEGEMT School "Marine Coatings", 10−14 July **2000**.

(161) Schmidt, D. L.; Brady; Lam, K.; Schmidt, D. C.; Chaudhury, M. K. *Langmuir* **2004**, *20*, 2830.

(162) Brady, R. F. Robust nontoxic antifouling elastomers. US20030190482, **2003**.

(163) Yarbrough, J. C.; Rolland, J. P.; DeSimone, J. M.; Callow, M. E.; Finlay, J. A.; Callow, J. A. *Macromolecules* **2006**, *39*, 2521.

(164) Barbey, R.; Lavanant, L.; Paripovic, D.; Schuwer, N.; Sugnaux, C.; Tugulu, S.; Klok, H.-A. *Chem. Rev.* **2009,** *109,* 5437.

(165) Lee, S. B.; Koepsel, R. R.; Morley, S. W.; Matyjaszewski, K.; Sun, Y. J.; Russell, A. J. *Biomacromolecules* **2004**, *5*, 877.

(166) Ramstedt, M.; Cheng, N.; Azzaroni, O.; Mossialos, D.; Mathieu, H. J.; Huck, W. T. S. *Langmuir* **2007**, *23*, 3314.

(167) Ignatova, M.; Voccia, S.; Gilbert, B.; Markova, N.; Cossement, D.; Gouttebaron, R.; Jerome, R.; Jerome, C. *Langmuir* **2006,** *22,* 255.

(168) Ma, H.; Wells, M.; Beebe, T. P., Jr.; Chilkoti, A. *Adv. Funct. Mater.* **2006**, *16*, 640.

(169) Ma, H.; Li, D.; Sheng, X.; Zhao, B.; Chilkoti, A. *Langmuir* **2006**, *22*, 3751.

(170) Singh, N.; Cui, X. F.; Boland, T.; Husson, S. M. *Biomaterials* **2007**, *28*, 763.

(171) Fan, X.; Lin, L.; Messersmith, P. B. *Biomacromolecules* **2006**, *7*, 2443.

(172) Bozukova, D.; Pagnoulle, C.; De Pauw-Gillet, M.-C.; Ruth, N.; Jerome, R.; Jerome, C. *Langmuir*, **2008**, *24*, 6649.

(173) Feng, W.; Brash, J. L.; Zhu, S. P. *Biomaterials* **2006**, *27*, 847.

(174) Tugulu, S.; Klok, H. A. *Biomacromolecules* **2008**, *9*, 906.

(175) Cho, Y.; Sundaram, H. S.; Weinman, C. J.; Paik, M. Y.; Dimitriou, M. D.; Finlay, J. A.; Callow, M. E.; Callow, J. A.; Kramer, E. J.; Ober, C. K. *Macromolecules* **2011**, *44*, 4783.

(176) Dimitriou, M. D.; Sundaram, H. S.; Cho, Y.; Paik, M. Y.; Condo, M.; Schmidt, K.; Fischer, D. A.; Ober, C. K.; Kramer, E. J. *Polymer* **2012**, *53*, 1321.

(177) Ishigami, T.; Amano, K.; Fujii, A.; Ohmukai, Y.; Kamio, E.; Maruyama, T.; Matsuyama, H. *Sep. Purif. Techonl.* **2012**, *99*, 1.

(178) Yang, W. J.; Pranantyo, D.; Neoh, K.-G.; Kang, E.-T.; Teo, S. L.-M.; Rittschof, D. *Biomacromolecules* **2012**, *13*, 2769.

(179) Yang, R.; Gleason, K. K. *Langmuir*, **2012**, *28*, 12266.

(180) Bhatt, S.; Pulpytel, J.; Ceccone, G.; Lisboa, P.; Rossi, F.; Kumar, V.; Arefi-Khonsari, F. *Langmuir*, **2011**, *27* , 14570.

(181) Pieracci, J.; Wood, D. W.; Crivello, J. V.; Belfort, G. *Chem. Mater.* **2000,** *12,* 2123.

(182) Ulbricht, M.; Matuschewski, H.; Oechel, A.; Hicke, H. G. *J. Membr. Sci.* **1996**, *115*, 31.

(183) Wang, Y.; Wang, T.; Su, Y.; Peng, F.; Wu, H.; Jiang, Z. *Langmuir*, **2005**, *21*, 11856.

(184) Yea, S. H.; Watanabea, J.; Iwasakib, Y.; Ishiharaa, K. *Biomaterials* **2003**, *24*, 4143.

(185) Ulbricht, M.; Belfort, G. *J. Membr. Sci.* **1996**, *111*, 193.

(186) Lopez, G. P.; Ratner, B. D.; Tidwell, C. D.; Hyacox, C. L.; Rapoza, R. J.; Horbett, T. A. *J. Biomed. Mater. Res.* **1992**, *26*, 415.

(187) Sanchez, C.; Julian, B.; Belleville, P.; Popall, M. *J. Mater. Chem.* **2005**, *15*, 3559.

(188) Sanchez, C.; Ribot, F. *New J. Chem.* **1994**, *18*, 1007.

(189) Van Olphen, H. *Science* **1966**, *154*, 645.

(190) M. Miller, National Geographic, **1995**, February, 50.

(191) Gomez-Romero, P. *Adv. Mater.* **2001**, *13*, 163.

(192) Arkles, B. *Mater. Res. Bull.* **2001**, *26*, 402.

(193) Warrick, E. *Forty Years of Firsts* McGraw- Hill, New York, **1990**, 212.

(194) Hazan, I.; Rummel, M. U.S. Patent No. 5162426, **1992**.

(195) Foscante, R. et al. U.S. Patent No. 4250074, **1981**.

(196) Sanchez, C.; Gomez-Romero, P. *Functional Hybrid Materials* Wiley VCH, Weinheim, **2004**.

(197) Itou, T.; Matsuda, H. *Key Eng. Mater.* **1998**, *67*, 150.

(198) Audebert, P.; Demaille, C; Sanchez, C. *Chem. Mater.* **1993**, *5*, 911.

(199) Livage, J.; Roux, C.; Da Costa, J. M.; Desportes, I.; Quinson, J.-F.; *J. Sol–Gel Sci. Technol.* **1996**, *7*, 45.

(200) Del Monte, R.; *J. Sol–Gel Sci. Technol.* **2000**, *18*, 291.

(201) Lopata, S. US Pat. No. 3056684, **1962**.

(202) Hagfeldt, A.; Gratzel, M. *Acc. Chem. Res.* **2000**, *33*, 269.

(203) Watanabe, M.; Uchida, H.; Igarashi, H. *Macromol. Symp.* **2000**, *156*, 223.

(204) Wen, J.; Wilkes, G. L. *Chem. Mater.* **1996,** *8,* 1667.

(205) Lenaerts, P.; Driesen, K.; Van Deun, R.; Binnemans, K. *Chem. Mater.* **2005,** *17,* 2148.

(206) Wang, D. M.; Zhang, J. H.; Lin, Q.; Fu, L. S.; Zhang, H. J.; Yang, B. *J. Mater. Chem.* **2003,** *13,* 2279.

(207) Goubard, F.; Vidal, F.; Bazzi, R.; Tillement, O.; Chevrot, C.; Teyssie´, D. *J. Lumin.* **2007,** *126,* 289.

(208) Dekker, R.; Klunder, D. J. W.; Borreman, A.; Diemeer, M. B. J.; Worhoff, K.; Driessen, A.; Stouwdam, J. W.; van Veggel, F. C. J. M. *Appl. Phys. Lett.* **2004,** *85,* 6104.

(209) Ji, J. M.; Coffer, J. L. *J. Phys. Chem. B* **2002,** *106,* 3860.

(210) Fukushima, Y.; Inagaki, S. *J. Inclusion Phenom.* **1987**, *5*, 473.

(211) Gilman, J. W. *Appl. Clay Sci.* **1999**, *15*, 31.

(212) Dolbecq, A.; Dumas, E.; Mayer, C. R.; Mialane, P. *Chem. Rev.* **2010**, *110*, 6009.

(213) Ray, S. S. *Acc. Chem. Res.* **2012**, *45*, 1710.

(214) Kickelbick, G. *Prog. Polym. Sci.* **2003**, *28*, 83.

(215) Lichtenhan, J. D.; Otonari, Y. A.; Carr, M. J. *Macromolecules* **1995**, *28*, 8435.

(216) Lee, A.; Lichtenhan, J. D. *Macromolecules* **1998**, *31*, 4970.

(217) Fu, B.X.; Hsiao, B. S.; Pagola, S.; Stephens, P.; White, H.; Rafailovich, M.; Sokolov, J.; Mather, P. T.; Jeon, H. G.; Phillips, S.; Lichtenhan, J.; Schwab, J. *Polymer* **2000**, *42*, 599.

(218) Haddad, T. S.; Lichtenhan, J. D. *Macromolecules* **1996**, *29*, 7302.

(219) Laible, R.; Hamann, K.; Polyreaktionen, P. *Angew. Makromol. Chem.* **1975**, *48*, 97.

(220) Huang, X.; Wirth, M. J. *Anal. Chem.* **1997**, *69*, 4577.

(221) Pyun, J.; Matyjaszewski, K. *Macromolecules* **2000**, *33*, 217.

(222) Bottcher, H.; Hallensleben, M. L.; Nu, S.; Wurm, H. *Polym. Bull.* **2000**, *44*, 223.

(223) Hoffmann, F.; Cornelius, M.; Morell, J.; Froba, M. *Angew. Chem. Int. Ed.* **2006**, *45*, 3216.

(224) Mal, N. K.; Fujiwara, M.; Tanaka, Y. *Nature* **2003**, *421*, 350.

(225) Radu, D. R.; Lai, C.-Y.; Wiench, J.W.; Pruski, M.; V Lin,. S.-Y. *J. Am. Chem. Soc.* **2004**, *126*, 1640.

(226) Lei, C.; Shin, Y.; Liu, J. E.; Ackerman, J. *J. Am. Chem. Soc.* **2002**, *124*, 11242.

(227) Macquarrie, D. J.; Jackson, D. B.; Tailland, S.; Utting, K. A. *J. Mater. Chem.* **2001**, *11*, 1843.

(228) Margolese, D.; Melero, J. A.; Christiansen, S. C.; Chmelka, B. F.; Stucky, G. D. *Chem. Mater.* **2000**, *12*, 2448.

(229) Jia, M.; Seifert, A.; Berger, M.; Giegengack, H.; Schulze, S.; Thiel, W. R. *Chem. Mater.* **2004**, *16*, 877.

(230) Mercier, L.; Pinnavaia, T. J. *Chem. Mater.* **2000**, *12*, 188.

(231) Macquarrie, D. J. *Chem. Commun.* **1996**, 1961.

(232) Lim, M. H.; Blanford, C. F.; Stein, A. *J. Am. Chem. Soc.* **1997**, *119*, 4090.

(233) Kim, D.-J.; Chung, J.-S.; Ahn, W.-S.; Kang, G.-W.; Cheongy, W.-J. *Chem. Lett.* **2004**, *33*, 422.

(234) Zhang, L.; Zhang, W.; Shi, J.; Hua, Z.; Li, Y.; Yan, J. *Chem. Commun.* **2003**, 210.

(235) Fukuoka, A.; Sakamoto, Y.; Guan, S.; Inagaki, S.; Sugimoto, N.; Fukushima, Y.; Hirahara, K.; Iijima, S.; Ichikawa, M.; *J. Am. Chem. Soc.* **2001**, *123*, 3373.

(236) Yang, Q.; Liu, J.; Yang, J.; Kapoor, M. P.; Inagaki, S.; Li, C. *J. Catal.* **2004**, *228*, 265.

(237) Hamoudi, S.; Royer, S.; Kaliaguine, S. *Microporous Mesoporous Mater.* **2004**, *71*, 17.

(238) Lu, Y.; Ganguli, R.; Drewien, C. A.; Anderson, M. T.; Brinker, C. J.; Gong, W.; Guo, Y.; Soyez, H.; Dunn, B.; Huang, M. H.; Zink, J. *Nature* **1997**, *389*, 364.

(239) Leuner, C.; Dressman, J. *Eur. J. Pharm. Biopharm.* **2000**, *50*, 47.

(240) Tachibana, T.; Nakamura, A. *Kolloid-Z. Polym.* **1965**, *203*, 130.

(241) Mayersohn, M.; Gibaldi, M. *J. Pharm. Sci.* **1966**, *55*, 1323.

(242) Walking, W. D. Povidone, in: A. Wade, P.J. Weller (Eds.), Handbook of Pharmaceutical Excipitients, American Pharmaceutical Association/The Pharmaceutical Press, Washington, DC/London, **1994**, pp. 392.

(243) Hilton, J. E.; Summers, M. P. *Int. J. Pharm.* **1986**, *31*, 157.

(244) Simonelli, A. P.; Metha, S. C. *J. Pharm. Sci.* **1969**, *58*, 538.

(245) Jachowicz, R. *Int. J. Pharm.* **1987**, *35*, 7.

(246) Risbud, M. V.; Hardikar, A. A.; Bhat, S. V.; Bhondeb, R. R. *J. Control. Release* **2000**, *68*, 23.

(247) Shan, C.; Yang, H.; Song, J.; Han, D.; Ivaska, A.; Niu, L. *Anal. Chem.* **2009**, *81*, 2378.

(248) Chuna, M.-K.; Chob, C.-S.; Choia, H.-K. *J. Control. Release* **2002**, *81*, 327.

(249) Lele, B. S.; Leroux, J.-C. *Macromolecules* **2002,** *35,* 6714.

(250) Benahmed, A.; Ranger, M.; Leroux, J.-C. *Pharm. Res.-Dordr.* **2001**, *18*, 323.

(251) Feldstein, M. M.; Tohmakhch, V. N.; Malkhazov, L. B.; Vasiliev, A. E.; Plat, N. A. *Int. J. Pharmaceut.* **1996**, *131*, 229.

(252) Sun, Y. G.; Xia, Y. N. *Science* **2002**, *298*, 2176.

(253) Chou, K.-S.; Lai, Y.-S. *Mater. Chem. Phys.* **2004**, *83*, 82.

(254) Teranishi, T.; Miyake, M. *Chem. Mater.* **1998**, *10*, 594.

(255) Narayanan, R.; El-Sayed, M. A. *J. Am. Chem. Soc.* **2003**, *125*, 8340.

(256) Pastoriza-Santos, I.; Liz-Marzan, L. M. *Langmuir* **2002**, *18*, 2888.

(257) Graf, C. D.; Vossen, L. J.; Imhof, A.; van Blaaderen, A. *Langmuir* **2003**, *19*, 6693.

(258) Guo, Li.; Yang, S.; Yang, C.; Yu, P.; Wang, J.; Ge, W.; Wong, G. K. L. *Appl. Phys. Lett.* **2000**, *76*, 2901.

(259) O'Connell, M. J.; Boul, P.; Ericson, L. M.; Huffman, C.; Wang, Y.; Haroz, E.; Kuper, C.; Tour, J.; Ausman, K. D.; Smalley, R. E. *Chem. Phys. Lett.* **2001**, *342*, 265.

(260) Rieter, W. J.; Taylor, K. M. L.; Lin, W. *J. Am. Chem. Soc.* **2007**, *129*, 9852.

(261) Elghanian, R.; Storhoff, J. J.; Mucic, R. C.; Letsinger, R. L.; Mirkin, C. A. *Science* **1997**, *277*, 1078.

(262) Maxwell, D.; Taylor, J. J. R.; Nie, S. *J. Am. Chem. Soc.* **2002**, *124*, 9606.

(263) Yu, A.; Liang, Z.; Cho, J.; Caruso, F. *Nano Letters* **2003**, *3*, 1203.

(264) Grohn, F.; Bauer, B. J.; Akpalu, Y. A.; Jackson, C. L.; Amis, E. J. *Macromolecules* **2000**, *33*, 6042.

(265) Gibson, J. D.; Khanal, B. P.; Zubarev, E. R. *J. Am. Chem. Soc.* **2007**, *129*, 11653.

(266) Colfen, H.; Mann, S. *Angew. Chem. Int. Ed.* **2003**, *42*, 2350.

(267) Georgakilas, V.; Gournis, D.; Tzitzios, V.; Pasquato, L.; Guldie, D. M.; Prato, M. *J. Mater. Chem.* **2007**, *17*, 2679.

(268) Katz, E.; Willner, I. *Angew. Chem. Int. Ed.* **2004**, *43*, 6042.

(269) Dyal, A.; Loos, K.; Noto, M.; Chang, S. W.; Spagnoli, C.; Shafi, K. V. P. M.; Ulman, A.; Cowman, M.; Gross, R. A. *J. Am. Chem. Soc.* **2003**, *125*, 1684.

(270) Liao, M.-H.; Chen, D.-H.; *Biotechnol. Lett.* **2002**, *24*, 1913.

(271) Perez, J. M.; Simeone, F. J.; Saeki, Y.; Josephson, L.; Weissleder, R. *J. Am. Chem. Soc.* **2003**, *125*, 10192.

(272) Katz, E.; Sheeney-Haj-Ichia, L.; Willner, I. *Chem. Eur. J.* **2002**, *8*, 4138.

(273) Gao, J.; Gu, H.; Xu, Bing. *Acc. Chem. Res.* **2009**, *42*, 1097.

(274) Qu, A.; Wen, X.; Pi, P.; Cheng, J.; Yang, Z. *J. Colloid. Interf. Sci.* **2008**, *317*, 62.

(275) Niepceron, F.; Lafitte, B.; Galiano, H.; Bigarre, J.; Nicol, E.; Tassin, J.-F. *J. Membrane Sci.* **2009**, *338*, 100.

(276) Sung, C.-F.; Kekuda, D.; Chu, L. F.; Chen, F.-C.; Cheng, S.-S.; Lee, Y.-Z.; Wu, M.-C.; Chu, C.-W. *Org. Electron.* **2010**, *11*, 154.

(277) Judeinstein, P.; Sanchez C. *J. Muter. Chem.* **1996***, 6*, 511.

(278) Lancelle-Beltran, E.; Prene, P.; Boscher, C.; Belleville, P.; Buvat, P.; Sanchez, C. *Adv. Mater.* **2006,** *18,* 2579.

(279) Ferrer M. L.; del Monte, F. *J. Phys. Chem. B* **2005**, *109*, 80.

(280) Tajima, K.; Li, L.-S.; Stupp, S. I. *J. Am. Chem. Soc.* **2006**, *128*, 5488.

(281) Asefa, T.; MacLachlan, M. J.; Coombs, N.; Ozin, G. A. *Nature* **1999**, *402*, 867.

(282) Inagaki, S.; Guan, S.; Fukushima, Y.; Ohsuna, T.; Terasaki, O. *J. Am. Chem. Soc.* **1999**, *121*, 9611.

(283) Ding, H.; Sun, H.; Shan, Y. *J. Photoch. Photobio. A* **2005**, *169*, 101.

(284) Kim, D. H.; Sun, Z.; Russell, T. P.; Knoll, W.; Gutmann, J. S. *Adv. Funct. Mater.* **2005**, *15*, 1160.

(285) Yang, D; Qi, L. M.; Ma, J. M. *J. Mater. Chem.* **2003**, *13*, 1119.

(286) Zhao, Y.; Yan, B. *J. Colloid. Interf. Sci.* **2013**, *395*, 145.

(287) Ohno, K.; Morinaga, T.; Koh, K.; Tsujii, Y.; Fukuda, T. *Macromolecules* **2005**, *38*, 2137.

(288) Kong, H.; Gao, C.; Yan, D. *Macromolecules* **2004**, *37*, 4022.

(289) Farmer, S. C.; Patten, T. E. *Chem. Mater.* **2001**, *13*, 3920.

(290) Li, C.; Benicewicz, B. C. *Macromolecules* **2005**, *38*, 5929.

(291) Boyer, C.; Whittaker, M. R.; Luzon, M.; Davis, T. P. *Macromolecules* **2009**, *42*, 6917.

(292) Kim, J.-H.; Lee, T. R. *Chem. Mater.* **2004**, *16*, 3647.

(293) Srivastava, S.; Kotov, N. A. *Acc. Chem. Res.* **2008**, *41*, 1831.

(294) Moore, G. E. "Cramming more components onto integrated circuits" Electronics Magazine, p. 4, **1965**.

(295) Andrus, J. and Bond, W. L. "Photoengraving in Transistor Fabrication," in F. J. Biondi et al, eds., Transistor Technology, Vol. III, Princeton, NJ: D. Van Nostrand, **1958**, 151–162.

(296) Sanders, D. P. *Chem. Rev.* **2010,** *110,* 321.

(297) Suss, O. *Liebigs. Ann. Chem.* **1944**, *556*, 65.

(298) Ito, H. *Adv. Polym. Sci.* **2005**, *172*, 37.

(299) Ito H.; Willson, C. G.; Frechet, J. M. J. Digest of Technical Papers of 1982 Symposium on VLSI Technology, p 86, **1982**.

(300) Ito H.; Flores, E. *J. Electrochem. Soc.* **1988**, *135*, 2322.

(301) Dektar, J. L.; Hacker, N. P. *J. Org. Chem.* **1988**, *53*, 1833.

(302) Dektar, J. L.; Hacker, N. P. *J. Photochem. Photobiol. A* **1989**, *46*, 233.

(303) Tsunooka, M.; Yanagi, H.; Kitayama, M.; Shirai, M. *J. Photopolym. Sci. Technol.* **1991**, *4*, 239.

(304) Buhr, G.; Dammel, R.; Lindley, C. R. *Proc. ACS. Div. Polym. Mater. Sci. Eng.* **1989**, *61*, 269.

(305) Lamanna, W. L.; Kessel, C. R.; Savu, P. M.; Cheburkov, Y.; Brinduse, S.; Kestner, T. A.; Lillquist, G. J.; Parent, M. J.; Moorhouse, K. S.; Zhang, Y.; Birznieks, G.; Kruger, T.; Pallazzotto, M. C. *Proc. SPIE* **2002**, *4690*, 817.

(306) Przybilla, K.-J.; Dammel, R.; Roschert, H.; Spies, W.; Pawlowski, G. *J. Photopolym. Sci. Technol.* **1991**, *4*, 421.

(307) Ito H.; Willson, C. G.; Frehet, J. M. J. *Proc. SPIE* **1987**, *771*, 24.

(308) Ito, H.; Ueda, M. *Macromolecules* **1988**, *21*, 1475.

(309) Jiang. Y.; Bassett, D. R. In: Thompson, L. F.; Willson, C. G.; Tagawa, S. (eds) Polymers for microelectronics.ACS Symposium Series 537, American Chemical Society, Washington, D.C., p 40, **1994**.

(310) Ito, H.; Breyta, G.; Hofer, D.; Sooriyakumaran, R.; Petrillo, K.; Seeger, D. *J. Photopolym. Sci. Technol.* **1994**, *7*, 433.

(311) Pawlowski, G.; Przybilla, K.-J.; Spiess, W.; Wengenroth. H.; Roschert, H. *J. Photopolym. Sci. Technol.* **1992**, *5*, 55.

(312) Allen, R. D.; Wallraff, G. M.; DiPietro, R. A.; Kunz, R. R. *J. Photopolym. Sci. Technol.* **1994**, *7*, 507.

(313) Silva, A. D.; Lee, J.-K.; Andre, X.; Felix, N. M.; Cao, H. B.; Deng, H.; Ober, C. K. *Chem. Mater.* **2008**, *20*, 1606.

(314) Trikeriotis, M,; Krysaki, M.; Chung, Y. S.; Ouyang, C.; Cardineau, B.; Brainard, R.; Ober, C. K.; Giannelis, E. P.; Cho, K. *J. Photopolym. Sci. Technol.* **2012**, *25*, 583.

(315) Romang A. H.; Watkins, J. J. *Chem. Rev.* **2010**, *110*, 459.

(316) Wang, C. W.; Chang, R. T.; Lin, W. K.; Lin, R. D.; Liang, M. T.; Yang, J. F.; Wang, J. B. *J. Electrochem. Soc.* **1999**, *146*, 3485.

(317) Goldfarb, D. L.; de Pablo, J. J.; Nealey, P. F.; Simons, J. P.; Moreau, W. M.; Angelopoulos, M. *J. Vac. Sci. Technol. B* **2000**, *18*, 3313.

(318) Ota, K.; Tsutsumi, A. *J. Mech. Design.* **2008**, *2*, 619.

(319) Hoggan, E. N.; Wang, K.; Flowers, D.; DeSimone, J. M.; Carbonell, R. G. *IEEE Trans. Semicond. Manuf.* **2004**, *17*, 510.

(320) Felix, N. M.; Silva, A. D.; Ober, C. K. *Adv. Mater.* **2008**, *20*, 1303.

(321) Blackburn, J. M.; Long, D. P.; Watkins, J. J. *Chem. Mater.* **2000**, *12*, 2625.

(322) Cabanas, A.; Blackburn, J. M.; Watkins, J. J. *Microelectron. Eng.* **2002**, *64*, 53.

(323) Zhao, B.; Momose, T.; Ohkubo, T.; Shimogaki, Y. *Microelectron. Eng.* **2008**, *85*, 675.

(324) Gougousi, T.; Barua, D.; Young, E. D.; Parsons, G. N. *Chem. Mater.* **2005**, *17*, 5093.

(325) Bessel, C. A.; Denison, G. M.; DeSimone, J. M.; DeYoung, J.; Gross, S.; Schauer, C. K.; Visintin, P. M. *J. Am. Chem. Soc.* **2003**, *125*, 4980.

(326) Shan, X. Y.; Watkins, J. J. *Thin Solid Films* **2006**, *496*, 412.

(327) Jones, C. A.; Yang, D. X.; Irene, E. A.; Gross, S. M.; Wagner, M.; DeYoung, J.; DeSimone, J. M. *Chem. Mater.* **2003**, *15*, 2867.

(328) Weibel, G. L.; Ober, C. K. *Microelectron. Eng.* **2003**, *65*, 145.

(329) Tekin, E.; Smith, P. J.; Schubert, U. S. *Soft Matter* **2008**, *4*, 703.

(330) Fromm, J. E. *IBM J. Res. Dev.* **1984**, *28*, 322.

(331) Sirringhaus, H.; Kawase, T.; Friend, R. H.; Shimoda, T.; Inbasekaran, M.; Wu, W.; Woo, E. P. *Science* **2000**, *290*, 2123.

(332) Sele, C. W.; Werne, T.; Friend, R. H.; Sirringhaus, H. *Adv. Mater.* **2005**, *17*, 997.

(333) Paul, K. E.; Wong, W. S.; Ready, S. E.; Street, R. A. *Appl. Phys. Lett.* **2003**, *83*, 2070.

(334) Lee, H.-H.; Chou, K.-S.; Huang, K.-C. *Nanotechnology* **2005**, *16*, 2436.

(335) Lee, Y.; Choi, J.; Lee, K. J.; Stott, N. E.; Kim, D. *Nanotechnology* **2008**, *19*, 415604.

(336) Redinger, D. R.; Molesa, S.; Yin, S.; Farschi, R.; Subramanian, V. *IEEE Trans. Electron. Devices* **2004**, *51*, 1978.

(337) Tekin, E.; Wijlaars, H.; Holder, E.; Egbe, D. A. M.; Schubert, U. S. *J. Mater. Chem.* **2006**, *16*, 4294.

(338) Hoth, C. N.; Choulis, S. A.; Schilinsky, P.; Brabec, C. J. *Adv. Mater.* **2007**, *19*, 3973.

(339) Voit, W.; Zapka, W.; Belova, L.; Rao, K. V. *Proc. Sci. Meas. Technol.* **2003**, *150*, 252.

(340) Borberl, M.; Kovalenko, M. V.; Gamerith, S.; List, E. J. W.; Heiss, W. *Adv. Mater.* **2007**, *19*, 3574.

(341) Roth, E. A.; Xu, T.; Das, M.; Gregory, C.; Hickman, J. J.; Boland, T. *Biomaterials* **2004**, *25*, 3707.

(342) Heanue, J. F.; Bashaw, M. C.; Hesselink, L. *Science* **1994**, *265*, 749.

(343) Lawrence, J. R.; O'Neill, F. T.; Sheridan, J. T. *Optik* **2001**, *112*, 449.

(344) Hesselink, L.; Orlov, S. S.; Bashaw, M. C. *Proc. IEEE* 2004, 92, 1231.

(345) Buse, K.; Adibi, A.; Psaltis, D *Nature* **1998**, *393*, 665.

(346) von der Linde, D.; Glass, A. M.; Rodgers, K. F. *Appl. Phys. Lett.* **1975**, *26*, 22.

(347) von der Linde, D.; Glass, A. M.; Rodgers, K. F. *J. Appl. Phys.* **1976**, *47*, 217.

(348) Vormann H.; Kratzig, E. *Solid State Commun.* **1984**, *49*, 843.

(349) Ostroverkhova, O.; Moerner, W. E. *Chem. Rev.* **2004**, *104,* 3267.

(350) Wright, D.; Gubler, U.; Roh, Y.; Moerner, W. E.; He, M.; Twieg, R. J. *Appl. Phys. Lett.* **2001**, *79*, 4274.

(351) Bai, Y.; Chen, X.; Wan, X.; Zhou, Q. F.; Liu, H.; Zhang, B.; Gong, Q. *Appl. Phys. Lett.* **2002**, *80*, 10.

(352) Ostroverkhova, O.; Gubler, U.; Wright, D.; Moerner, W. E.; He, M.; Twieg, R. *Adv. Function. Mater.* **2002**, *12*, 621.

(353) Winiarz, J.; Prasad, P. *Opt. Lett.* **2002**, *27*, 1330.

(354) Hackel, M.; Kador, L.; Kropp, D.; Schmidt, H.-W. *Adv. Mater.* **2007**, *19*, 227.

(355) Wang, F.; Chen, Z. J.; Zhang, B.; Gong, Q. H.; Wu, K. W.; Wang, X. S.; Zhang, B. W.; Tang, F. Q. *Appl. Phys. Lett.* **1999**, *75*, 3243.

(356) Close, D. H.; *Appl. Phys. Lett.* **1969**, *14*, 159.

(357) Sugawara, S.; Murase, K.; Kitayama, T.; *Appl. Opt.* **1975**, *14*, 378.

(358) Zhao F.; Frietmann, E. E. E.; Li, X. *Proc. SPIE* **1998**, *3468*, 317.

(359) Oliveira, P. W.; Krug, H.; Miller, P.; Schmidt, H. *Mater. Res. Soc. Symp. Proc.* **1996**, *435*, 553.

(360) Suzuki, N.; Tomita,Y.; Kojima, T. *Appl. Phys. Lett.* **2002**, *81*, 4121.

CHAPTER TWO:

IMPROVED ANTIFOULING PROPERTIES OF REVERSE OSMOSIS MEMBRANES USING A 'LAYER-BY-LAYER' MEDIATED METHOD*

*Lin Chen, Héloïse Thérien-Aubin, Mavis C.Y. Wong, Eric M.V. Hoek and Christopher K. Ober. *Submitted to Journal of Materials Chemistry B*.

2.1 Introduction

Biofouling has been referred to as the 'Achilles heel' of reverse osmosis (RO) membranes, causing decline of water flux and loss in the salt rejection properties of the RO membrane, thus increasing the energy cost and shortening the membrane lifetime.[1-4] The fundamental problem lies with the fact that modern RO membranes cannot tolerate continuous exposure to chlorine and other oxidative disinfectants. Unlike colloidal and particulate fouling, which can be mitigated through pre-filtration, microbiological fouling is a much more difficult, dynamic problem to deal with.[1] Bacteria grow, reproduce and produce extra-cellular polymeric substances (EPS) in response to available nutrients and other stressors (i.e., low molecular weight solutes not removed by pre-filtration); hence, only trace amounts of attached cells are needed to eventually form an overwhelming biofilm.[5] Suspended bacteria cells initially deposit to RO membranes through non-specific interactions, e.g., van der Waals, electrostatic and hydration forces.[6] Once attached, cells change their surface chemistry and produce EPS, which render bacterial attachment irreversible; even if initial environmental conditions do not support biofilm formation, later perturbations in nutrient supply can stimulate rapid biofilm formation and subsequent performance decline.

In general, the pursuit to combat RO membrane biofouling has fallen into three approaches: (1) synthesize chlorine tolerant RO membranes, (2) synthesize or modify membranes that resist initial bacterial attachment, and (3) synthesize or modify membranes that inactivate bacteria, rendering them no more than inert deposits of organic matter. Polymer brushes with selected functional groups have been considered

as good candidates for antifouling purposes.[7,8] Polymers with quaternary ammonium functionalities are good antimicrobial agents, which can kill attached bacteria.[9-11] Poly(ethylene glycol) (PEG) and its derivatives, due to their high hydration forces, have been developed to reduce protein and cell adhesion.[12-14] Zwitterionic structures, containing both positive and negative charges within one molecule, have recently been found capable of preventing initial, non-specific adhesion of microorganisms.[15-17] Fluoro-polymers have been used as excellent fouling release coatings due to their low surface energy and good non-stick characteristics.[18-20] Copolymers of such polymer brushes have also been synthesized and used in various antifouling coatings.[21-23]

In order to improve the antifouling properties of RO membranes, several methods have been developed to grow polymer brushes on a membrane surface. Belfer et al. used an *in-situ* redox initiation process to grow poly(ethylene glycol) methacrylate brushes on commercial RO membranes.[24] Sagle et al. coated a membrane surface with a series of crosslinked PEG-based hydrogel films by using UV-induced photopolymerization.[25] Lin et al. introduced an atmospheric pressure plasma induced graft polymerization reaction to attach poly(methacrylic acid) and poly(acrylamide) brushes.[26] Other methods include casting thin film composite RO membranes using monomers modified with functional groups for the growth of polymer brushes.[27,28] However, almost all the approaches mentioned above will greatly modify the barrier layer structure, which may negatively impact basic separation performance.

Herein, we introduce a 'layer by layer' (LBL) method to grow antifouling polymer brushes on a membrane surface without adversely affecting water flux or salt rejection

of the modified membranes. The method of LBL coatings was first introduced in 1993.[29] Through electrostatic interactions, multiple alternating layers of polycations and polyanions can be firmly coated onto different kinds of substrates.[30-32] Since LBL films are assembled by physical intermolecular forces, the original membrane is not altered. While some of the polyelectrolytes do contain reactive chemical groups, e.g., polyallylamine hydrochloride (PAH), LBL films will generally not only protect the surface from being directly exposed to potential damage, but also help to amplify the number of reaction sites on the substrate. By taking advantage of the native negative charge of the polyamide surface, we first deposit a multilayer LBL film on the membrane. In order to construct surfaces with various functional antifouling polymer brushes, further modifications of the coated membrane surfaces are done by either a 'grafted to' or a 'grafted from' approach. Attached polymers consist of chains with either uncharged PEG side groups or charged zwitterionic groups, both of which are known to have antifouling characteristics to a range of species. In one approach, we use reversible addition-fragmentation chain transfer (RAFT) polymerization to grow brushes and then carry out a Michael addition to attach the fouling resistant brushes [33]. In a second approach, we demonstrate modification of the LBL film by atom-transfer radical-polymerization (ATRP) initiator sites and grow fouling resistant brushes by a surface initiated ATRP process. [34,35] These brushes were characterized and their surface properties assessed using attenuated total reflectance-Fourier transform infrared spectroscopy (ATR-FTIR) spectroscopy, X-ray photoelectron spectroscopy (XPS) and water contact angle measurements.

2.2 Experimental

2.2.1 Materials

The commercial seawater RO membrane (SWC4+) was kindly provided by Hydranautics (Oceanside, California, USA). Silicon wafer was purchased from WRS Materials Company (San Jose, California, USA) and modified as described below. Hydrogen peroxide (H_2O_2, 30-32%), sodium chloride (NaCl), sodium bicarbonate ($NaHCO_3$) and sulfuric acid (H_2SO_4, 96%) was purchased from J.T. Baker Chemicals (Center Valley, Pennsylvania, USA). (3-aminopropyl) trimethoxysilane (ATS, 97%), poly(sodium 4-styrenesulfonate) (PSS, average Mw~70,000), poly(allylamine hydrochloride) (PAH, average Mw~15,000), acrylic acid (99%), N-(3-dimethylaminopropyl)-N'-ethylcarbodiimide hydrochloride (EDC), N-hydroxysuccinimide (NHS, 98%), 2-bromo-2-methylpropionic acid (BMA, 98%), poly(ethylene glycol) methyl ether methacrylate (PEGMA, average Mn~500), [2-(methacryloyloxy)ethyl] dimethyl-(3-sulfopropyl) ammonium hydroxide (SBMA, 97%), 2-phenyl-2-propyl benzodithioate (CTA, 96%), 2,2′-azobis(2-methylpropionitrile) (AIBN, 98%), triethylamine, copper (I) bromide (CuBr), copper (II) bromide (CuBr), 2,2'-bipyridyl (bpy) were purchased from Sigma Aldrich (St. Louis, Missouri, USA) and used as received except PEGMA and SBMA, which were purified over an alumina column. Hydrochloric acid (HCl) and solvents were purchased from Fisher Scientific (Pittsburgh, Pennsylvania, USA) and used as received.

2.2.2 Layer by Layer Coatings

RO membranes were first washed in deionized water for 5 days to release any irreversibly bound coatings or preservatives from their surfaces. The membrane was then cut into 5 cm x 10 cm (2 in x 4 in) pieces for modifications and characterizations.

Coating LBL films on membranes was following a standard protocol.[29] The membrane was first soaked in a PAH solution (0.1 g of PAH and 0.585 g of NaCl in 100 ml of H_2O) for 10 min. It was then placed in 100 ml of water for 2 minutes, which was repeated two times with clean water to wash off excessive absorbed polyelectrolytes. The membrane was soaked in a HCl solution (pH 3) for another 2 minutes. Then it was put in a PSS solution (0.1 g of PSS and 0.585 g of NaCl in 100 ml of H_2O) for another 10 minutes, washed in 100 ml of H_2O for 2 minutes and repeated three times. This finishes one cycle of LBL coatings. The membrane was then put in the PAH solution again to start a new cycle. After a desired number of coating cycles, the membrane was soaked in 100 ml of H_2O for 30 minutes and air-dried overnight.

2.2.3 Adding Chemical Functionalities on RO Membranes

Before adding any functional chemical groups, the membranes coated with LBL films were soaked in a $NaHCO_3$ solution (0.1M) for 3 hours to neutralize the PAH layer. The carbon-carbon double bond (C=C) was reacted onto the surface through an acid-amine coupling reaction. Acrylic acid (0.05 M, 0.087 ml), EDC (0.06 M, 0.288 g) and NHS (0.06 M, 0.176 g) were stirred in 25 ml of H_2O for 3 hours. 0.21 g $NaHCO_3$ (0.1 M) was added into the solution to adjust the pH to about 6. The membranes were

then soaked in the solution and stirred for 24 hours, after which the membranes were washed with H_2O for several times and vacuum dried overnight. Tertiary bromide was added onto the membrane surface through the same reaction, but using BMA instead.

2.2.4 Grafting Polymer Brushes

A simple thiol-ene Michael addition reaction was used to graft the antifouling polymer brushes onto the membranes.[33] The polymer was first synthesized through reversible addition-fragmentation chain transfer (RAFT) polymerization. A mixture of 8 ml of PEGMA monomer and 51.2 mg of CTA was dissolved in 40 ml of toluene, and then freeze-thawed three times. The solution was transferred into a Schlenk tube containing 7.6 mg of AIBN, and reacted at 80 ^oC for 8 hours under argon (Ar). The solvent was evaporated and the polymer was redissolved in minimum amount of tetrahydrofuran (THF) and precipitated in hexane/ethyl ether mixture (1:1 volume ratio, 40 ml for each) for several times to get rid of any unreacted monomer. 5 g of the as-synthesized polymer (Mn~33,000; PDI~1.08) and 0.15 ml of propylene amine were added in 25 ml of THF. After reacting for 8 hours at room temperature, the polymer end groups were reduced to be thiol groups. 1 g of the thiol-ended polymer was dissolved in 20 ml of H_2O, into which the RO membranes with 'C=C' bonds were soaked. 3 μl of triethylamine was then added as catalyst and the reaction was allowed to go for 24 hours. The as-modified membranes were then washed with H_2O and air-dried overnight.

Surface initiated atom-transfer radical-polymerization (SI-ATRP) process was also used to grow polymer brushes directly from the membrane surfaces. PEGMA

monomer (5 g) was dissolved in 20 ml of H_2O. After purged with Ar for 1 hour, the solution was transferred into a Schlenk tube containing 143 mg of CuBr, 15 mg of $CuBr_2$, 312 mg of 2,2'-bipyridyl (bpy) and the membranes with tertiary bromide ATRP initiators. After reacting for 2 hours under Ar at room temperature, the membrane were washed with H_2O and air-dried.

2.2.5 Membrane Performance Test

To obtain the water permeability and salt permeability coefficients for the membranes, a custom designed reverse osmosis system was employed. The system is a cross-flow system consisting of six stainless steel cells operating under the same pressure. Each cell has an effective membrane area of 19 cm^2 and a channel height of 2 mm. The feed solution was pressurized in the system by a diaphragm pump (Hydracell; Wanner Engineering). The feed solution was kept at a constant temperature by a large stainless steel coil, submerged in the feed tank, connected to a water chiller (NTE RTE7; Fisher Scientific).

Membrane coupons were compacted at 850 psi for 16 hours prior to testing. To determine the intrinsic pure water permeability, the feed tank was filled with Milli-Q water produced from Super-Q water systems (Millipore Corp.), and the permeate flow rate was measured by a digital flow meter (Optiflow 1000; Agilent Technology) at 800 psi and 25 °C. The intrinsic salt permeability was determined by using 32 g/L sodium chloride (NaCl; Fisher Scientific) feed solution, and measuring the resulting permeate conductivity with a calibrated conductivity meter (Accumet XL20; Cole Parmer).

2.2.6 Antifouling Test

Static protein adsorption tests were realized by immersing the membrane in a 0.5 g/L solution of FITC-BSA in 0.1 M phosphate buffer at pH 7.4 containing 3.5% of NaCl for 48 h; the amount of protein bounded to the membrane was evaluated by the signal intensity obtained by fluorescence microscopy.

The direct observation system used for the real-time antifouling experiments was developed by Huang et al., and described in detail previously.[5] A customized stainless steel flow cell with a flow channel 69.86 mm long, 25 mm wide and 2.55 mm high was used in the experiments. The cell was also designed with a polycarbonate window to allow for microscopic observation of the membrane during experimentation. After membrane coupons were placed into the flow cell, and the assembled flow cell was mounted to an optical microscope (BX51WI; Olympus) equipped with a reflected fluorescence system (Sutter Instrument Co.). The membrane surfaces were viewed through a 10× microscope objective lens (UPlanFI 10×/0.30; Olympus), while a high resolution charged-couple device camera (F-View II; Soft Imaging System Co.) installed on the top of the microscope for image acquisition provided an additional 4× magnification.

Membrane coupons were first compacted at 850 psi for 30 min using a salt solution consisting of 32 g/L of a commercial sea salt comprised mostly of Na^+, Cl^-, Mg^{2+}, SO_4^{2-}, K^+, Ca^{2+} and HCO_3^- (Instant Ocean®; Spectrum Brands Inc.). After compaction and system stabilization, the solution crossflow was adjusted to 1.4 – 1.8 gallons per hour (gph) and a temperature of 25 °C. A prepared solution of *Halimonas*

pacifica stained with Syto 9 green fluorescent probes (Life Technologies Corp.) was injected into the feed solution immediately after the system was stabilized. The feed concentration was approximately 10^9 cells/L verified by diluted feed counts using a cytometer. Images were taken every 5 min during the deposition experiments, and the attached cells were counted.

2.2.7 Membrane Characterizations

LBL film thicknesses were measured on a Nanofilm EP3 ellipsometer. XPS experiments were carried out on Surface Science Instruments (SSI) model SSX-100. ATR-FTIR experiments were carried out on a Nicolet iZ-10 instrument equipped with a diamond ATR crystal. Water contact angles were measured using a Rame-Hart 100-00 contact angle goniometer. Atomic Force Microscopy (AFM) images were taken on a Veeko Icon AFM instrument. Scanning Electron Microscopy (SEM) images were taken on a Zeiss Supra 55 microscope.

2.3 Results and Discussion

Scheme 2.1 shows the designed modification process of the membrane surface. Due to the process and materials used to form the polyamide thin films, there are pendent carboxylic acid groups at the outer membrane interface. Therefore, under normal operating conditions, i.e.200-800 psi at room temperature, the surface of the membrane has a slight negative charge,[36] which provides a good substrate for LBL coatings. The LBL films were coated onto the membrane surface using a standard dip-

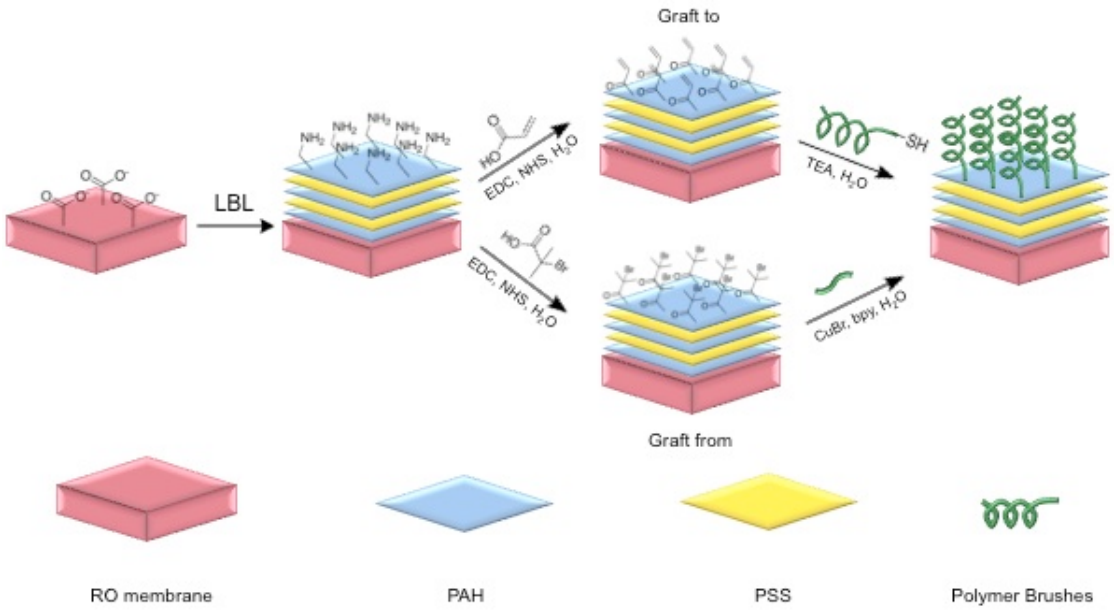

Scheme 2.1. Modification process of RO membranes. PAH and PSS layers were alternately coated onto the membrane surface. Polymer brushes were then attached using the surface through either 'grafted to' or 'grafted from' approaches.

coating protocol such that alternate layers of polycations and polyanions were alternately attached by electrostatic interactions. The membrane surfaces were then modified with functional groups for subsequent incorporation of antifouling polymer brushes.

In this study two methods were used to grow polymer brushes, i.e. 'grafted to' and 'grafted from' approaches. For the 'grafted to' approach, the membrane surfaces were first functionalized with 'C=C' bonds. The brush polymers to be attached were first synthesized by RAFT polymerization and reduced to form thiol end groups, which could then be added to the coatings through a Michael addition reaction. For the 'grafted from' method, the membrane surfaces were functionalized with tertiary bromide groups serving as ATRP initiators for polymer brush growth from the surface by the ATRP. Two antifouling polymer brush types, i.e. PEGMA and SBMA, were selected. In our experience, having several types of coatings is important in anti-fouling applications because the adhesion strategies used by different biological species can vary widely.[22,28] It is worth noting that all membrane modification reactions were conducted in aqueous solution. No organic solvents were used since they could either dissolve or swell the membrane, thus affecting the membrane structure and performance.

ATR spectra were used to confirm the growth of the LBL films. A typical spectrum of the RO membrane is shown as curve (a) in Figure 2.1. Characteristic peaks around 1660 cm^{-1} from the active polyamide layer and peaks around 1580 cm^{-1}

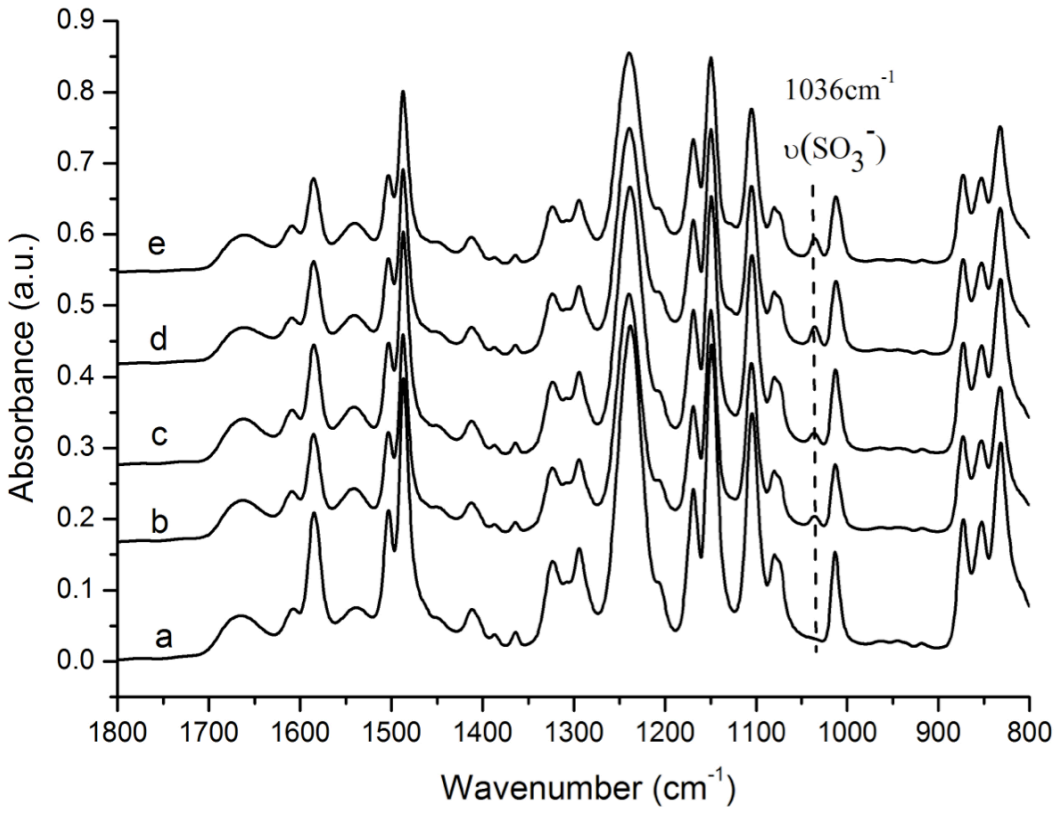

Figure 2.1. ATR spectra of LBL films on RO membranes coated with different layers of LBL films before and after the membrane performance test: a – virgin membrane; b – membrane modified with 5 cycles of LBL films before performance test; c – membrane modified with 5 cycles of LBL films after performance test; d – membrane modified with 10 cycles of LBL films before performance test; e – membrane modified with 10 cycles of LBL films after performance test.

and 1483 cm^{-1} from the supporting polyethersulfone layer were observed.[37] After the membranes were modified with LBL films, a specific peak at 1036 cm^{-1} appeared, which was attributed to the symmetrical vibrational adsorption of SO_3^- group in the PSS layer.[38] XPS results (Table 2.1) also showed an increase of sulfur content on the surface from 0.06 to 5.57 % after modifications, indicating the successful growth of LBL films on the surface of the RO membranes.

To test the stability of the LBL films on the membrane surfaces, ATR and XPS results of the coated films were measured before and after the membrane performance test. Not only did the peak of the SO_3 group still exist (Fig. 2.1) after the test, but also the surface composition of the membranes showed little change (Table 2.1). This proved that the LBL films were quite stable on the membrane surfaces, at least under the pressurized cross-flow testing conditions.

Chemical functionalities were then added on top of the LBL films. Water contact angle measurements were used to detect possible changes of the membrane surface properties (Fig. 2.2). The virgin membrane showed a contact angle of 55^o, while it dropped to 15^o after LBL coatings were added, indicating a significant change from a mildly hydrophobic to a highly hydrophilic surface. Adding chemical functionalities only increased the contact angle by 2~3^o, consistent with a monolayer of 'C=C' and 'Br', the presence of which was confirmed by XPS analysis (~1.61% Br on the surface, Table 2.2). Two different polymers were then selected to further modify the LBL coated membranes, i.e., PEGMA and SBMA. After growth of the polymer brushes, the contact angle increased to about 25^o (Fig. 2.2). In ATR spectra (Fig. 2.3), specific

Table 2.1. XPS results of atomic percentage of elements on membrane surfaces coated with different layers of LBL films before and after the membrane performance test.

	virgin membrane	LBL 5cycles	LBL 5cycles after test	LBL 10cycles	LBL 10cycles after test
C 1s	75.34	67.90	69.21	68.56	69.30
O 1s	16.02	20.56	20.01	19.81	20.22
N 1s	8.40	5.97	5.65	5.64	5.18
S 2p	0.06	5.57	5.13	5.99	5.30

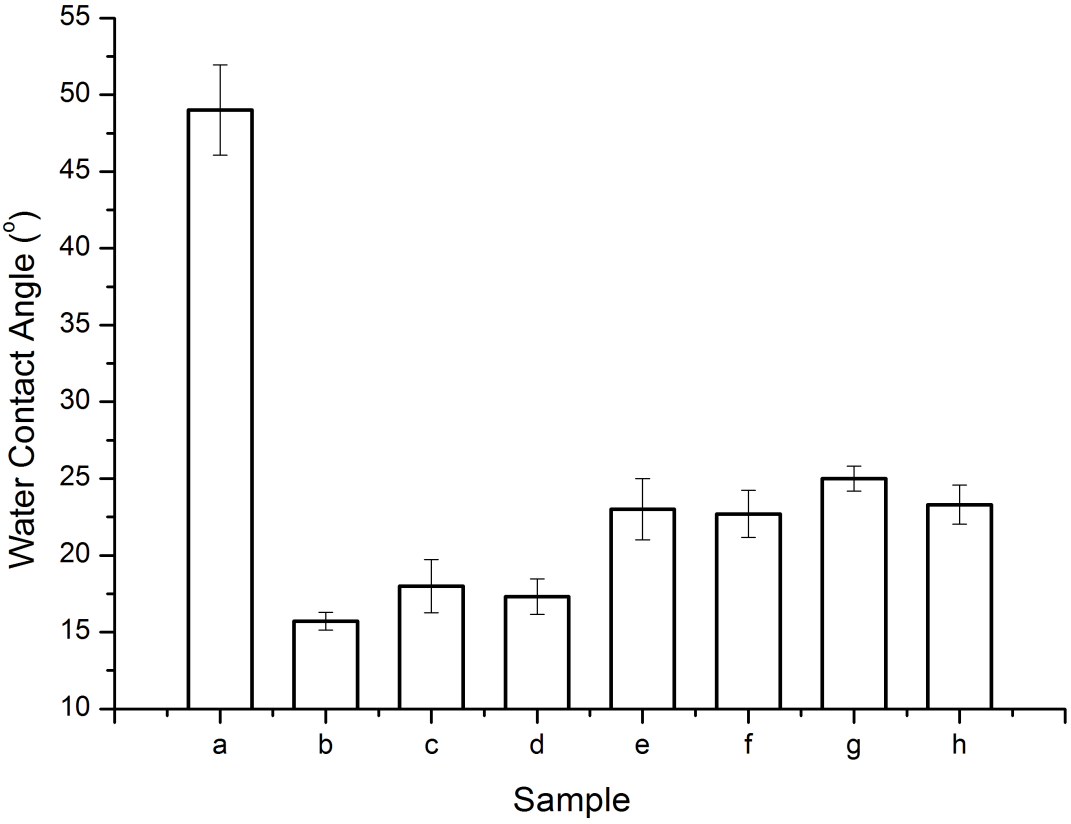

Figure 2.2. Water contact angle measurements of the modified membranes: a - virgin membrane; b – membranes with LBL films. c – membranes with 'C=C'; d – membrane with 'Br'; e – membranes with PEGMA polymer by 'grafted to' method; f – membranes with SBMA polymer by 'grafted to' method; g – membranes with PEGMA polymer by 'grafted from' method; h – membranes with SBMA polymer by 'grafted from' method.

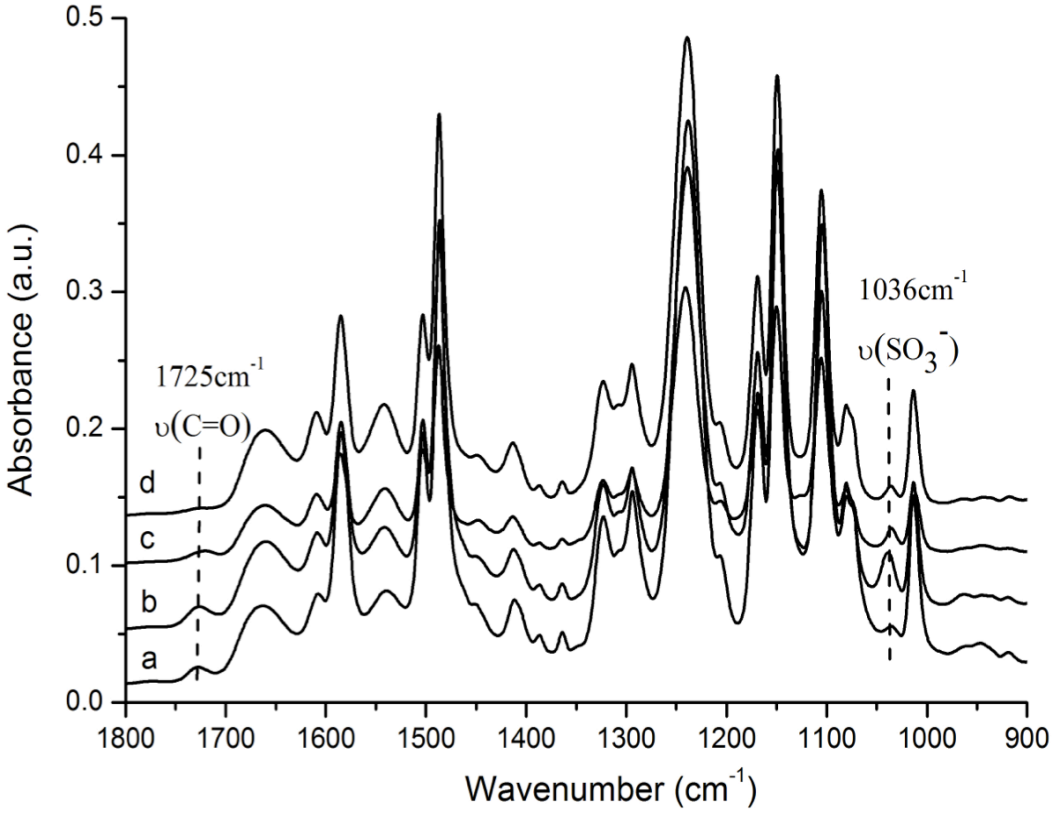

Figure 2.3. ATR spectra of the modified membranes with polymer brushes grown through either 'grafted to' or 'grafted from' approaches: a – membranes with PEGMA polymer by 'grafted to' method; b – membranes with SBMA polymer by 'grafted to' method; c – membranes with PEGMA polymer by 'grafted from' method; d – membranes with SBMA polymer by 'grafted from' method.

Table 2.2. XPS results of membrane surfaces modified with LBL films, chemical functionalities and polymer brushes through ‘grafted to’ or ‘grafted from’ approaches..

	LBL 5.5cycles	-C=C	-Br	GT_PEGMA*	GT_SBMA	GF_PEGMA*	GF_SBMA
C 1s	66.90	64.95	63.22	63.71	63.88	63.79	63.79
O 1s	19.77	21.49	21.40	23.43	23.13	23.52	22.54
N 1s	7.41	8.26	8.39	8.35	8.07	7.74	7.63
S 2p	5.92	5.30	5.38	4.51	4.92	3.95	4.73
Br 3p	-	-	1.61	-	-	0.99	1.14

* ‘GT’ stands for ‘grafted to’’; ‘GF’ stands for ‘Grafted from’.

peaks at 1720cm^{-1} could be observed, which are characteristic of the C=O groups on both polymers. The slight increase of oxygen and decrease of sulfur content from XPS analysis (Table 2.2) also indicated the composition change on the membrane surface, proving the successful growth of the polymer brushes. Transmission IR spectra for the polyamide layers only provided further solid evidences of the strong chemical bondings between polymer brushes and membrane surfaces (Fig. 2.4).

In order to measure the thickness of LBL films and polymer brushes on membrane surfaces, SEM and AFM were applied to observe the membrane structure from both side and top views. However, since the polysulfone supporting layer is much thicker (~30 μm, Fig. 2.5) than the polyamide dense layer (100-200 nm) and surface roughness on all membranes (virgin and as-modified) appeared to be high (60-100 nm, Fig. 2.6), it is hard to track the thickness change on the membrane surface. A model reaction on silicon wafer was then adopted as a reference. Treatment of silicon wafer was described in detail in supporting information. Ellipsometry was then used to measure the thickness of LBL films coated on the substrate. A good linear relationship between the film layers and thicknesses was observed (Fig. 2.7), which is in accordance with previous reports. [29,31] The average thickness of one cycle, i.e., two layers, was estimated to be 2 nm. The thickness of polymer brushes was estimated to be 10 nm for 'grafted to' method and 5 nm for 'grafted from' method. In addition to film growth, the stability of the LBL coatings on a silicon wafer was also tested as shown in Fig. 2.8. Wafers with 5 and 10 cycles of LBL film deposition were soaked in a NaCl solution, the concentration of which is similar to that of seawater (~32 g/L). Samples were taken on a regular basis to track the change in thickness with time. As

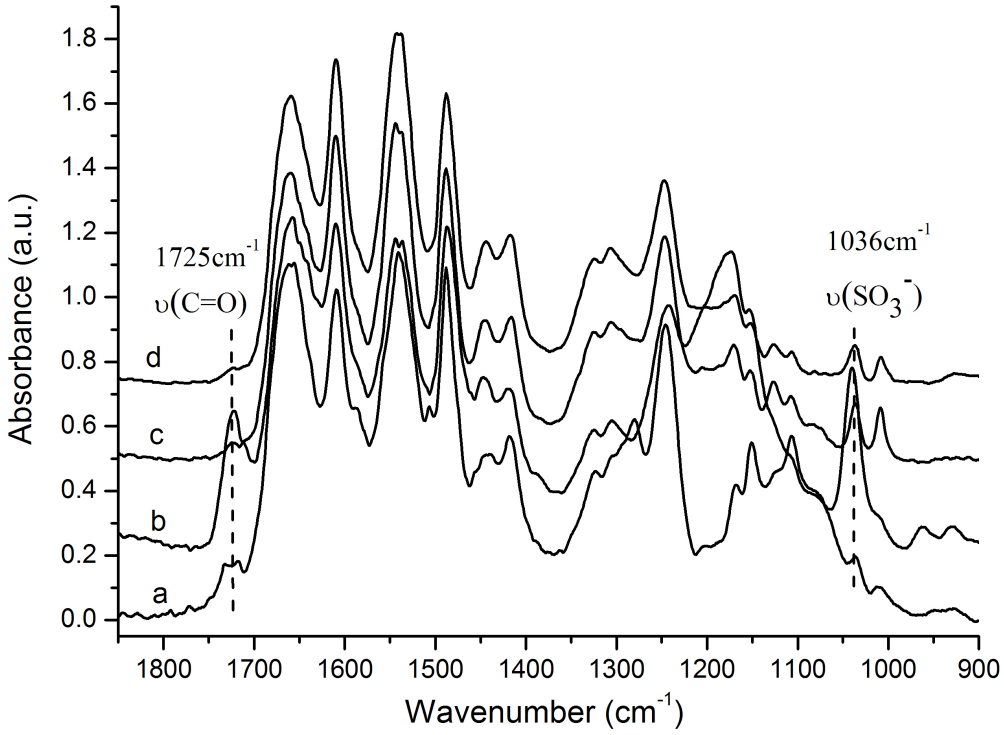

Figure 2.4. Transmission IR spectra of membranes modified with polymer brushes grown through either 'grafted to' or 'grafted from' approaches: a-grafted to_PEGMA; b-grafted to_SBMA; c-grafted from_PEGMA ; d-grafted from_SBMA.

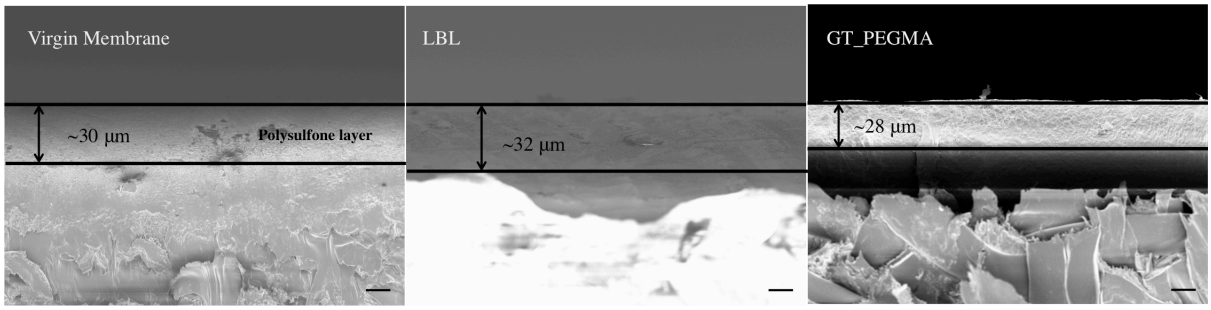

Figure 2.5. SEM images of RO membranes. Left: virgin membrane; Center: membrane modified with LBL film; Right: membrane modified with PEGMA polymer brushes through 'grafted to' approach. Scale bar: 10 µm.

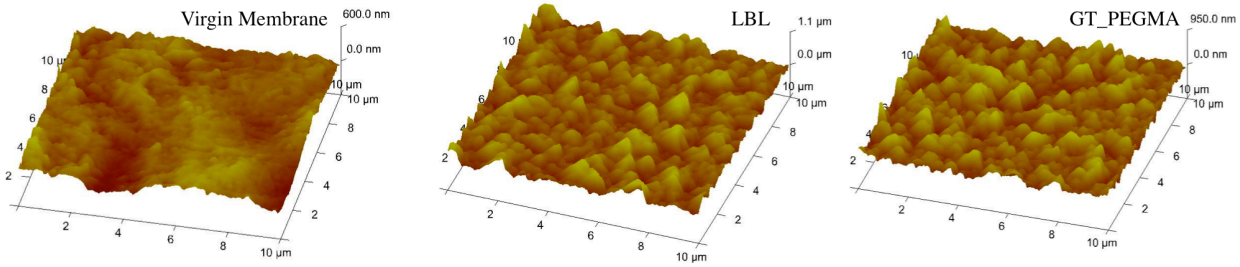

Figure 2.6. AFM images of RO membranes. Left: virgin membrane; Center: membrane modified with LBL film; Right: membran modified with PEGMA polymer brushes through 'grafted to' approach. Average surface roughness ~ 50 nm.

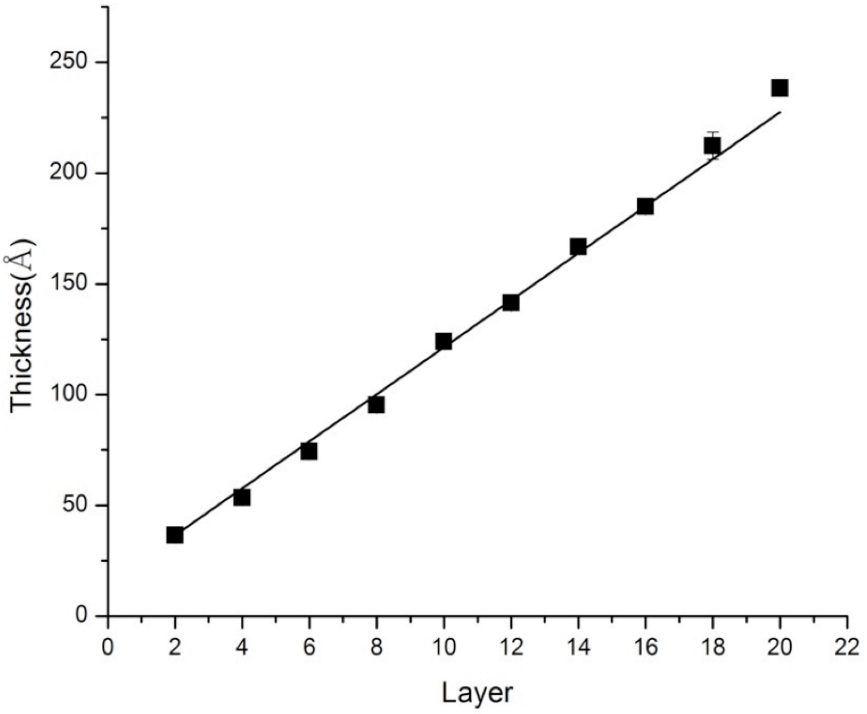

Figure 2.7. LBL film growth on silicon wafers. Linear relationship can be observed between LBL film thickness versus layer numbers.

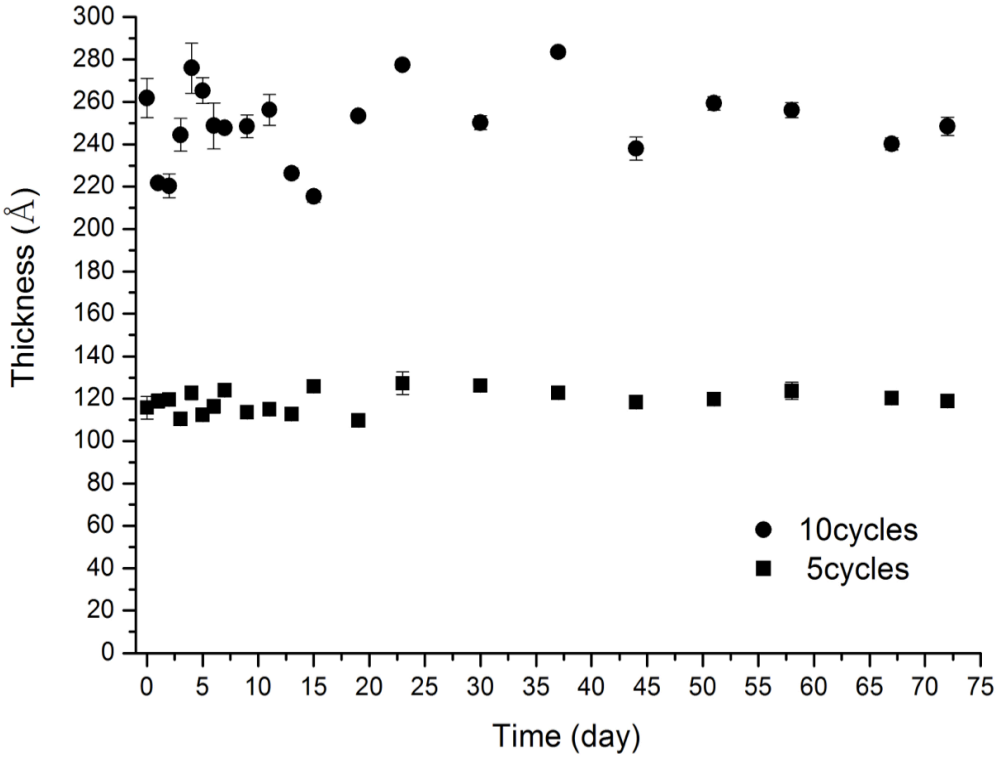

Figure 2.8. Stability test of LBL films on silicon wafers. One cycle refers to one bi-layer applied. Average thickness remains constant through a period of two and a half months.

can be seen from the results, although variations occurred, the average thickness of the LBL films remained constant during the entire testing period, indicating that the LBL films were quite stable on the substrate for at least 74 days.

Membrane performance tests were done to see whether the entire modification process would affect membrane water permeability and salt rejection. Table 2.3 lists some key parameters of the RO membranes before and after modifications. As shown in the table, the pure water permeability did not decrease for membranes with LBL films and polymer brushes grown through the 'grafted to' method, and increased a little bit with polymer brushes grown by the 'grafted from' method. As for the NaCl salt rejection, all modified membranes showed relatively better results than the virgin membrane, possibly due to the extra resistance to permeation from the coatings on the membrane surfaces.

Antifouling tests of the as-modified membranes were first done by static protein adsorption tests. As shown in Fig. 2.9, it is interesting to find that membrane modified with LBL films adsorbed more proteins than the virgin membrane, possibly due to the highly charged surface and enhanced electrostatic interactions between the surface and protein. After polymer brush growth by 'grafted to' method, less BSA was adsorbed, indicating a slight improvement of antifouling properties. Membranes modified with polymer brushes by 'grafted from' method, however, showed significant reduction of protein attachment, constructing much better antifouling surfaces.

In addition to protein adsorption tests, real-time antifouling measurements of the as-modified membrane under normal working conditions were investigated through

Table 2.3. Membrane Performance of the modified membranes. with LBL films and polymer brushes grown through either ‘grafted to’ or ‘grafted from’ approaches.

	Pure Water Flux at 800psi (μm/s)	Pure Water Permeability A (μm/s-MPa)	NaCl Permeate Flux (μm/s)	NaCl Permeability B (10^{-7} m/s)	NaCl Rejection (%)
Virgin	9.68 ± 0.00	1.76 ± 0.00	4.73 ± 0.02	9.51 ± 0.04	96.20 ± 0.03
LBL	9.89 ± 0.00	1.79 ± 0.00	4.96 ± 0.01	3.19 ± 0.04	96.88 ± 0.06
GT_PEGMA	9.86 ± 0.03	1.79 ± 0.01	4.89 ± 0.01	3.96 ± 0.04	96.14 ± 0.06
GT_SBMA	9.65 ± 0.08	1.75 ± 0.00	4.73 ± 0.08	4.41 ± 0.01	95.63 ± 0.07
GF_PEGMA	12.2 ± 0.00	2.22 ± 0.00	3.00 ± 0.00	7.00 ± 0.01	94.57 ± 0.02
GF_SBMA	13.6 ± 0.00	2.47 ± 0.00	3.41 ± 0.00	5.87 ± 0.01	95.86 ± 0.02

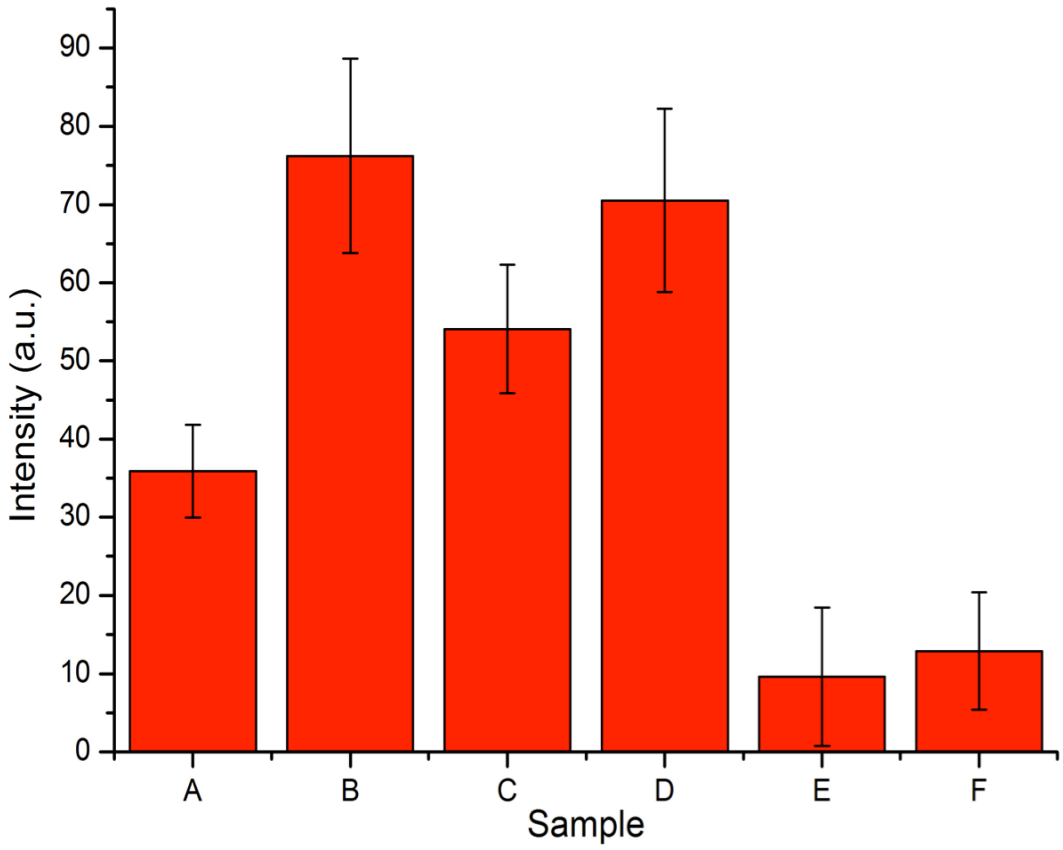

Figure 2.9. Static protein adsorption tests on as-modified membranes: A - virgin membrane; B – membranes with LBL films; C – membranes with PEGMA polymer by ‘grafted to’ method; D – membranes with SBMA polymer by ‘grafted to’ method; E – membranes with PEGMA polymer by ‘grafted from’ method; F – membranes with SBMA polymer by ‘grafted from’ method.

direct observation of the attachment of *H. pacifica* as a function of time. It could be clearly observed from the microscope images that more cells tended to attach onto the virgin membrane than the as-modified membranes (Fig. 2.10). Figure 2.11 showed the quantification plot of the images. It can be seen that results of the real-time antifouling tests were quite different from those of the static adsorption tests. Even from the very start, the untreated membrane has higher bacterial fouling than any of the modified membranes. The number of cells per mm^2 increased about 56% on the untreated membrane during the testing period. Membranes coated with only LBL films and the 'grafted to' PEGMA brushes showed the lowest attachment of bacteria throughout the entire process. Coatings with charged SBMA brushes modified through either 'grafted to' or 'grafted from' approaches also showed excellent antifouling behaviors. Although the neutral 'grafted from' PEGMA coating was not as effective as the others, the cell attachment was still lower than the virgin membrane. Current testing period is relatively short (only 60 min), but simple trend lines indicate that the virgin membrane will probably attract more bacteria than the as-modified membranes in a long run (Fig. 2.11).

It is no surprise that membranes coated with only LBL films exhibited good antifouling properties against certain microorganisms. Recent studies showed that due to high hydrophilicity and low surface roughness, LBL films could be used as good antifouling layers.[39,40] However, static adsorption tests revealed that LBL films could also be easily fouled by other types of foulants such as BSA proteins. Comparing the results between cell attachment and protein adsorption indicates that a single type of surface coatings may not be sufficient to prevent adhesion and growth of a range of

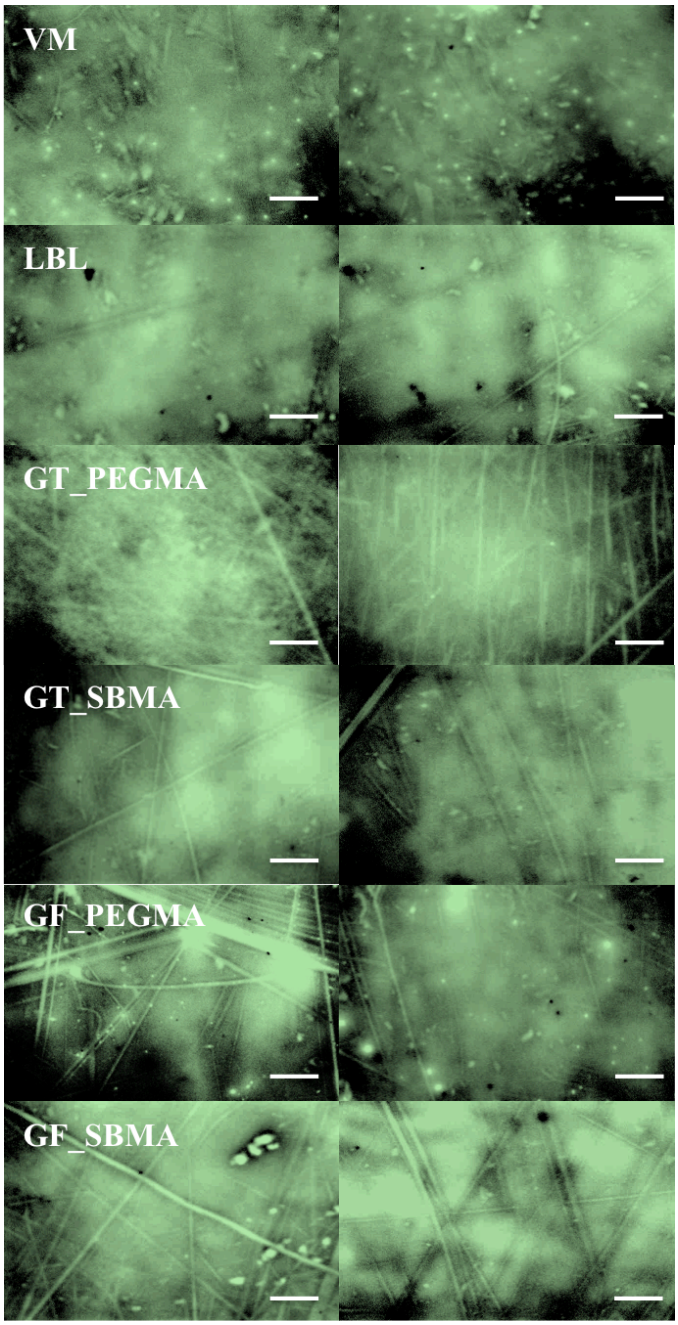

Figure 2.10. Microscope images of cell attachment measurements on membranes modified with LBL films and polymer brushes grown through either 'grafted to' or 'grafted from' approaches. Left -15min; Right - 60min; Bright spots are where the cells are attached. Scale bar: 620 μm.

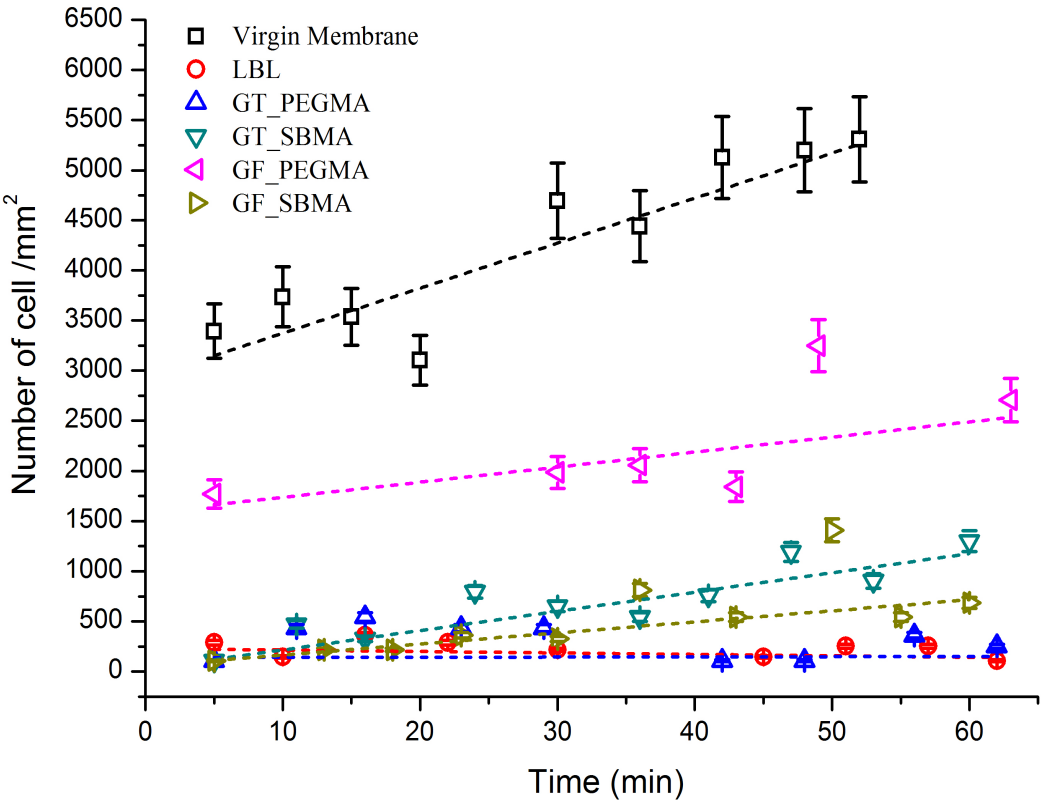

Figure 2.11. Real-time antifouling tests on modified RO membranes. LBL films and polymer brushes grown through different approaches. Membranes modified with LBL films and PEGMA brushes through 'grafted to' method have best behavior.

potential fouling species. It is necessary therefore to build up surfaces with different types of antifouling layers against various kinds of foulants. [41,42] In this report, not only the LBL-film coated membrane showed low cell attachment, but membranes with both neutral PEGMA and charged SBMA polymer brushes were successful, which provides the potential for the modified membranes to be applied in complex biological environments.

2.4 Conclusion

Commercial RO membranes were modified with antifouling polymer brushes by using a 'layer by layer' method. The LBL films not only protected the membranes from potential chemical damage, but also amplified the reaction sites on the membrane surfaces. Detailed studies and surface characterizations by ATR-FTIR and XPS methods showed successful growth of different polymer brushes through the two grafting methods. The LBL coatings also showed a pretty good stability on the membrane surfaces. Although there might be concerns about growing polymer brushes not only on the active polyamide layer, but also on the supporting polyethersulfone and the substrate polyester layers, performance tests showed that pure water flux and salt rejection of the membranes were maintained after all modifications. Moreover, antifouling testing of the attachment of *H. pacifica* on the membrane surfaces exhibited improved antifouling properties of the modified membranes compared to the virgin membrane. Surfaces with different types of antifouling coatings were successfully obtained.

2.5 Acknowledgments

The author is grateful to the Cornell-KAUST research center for financial support (Award No. KUS-C1-018-02), to both the Nanobiotechnology Center (NBTC) and Cornell Center for Materials Research (CCMR), which are supported by National Science Foundation (NSF), for use of their facilities. The author is also grateful to Dr. Héloïse Thérien-Aubin for her help in polymer synthesis, Mavis Wong and Professor Eric Hoek from University of California, Los Angeles for their help in the membrane performace tests.

REFERENCES

(1) Flemming, H. C.; Schaule G.; Griebe T.; Schmitt J.; Tamachkiarowa A. *Desalination* **1997**, *113*, 215-225.

(2) Herzberg, M.; Elimelech, M. *J. Membrane Sci.* **2007**, *295*, 11–20.

(3) Pang, C. M.; Hong, P.; Guo, H.; Liu, W.-T. *Environ. Sci. Technol.* **2005**, *39*, 7541-7550.

(4) Hoek, E. M.V.; Allred, J.; Knoell, T.; Jeong, B.-H. *J. Membrane Sci.* **2008**, *314*, 33–49.

(5) Huang, X.; Guillen G. R.; Hoek E. M. V. *J. Membrane Sci.* **2010**, *364*, 149-156.

(6) Kang, S.-T.; Subramani, A.; Hoek, E. M. V.; Deshusses, M.A.; Matsumoto, M. R. *J. Membrane Sci.* **2004**, *244*, 151–165.

(7) Rana, D.; Matsuura, T. *Chem. Rev.* **2010**, *110,* 2448–2471.

(8) Fristrup, C. J.; Jankova, K.; Hvilsted, S. *Soft Matter* **2009**, *5*, 4623–4634.

(9) Kenawy, E.-R.; Worley, S. D.; Broughton, R. *Biomacromolecules* **2007**, *8*, 1359-1384.

(10) Banerjee, I.; Pangule, R. C.; Kane, R. S. *Adv. Mater.* **2011**, *23*, 690–718.

(11) Ye, S.; Majumdar, P.; Chisholm, Bret.; Stafslien, S.; Chen, Z. *Langmuir* **2010**, *26*, 16455–16462.

(12) Dalsin, J. L.; Hu, B.-H.; Lee, B. P.; Messersmith, P. B. *J. Am. Chem. Soc.* **2003**, *125*, 4253-4258.

(13) Efremova, N. V.; Sheth, S. R.; Leckband, D. E. *Langmuir* **2001**, *17*, 7628–7636.

(14) Caro, A.; Humblot, V.; Méthivier, C.; Minier, M.; Salmain, M.; Pradier, C.-M. *J. Phys. Chem. B* **2009**, *113*, 2101–2109.

(15) Chang, Y.; Liao, S.-C.; Higuchi, A.; Ruaan, R.-C.; Chu, C.-W.; Chen, W.-Y. *Langmuir* **2008**, *24*, 5453–5458.

(16) Chen S.; Li, L.; Zhao, C.; Zheng, J. *Polymer* **2010**, *51*, 5283-5293.

(17) Sun, Q.; Su, Y.; Ma, X.; Wang, Y.; Jiang, Z. *J. Membrane Sci.* **2006**, *285*, 299–305.

(18) Jan, G.; Kirill, E. *Biofouling* **2006**, *22*, 339-360.

(19) Yebra, D. M.; Kiil, S.; Dam-Johansen, K. *Prog. Org. Coat.* **2004**, *50*, 75–104.

(20) Callow, J. A.; Callow, M. E. *Nat. Commun.* **2011**, *2*, 244.

(21) Gudipati, C. S.; Greenlief, C. M.; Johnson, J. A.; Prayongpan, P.; Wooley, K. L. *J. Polym. Sci. Part A-Pol. Chem.* **2004**, *42*, 6193-6208.

(22) Cho, Y.; Sundaram, H. S.; Weinman, C. J.; Paik, M. Y.; Dimitriou, M. D.; Finlay, J. A.; Callow, M. E.; Callow, J. A.; Kramer, E. J.; Ober, C. K. *Macromolecules* **2011**, *44*, 4783-4792.

(23) Finlay, J. A.; Krishnan, S.; M. E.; Callow, J. A.; Dong, R.; Asgill, N.; Wong, K.; Kramer, E. J.; Ober, C. K. *Langmuir***, 2008**, *24*, 503–510.

(24) Belfer, S.; Purinson, Y.; Fainshtein, R.; Radchenko, Y.; Kedem, O. *J. Membrane Sci.* **1998**, *139*, 175-181.

(25) Sagle, A. C.; VanWagner, E. M.; Ju, H.; McCloskey, B. D.; Freeman, B. D.; Sharma, M. M. *J. Membrane Sci.* **2009**, *340*, 92–108.

(26) Lin, N. H.; Kim, M.; Lewis, G. T.; Cohen, Y. *J. Mater. Chem.* **2010**, *20*, 4642-4652.

(27) Kang, G.; Liu, M.; Lin, B.; Cao, Y.; Yuan, Q. *Polymer* **2007**, *48*, 1165-1170.

(28) Thérien-Aubin H.; Chen, L.; Ober, C. K. *Polymer* **2011**, *52*, 5419-5425.

(29) Decher, G.; *Science* **1993,** *277*, 1232-1237.

(30) Hammond, P. T. *Adv. Mater.* **2004**, *16*, 1271-1293.

(31) Bertrand, P.; Jonas, A.; Laschewsky, A.; Legras, R. *Macromol. Rapid Commun.* **2000**, *21*, 319–348.

(32) Peyratout, C. S.; Dähne, L. *Angew. Chem. Int. Ed.* **2004**, *43*, 3762-3783.

(33) Naidu, B. N.; Sorenson, M. E.; Connolly, T. P.; Ueda, Y. *J. Org. Chem.* **2003**, *68*, 10098-10102.

(34) Deshrnukh, S. S.; Childress, A. E. *Desalination* **2001**, *140*, 87-95.

(35) Sja, N. K.; Joshi, S. V. *J. Membrane Sci.* **2009**, *342*, 60-69.

(36) Yang, J. C.; Jablonsky, M. J.; Mays, J. W. *Polymer* **2002**, *43*, 5125–5132.

(37) Ishigami T.; Amano, K.; Fujii, A.; Ohmukai, Y.; Kamio, E.; Maruyama, T.; Matsuyama, H. *Sep. Purif. Technol.* **2012,** *99*, 1-7.

(38) Wong, S. Y.; Han, L.; Timachova, K.; Veselinovic, J.; Hyder, M. N.; Ortiz, C.; Klibanov, A. M.; Hammond, P. T. *Biomacromolecules* **2012**, *13*, 719−726.

(39) Sundaram, H. S.; Cho, Y.; Dimitriou, M. D.; Finlay, J. A.; Cone, G.; Williams, S.; Handlin, D.; Gatto, J.; Callow, M. E.; Callow, J. A.; Kramer, E. J.; Ober, C. K. *ACS Appl. Mater. Interfaces* **2011**, *3*, 3366–3374.

(40) Cho, Y.; Sundaram, H. S.; Finlay, J. A.; Dimitriou, M. D.; Callow, M. E.; Callow, J. A.; Kramer, E. J.; Ober, C. K. *Biomacromolecules* **2012**, *13*, 1864−1874.

CHAPTER THREE:

FABRICATION OF POLYARAMIDE MEMBRANES WITH ANTIFOULING COATINGS*

* Portions of the chapter were adapted from the article "Fouling-resistant polymer brush coatings". Héloïse Thérien-Aubin, Lin Chen and Christopher K. Ober. *Polymer* **2011**, *52*, 5419.

3.1 Introduction

Biofouling is a serious problem occurring on almost any system exposed to a marine environment. During the last few decades much effort has been spent on developing highly efficient bio-friendly antifouling coatings for membranes and other surfaces. [1-4] These coatings have been designed to efficiently inhibit the settlement of algae and bacteria on the treated surfaces (fouling-resistant coatings) and/or provide weak foulant/surface adhesion so that the foulant can be easily washed off (fouling-release coatings). Traditional antifouling coatings for biomedical studies are usually composed of highly hydrophilic polymers such as polyethylene glycol (PEG) [5, 6] or zwitterionic polymers. [7-9] Recent work has been focused on both fouling-resistant coatings and fouling-release coatings. A fouling-resistant coating inhibits the settlement of the substrate surface by protein, algae or bacteria due to their strong interaction with water molecules, while a fouling-release coating has a low surface energy so that the foulant can be easily washed off with the application of a limited shear force.

Due to their exceptional mechanical properties, good thermal resistance and chemical stability, polyaramides are widely used as the selective material in the preparation of separation membranes such as ion exchange, [10] gas permeation, [11] nanofiltration [12] and reverse osmosis membranes. [13] However, significant biofouling is always a severe problem occurring on surfaces of the membranes, restricting the performance of the purification process. [14-16] In order to prevent surface fouling problems, a variety of modification methods have been introduced and explored. Neutral polymers such as polyvinyl alcohol (PVA) are simply deposited and non-

covalently bound to the commercially used membrane surfaces. [17] A high degree of functionalization of the membranes with antifouling reagents has been achieved using redox or plasma initiated grafting from polymerization processes. [18-20] Reactions on dangling amine or acid groups on the polyaramide membranes have also been developed to introduce antifouling functionalities. [21, 22]

In the present work, functional groups are first introduced in the polyamide building blocks during the fabrication of the polyaramide membranes to act as potential post-polymerization grafting sites for growth of polymer brushes. Poly(methacrylic acid) (PMAA) brushes are then grown from those sites using a surface initiated-atom transfer radical polymerization (SI-ATRP) process. Finally, a variety of side-chains such as perfluorinated and PEG side chains are reacted onto the brushes to fine-tune the antifouling properties of the membranes with either fouling-resistant or fouling-release surfaces.

3.2 Experimental

3.2.1 Materials

3,5-Diaminobenzoic acid, 2-bromo-2-methylpropionyl bromide, ethyl-2-bromo-2-methylpropionate, 1,3-dicyclohexylcarbodiimide (DCC), anhydrous triethylamine (TEA), 4-(dimethylamino) pyridine (DMAP), di-tert-butyldicarbonate (Boc_2O), m-phenylene diamine (MPD), trimesoyl chloride (TMC), sodium methacrylate, copper (I) bromide, copper (II) bromide, 2,2'-bipyridine (Bipy), polyethylene glycol monomethyl ether (PEG), Zonyl FSO-100^{TM} (a PEGylated fluoroalkyl surfactant),

1H,1H-perfluoro-1-nonanol (C9F17), chlorohydroxypropyltrimethyl ammonium chloride (QA) and polydimethylsiloxane monohydroxy terminated (PDMS) were purchase from Sigma Aldrich and used as received except for methacrylic acid (purified over an alumina column) and copper (I) bromide (washed with glacial acetic acid). Solvents were purchased from Fisher Chemical and used as received with the exception of THF that was refluxed and distilled over sodium and benzophenone.

3.2.2. Monomer Synthesis

Bromoisobutoxyethyl-3,5-diaminobenzoate or Br-MPD (1) was synthesized as follows (Scheme 3.1): 10 g of 3,5-diaminobenzoic acid was reacted with 43 g of Boc_2O in 350 mL of THF in presence of 27.5 mL of TEA, the reaction mixture was stirred at 70 ^oC for 16 h. The solvent was evaporated and the crude product was re-dissolved in ethyl acetate and extracted with a 0.2 M HCl solution, a 0.2 M $NaHCO_3$ solution and finally with brine. The organic phase was dried over magnesium sulfate and evaporated. The remaining product was then purified with a silica gel column with hexane/ ethyl acetate (2:3) as eluent. Yield = 94%. ^1H NMR [$CDCl_3$] 1.47 (s, 18H), 7.7 (s, 1H), 8.3 (m, 2H).

10 g of the resulting Boc protected 3,5-diaminobenzoic acid was esterified with ethylene glycol (100 mL) in dry THF (400 mL) in presence of 8.8 g of DCC, 2.1 g of DMAP and 0.8 mL of TEA under reflux for 8 h. After solvent evaporation, the resulting Boc protected 3,5-diaminobenzoate ethylene glycol ester was purified by extraction between dichloromethane and 0.2 M HCl, the organic phase was then washed with brine and dry with $Mg(SO_4)_2$. The crude product obtained was then

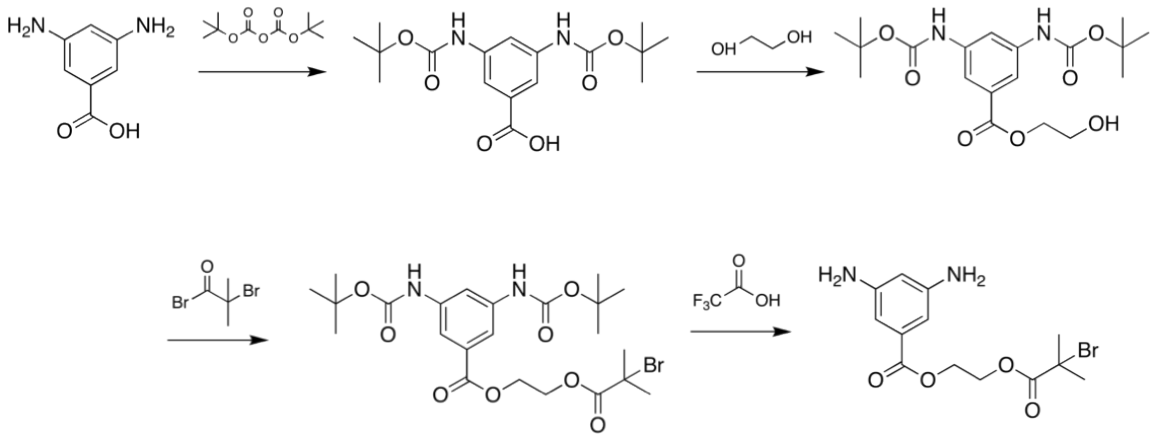

Scheme 3.1. Monomer synthesis of Br-MPD through the protection, esterification, halogenation and deprotection reactions.

further purified with a silica gel column with hexane/ethyl acetate (2:3) as eluent. Yield = 87%. ^{1}H NMR [$CDCl_3$] 1.5 (s,18H), 3.8 (m, 2H), 4.2(m, 2H), 7.6 (m, 1H), 8.0 (m, 2H).

The ATRP initiating group was introduced when 6.3 mL of 2-bromo-2-methylpropionyl bromide was added drop-wise to a solution of 10 g of Boc-protected 3,5-diaminobenzoate ethylene glycol ester in 250 mL of anhydrous dichloromethane containing 4.1 mL of pyridine and 0.77 g of DMAP. The solution was then agitated at room temperature for 18 h. The dichloromethane was then washed with a 0.2 M solution of $NaHCO_3$ followed by 0.2 M HCl and finally brine, the organic phase was dried with anhydrous $Mg(SO_4)_2$ and evaporated. The crude product obtained was then further purified with a silica gel column with hexane/ethyl acetate (1:1) as eluent. Yield = 98%. ^{1}H NMR [$CDCl_3$] 1.6-1.8 (m, 24H), 4.4 (m, 4H), 7.7 (m, 1H), 8.1 (m, 2H).

Finally, the deprotection of the amine groups was carried out by dissolving 10 g of Boc-protected bromoisobutoxyethyl 3,5-diaminobenzoate in 200 mL of DCM, 50 mL of trifluoroacetic acid was then added and the solution was agitated at room temperature for 4 h. The bromoisobutoxyethyl-3,5-diaminobenzoate was purified by multiple extractions with $NaHCO_3$ 0.2 M and dried with $Mg(SO_4)_2$ and the solvent evaporated. The product obtained was then purified with an alumina gel column using hexane/ethyl acetate (1:3) as eluent. Yield = 68%. ^{1}H NMR [$CDCl_3$] 1.9 (s, 6H), 4.4 (m, 4H), 7.0 (m, 1H), 7.4 (m, 2H).

3.2.3 Membrane Casting

A polysulfone membrane (PS-20 from Sepro Membrane) was soaked in a 3.4% wt aqueous solution of MPD for 2 min and dried with an air-knife. The membrane was then soaked in a 0.15% wt solution of TMC in hexane for 1 min, and dried for 2 min. After that, the membrane was soaked in a 5% wt solution of Br-MPD in diethyl ether (or in plain diethyl ether for "regular" polyamide standard) for 30 s and dried with an air-knife. The polymerization of the polyamide layer was then promoted by curing the membrane in 95 ^{o}C DI water for 2 min. Afterwards, the membrane was washed for 2 min with a 200 ppm aqueous solution of sodium hypochlorite, followed by 30 s immersion in a 1000 ppm sodium bisulfite solution. The result is a polyamide layer physically tethered to the porous polysulfone support membrane (Scheme 3.2).

3.2.4 Polymer Brush Growth

The surface-initiated ATRP polymerization was carried out on a 50 cm^2 membrane; 1 g of sodium methacrylate was dissolved in water (50 mL) the pH of the solution was adjusted to 9.0 with NaOH (0.05 N). The mole ratio of CuBr/$CuBr_2$/Bipy/monomer used during polymerization was 1:0.1:2.2:100. After a polymerization time of 18 h, the membrane was removed from the solution, washed with 0.01 N HCl and cleaned by soxhlet extraction with water for 24 h.

3.2.5 Brush Functionalization

The esterification of methacrylic acid brushes was carried out by immersing a piece of 50 cm^2 of membrane in 50 mL of anhydrous acetonitrile with 17 mg of DCC, 3 mg of DMAP and an excess of alcohol (or a mixture of alcohol in the case of the

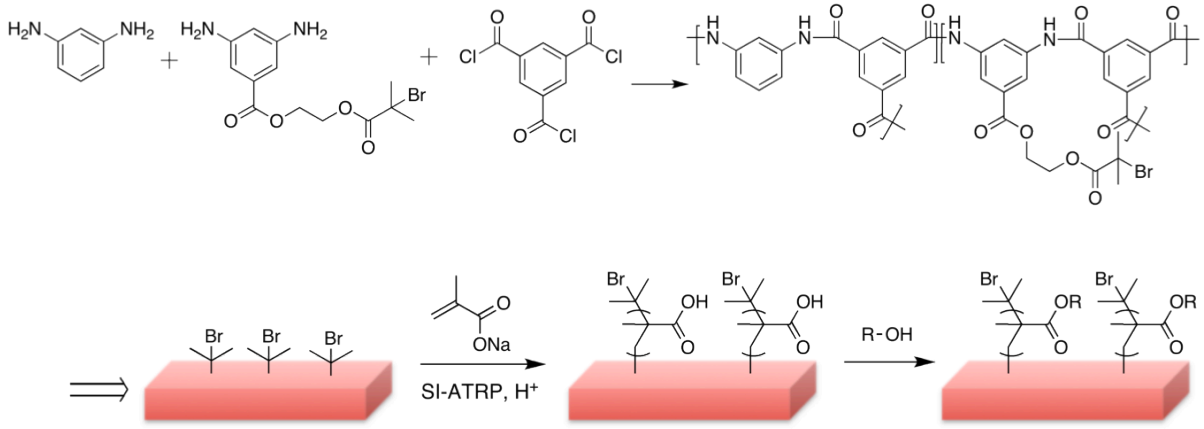

Scheme 3.2. Fabrication and functionalization of polyaramide membranes through surface-initated polymerization reaction and esterification reactions of the side chains.

C9F17/PEG 1:1 membrane). The membrane was cleaned by soxhlet extraction with acetonitrile for 24 h (Scheme 3.2).

3.2.6 Membrane Characterizations

XPS experiments were carried out on Surface Science Instruments (SSI) model SSX-100. ATR-FTIR experiments were carried out on a Nicolet iZ-10 instrument equipped with a diamond ATR crystal. Contact angle were measured using a Rame-Hart 100-00 contact angle goniometer. SEM images where obtained on a Keck LEO 1550 FESEM. Membrane roughness was measured using a Veeco Dimension 3100 AFM in tapping mode. Thicknesses were measured on a Nanofilm EP3 ellipsometer after dissolution of the polysulfone support layer in THF. Protein absorption tests were realized by immersing the membrane in a 0.5 g/L solution of FITC-BSA in 0.1 M phosphate buffer at pH 7.4 containing 3.5% of NaCl for 48 h; the amount of protein bounded to the membrane was evaluated by the signal intensity obtained by fluorescence microscopy. Protein release tests were conducted by blasting a water stream with an incoming pressure varying between 0 and 100 psi on the membrane with an incident angle of 15^{o} and measuring the decrease in the fluorescence of the BSA.

3.3 Results and Discussion

Table 3.1 shows the composition and hydrophilicity of the membrane surfaces before and after modification. An amount of 0.35 atomic % of bromine atoms on the Br-polyamide membrane surface confirmed the successful introduction of the ATRP

Table 3.1. Surface properties of the membranes. Calculated degree of substitution, measured water contact angle, surface roughness and XPS analysis.

Membrane	**Subs.** (%)	θ_w (°)	R_a (nm)	**Composition (XPS)**			
				N/C	O/C	Br/C	F/C
Polyamide	-	66 ± 4	43 ± 5	0.09	0.20	-	-
Br-Polyamide	-	55 ± 2	52 ± 4	0.07	0.16	4e-3	-
PMAA	-	37 ± 3	51 ± 5	0.04	0.25	2e-3	-
PEG	90 ± 6	35 ± 3	49 ± 4	0.03	0.26	3e-4	-
C9F17	98 ± 2	70 ± 7	43 ± 5	0.03	0.17	4e-4	0.12
Zonyl	82 ± 10	43 ± 5	48 ± 7	0.04	0.25	3e-4	0.06
QA	87 ± 6	40 ± 4	49 ± 6	0.09	0.20	2e-4	-
PDMS	85 ± 4	74 ± 6	47 ± 5	0.04	0.21	-	-
PEG/C9F17	93 ± 6	42 ± 7	47 ± 5	0.04	0.28	5e-5	0.04

Subs.: degree of substitution measured by FTIR;

θ_w: water contact angle;

R_a: Average surface roughness;

initiator during the fabrication of the membrane. After the polymerization of the sodium methacrylate, the membranes were washed in slightly acidic conditions to produce poly(methacrylic acid) brushes. XPS analysis also shows an increase in the O(1 s) signal at 529 eV indicative of the presence of the acid groups at the surface. In addition, no typical signals of Na (2 s) at 63 or (1 s) at 1070 eV were observed, confirming the complete conversion of the surface functional groups from acetate to acid. A decrease of water contact angle from 55^{o} to 37^{o} indicates a more hydrophilic surface after the acid conversion. To further control and modify the surface properties of the membrane, the esterification of the PMAA brushes was realized with different alcohols, providing a variety of functional groups as side-chains such as polyethylene glycol (PEG), perfluorinated alkane (C9F17), quaternary ammonium (QA), poly(dimethylsiloxane) (PDMS), amphiphilic (Zonyl) or a equimolar mixture of poly(ethylene glycol) and perfluorinated alkane (PEG/C9F17 1:1).The appearance of fluorine atoms and variations of surface compositions after functionalization of PMAA with different side chains confirmed successful esterification reactions between the acids and alcohols. Changes of water contact angle, e.g. an increase to 70^{o} and 74^{o} for C9F17 and PDMS respectively, also indicate different surface hydrophilicity after side-chain functionalization.

ATR-FTIR spectra were measured to further confirm and quantify the extent of the brush functionalization. In the ATR-FTIR spectra of the modified membranes, most of the relevant information below 1800 cm^{-1} is hidden by the overwhelming polysulfone peaks (1500 and 1600 cm^{-1}) (Figure 3.1A). If the polysulfone is carefully dissolved, a transmission spectrum of the thin polyamide layer could be obtained, thus revealing

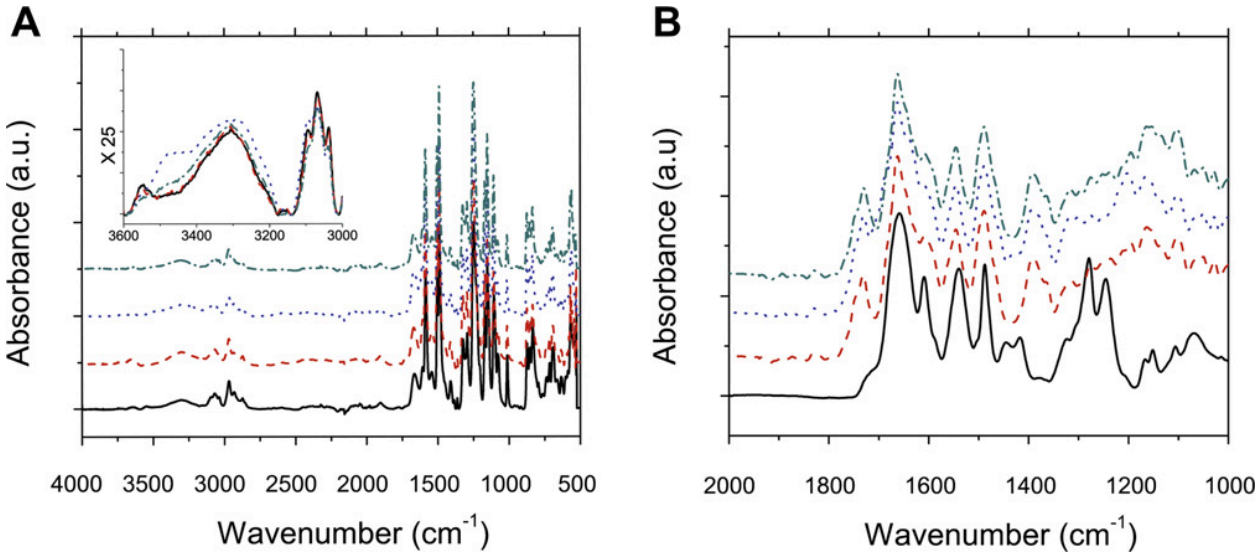

Figure 3.1. FTIR spectra of as-modified membranes. A) ATR-FTIR of the membranes and B) Transmission FTIR spectra of polyamide layers. Unmodified polyaramide (—), Br-polyaramide (----), Br-Polyaramide + PMAA brushes (••••) and Br-Polyaramide + PMAA + PEG side chains (-••-•).

spectral features (Figure 3.1B) in keeping with the membrane modification. the Br-polyamide has a carbonyl stretching peak at 1733 cm^{-1} attributed to the two ester linkages in the Br-MPD monomer. After the poly(methacrylic acid) brush polymerization, a clear shoulder appears in the carbonyl region at 1689 cm^{-1} attributed to the C=O stretching of the acid function. After the functionalization with PEG side-chains, the ether C-O stretching peak is observed at 1147 cm^{-1}. Degrees of side-chain substitutions can be calculated as follows:

$$\text{Sub}\ (\%) = \ 100 \times \left(1 - \frac{A_3 - A_1}{A_2 - A_1}\right) \qquad \textbf{Equation 3.1}$$

where A is the area of the O-H/N-H stretching peak at ca. 3300 cm^{-1} and the subscript 1, 2, and 3 represent the Br-polyamide membrane, the PMAA brush membrane, and the functionalized membrane respectively. The degree of substitution (Table 3.1) varies from 82% in the case of the bulky Zonyl ^{TM} side-chains to 98% in the case of the perfluoroalkane C9F17 side-chains, the degree of substitution of the other side-chains varying between those two limits.

The membranes have similar morphologies (Figure 3.2) and roughness (R_a ~ 40-55 nm, Table 3.1) before and after functionalization. However, the Br-polyamide membrane has a thicker polyamide layer, as measured by ellipsometry, of 115 nm in comparison with 95 nm in thickness for the unmodified polyamide membrane. To determine the grafting density of the polymer brushes, free ATRP initiator was added to the polymerization reaction and the molecular weight (Mn) of the free polymer was quantified by NMR. Assuming that the molecular weight of the free polymer is the same as the surface tethered brushes, the grafting density (σ) was estimated using [23]:

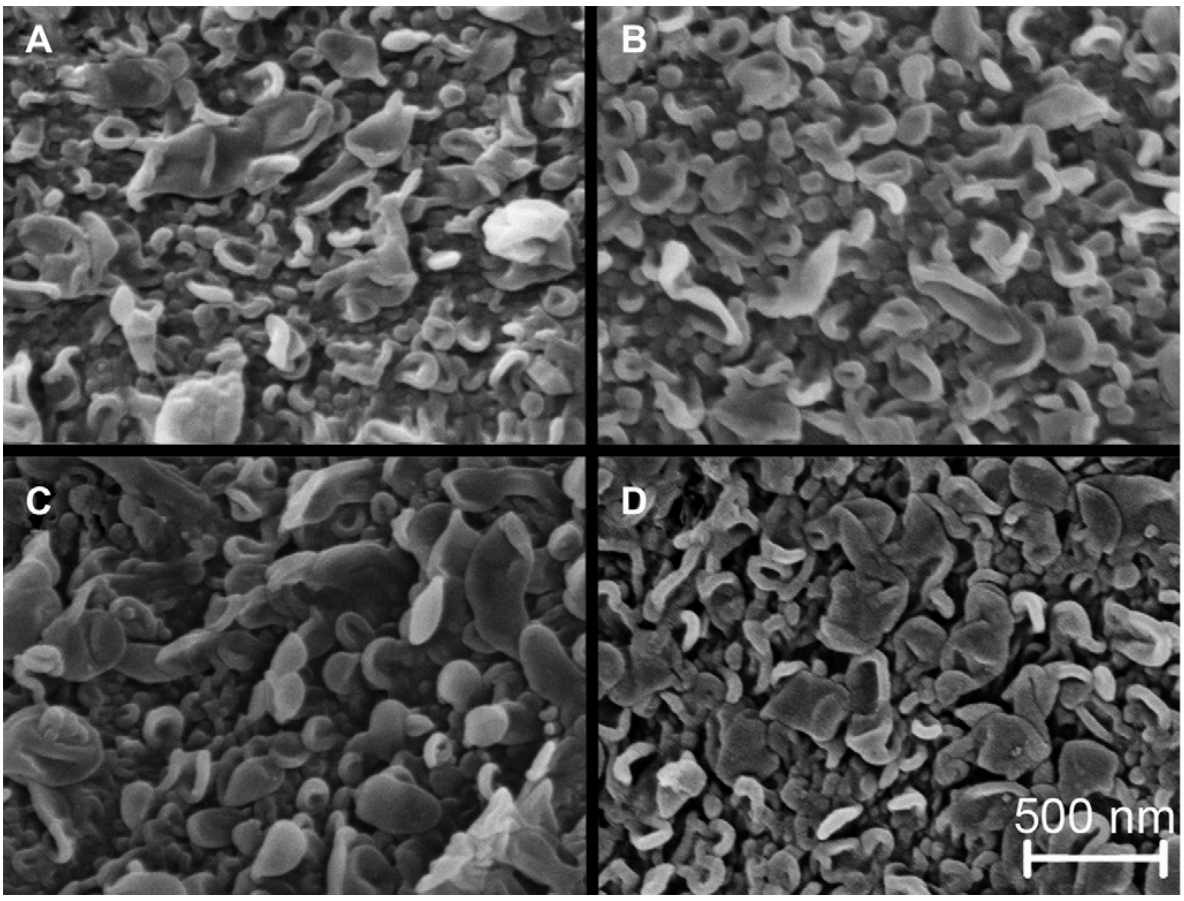

Figure 3.2. SEM images of the membrane surfaces: A) Regular Polyaramide; B) Br-Polyaramide; C) Br-Polyaramide + PMAA brushes; D) Br-Polyaramide + PMAA + PEG side chains.

$$\sigma = \frac{h\rho N_A}{M_n} \qquad \textbf{Equation 3.2}$$

where h is the thickness measured by ellipsometry, N_A the Avogadro number and ρ the estimated density of the PMAA layer (1.05 g/cm^3). After the polymerization, the membrane is covered by a 27 nm thick layer of polymethacrylic acid, with an average grafting density of 0.44 chains/nm^2, leading to uniform coverage of the membrane with the polymer brush. As observed in Fig. 3.3, a decrease in the polymerization rate after 6 h is observed and could be attributed to a termination reaction leading to limited polymer brush growth after that point.

The long-term stability of those coatings was also quantified over a two months period by the immersion of the modified membranes in water solution at pH 3 and 11 (Fig. 3.4). Polyacrylic acid ester was used as a comparison. As is shown, less than ±2^o of variation of the surface contact angle is observed for methacrylic acid ester, while significant change, up to a variation of 35^o in basic conditions, is observed with polyacrylic acid ester, which indicates that no significant hydrolysis of the various side-chains occurred with the methacrylic esters. The methacrylic acid ester brushes are more stable than the acrylic acid ester possibly due to the steric hindrance created by the methyl group on the backbone, limiting the hydrolysis. All the fouling experiments were realized with membranes modified by methacrylate ester brushes to avoid any bias created by the hydrolysis of the side chains.

In order to get a better understanding on the antifouling properties of the membranes with different functional groups, bovine serum albumin (BSA) was used

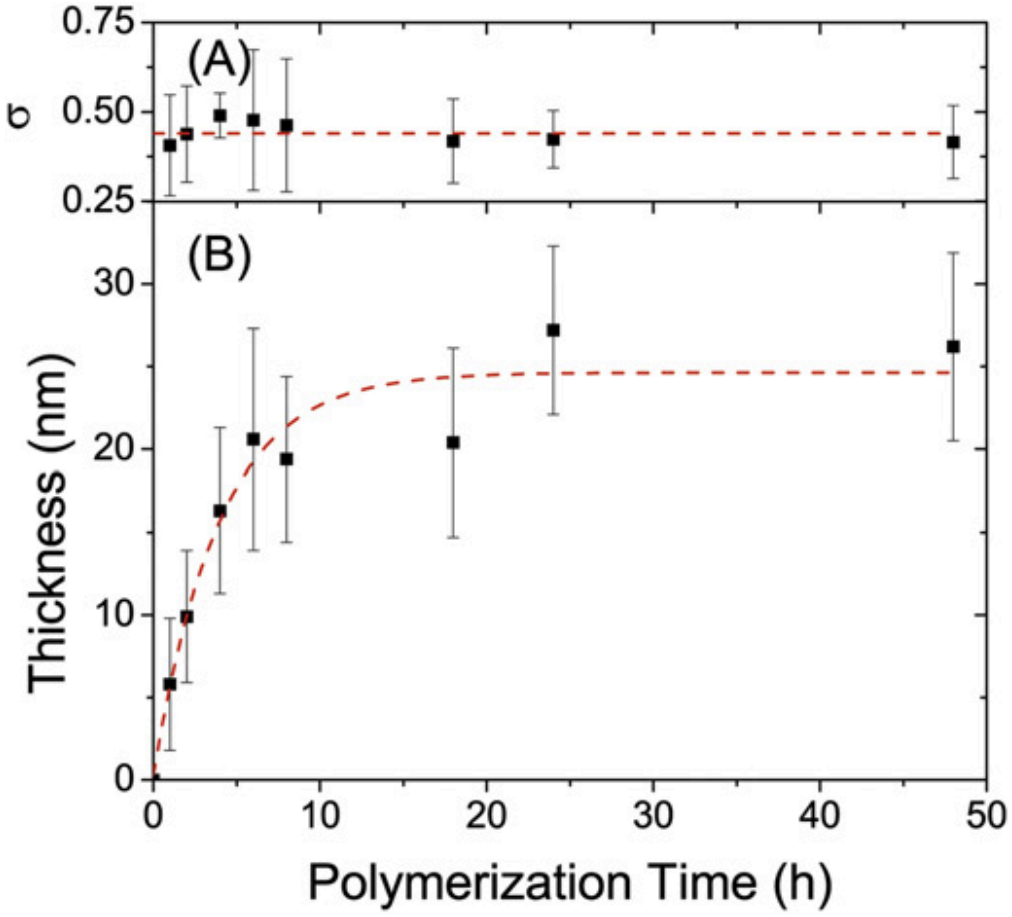

Figure 3.3. Polymerization of PMAA brushes as a function of time. A) Grafting density; B) Brush thickness. Grafting density keeps the same while brush thickness reaches maximum after 10 hours reaction time.

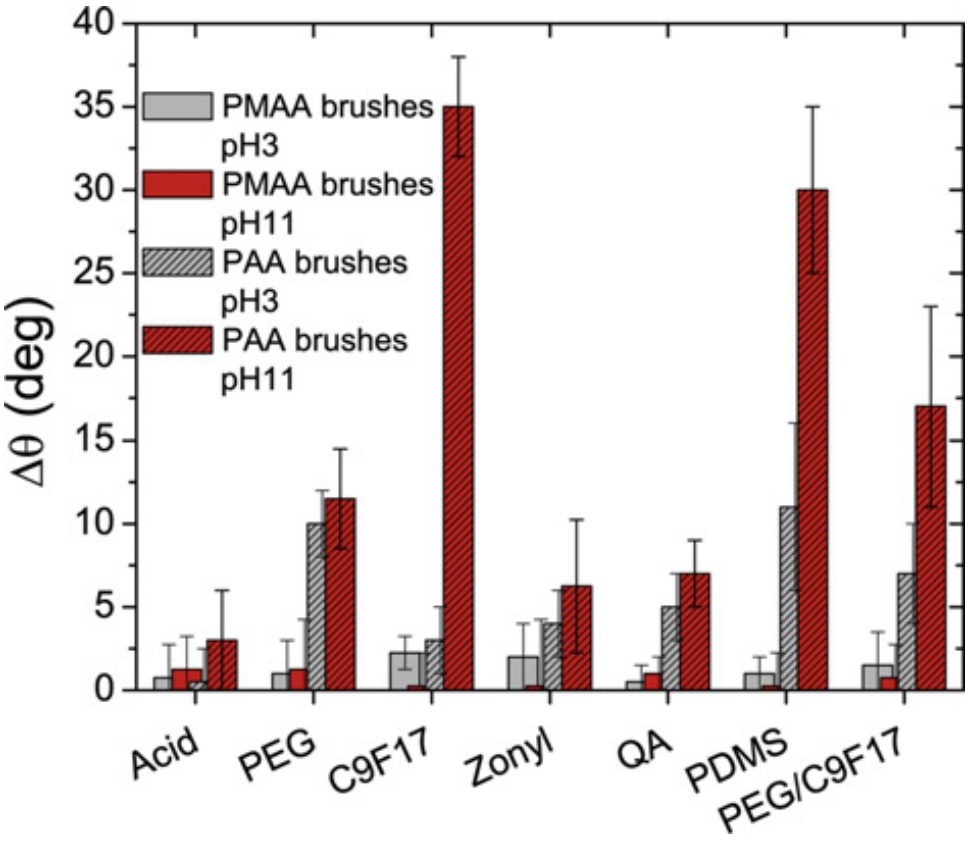

Figure 3.4. Stability of the side-chains after 2 months immersion in a solution of NaCl 0.55 M. Functional groups from left to right: Acid, PEG, C9F17, Zonyl, Quaternary ammonium, PDMS and PEG/C9F17 mixture.

as a model foulant for the antifouling tests. Both of the fouling-resistant and fouling-release characteristics of the polyaramide membranes were evaluated. The fouling-resistant behavior was evaluated by the fluorescence intensity of the fluorescently labeled BSA adsorbed to the membrane after an immersion of 48 h in the absence of flow. While the fouling-release property was measured by exposing a fouled piece of membrane to a controlled tangential flow creating a predetermined shear stress (s) generated by a jet of pressurized saline solution. The shear force on the membrane was estimated as:

$$\tau = \frac{F\sqrt{2\rho P cos(\theta)}}{A} \qquad \textbf{Equation 3.3}$$

where F is the flow and ρ the density of the washing solution, P the pressure of the solution jet, q the angle of incidence of the jet and A the area of membrane washed with the jet.

The different surface compositions result in very different adsorption and release of BSA on the membrane. The protein binding study allows one to get new insights concerning the settlement of biomaterial and the colonization of the membrane. Typically, it is widely accepted that the more hydrophilic a surface is the lower the fouling is, [9, 24] which is also observed in our case (Fig. 3.5). Protein binding decreases with the increase of hydrophilicity of the membrane. The fouling on the hydrophobic coatings (PDMS, C9F17) increases by a factor of two in comparison to the native polyamide membrane, while in the case of the hydrophilic coating like PEG, a 70% decrease in protein adsorption is obtained. Those results imply that the fouling-

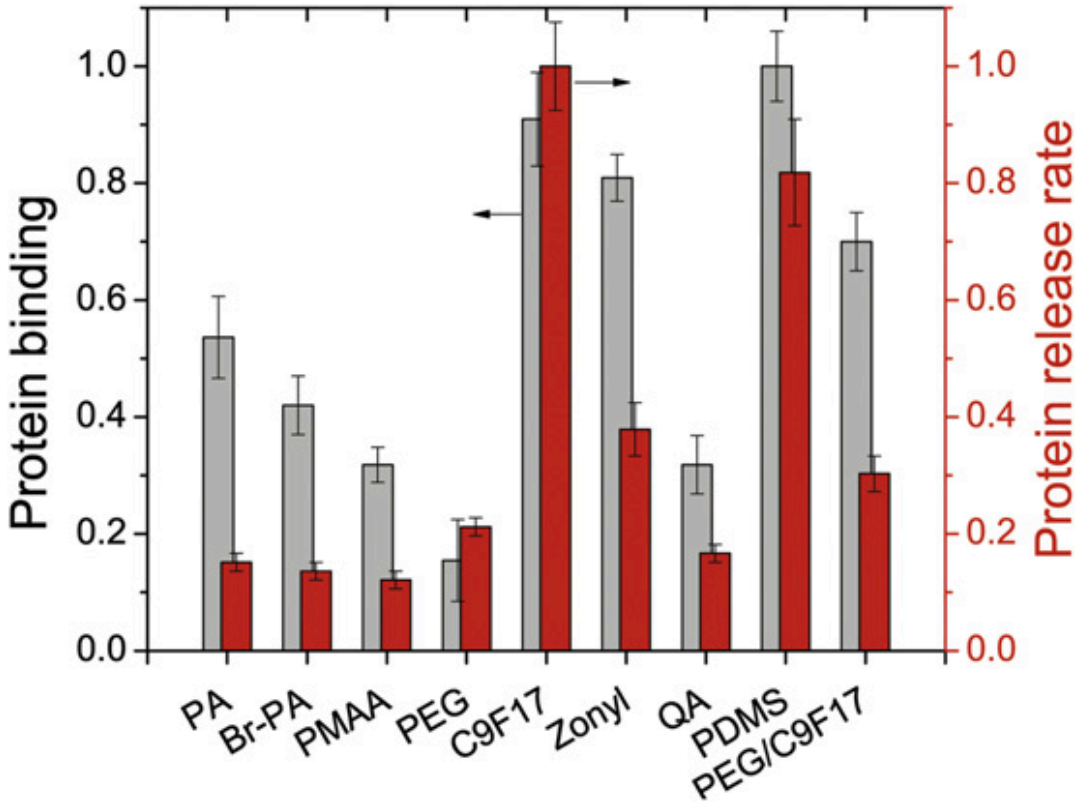

Figure 3.5. Protein binding and release from the membrane. Functional groups from left to right: Acid, PEG, C9F17, Zonyl, Quaternary ammonium, PDMS and PEG/C9F17 mixture.

resistant behavior of the membrane is related to the ability of the coating to coordinate water molecules on its surface. Settlement of bio-foulants such as BSA is easier to occur on more hydrophobic surfaces, of which the hydration energy is not high enough to prevent the displacement of the water molecules with foulants as observed for other systems. [9, 25]

Fouling-release properties of the as-modified membranes were measured by using a water jet system, varying the pressure of the jet and thus the shear force at the surface of the membrane. The release observed (Fig. 3.6) increases with the shear force at the interface, and varied significantly with the chemical composition of the surface coating. The release curves were used to measure the protein release rate of each membrane, (Fig. 3.5) which corresponds to the self-cleaning potential of each membrane. The membrane with PDMS and perfluoroalkane C9F17 side-chains showed the highest release rate, while the unmodified membrane, the membrane with the unsubstituted PMAA brushes and the membrane with quaternary ammonium side-chains showed low release (less than 8%) at the highest shear force used, indicative of the limited self-cleaning potential of those membranes. The results obtained show that the lower the surface energy, the higher the self-cleaning potential of the membrane, i.e. the higher the protein release; the release rates of the low surface energy coatings (PDMS and perfluoroalkane C9F17) are 5-fold what is observed with the unmodified membrane. Therefore, it is reasonable to suggest that if a foulant (protein or bacteria) does deposit on the membrane, when there is a weak adhesion force between the membrane and the foulant, for example, with C9F17 side-chains, the shear force

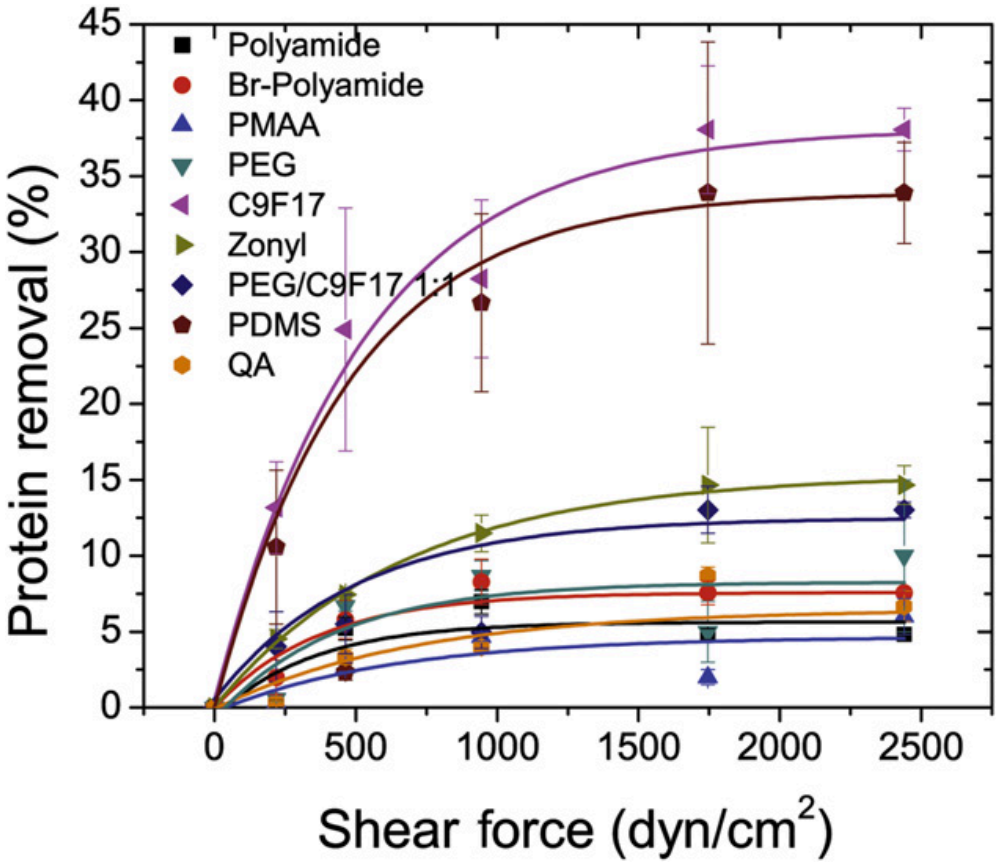

Figure 3.6. Protein release from the membrane after application of a tangential force. Polymer brushes with functional grouos of C9F17 and PDMS release the most adsorbed proteins.

created by tangential water flow will clean the membrane, in keeping with results obtained for other modified surfaces. [26, 27]

3.4 Conclusion

Antifouling functional polyaramide membranes were successfully fabricated followed by modification of the surface by SI-ATRP of poly(methacrylic acid) brushes. A Br-substituted polyamide is an efficient way to chemically tether polymer brushes to the membrane using controlled living polymerization. The results demonstrated a control over the thickness of the polymer brushes and a high grafting density. The composition of the brush coating determined the characteristics of the surface and could be modified through esterification with different functional groups. The esterified brushes were stable toward hydrolysis for a relatively long period of time.

The fouling by bacteria was correlated with the adsorption and release of protein on the membrane. Generally the adsorption decreased with increasing hydration energy of the membrane. Yet it is not necessary to have a highly hydrophilic surface to obtain a fouling-resistant membrane. The surface energy of the membrane is also crucial, since the lower the surface energy, the easier it is to clean the membrane. The results obtained here suggest that the use of low surface energy materials could form optimal fouling-release membranes with efficient antifouling properties.

3.5 Acknowledgements

The author is grateful to the Cornell-KAUST research center for financial support, to both the Nanobiotechnology Center (NBTC) and Cornell Center for Materials Research (CCMR), which are supported by NSF, for use of their facilities and to NSF as well. The author would also like to acknowledge Dr. Héloïse Thérien-Aubin for her crucial contribution as the first author of the publication of this work.

REFERENCES

(1) Mansouri, J.; Harrisson, S.; Chen, V. *J. Mater. Chem.* **2010**, *20*, 4567.

(2) Rana, D.; Matsuura, T. *Chem. Rev.* **2010**, *110*, 2448.

(3) Krishnan, S.; Wang, N.; Ober, C.; Finlay, J. A.; Callow, M. E.; Callow, J. A. et al. *Biomacromolecules* **2006**, *7*, 1449.

(4) Weinman, C. J.; Finlay, J. A.; Park, D.; Paik, M. Y.; Krishnan, S.; Sundaram, H. S. et al. *Langmuir* **2009**, *25*, 12266.

(5) Schilp, S.; Kueller, A.; Rosenhahn, A.; Grunze, M. *Biointerphases* **2007**, *2*, 143.

(6) Kang, S.; Asatekin, A.; Mayes, A. M.; Elimelech, M. *J. Membr. Sci.* **2007**, *296*, 42.

(7) Sun, Q.; Su, Y.; Ma, X.; Wang, Y.; Jiang, Z. *J. Membr. Sci.* **2006**, *285*, 299.

(8) Chen, S.; Cao, Z.; Jiang, S. *Biomaterials* **2009**, *30*, 5892.

(9) Chen, S.; Li, L.; Zhao, C.; Zheng, J. *Polymer* **2010**, *51*, 5283.

(10) Jo, T. S.; Ozawa, C. H.; Eagar, B. R.; Brownell, L. V.; Han, D.; Bae, C. *J. Polym. Sci. Part A Polym. Chem.* **2009**, *47*, 485.

(11) Peng, N.; Chung, T. S.; Li, K. Y. *J. Membr. Sci.* **2009**, *343*, 62.

(12) Vandezande, P.; Gevers, L. E. M.; Vankelecom, I. F. J. *Chem. Soc. Rev.* **2008**, *37*, 365.

(13) Baker, R. W. Membrane technology and applications. 2nd ed. New York: John Wiley & Sons; **2004**.

(14) Flemming, H. C.; Schaule, G.; Griebe, T.; Schmitt, J.; Tamachkiarowa, A. *Desalination* **1997**, *113*, 215.

(15) Li, D.; Wang, H. *J. Mater. Chem.* **2010**, *20*, 455.

(16) Subramani, A.; Hoek, E. M. V. *Desalination* **2010**, *257*, 73.

(17) Hachisuka, H.; Ikeda, K. **1997**, WO9734686.

(18) Belfer, S.; Purinson, Y.; Fainshtein, R.; Radchenko, Y.; Kedem, O. *J. Membr. Sci.* **1998**, *139*, 175.

(19) Bernstein, R.; Beller, S.; Freger, V. *Langmuir* **2010**, *26*, 12358.

(20) Lin, N. H.; Kim, M. M.; Lewis, G. T.; Cohen, Y. *J. Mater. Chem.* **2010**, *20*, 4642.

(21) Mickols, W. E. **2000**, WO0076641.

(22) Kang, G. D.; Liu, M.; Lin, B.; Cao, Y. M.; Yuan, Q. *Polymer* **2007**, *48*, 1165.

(23) Ejaz, M.; Ohno, K.; Tsujii, Y.; Fukuda, T. *Macromolecules* **2000**, *33*, 2870.

(24) Krishnan, S.; Weinman, C.; Ober, C. *J. Mater. Chem.* **2008**, *18*, 3405.

(25) Schilp, S.; Rosenhahn, A.; Pettitt, M. E.; Bowen, J.; Callow, M. E.; Callow, J. A. et al. *Langmuir* **2009**, *25*, 10077.

(26) Grozea, C. M.; Walker, G. C. *Soft Matter* **2009**, *5*, 4088.

(27) Bennett, S. M.; Finlay, J. A.; Gunari, N.; Wells, D. D.; Meyer, A. E.; Walker, G. C. et al. *Biofouling* **2010**, *26*, 235.

CHAPTER FOUR:

SYNTHESIS OF SUPERCRITICAL CARBON DIOXIDE DISPERSIBLE NANOPARTICLES AS PROSPECTIVE TRACERS FOR SUBSURFACE MAPPING TECHNOLOGIES*

---

* Lin Chen, Yisheng Xu, Yushi (Russell) Zhao, Lawrence M. Cathles, Christopher K. Ober. *To be submitted*

4.1 Introduction

Supercritical carbon dioxide ($scCO_2$), regarded as a 'greener' solvent compared to traditional hydrocarbon solvents, has been widely applied in extraction processes such as extraction of caffeine from green tea and coffee, dry cleaning etc. [1,32] The liquid character of $scCO_2$ facilitates mass dissolution and transport, while the gas-like properties enable enhanced diffusion behavior of $scCO_2$. Recently, $scCO_2$, due to its low viscosity and zero surface tension, has become a promising medium for microelectronics processing such as pattern drying and photoresist stripping.. [3, 4] One of the most important applications of $scCO_2$ is to utilize it for enhanced oil recovery (EOR), which has been applied in real oil fields for more than 30 years. [5, 6] Taking advantage of the unique properties of $scCO_2$, more than 50% of the oil stored underground can be recovered. Recently, it has also found applications in enhanced coal bed methane (ECBM) production. [7] Moreover, sequestration of carbon dioxide by storage in depleted oil reservoirs and gas shale is an efficient method to manage the "green house" effect. [8]

In order to track the flow of $scCO_2$ underground for evaluation of EOR efficiency and CO_2 storage capacity, subsurface mapping technologies are highly desired, which will determine important factors such as porous heterogeneity of underground shales and degrees of fracture formation in shale layers etc. [9, 10] One of the most attractive methods is to use a dual-tracer diffusion system, which has been successfully developed in aqueous systems. [11] Two tracers with at least one order of magnitude difference in response were dissolved and injected simultaneously into a diffusion cell. Organic C-dot nanoparticles remained inside a permeable core channel while a much

smaller chemical tracer (KBr) diffused into a compact and uniform matrix. Diffusion behaviors of both tracers were well predicted by selecting proper parameters and models according to the style of the flow cells. [11] This success in water suggests that a similar strategy could be adopted for $scCO_2$ system. It is therefore necessary to design new tracers which are compatible with $scCO_2$. The tracers are required to be uniform, small (usually less than 50 nm for NP tracer) and easily detectable.

Surprisingly, as far as we know, applications of nanoparticles in $scCO_2$ have not yet been fully recognized. Little research has been done on the preparation of $scCO_2$ dispersible nanoparticles. Grignard et al. [12] synthesized macroligands with thiol end groups and grafted them onto silica particles, which were then used as chelating agents in atom transfer radical polymerization (ATRP) of trifluoroethyl methacrylate in $scCO_2$. Little information about the solubility of these silica-macroligands or others in $scCO_2$ is available. It is therefore necessary to develop and demonstrate functional materials that are soluble and applicable in $scCO_2$.

Herein, we report a simple strategy for synthesis of $scCO_2$-philic nanoparticles. The particle is composed of an inorganic core with a corona of fluoropolymers, which is covalently bonded on the core through a surface-initiated atom transfer radical polymerization (SI-ATRP) reaction. The as-synthesized nanoparticles exhibit good solubility in both $scCO_2$ and hydrofluoroether (HFE), the latter of which is used as an analogue to $scCO_2$ for characterization under ambient pressure conditions. Incorporation of fluorescent labels in the polymer matrix helps to improve the

detectability of the particles. Applications of the nanoparticles as prospective tracers for subsurface mapping of shales are subsequently explored.

4.2 Experimental

4.2.1 Materials

Ferrous sulfate deptahydrate ($FeSO_4 \cdot 7H_2O$), ferric chloride hexahydrate ($FeCl_3 \cdot 6H_2O$), oleic acid (OA), (3-aminopropyl) trimethoxysilane, α-bromoisobutyryl bromide, copper (I) bromide, N, N, N′, N″, N″-pentamethyldiethylenetriamine (99%), 3,3,4,4,5,5,6,6,7,7,8,8,9,9,10,10,10 - Heptadecafluorodecyl methacrylate (97%), triethylamine (TEA), α,α,α-trifluorotoluene (TFT), toluene anhydrous (99.8%), N, N-dimethylformamide (DMF), tetrahydrofuran (THF) and Ludox SM30 silica nanoparticles (NPs) were purchased from Sigma Aldrich. 1-Pyrenylmethyl methacrylate was purchased from Polysciences. Ethoxy-nonafluorobutane (HFE 7200) was purchased from 3M. Heptadecafluorodecyl methacrylate was passed through an alumina column to remove inhibitor. 1-Pyrenylmethyl methacrylate dissolved in THF was passed through a silica column to remove inhibitor. All other solvents and reagents were used as received without further purifications.

4.2.2 Synthesis of 2-bromo-2-methyl-N-(3-(trimethoxysilyl)propyl) propanamide (BMTP)

α-Bromoisobutyryl bromide (6.72 mL, 0.053 mol) dissolved in 20 mL methylene chloride was added dropwise into a mixture of (3-aminopropyl) trimethoxysilane (12 mL, 0.067 mol) and TEA (13.96 mL, 0.1 mol) and 60 mL methylene chloride at 0 ºC.

After 4 hour reaction at room temperature, white precipitate was removed by vacuum filtration. The filtrate was washed with HCl (pH 2-3), brine and distilled water respectively and dried over anhydrous magnesium sulfate. The final product was obtained as colorless liquid after rotary vaporization (9.30 g, yield = 53.2%). ^{1}H NMR (300 MHz, $CDCl_3$): δ = 3.58 (s, 9H, -Si-O-C*H*$_3$), 3.26 (t, 2H, -C*H*$_2$-NH-), 1.96 (s, 6H, -C*H*$_3$), 1.65 (m. 2H, -CH_2-C*H*$_2$-CH_2-), 0.67 (t, 2H, -Si-C*H*$_2$-)

4.2.3 Synthesis of Mono-dispersed Fe_3O_4-NPs

The synthetic procedure was followed by the method described by Sun et al. [13] 2.35 g $FeSO_4 \cdot 7H_2O$ and 4.1 g $FeCl_3 \cdot 6H_2O$ were dissolved into 100 mL distilled water in a 250 mL flask. Iron oxide NPs were prepared by quickly adding 25 mL 27% (w/w) ammonium hydroxide under vigorous stirring at room temperature. 1 mL OA was then dropped into the formed black NP precipitates at 80 ºC for 1 hour. The above reactions were carried out under nitrogen atmosphere. This OA functionalized NPs were then extracted with 25 mL toluene twice in the presence of small amount of sodium chloride in order to disperse the NP into organic solvent. Finally, the NP dispersion was dried over anhydrous sodium sulfate and the concentration of the NP dispersion was determined to be 15 mg/mL.

4.2.4 Preparation of Initiator Modified Fe_3O_4-NPs

BMTP (1.19 g), 20 mL TEA (2M) and 30 mL magnetic NPs in toluene were mixed together in a round flask. The mixture was allowed to react under nitrogen for 24 hours. After reaction, 20 mL petroleum ether was added to precipitate the NPs followed by magnetic separation of NPs. The NPs were then re-dispersed in 15 mL

toluene. Such process was repeated 3 times to remove the unreacted BMTP and remaining OA. The NPs were finally vacuum dried and ready for polymerization. TGA analysis shows the initiator immobilized on Fe_3O_4 is ~ 22 % (w/w) of total mass.

4.2.5 Surface Polymerization on Initiator Modified Fe_3O_4-NPs

10 mg of initiator modified Fe_3O_4-NP was dissolved with co-solvent of DMF and TFT (50 : 50 v/v) in a Schlenk flask followed by 30 minutes purge with argon. In another flask, CuBr (4.7 mg, 0.03 mmol), PMDETA (8 μL, 0.038 mmol), heptadecafluorodecyl methacrylate (0.67 mL, 2 mmol), and 1-Pyrenylmethyl methacrylate (20 mg, 0.07 mmol) were dissolved in 3 mL co-solvent of DMF and TFT (50 : 50 v/v). The mixture was freeze-thawed three times to remove oxygen, which was then transferred into the NP solution under argon atmosphere. The reaction was carried out at 70 ºC for 7 hours. The polymer functionalized NPs were precipitated and collected through vacuum filtration. To remove copper catalysts, the solid was stirred in methanol overnight and the polymer modified NP powder was collected.

4.2.6 Preparation of Initiator Modified SiO_2-NPs

Silica particle dispersions in water (Ludox SM 30) were first passed through cation exchange resin to protonate the NP solution. Solvent exchange of water with DMF was done through dialysis in DMF by using a cellulose membrane (MW cutoff: 7 K) for 48 hours with 1 change of DMF. Concentration of silica NPs in DMF solution was determined to be 115 mg/mL. 1 mL of the solution was further diluted in 9 mL DMF. 11.45 g initiator was added into the solution, which was stirred at room temperature for 24 hours. The excess initiator was removed by dialysis against DMF for 96 hours

with 4 changes of DMF. To determine the particle concentration, the SiO_2 NPs were precipitated by HFE followed by centrifugation and then dried. The content of SiO_2 was finally determined to be 8 mg/mL. TGA analysis shows the initiator immobilized on SiO_2 is ~ 25 % (w/w) of total mass.

4.2.7 Surface Polymerization on Initiator Modified SiO_2-NPs

1 mL of initiator modified SiO_2-NP solution was added in a Schlenk flask followed by 30 minutes purge with argon. In another flask, CuBr (5.7 mg, 0.04 mmol), PMDETA (10 μL, 0.048 mmol), heptadecafluorodecyl methacrylate (0.59 mL, 1.8 mmol), and 1-Pyrenylmethyl methacrylate (10 mg, 0.035 mmol) were dissolved in 3 mL DMF. The mixture was freeze-thawed three times to remove oxygen. The mixture was then transferred into the NP solution under argon atmosphere and the reaction was carried out at 70 ºC for 7 hours. The polymer functionalized NPs were precipitated and collected through vacuum filtration. To remove copper catalysts, the solid was stirred in methanol overnight and the polymer modified NP powder was collected.

4.2.8 Particle Characterizations

ATR-FTIR experiments were carried out on a Nicolet iZ-10 instrument equipped with a diamond ATR crystal. Thermogravimetric analysis (TGA) was done on RT Instrument model Exstar SII TG/DTA 6200. Dynamic light scattering (DLS) measurements were carried out on Malvern Zeta Sizer model Nano-ZS. Ultraviolet–visible (UV-vis) and fluorescent spectroscopy was done on Molecular Devices model Spectramax M2. TEM was performed with a LEO 1550 FESEM under TEM mode at

30 kV. $scCO_2$ solubility tests were performed in a supercritical fluid phase monitor (SFT-phase monitor II) instrument.

4.2.9 Dual Tracer Diffusion Experiments

The glass Hele Shaw diffusion cells, with a core channel with dimensions of 8mm x 8mm x 100mm and a diffusion slit with dimensions of 2mm x 80mm x 100mm, were designed and used for the diffusion tests. The chemical tracer (TFT) and the SiO_2 or Fe_3O_4 NP tracers were premixed at a known concentration in HFE 7200. The solution is held in a 50 ml glass syringe mounted on a high precision syringe pump. The injection rate is controlled at 1.44 cc/day. TFT tracer was detected by UV spectrometer at 255 nm and NP tracers were detected by fluorometer at 390 nm.

4.3 Results and Discussion

4.3.1 Preparation of Fluoropolymer Functionalized Fe_3O_4- and SiO_2-NPs

Iron oxide NPs were prepared through a ligand exchange method as was previously reported (Scheme 4.1). [13] Firstly, stable mono-dispersed NPs were prepared by co-precipitation in the presence of oleic acid (OA). After extraction with toluene, the monodispersed NPs were stabilized by exposing hydrophobic alkyl moieties in toluene. Initiator was then covalently functionalized on the NPs by ligand exchange with surfactant OA. After precipitation and re-dispersion of the NPs with petroleum and toluene respectively, unattached initiator molecules were removed and the NPs were dried under vacuum. Such NPs could be well dispersed in DMF for further SI-

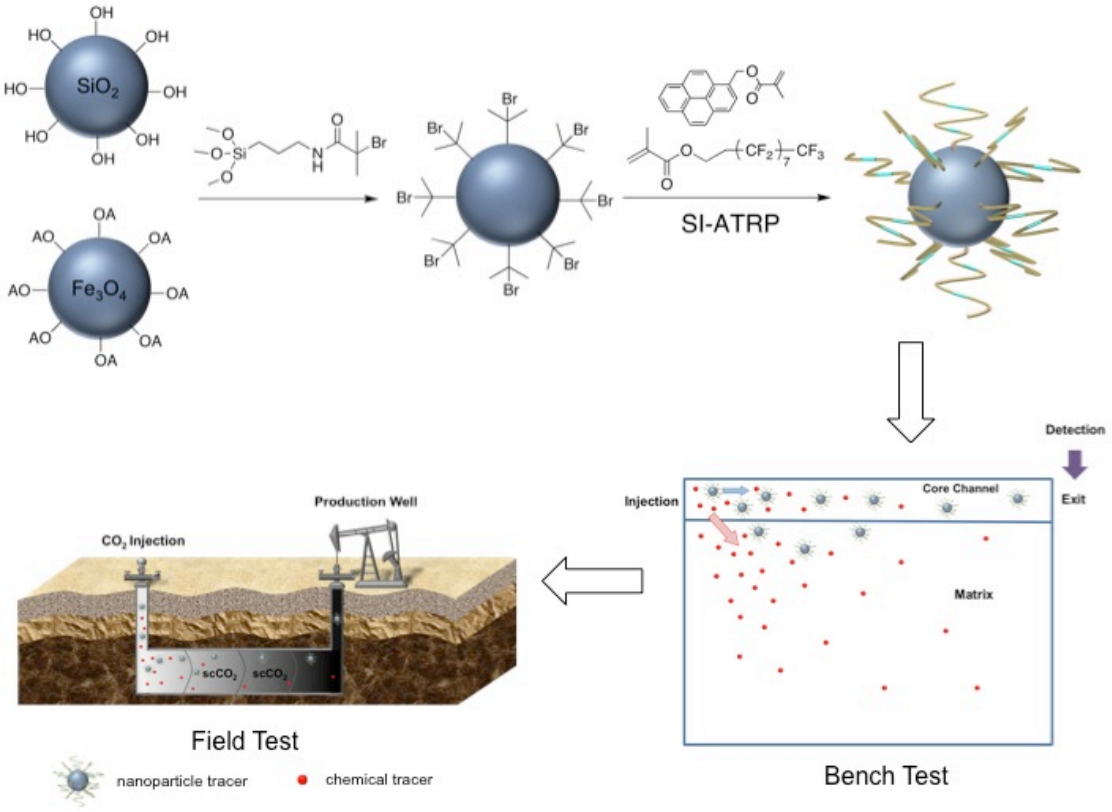

Scheme 4.1. Modification of silica and iron oxide cores with fluorinated polymers through surface-initiated ATRP reaction. As-modified nanoparticles are applied in diffusion test on bench scale and further applied in field test.

ATRP processing. A mixed solution of DMF and TFT was used for the polymer grafting and the as-prepared nanoparticles were precipitated after the polymerization reactions.

Modifications of SiO_2-NP surfaces were performed by using similar approaches. Since the silica NPs were more liable to aggregate, it was necessary to keep the nanoparticles dispersed in solution through the entire preparation process. Therefore instead of solid powders, Ludox particles in aqueous solution were selected as the initial core source and then solvent exchanged with DMF for further modifications.

4.3.2 Characterizations of Fe_3O_4- and SiO_2-NPs

ATR-IR spectra were measured to confirm successful NP functionalization. For Fe_3O_4-NPs, as shown in Figure 4.1 (a), the stretching modes of alkyl moieties from OA could be clearly observed between 2800 and 3000 cm^{-1} and the carboxylate group of OA at 1701 cm^{-1}. After ligand exchange, amide I and II peaks appeared at 1645 and 1534 cm^{-1} respectively, indicating successful attachment of initiator. The disappearance of high frequency stretching peaks and carboxylate peaks at 1701 cm^{-1} further proved the high extent of ligand exchange with no OA molecules attached. When polymerization took place in TFT/DMF=1:9 solvent mixture, very little carbonyl stretching at 1728 cm^{-1} could be detected and the entire spectrum was very similar to that of initiator-modified NPs. However, increasing the TFT/DMF ratio to 1 dramatically increased the peak intensity at 1728 cm^{-1}, indicating efficient coverage by polymer brushes on the NP surface. Spectra of SiO_2-NPs showed similar

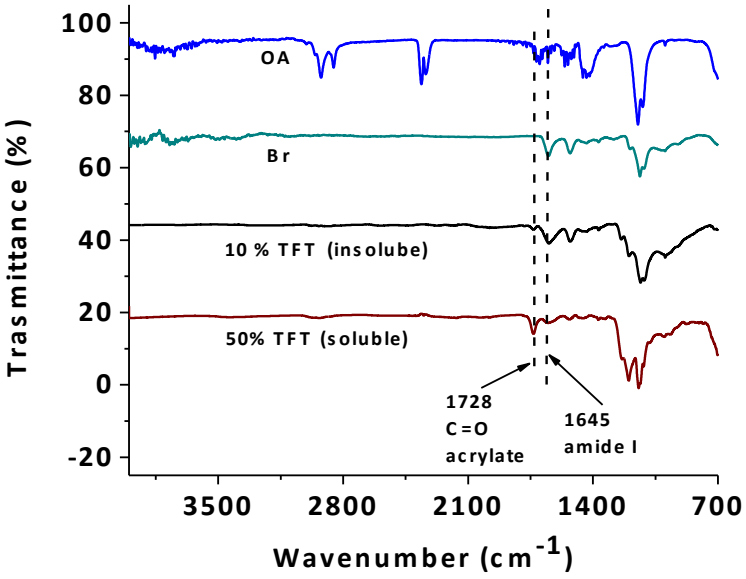

(a)

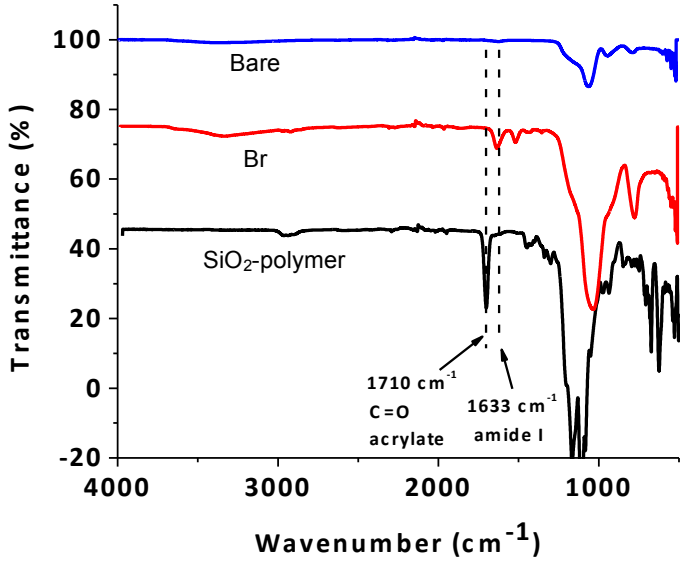

(b)

Figure 4.1. ATR Spectra of as-prepared nanoparticles: (a) Fe_3O_4-NPs; (b) SiO_2-NPs. Specific peaks of the initiator and fluoropolymers can be observed.

characteristics as those of Fe_3O_4-NPs. Specific peaks of the initiator and fluoropolymers appeared after corresponding modifications (Figure 4.1 (b)).

TGA was used to establish the composition of NPs (Figure 4.2). Mass content of initiator and polymer brush on the Fe_3O_4-NPs is about 25% and 65% respectively, and is about 20% and 70% for SiO_2-NPs. It is worth noting that Fe_3O_4-NPs prepared in a TFT/DMF=1:9 solvent mixture showed little increase of organic content after polymerization, indicating few polymers were grafted on the particle cores, which is consistent with the ATR analysis. Grafting density of the initiator and polymers can then be estimated by the following equation as reported by Liu et al. [14]

$$GD = \frac{a\, N_A}{\frac{S}{\rho\, V}} \qquad \textbf{Equation 4.1}$$

where GD is grafting density, a is number of moles of initiator/polymer per gram of NP, N_A is Avogadro's number, S is the surface area of NP, V is the volume of NP, and ρ is the density of NP. Table 4.1 lists the calculated parameters and grafting densities of Fe_3O_4- and SiO_2-NPs.

TEM images were taken to investigate the particle size in its dry state. Figure 4.3 (a) & (b) show images of the bare Fe_3O_4 and SiO_2 cores. Particles with spherical morphologies were observed. The average diameter is 9 and 7 nm for Fe_3O_4 and SiO_2 respectively. Figure 4.3 (c) & (d) are images of polymer-functionalized NPs. Since the particles were in their dry state, agglomeration was inevitable and observed for both NPs. The contrast between bright ion oxide core and dark polymer corona can be

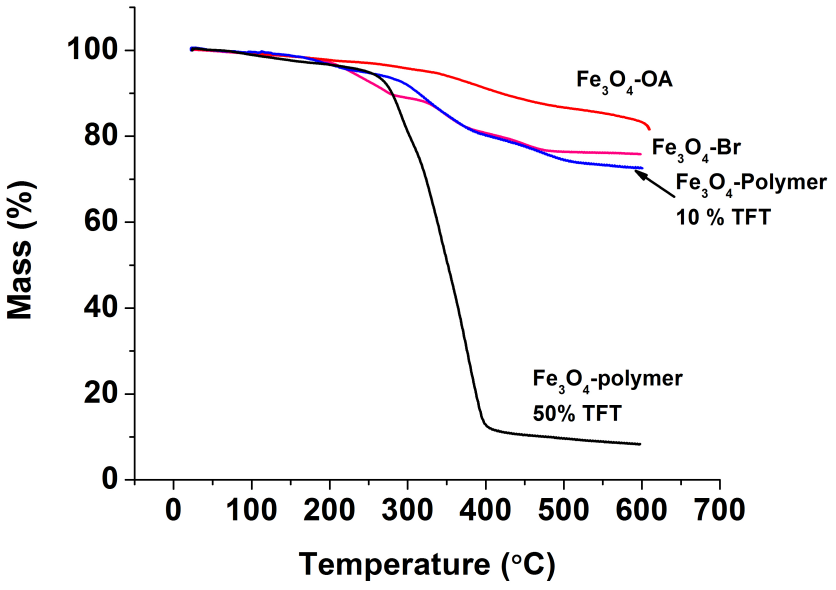

(a)

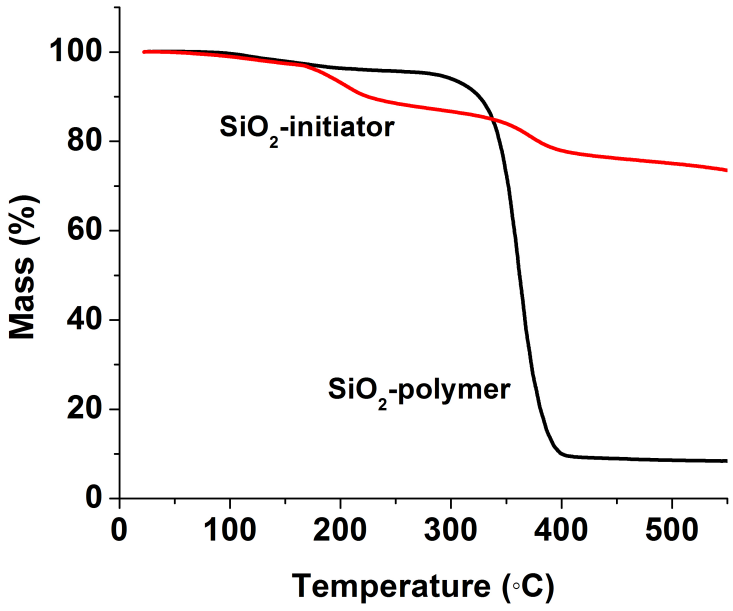

(b)

Figure 4.2. TGA measurements of NPs: (a) Fe_3O_4-NPs; (b) SiO_2-NPs. Weight loss is 20 % and 80% for NPs modified with initiator and fluoropolymers respectively.

Table 4.1. Physical properties and grafting density of initiator and polymers on NPs.

	Mass (g/1g)	Mw* (g/mol)	a (mol/g)	ρ (g/cm^3)	r (nm)	S (nm^2)	V (nm^3)	GD ($\#/nm^2$)
Fe_3O_4-ini.	0.250	235	1.06×10^{-3}	5.00	5.0	3.14×10^{2}	5.24×10^{2}	5.32
SiO_2-ini.	0.250	235	1.06×10^{-3}	2.65	3.5	1.54×10^{2}	1.80×10^{2}	1.95
Fe_3O_4-poly.	0.662	23,000	2.88×10^{-5}	5.00	5.0	3.14×10^{2}	5.24×10^{2}	0.144
SiO_2-poly.	0.666	22,000	3.02×10^{-5}	2.65	3.5	1.54×10^{2}	1.80×10^{2}	0.056

* Molecular weight of polymers was measured on fluoro-polymers prepared by ATRP of pure initiator at the same conditions as NPs were synthesized.

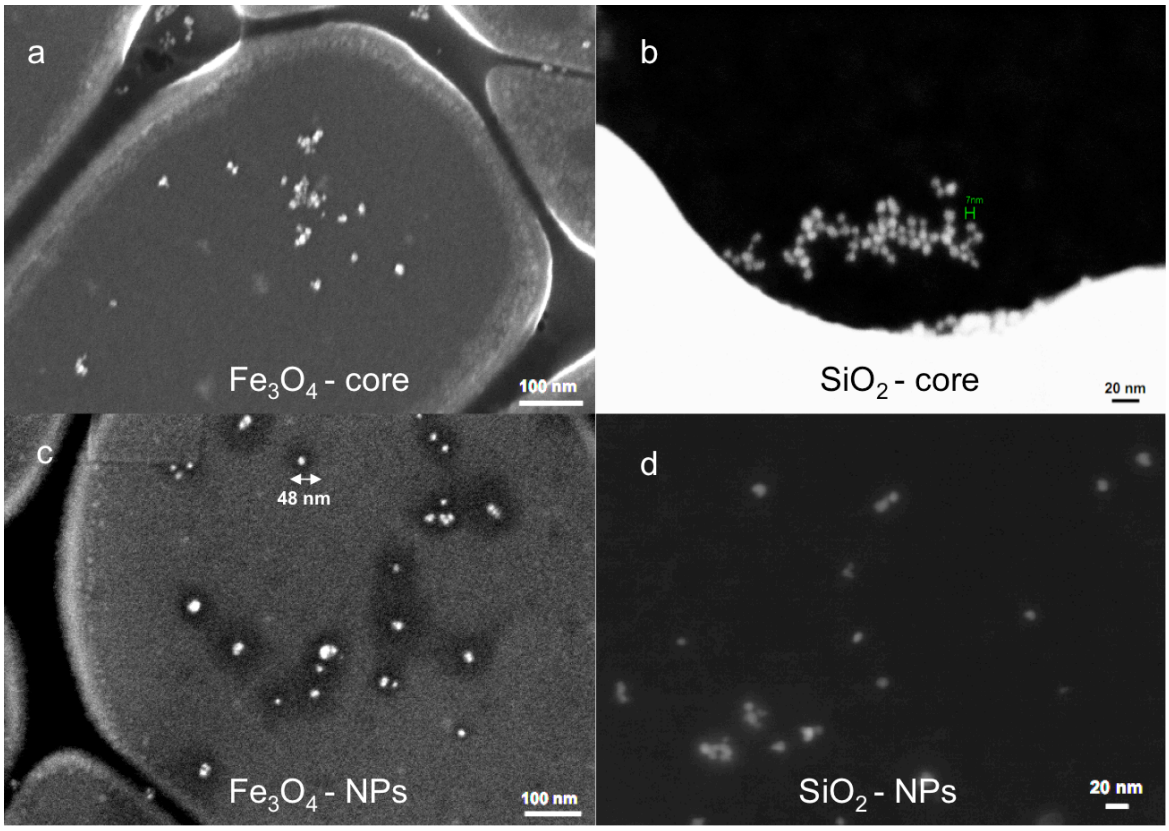

Figure 4.3. TEM images of NPs. (a) Fe_3O_4 core; (b) SiO_2 core; (c) Fe_3O_4 nanoparticle; (d) SiO_2 nanoparticle.

clearly seen in Fe_3O_4-NPs, while the contrast of SiO_2-NPs is not that obvious. An average particle size of 45 nm in diameter was measured.

DLS was used to explore the particle size in solution. Since fluoropolymers dissolve well in both $scCO_2$ and HFE, the latter was used here as an analogue solvent to $scCO_2$ due to its $scCO_2$-like properties such as low surface tension and viscosity. Clear, well-dispersed solutions of both NPs were obtained and used for DLS measurements in HFE. Results show that the hydrodynamic diameters for Fe_3O_4 and SiO_2 nanoparticles are 9 and 6 nm respectively (Figure 4.4), and consistent with the TEM results. Adding initiator barely changed the particle size, while after modifications with fluoro-polymers, particle sizes were increased to 43 and 39 nm respectively for Fe_3O_4 and SiO_2 nanoparticles. Considering the dry particle size measured from TEM, it is reasonable to suggest that the as-prepared NPs were well mono-dispersed in HFE solutions.

Figures 4.5 & 4.6 show UV-vis spectra and fluorescence properties of Fe_3O_4- and SiO_2-NPs when 3.5% (mol) fluorescent monomer 1-pyrenylmethyl methacrylate was incorporated in the nanoparticles. The UV-spectrum of Fe_3O_4-NPs shows a peak at 340 nm, which corresponds to the characteristic peak of 1-pyrenylmethyl methacrylate, and the peak at 445 nm, which is attributed to the absorption of the Fe_3O_4 core (Figure 4.5 (a)). The NPs show very intense fluorescence upon exposure to an excitation light source (Figure 4.5 (b)). However, due to absorption of the core, only the top solution under excitation is fluorescent and the bottom solution still exhibits the brown

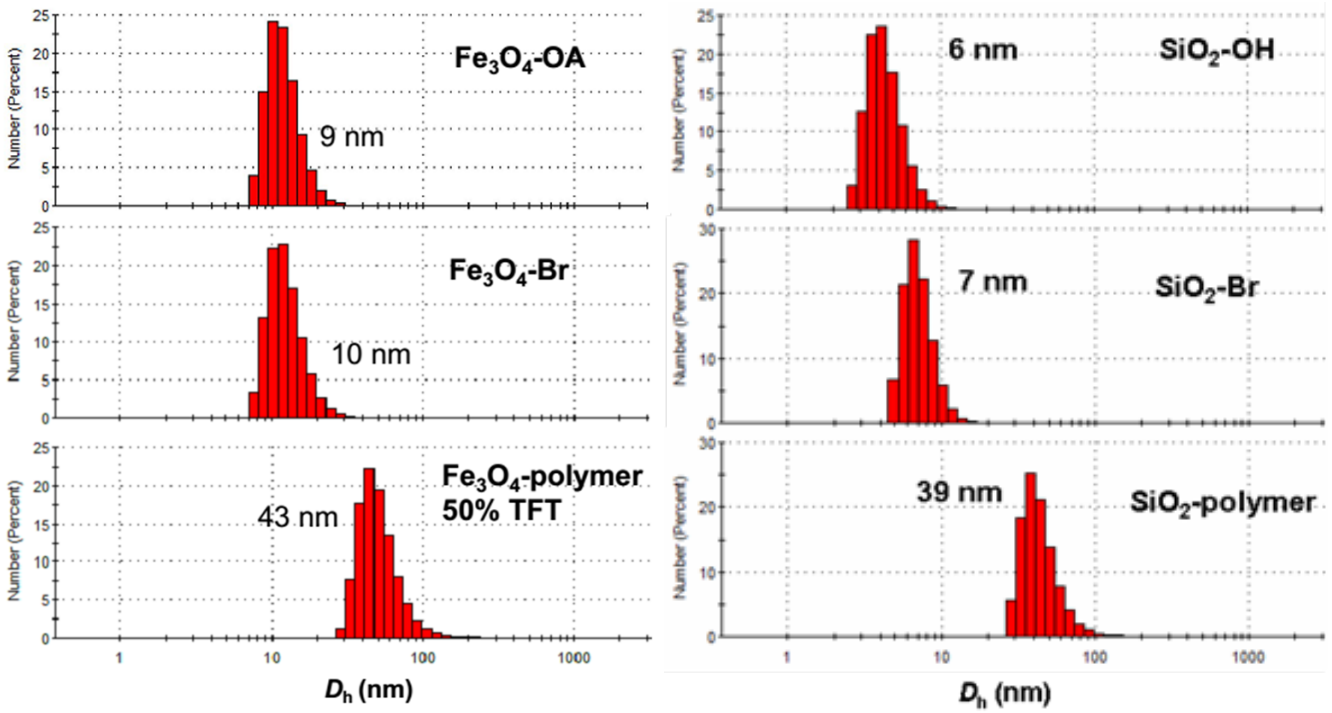

Figure 4.4. DLS measurements of hydrodynamic diameters of NPs: (a) Fe_3O_4-NPs modified with OA, initiator and fluoropolymers; (b) SiO_2-NPs with bare core and NPs modified with initiator and fluoropolymers

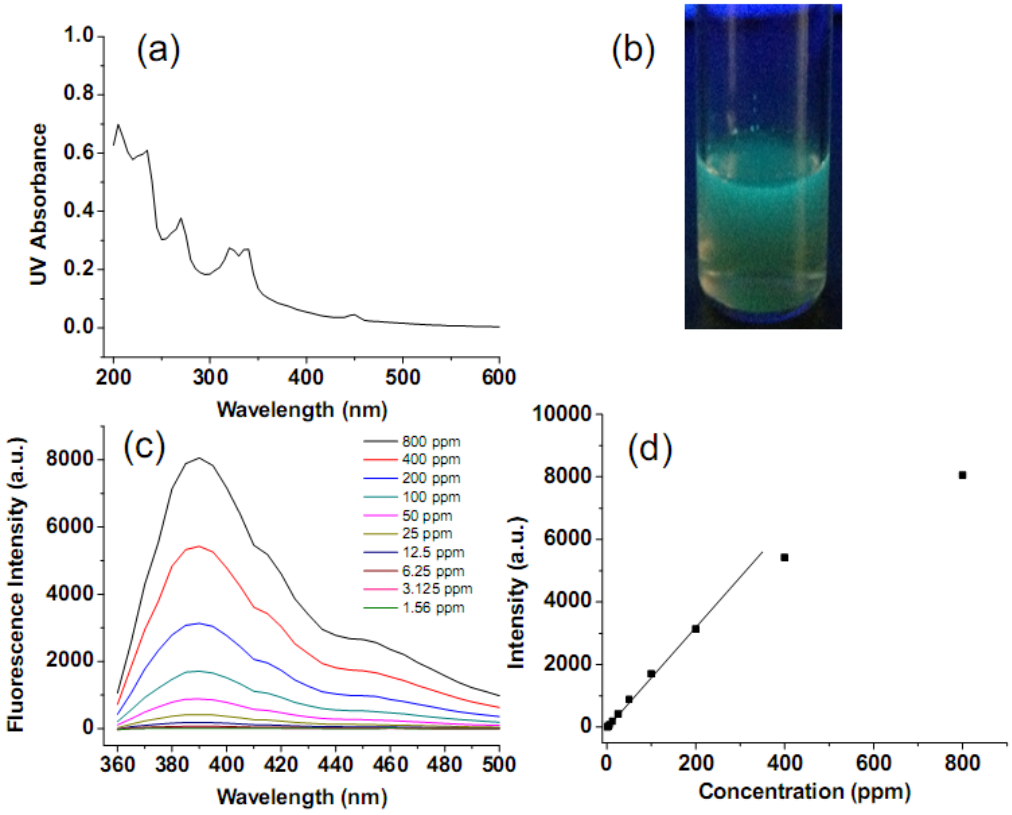

Figure 4.5. Fluorescent properties of Fe_3O_4-NPs. (a) UV-vis spectrum; (b) picture of fluorescent particle solution; (c) fluorescence spectrum; (d) relationship between intensity of fluorescence and particle concentrations.

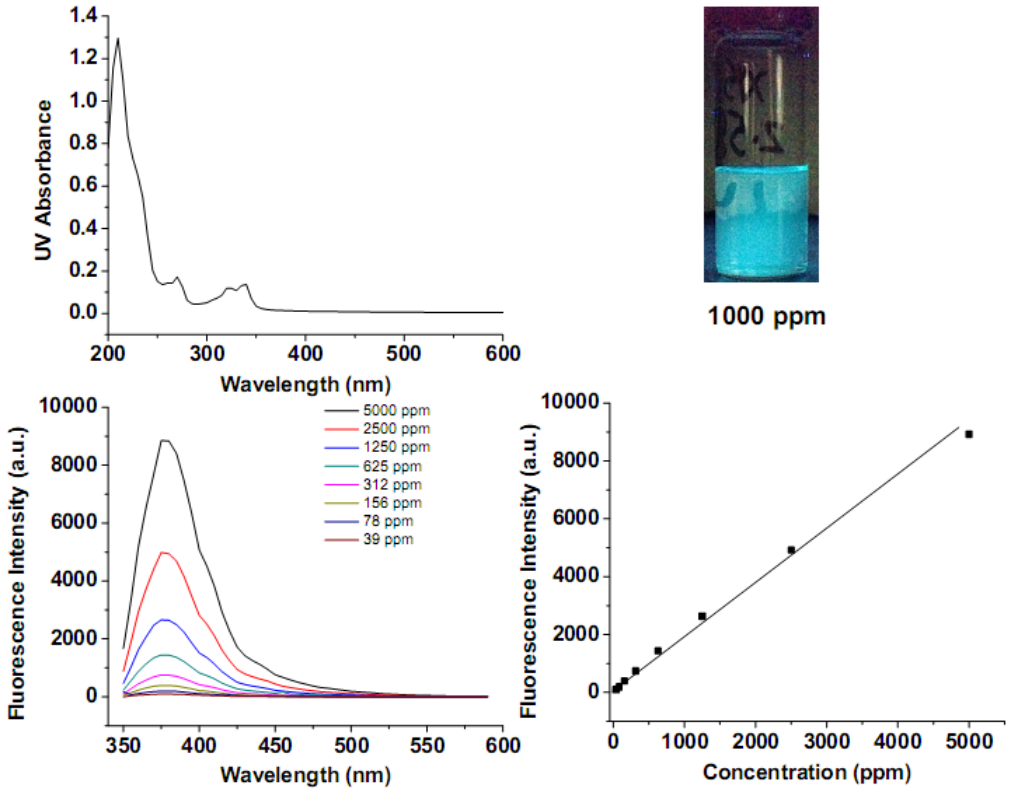

Figure 4.6. Fluorescent properties of SiO_2-NPs. (a) UV-vis spectrum; (b) picture of fluorescent particle solution; (c) fluorescence spectrum; (d) relationship between intensity of fluorescence and particle concentrations.

characteristic color of Fe_3O_4-NPs. The fluorescence intensity increased with the increase of the NP concentration (Figure 4.5 (c)). A correlation curve of the intensity with concentration shows a linear relationship between the intensity and NP concentration when the concentration is below 400 ppm (Figure 4.5 (d)). Deviation from a linear curve was observed at high NP concentration. Such a phenomenon is probably due to the strong background absorption of Fe_3O_4-cores, which reduces the light energy for fluorophore excitation. While at low concentrations, the background absorption is greatly reduced and the incident light is mainly absorbed by fluorophore molecules. A UV-vis spectrum of SiO_2-NPs in Figure 4.6 (a) shows the same characteristic peak of 1-pyrenylmethyl methacrylate at 340 nm, while no strong baseline absorption was found for SiO_2-NPs. Therefore, unlike Fe_3O_4-NPs, SiO_2-NP solutions show uniformly fluorescent emission from the bottom to top as shown in Figure 4.6(b). Plotting the fluorescence intensity versus the particle concentration gives a linear relationship even at concentrations as high as 5000 ppm (Figure 4.6 (d)). However, the fluorescence of SiO_2-NPs is found to be much lower than that of Fe_3O_4-NPs at the same concentration.

4.3.3 Solubility of Fe_3O_4- and SiO_2-NPs in $scCO_2$

In order to confirm dispersion properties of the NPs in $scCO_2$, solubility tests were done in a supercritical fluid phase monitor instrument. 20 mg of the NPs were placed in a 30 ml cell and the tests were then performed under various temperatures and pressures. Pictures taken at different dissolution stages are shown in Figure 4.7. Both Fe_3O_4- and SiO_2-NPs were insoluble at low temperatures and pressures when CO_2 is in

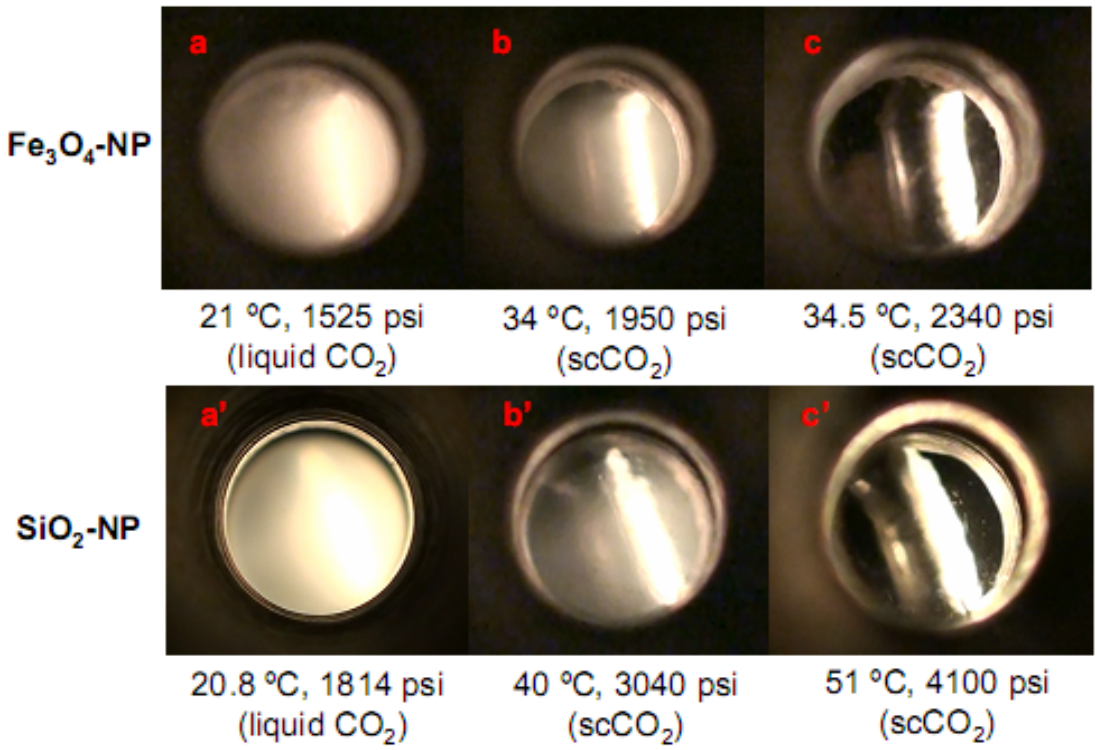

Figure 4.7. $scCO_2$ solubility of NPs. (a) Fe_3O_4-NP in liquid CO_2; (b) Fe_3O_4-NP partially dissolved in $scCO_2$; (c) Fe_3O_4-NP fully dissolved in $scCO_2$; . (a') SiO_2-NP in liquid CO_2; (b') SiO_2-NP partially dissolved in $scCO_2$; (c') SiO_2-NP fully dissolved in $scCO_2$

its liquid state (Figure 4.7 (a) & (a')). Increasing the temperature and pressure turned CO_2 into the supercritical state and facilitated the dissolution of NPs (Figure 4.7 (b) & (b')). While beyond a certain critical point, i.e. the 'cloud point', the solution suddenly became completely clear (Figure 4.7 (c) & (c')). The observed cloud point was 34.5 ^oC and 2340 psi for Fe_3O_4-NPs, while the SiO_2-NPs had a higher cloud point with a higher critical temperature (51 ^oC) and pressure (4100 psi). The clear dispersion solutions proved the good solubility of the NPs in $scCO_2$.

4.3.4 Diffusion Tests of Fe_3O_4- and SiO_2-NPs

To explore potential applications of the NPs in a 'dual tracers system' used to evaluate the subsurface heterogeneity for enhanced oil recovery and CO_2 sequestration, diffusion behavior of the NP tracers and chemical tracer (TFT) were investigated in a Hele Shaw style diffusion cell. The time dependent diffusion resulting from combination of NPs and chemical tracers are provided in Figure 4.8. The fact that the NP tracer arrives in the effluent before the chemical tracer in both experiments suggests that the chemical tracer (TFT) diffuses vertically into the matrix adjacent to the core flow channel in addition to a horizontal flow, while very slight vertical diffusion is observed for NPs due to its small diffusion coefficient. The experimental results suggest that in real geological settings, the NPs will flow mainly through the fractures or cracks whereas small chemical tracers will broadly diffuse into the dense porous matrix since it has a much larger diffusion coefficient than NPs do. On the other hand, the prediction of effluent concentration curves of TFT and NP tracers was then calculated by the streamline model, [15] which helps to translate the experimental

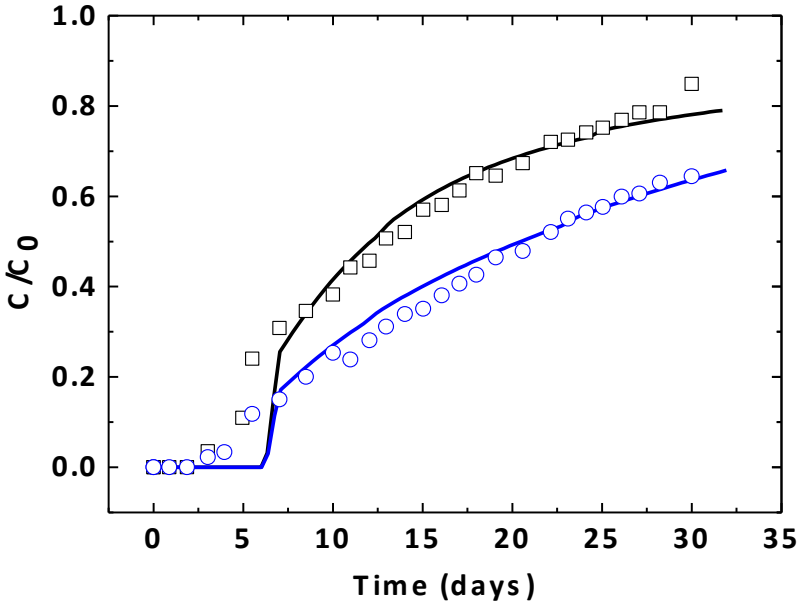

(a)

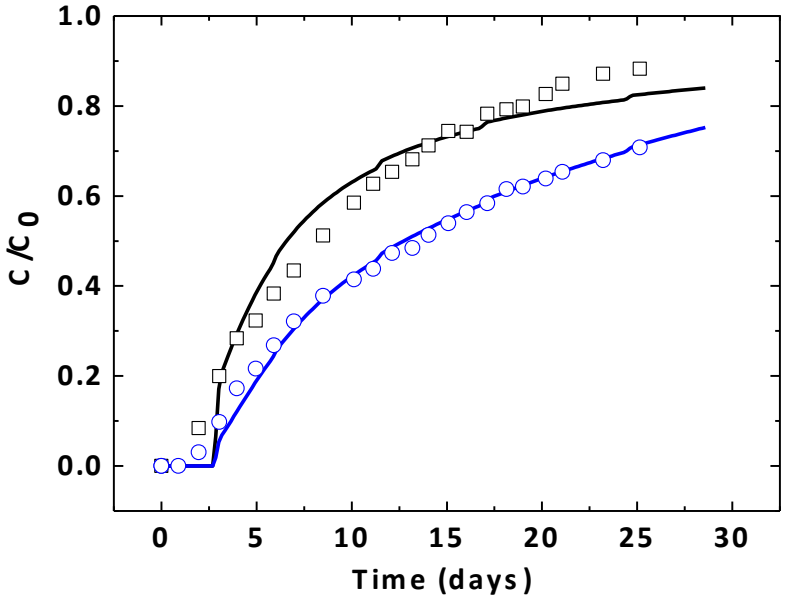

(b)

Figure 4.8. Comparison of the effluent TFT (blue) and NP (black) concentration as a function of time (square data points) to the concentrations predicted by the advection-diffusion model (solid lines): (a) Fe_3O_4; (b) SiO_2.

results and to demonstrate the fracture information of targeted geological formations. Agreement between predictive and experimental results for both the chemical and NP curves indicate that this $scCO_2$-philic dual-tracer system is a promising tool for diffusion measurements and subsurface fracture-matrix prediction during CO_2 sequestration in shales.

4.4 Conclusion

Nanoparticles with different inorganic cores (Fe_3O_4, SiO_2) and covalently bonded fluoropolymer corona were prepared by a surface-initiated ATRP process. Successful attachment of polymers was proved by ATR spectra and detailed compositions of the nanoparticles were measured by TGA. TEM and DLS results show that the particles were well mono-dispersed in HFE solution. Incorporation of fluorescent labels improved the detectability of NPs. Finally, solubility and diffusion tests in $scCO_2$ confirmed that the as-prepared nanoparticles could be well dispersed in $scCO_2$ and applied as tracers for subsurface mapping and evaluation of enhanced oil recovery and CO_2 sequestrations.

4.5 Acknowledgments

The author is grateful to the Cornell-KAUST research center for financial support, to both the Nanobiotechnology Center (NBTC) and Cornell Center for Materials Research (CCMR), which are supported by National Science Foundation (NSF), for use of their facilities. The author is also thankful to Dr. Yisheng Xu for preparation of

nanoparticles, Yushi (Russell) Zhao and Professor Lawrence M. Cathles for diffusion tests and modeling.

REFERENCES

(1) Kim, W.-J.; Kim, J.-D.; Kim, J.; Oh, S.-G.; Lee, Y.-W. *J. Food. Eng.* **2008**, *89*, 303.

(2) Klara, S. M.; Srivastava, R. D.; McIlvried, H. G. *Energ. Convers. Manage.* **2003**, *44*, 2699.

(3) Romang, A. H.; Watkins, J. J. *Chem. Rev.* **2010**, *110*, 459.

(4) Weibel G. L.; Ober C. K. *Microelectron. Eng.* **2003**, *65*, 145.

(5) Damen, K.; Faaij, A.; van Bergen, F.; Gale, J.; Lysen, E. *Energy* **2005**, *30*, 1931.

(6) Bachu, S. *Prog. Energ. Combust.* **2008**, *34*, 254.

(7) Busch, A.; Gensterblum, Y. *Int. J. Coal. Geol.* **2011**, *87*, 49.

(8) Holloway, S. *Energy* **2005**, *30*, 2318.

(9) Juanes, R.; Spiteri, E. J.; Orr, F. M.; Blunt, M. J. *Water Resources Research* **2006**, *42*, W12418.

(10) McCarthy, J. F.; McKay, L. D.; Bruner, D. D. *Environmental Science & Technology* **2002**, *36*, 3735.

(11) Subramanian, S. K.; Li, Y.; Cathles, L. M. *Water Resources Research* **2013**, *49*, 29.

(12) Grignard, B.; Calberg, C.; Jérôme, C.; Wang, W.; Howdle, S.; Detrembleur, C. *Chem. Comm.* **2008**, 5803.

(13) Sun, Y.; Ding, X.; Zheng, Z.; Cheng, X.; Hu, X.; Peng, Y. *Eur. Polym. J.* **2007**, *43*, 762.

(14) Liu, J.; He, W.; Zhang, L.; Zhang, Z.; Zhu, J.; Yuan, L.; Chen, H.; Cheng, Z.; Zhu, X. *Langmuir* **2011**, *27*, 12684.

(15) Xu, Y.; Chen, L.; Zhao, Y.; Cathles, L. M.; Ober, C. K. *Energ. Environ. Sci.* (to be submitted)

CHAPTER FIVE:

SUPERCRITICAL CARBON DIOXIDE APPLICATIONS IN MICROELECTRONICS PROCESSING

5.1 Introduction

With the continuously reduced dimensions of microelectronic devices, smaller and smaller features are required on the nanoscale level for high-resolution lithographic patterning. Currently, 45 nm nodes have already been achieved in industrial production lines, while 22 nm nodes are being developed [1, 2]. Meanwhile, in order to have successful pattern transfer at such small dimensions, high aspect ratio pattern features are necessary. Fine pattern structures with aspect ratios higher than 7 have been obtained for different polymeric materials using a variety of lithographic methods [3-5]. However, small features with high aspect ratios can easily collapse during post-patterning processes such as post-exposure development or post-etch cleaning[6-8]. Due to the high surface tensions of many of the liquids used in such processes, capillary forces are induced between the pattern features. The relationship between capillary force (F) and surface tension (γ) is expressed in Equation 5.1, in which d is the spacing width, θ is the contact angle, and H/t is the aspect ratio of imaged patterns. Collapse of lithographically defined features is possible upon solvent evaporation or removal. The critical aspect ratio of collapse (CARC) decreases from 5 to 3.7 as the space width is decreased from 400 nm to 150 nm [9].

$$F = \frac{6 \bullet \gamma \bullet \cos\theta}{d}\left[\frac{H}{t}\right]^2 \qquad \textbf{Equation 5.1}$$

Supercritical carbon dioxide ($scCO_2$) has emerged over the last 20 years as a promising and eco-friendly solvent for pattern processing [10-12]. Due to the relatively low critical temperature and pressure (31.2 ^{o}C, 1043 psi), it is straightforward to reach

the supercritical state of CO_2 and provide potential scale-up for $scCO_2$ processing. The liquid-like properties of $scCO_2$ make it a good medium for mass transport and reagent dissolution, while its gas-like properties such as low viscosity and zero surface tension make it an ideal candidate for microelectronics processing with minimum pattern collapse. Moreover, compared to traditional aqueous or organic solvents, $scCO_2$ is more environmentally benign, making it a versatile greener solvent for many applications. The unique solubility characteristics of $scCO_2$, however, provide challenges in the use of this solvent.

Applications of $scCO_2$ in microelectronics processing include photoresist stripping, wafer cleaning, and metal etching. Goldfarb first explored the possibility of $scCO_2$ dry processing to prevent pattern collapse [13]. Combined with a co-solvent such as n-hexane, $scCO_2$ was successfully used as a drying medium for photolithographic patterning with an aspect ratio of 6.8 and no pattern collapse was observed. Wagner first synthesized a $scCO_2$-compatible salt (CCS) as an extreme ultraviolet photoresist in $scCO_2$ [14]. Ober et al. further developed a series of fluorinated quaternary ammonium salts (QAS) as additives in $scCO_2$ to help develop several negative tone resists. The QAS was shown to be a surfactant in $scCO_2$ that when used as an additive in $scCO_2$ provided a fluorine free resist dissolution rate as high as 40 nm/min [2]. Passemard et al. studied the efficiency of $scCO_2$ in cleaning oxidized copper after an etching process [15]. In the presence of sulfonic acid and chelating agents such as β-diketones, double layers of oxidized copper with a thickness of about 4 nm could be efficiently removed with no pitting corrosion. Katsuhiro et al. used a $scCO_2$-pulse cleaning method to remove contamination in high aspect ratio trenches and microholes of highly

integrated semiconductor devices [16]. More than 50 nm fine particles from deep microholes could be efficiently cleaned. DeSimone et al. developed etchant solutions composed of organic peroxide and fluoro-ligands to etch copper (0) in $scCO_2$ dry environment. Up to 34 wt% of a copper coupon could be etched away after 20 h processing time [17]. Hydrofluoric acid (HF) was used as a co-solvent in $scCO_2$ for silicon dioxide dry etching process. Etching rates varied from 0.5 nm/min to 2 nm/min with different concentrations of HF and different processing times [18, 19].

Here in this project, we expected to achieve two goals. We first studied the removal of post-etch organic photoresist residue in the presence of co-solvents and additives in $scCO_2$. Different co-solvents were used and QAS was synthesized and applied as an additive. Various processing conditions were adopted to achieve the most effective cleaning procedure. Then, selective dry etching of titanium nitride (TiN) in $scCO_2$ was investigated. A novel formulation containing strong organic acids, strong organic peroxides and stabilizers were tested. The etchant solution worked efficiently for wet etching in organic solvents, while promising results were obtained for $scCO_2$ dry etching processes.

5.2 Experimental

5.2.1 Materials

Patterned silicon wafers were prepared by using p(MAdMA-co-GBLMA) photoresist and etched with plasma. Silicon wafers with TiN coatings (~25 nm) were

provided by Samsung. All chemicals, unless otherwise noted, were purchased from Sigma-Aldrich.

5.2.2 Quaternary Ammonium Salt (QAS) Synthesis

QAS was synthesized according to a previous report [2]. Typical procedures are the following:

5.2.2.1 Synthesis of 1,1,1,2,2,3,3,4,4,5,5,6,6-Tridecafluoro-9-iodononane (P-1)

4,4,5,5,6,6,7,7,8,8,9,9,9-Tridecafluorononan-1-ol (25 g, 66.1 mmol, purchased from SynQuest), triphenyl phosphine (26.0 g, 99.2 mmol), and imidazole (26.0 g, 99.2 mmol) were dissolved in 300 mL of anhydrous THF and cooled to -78 ^{o}C. Iodine (25.2 g, 99.2 mmol) was then added slowly to the solution at-78 ^{o}C. The mixture was stirred for 1 h at-78 ^{o}C and then warmed up to room temperature. After stirring for 2 h at room temperature, the mixture was quenched by adding 100 mL of water. The product was extracted with 100 mL of diethyl ether three times and washed twice with 100 mL of water. The solvent was evaporated, and then 300 mL of hexanes was added to precipitate the byproduct, phosphonium oxide. After the precipitate was filtered off, the solvent was evaporated under vacuum and the product was purified by distillation under vacuum. The product obtained was a colorless viscous liquid (17.3 g, yield = 50.6%). ^{1}H NMR (300 MHz, $CDCl_3$, Figure 5.1 (a)): δ=3.25 (t, 2H, -CF_2-CH_2-), 2.20 (m, 2H, -CH_2-), 2.15 (t, 2H, -CH_2-I).

5.2.2.2 Synthesis of N-Ethyl-4,4,5,5,6,6,7,7,8,8,9,9,9-tridecafluoro-N-methylnonan-1-amine (P-2)

Ethyl methyl amine (7.42 mL, 83.0 mmol) was added dropwise to a mixture of P-1 (9 g, 18.5 mmol) and pyridine (20 mL). The mixture was stirred for 4 h at 80 ^{o}C after which the lower phase (yellow liquid) of the mixture solution was collected. The remaining upper phase (red liquid) was washed with 10 wt% NaOH aqueous solution for 1 h at 50 ^{o}C and allowed to stand. The lower phase was collected and combined with the previous yellow liquid. The collected liquid was washed with a 10 wt% NaOH aqueous solution and dried with magnesium sulfate. After distillation under vacuum, the product obtained was a colorless viscous liquid (5.75 g, yield = 74.4%). ^{1}HNMR(300 MHz, dimethylformamide-d_7, Figure 5.1 (b)): δ=2.58 (m, 2H, -CH_2-N-), 2.52 (m, 2H, -N-CH_2-), 2.32 (s, 3H, -N-CH_3), 2.48 (m, 2H, -CF_2-CH_2-), 1.89 (m, 2H, -CH_2-CH_2-CH_2-), 1.16 (t, 3H, -CH_2-CH_3).

5.2.2.3 Synthesis of N-Ethyl-4,4,5,5,6,6,7,7,8,8,9,9,9-tridecafluoro-N-methyl-N-(4,4,5,5,6,6,7,7,8,8,9,9,9-tridecafluorononyl)nonan-1-aminium iodide (P-3)

A mixture of P-1 (8.55 g, 17.6 mmol) and P-2 (5.75 g, 13.8 mmol) was stirred for 24 h at 80 ^{o}C. After the reaction, the crude product was washed with copious amounts of diethyl ether to remove remaining reactants, and then dried under vacuum. The product obtained was a white powder (4.58 g, yield = 36.7%). 1H NMR (300 MHz, dimethylformamide-d_7, Figure 5.1 (c)): δ=3.89-3.87 (m, 6H, -N-CH_2-), 3.51 (s, 3H, -N-CH_3), 2.69 (m, 4H, -CF_2-CH_2-), 2.40 (m, 4H, -CH_2-CH_2-CH_2-), 1.62 (t, 3H, -CH_2-CH_3).

5.2.2.4 Synthesis of QAS

500 mL of a basic solution of sodium hydroxide (2M) was passed slowly through an ion exchange column filled with 25 g of an anion exchange resin (Dowex 1 X 4 chloride form, 20-50 mesh), which was converted to hydroxyl form. Another 500 mL of water was passed through to wash the column neutral. 200 mL of acetic acid was then added to convert the hydroxyl ions to acetic ions. An acetic solution (20 mL) with P-3 (0.5 g, 0.55 mmol) was passed through the column. The solvent was evaporated under vacuum, and the product was fully dried at 80 ^{o}C under vacuum to yield QAS as a white solid (0.46 g, yield = 99.4%) ^{1}HNMR(300MHz, dimethylformamide-d_7, Figure 5.1 (d)): δ=3.89-3.87 (m, 6H, -N-CH_2-), 3.51 (s, 3H, -N-CH_3), 2.69 (m, 4H, -CF_2-CH_2-), 2.40 (m, 4H, -CH_2-CH_2-CH_2-), 2.03 (s, 3H, CH_3-COO^-), 1.62 (t, 3H, -CH_2-CH_3).

5.2.2.5 TiN Etching

Wet etching of TiN was performed in organic solvents. Typically, 1.667 mL of heptafluorobutyric acid (F3 acid), 0.153 mL of *tert*-butyl peroxybenzoate (t-BPB) and 2 mL of isopropanol (IPA) was mixed together and pre-reacted at 65^{o}C for 2 hours. A piece of TiN-deposited silicon wafer (1 cm x 1 cm) was then put into the solution. The etching process was kept at 65^{o}C for different reaction times.

Dry etching of TiN followed a similar protocol as wet etching. After pre-reaction of the mixture, a TiN wafer was processed in the $scCO_2$ chamber at 65^{o}C under different pressures with different processing times.

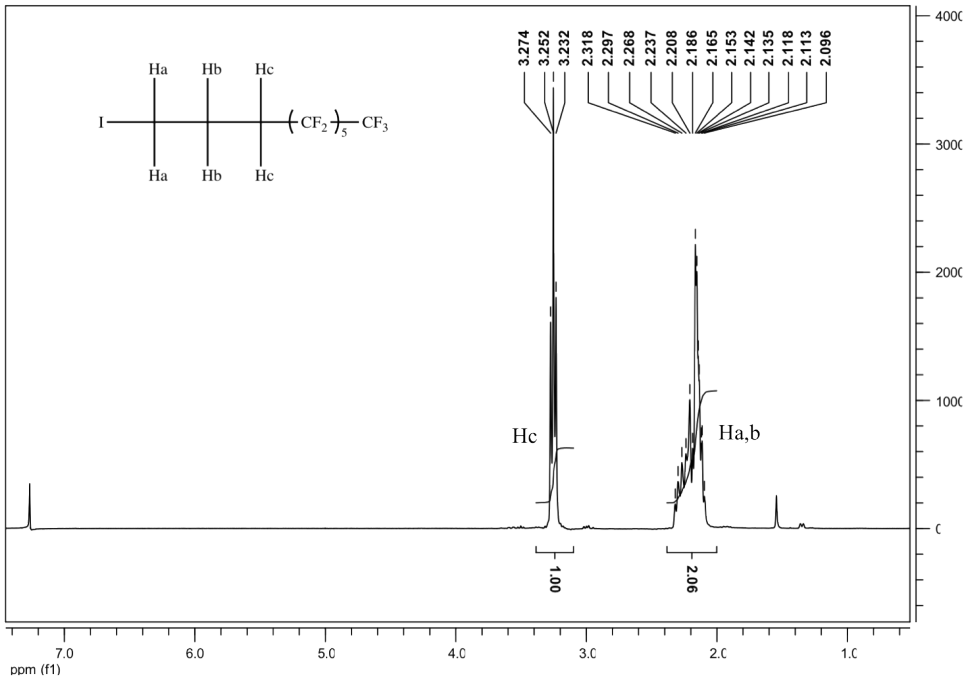

Figure 5.1 (a) ^{1}HNMR Spectrum of P-1.

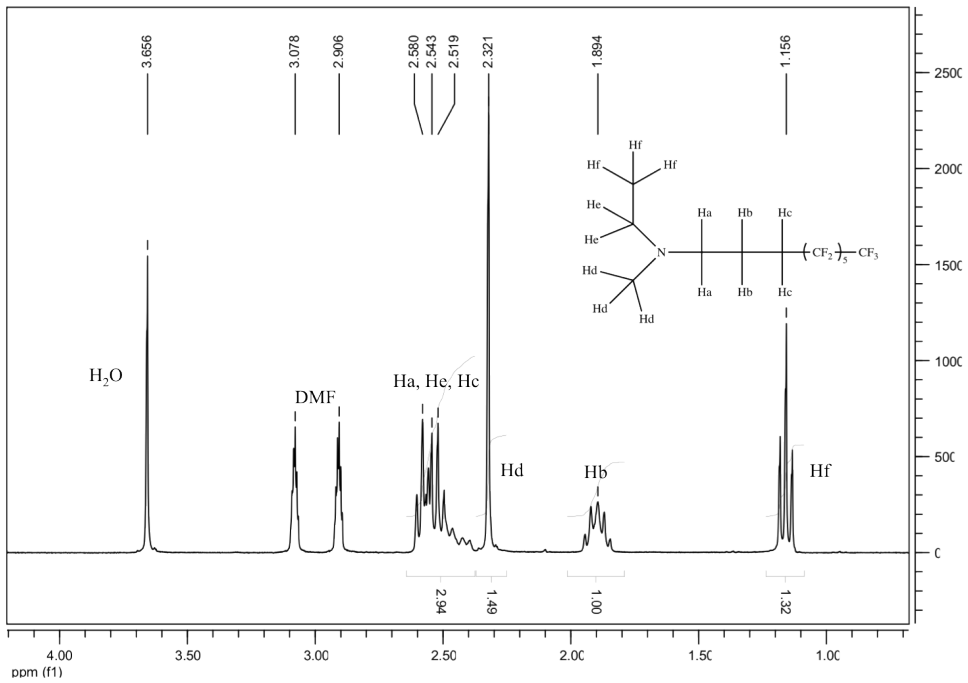

Figure 5.1 (b) ^{1}HNMR Spectrum of P-2.

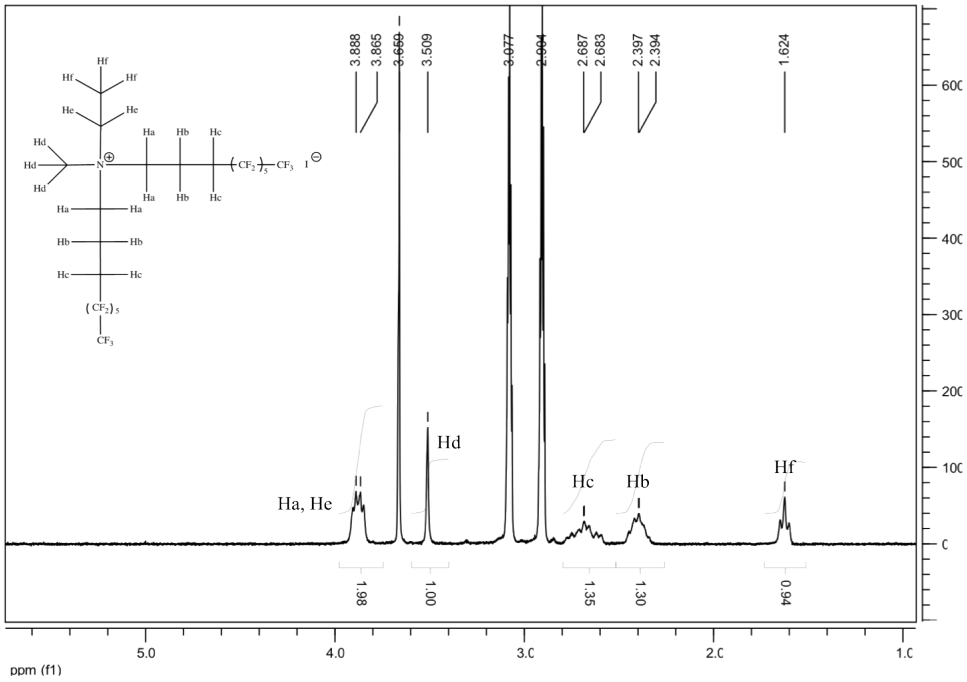

Figure 5.1 (c) ^{1}HNMR Spectrum of P-3

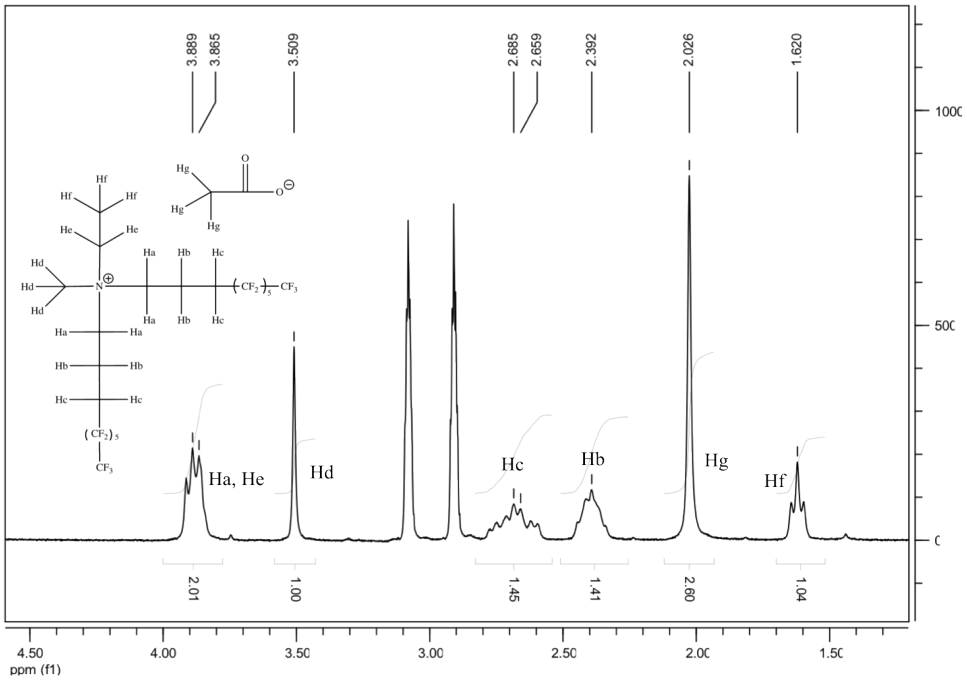

Figure 5.1 (d) ^{1}HNMR Spectrum of QAS

5.2.3 Instrumentation

5.2.3.1 $scCO_2$ Processing System

Scheme 5.1 shows the setup for $scCO_2$ processing. CO_2 gas was chilled into liquid state in the Spe-ed SFE pressure regulator under high pressure. Liquid CO_2 was pumped into the heating oven to reach the supercritical state. Co-solvents and additives were premixed in the pre-mixing chamber. The mixed solution was then pumped into the processing chamber to clean the target wafers.

5.2.3.2 Cloud Point Measuring System

Scheme 5.2 shows the instrument used in measuring the cloud point in order to study the solubility of co-solvents and additives. Co-solvents and additives were pre-loaded in the chamber. High-pressure CO_2 gas was pumped into the processing chamber and then heated and pressurized into its supercritical state to dissolve co-solvents and additives under stirring. A camera was set at the back of the chamber. The cloud point was determined by observing the state of the mixtures in the processing chamber.

5.2.4 Characterizations

Scanning Electron Microscope (SEM) images were taken on a Zeiss Supra Scanning Electron Microscope. Fourier Transform Infrared Spectroscopy (FTIR) was measured on Bruker Hyperion FT-IR Spectrometer & Microscope. Film thicknesses were measured on a Nanofilm EP3 Imaging Ellipsometer. ^{1}H and ^{13}C NMR spectra were recorded on a Varian Mercury-300 (300 MHz) spectrometer at room temperature.

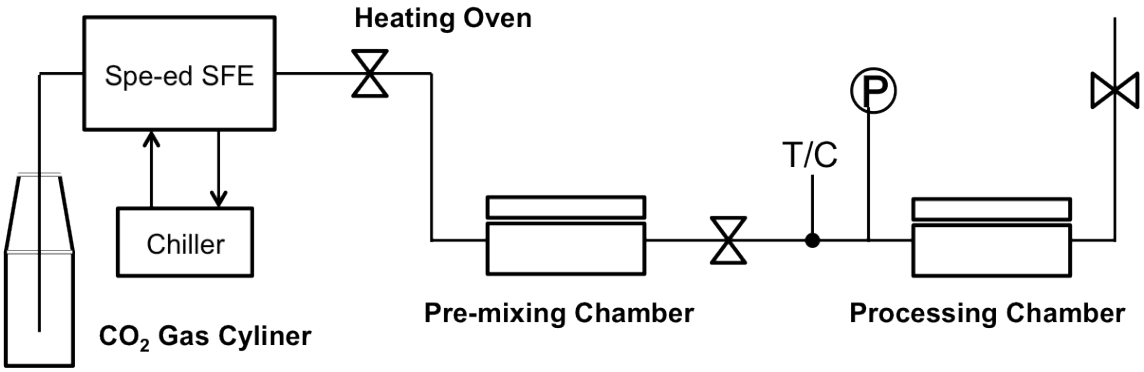

Scheme 5.1. $scCO_2$ processing system. CO_2 is chilled to liquid state and purged into the premixing chamber to reach supercritical state and mixed with additives and cosolvents, which is then purged into the processing chamber.

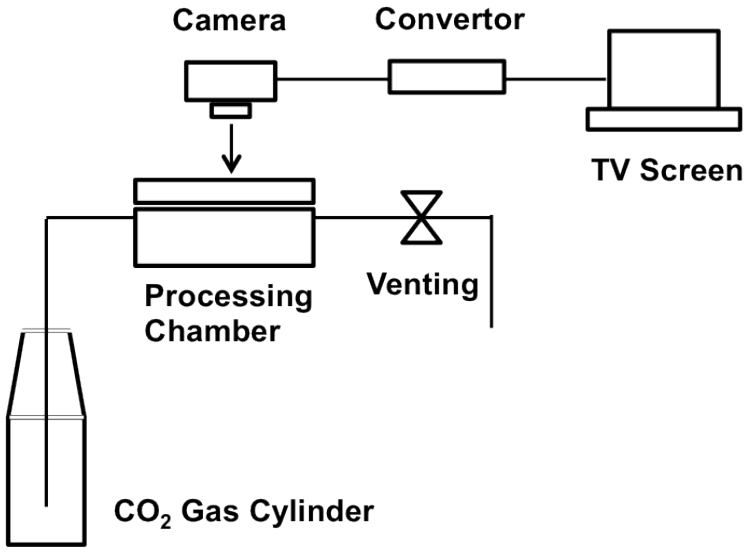

Scheme 5.2. Cloud point measuring system. Liquid CO_2 is purged into the processing chamber and heated and pressurized into the supercritical state. Miscibility of materials with $scCO_2$ can be observed through the camera at the back.

5.3 Results and Discussion

5.3.1 Organic Residue Removal

5.3.1.1 Effect of Co-solvents

Isopropanol (IPA, purchased from Fisher Scientific Co.), propylene carbonate (PC), dimethyl sulfoxide (DMSO), and propylene glycol methyl ether acetate (PGMEA) were selected as co-solvents. Different working conditions were used to study the effect of co-solvents in aiding with cleaning organic residue from wafer surfaces (see Table 5.1). The operating pressure and temperature were fixed at 2030 psi and 50 ^{o}C.

SEM images (Fig. 5.2) show the results of wafer cleaning using different processing conditions. It was found that under the same conditions, (e.g. same amount of solvent and processing time) PC compared with other solvents appeared to be the best co-solvent in removing photoresist residue. Transmission IR spectra (Fig. 5.3) also show consistent results. The uncleaned wafer revealed two specific sharp IR peaks around 1720 cm^{-1}, which were attributed to carbonyl groups within different chemical environments. This is possibly due to the oxidation of the photoresist after plasma etching and pattern transfer. Peaks at ~ 3000-2900 cm^{-1} were attributed to the presence of aliphatic hydrocarbon chains, indicating organic residue left on the wafer. These peaks were found to become weaker or even disappear for some samples after $scCO_2$ cleaning, e.g. the PC-3, DMSO-2 and DMSO-3. For other samples, e.g. IPA and PGMEA, peaks indicating organic residue were still present. This is consistent with the SEM results, which show that PC-3 is the best sample with almost no residue

Table 5.1 Working conditions for cleaning processes with different kinds and amounts of co-solvents and different pre-mixing time and processing time in $scCO_2$.

Co-solvent	Amount (ml)	Pre-mixing Time (min)	Processing Time (min)
PC-1	1	10	10
PC-2	3	10	10
PC-3	3	10	30
DMSO-1	1	10	10
DMSO-2	3	10	10
DMSO-3	3	10	30
IPA	1	10	3
PGMEA	1	10	10

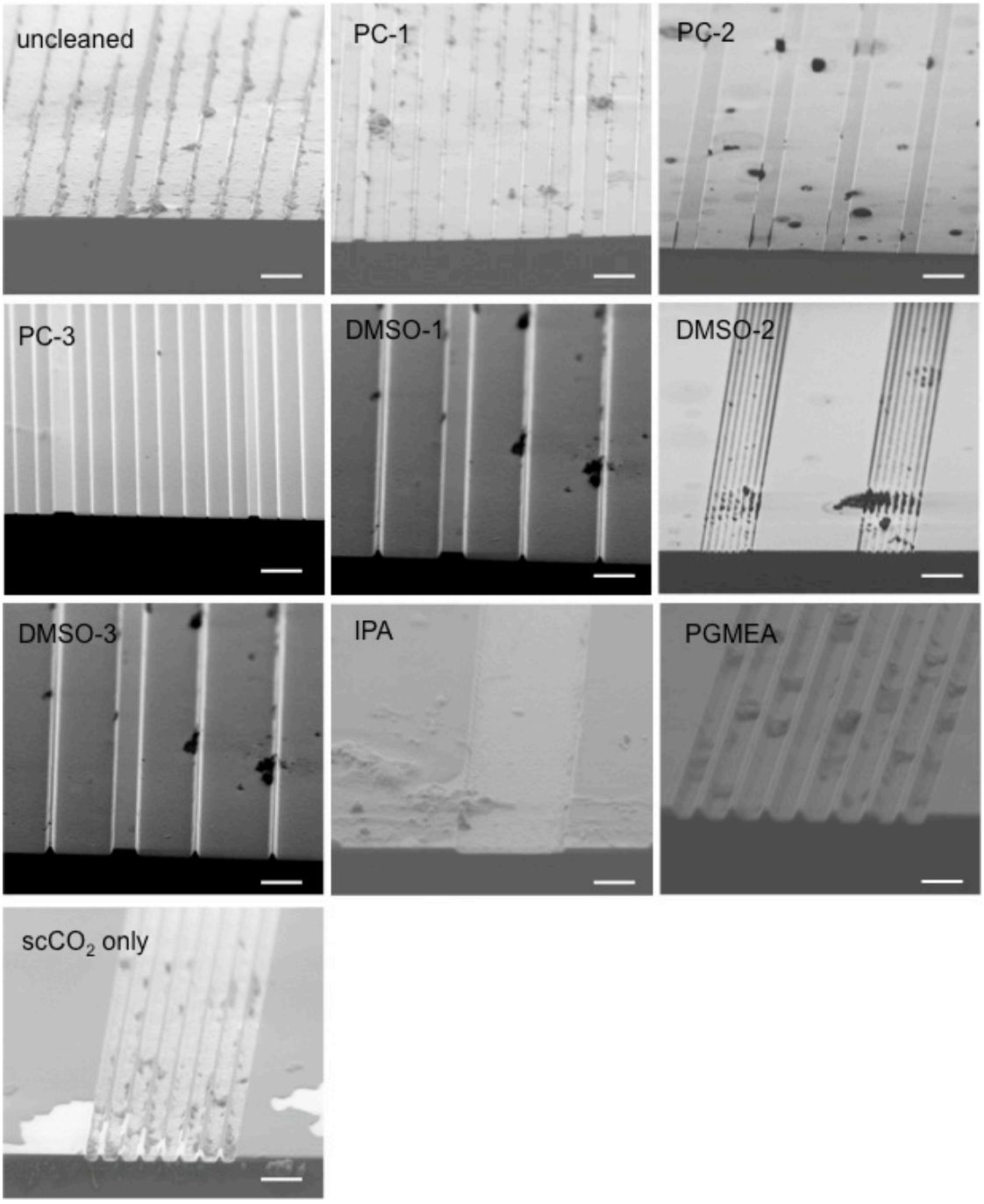

Figure 5.2. SEM images of wafer surfaces treated with different kinds and amounts of co-solvents and different pre-mixing time and processing time in $scCO_2$. Scale bar: 2 μm.

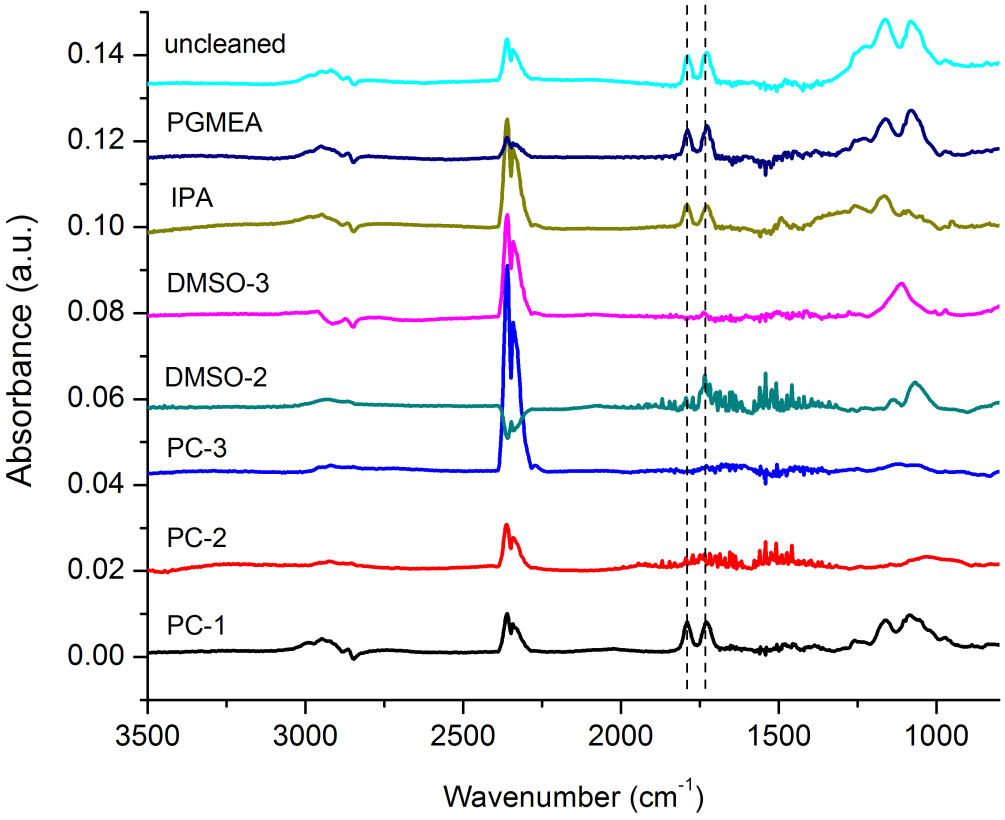

Figure 5.3. FTIR spectra of selected wafer samples cleaned with different kinds and amounts of co-solvents and different pre-mixing time and processing time in $scCO_2$.

left on the wafer.

Although both SEM images and IR spectra indicate that using PC only could have good cleaning results, a relatively long processing time, i.e. 30 min time, and a large amount of PC (3 mL) were needed in order to clean the surface thoroughly. Such processing conditions are feasible in laboratory, but not ideal for real industrial processing. Moreover, a small portion of PC remained in the pre-mixing chamber after venting, which may not meet the standards of practical applications. Reproducibility is another issue. As shown in Fig. 5.4, a second attempt using the same conditions with a different processing time resulted in inferior cleaning than the first attempt. Residue could be found all over the wafer. A possible reason is that the pre-etched wafers may contain different amounts and compositions of organic residue, which makes it difficult to determine the precise amount of co-solvent and the exact processing time needed for each cleaning. This may lead to irreproducible results. Similar situations could also be observed with other co-solvents.

5.3.1.2 Effect of Additives on the Cleaning Mixture

In addition to co-solvents, quaternary ammonium salts (QAS) were also synthesized and applied to help in removal of organic residue on wafer surfaces. Different amounts and operating pressures were used to optimize each set of working conditions (Table 5.2). The pre-mixing time and processing time were both fixed at 10 min, and the temperature was kept at 50 ^{o}C.

SEM images (Fig. 5.5) and IR spectra (Fig. 5.6) show that instead of cleaning the surface, the use of an excess of QAS (0.05 g, Q-1) without co-solvent could

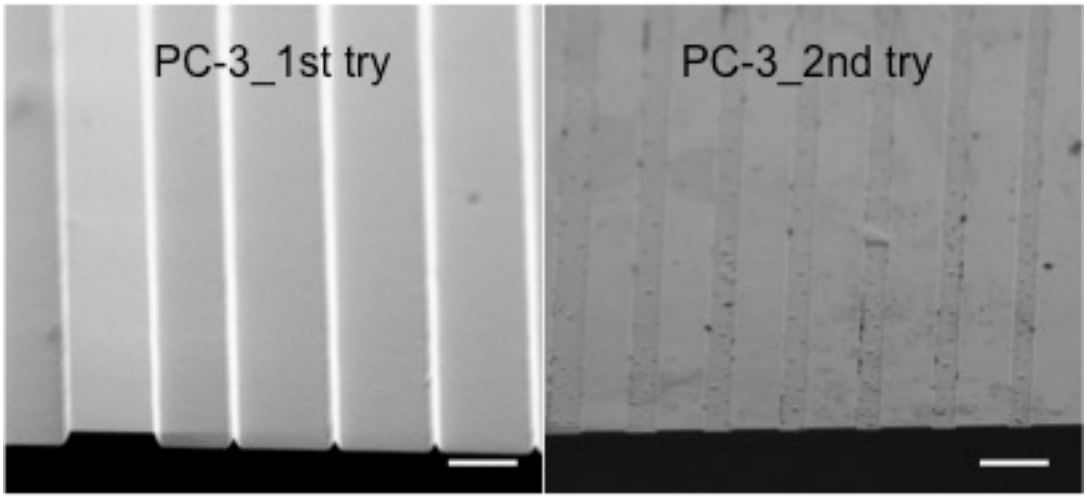

Figure 5.4. SEM images of wafers treated with PC-3 at different times. The cleaning results are not reproducible. Scale bar: 2 μm.

Table 5.2. Optimized conditions for QAS-assisted cleaning processes with different amounts of QAS and co-solvent under different working pressures.

Sample	Amount (mg)	Co-solvent	Pressure (psi)
Q-1	50	none	2030
Q-2	20	none	2030
Q-3	20	none	4060
Q-4	20	none	5000
Q-5	20	0.5 mL PC	2030
Q-6	7	none	5000
Q-7	7	0.5 mL PC	2030

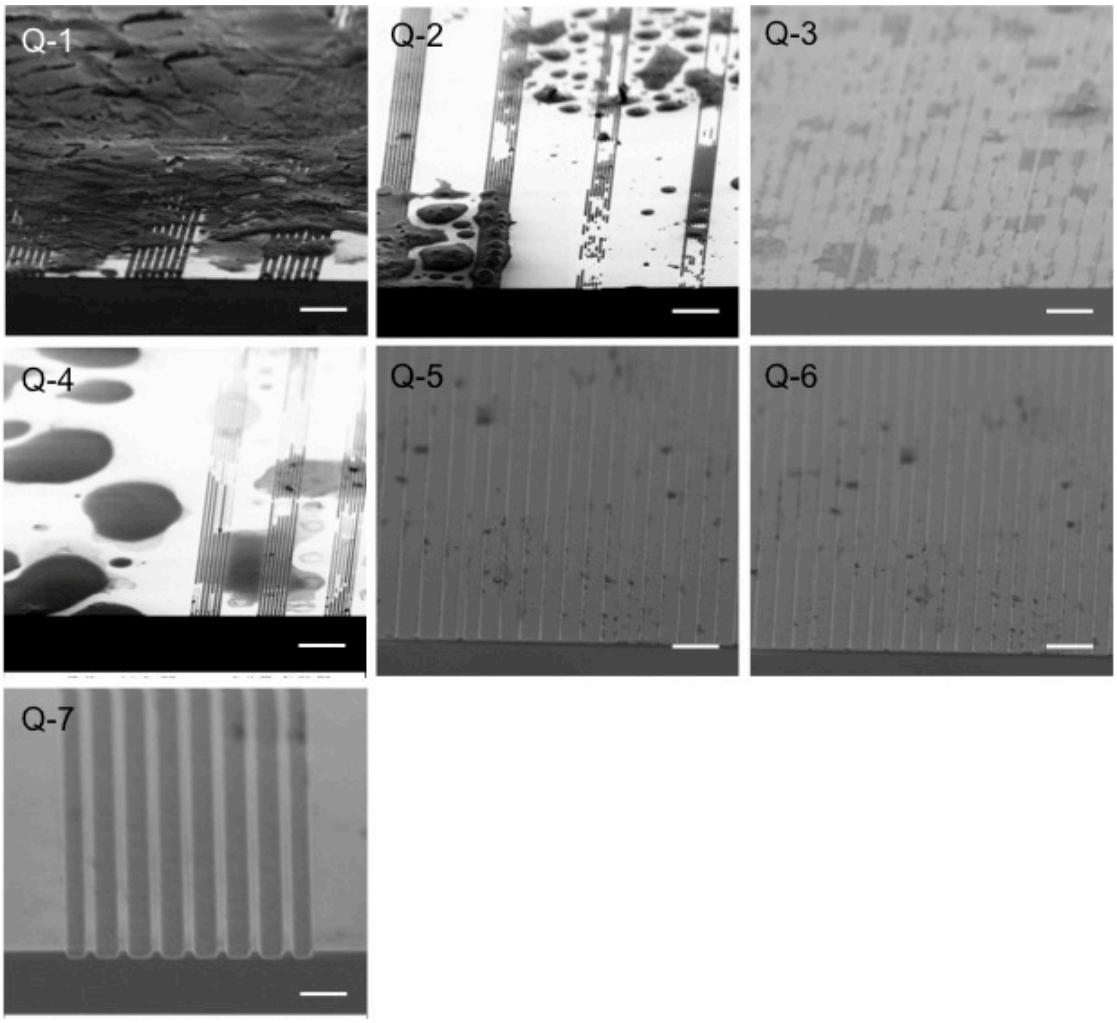

Figure 5.5. SEM images of wafer surfaces treated by QAS-assisted cleaning processes with different amounts of QAS and co-solvent under different working pressures. Scale bar: 2 μm.

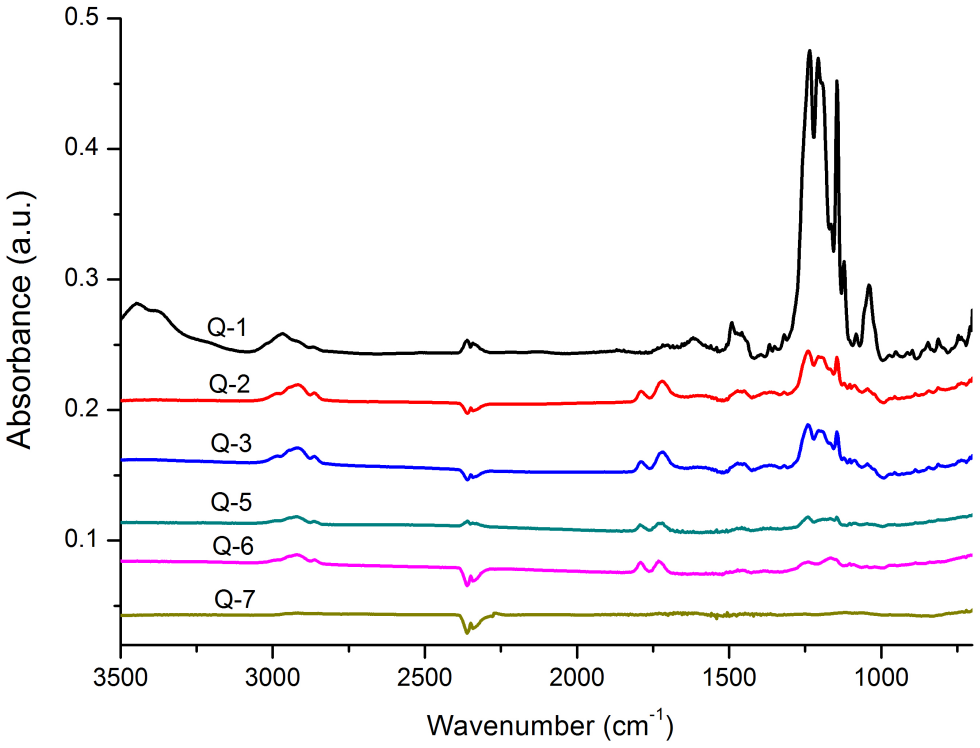

Figure 5.6. FTIR spectra of selected wafer samples cleaned by QAS-assisted cleaning processes with different amounts of QAS and co-solvents under different working pressures.

significantly contaminate the surface. Reducing the amount of QAS to 0.02 g and processing at the same pressure, i.e. 2030 psi, reduced the amount of QAS left on the wafer, but SEM images and IR spectra still showed the presence of both QAS salt and organic residue (Q-2). Increasing the working pressure to 4060 and 5000 psi did not effectively improve the result (Q-3 and Q-4). Addition of 0.5 mL PC as a co-solvent in the QAS cleaning condition was helpful in reducing the amount of residue. Compared to the previous conditions, much less residue could be observed on the wafer (Q-5). It is interesting to find that decreasing the amount of QAS applied (0.007 g) could also help to reduce the QAS contamination (Q-6), although a much higher operating pressure was required. The best cleaning result to date, i.e. Q-7, was obtained by combining QAS and PC in a proper ratio. Only small amounts of QAS and PC were used and the working pressure was as low as 2030 psi. Residue of both QAS and photoresist could hardly be observed on the wafer surface after the 10 min processing time.

It has been shown in Fig. 5.2 that using $scCO_2$ alone could not clean the wafer surface effectively. Using certain co-solvents may help to remove the organic residue produced by etching, while the cleaning results were irreproducible and unpredictable. However, adding small amounts of $scCO_2$-compatible salts such as QAS could improve the cleaning effects. It has been reported that QAS behaves as a surfactant in a $scCO_2$ processing environment [2, 14]. The electro-positive quaternary ammonium end can easily interact with the electro-negative oxygen atom in the carbonate group, forming micelles around the residue. While the long fluorinated chains help to stabilize and solubilize the micelles in $scCO_2$. In combination with co-solvents such as

PC which can further facilitate the dissolution of both QAS and organic residue, dry cleaning of wafers after etching was successfully achieved. The small amount used, relatively low operational pressure and a short cleaning time all provide potential possibilities for practical industrial processing applications.

5.3.2 TiN Etching

In microelectronics devices, titanium nitride has long been used as a diffusion barrier in aluminum and copper metallization since the 1980's [20-22]. Recently it has been recognized as a low-resistsnce, metallic material for gate electrodes in complementary metal–oxide–semiconductor (CMOS) technology [23-25]. TiN is commonly etched either in plasma or strong oxidation aqueous solutions such as SC-1 or 'piranha solution' [26-28]. Herein, we first report etching TiN in wet organic solutions and dry $scCO_2$ processing as well.

TiN etching was first done in organic solvents. To formulate a similar composition to traditional oxidation etching solution, a strong organic acid, a strong organic peroxide and an organic solvent were mixed. Chemical structures of the reagents used in organic wet etching processes are shown in Scheme 5.3.

Figure 5.7 shows the best results encountered for organic wet etching of TiN films. Compared to traditional SC-1 aqueous etching at room temperature, etching of TiN in IPA at 65^{o}C was even faster. The relatively slow etching in the first 15 min was believed to be etching of a thin layer of titanium dioxide (TiO_2), which was formed on top of the TiN film due to exposure of the film to air. Once the more robust TiO_2 layer (~2-3 nm) was etched away, a much faster etching process was achieved. About 20nm

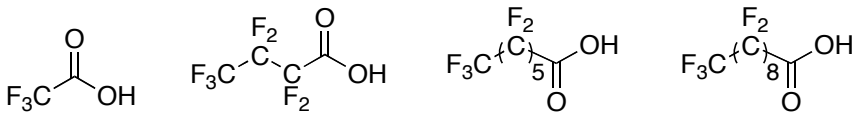

F1 acid F3 acid F6 acid F9 acid

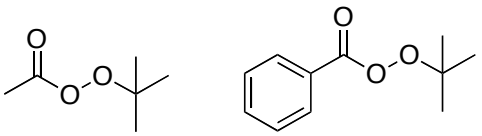

t-BPA t-BPB

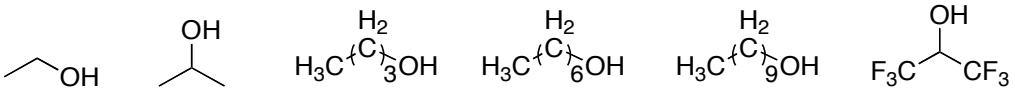

Ethanol IPA 1-butanol 1-heptanol 1-decanol F-IPA

Scheme 5.3. Chemicals used in TiN etching processes. Top: perfluorinated organic acids as strong acids; Middle: organic peroxides as strong oxidants; Bottom: alcohols as co-solvents and stabilizers.

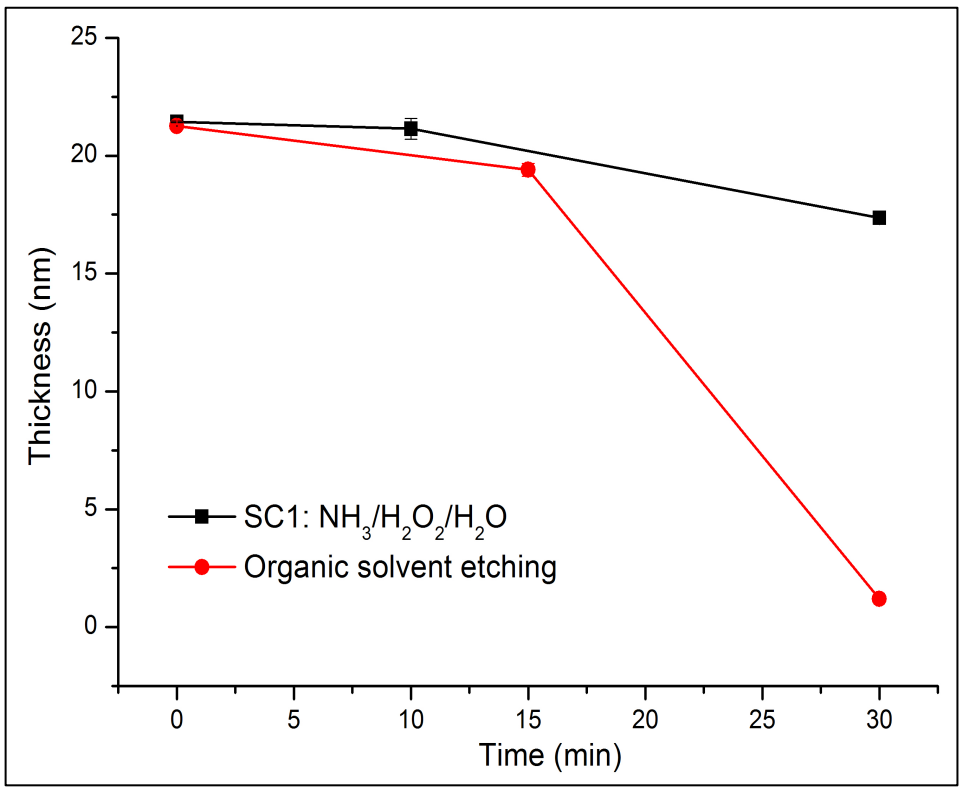

Figure 5.7. TiN wet etching in organic solvents compared with traditional SC1 solution. Volume ratio of F3/t-BPA/IPA=1.667/0.153/2. Reaction was done at 65°C.

of TiN was etched away within the latter 15 min. The etch rate is estimated to be 1.3 nm/min.

Detailed studies were performed to optimize the reaction conditions. Fig. 5.8 (a) shows different etching results with and without peroxide. It could be clearly seen that adding peroxide to the system is necessary to reach a relatively fast etch rate. Almost no etching could be observed without peroxide, while 20 nm of TiN was etched after 4 hours in the presence of peroxide. This indicates that peroxide dramatically facilitates the etching process. It is worth mentioning that during the first 2 hours, no etching was found whether the peroxide was used or not. Because this experiment was done with no pre-reaction time of the reagents, we assume that during the first 2 hours, instead of etching TiN, some reaction occurred among the reagents, especially between the F3 acid and the alcohol.

The amount of peroxide used is also critical to successful etching. As shown in Fig. 5.8 (b), no etching was achieved without peroxide, while the most effective etching was obtained when 1 mL of t-BPA was used. Increasing the amount of t-BPA makes a strong negative impact on TiN etching. Less than 5 nm of TiN was etched away when the amount of t-BPA was over 2 mL, indicating a seriously retarded etching process.

Concentrations of the acid and peroxide in the solution play another important role in affecting the etching results. Fig. 5.8 (c) shows that no etching was observed even after 7 hours of processing time when the volume ratio of t-BPA and IPA was below 0.15. Total etching of 20 nm of TiN was done after the volume ratio was increased to 0.2, which appeared to be a critical point for this working solution.

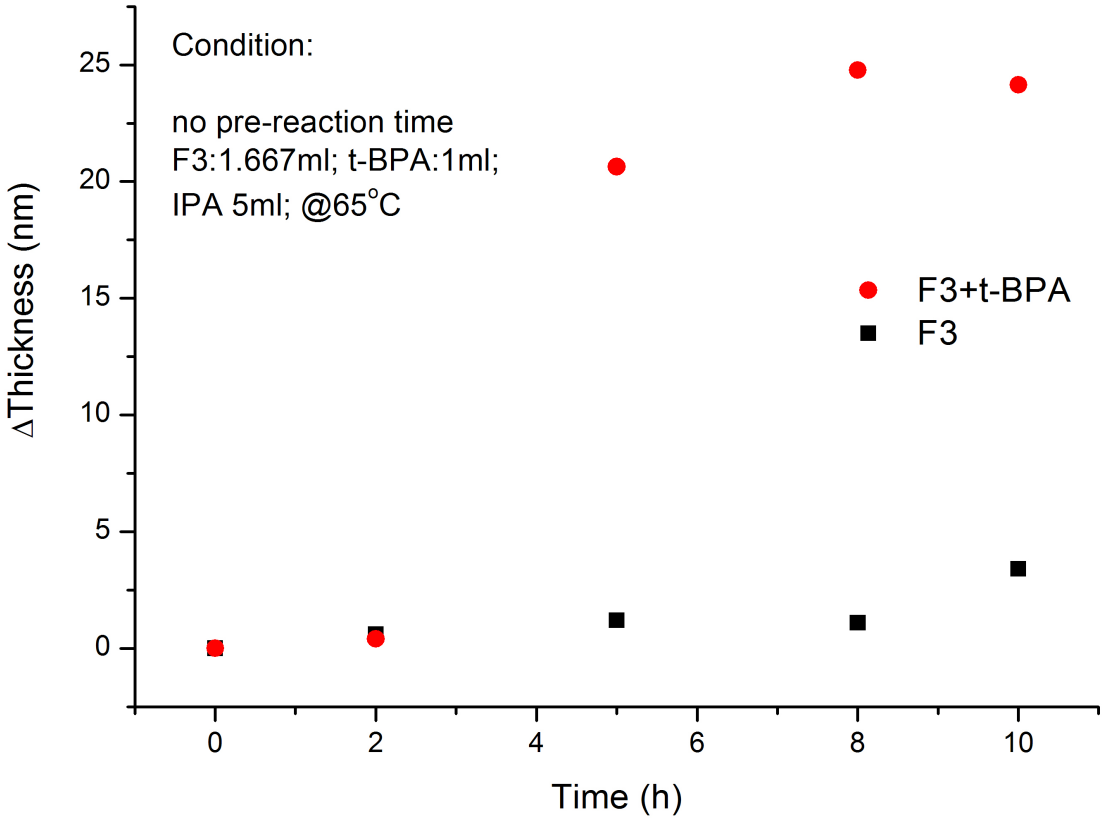

Figure 5.8 (a). Peroxide effect on TiN etching. Etching process is more effective in the presence of peroxide.

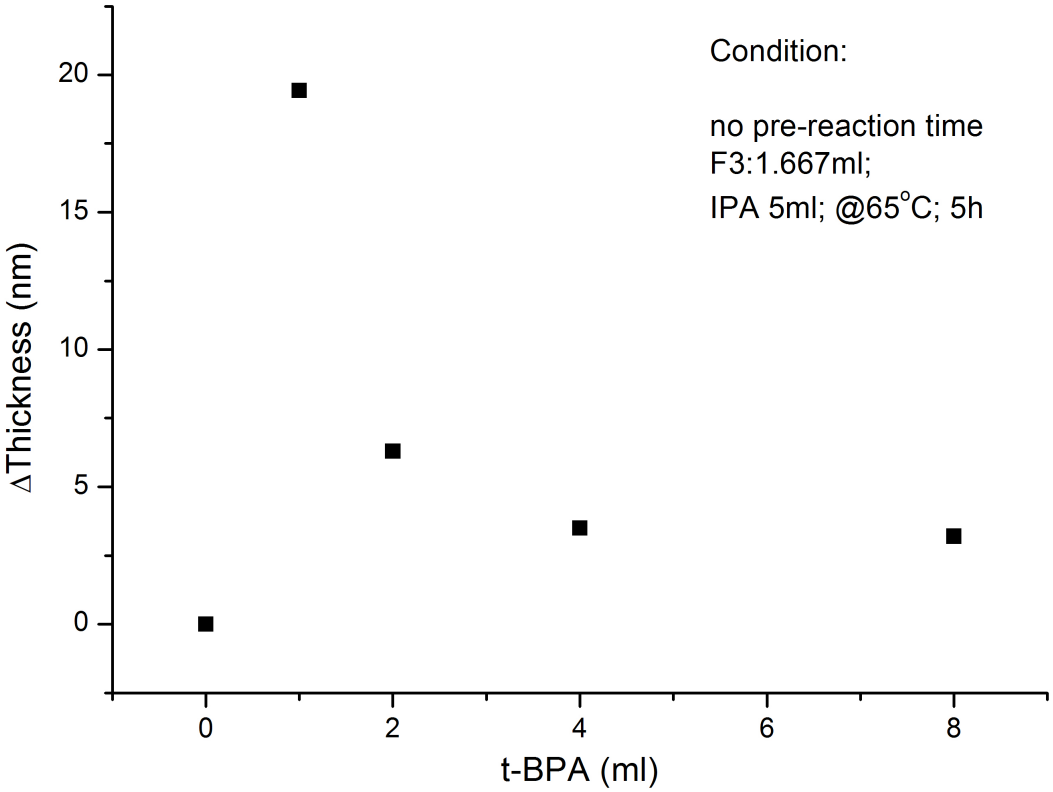

Figure 5.8 (b). Effect of amount of peroxide on TiN etching. Large amounts of peroxide are harmful for TiN etching.

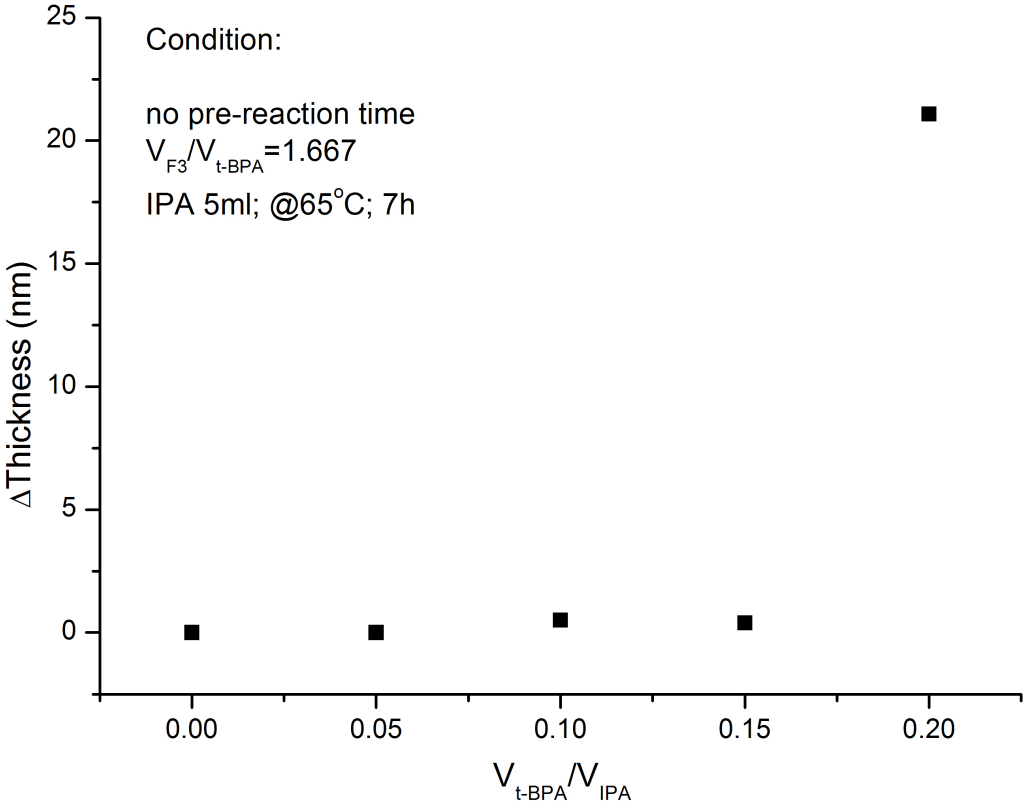

Figure 5.8 (c). Effect of concentration of acid and peroxide on TiN etching. Successful etching is achieved with high concentrations of acid and peroxide.

In order to study a detailed mechanism of this unique system, different reactants and reaction conditions were attempted. Table 5.3 lists the results of TiN wet etching in organic solutions. By comparing Entry 1 and 2, we find that the stronger the acid used, the faster the etch rate. Etch rate of F3 acid is 37.5 times faster than F1 acid. Stronger acids such as F-6 and F-9 were also used. Although exact etch rate still needs to be measured, total TiN etching could be achieved (Entries 3 & 4). Results of entries 5-10 provide a deeper understanding of the system. Acid alone, no matter how strong it is, resulted in zero etching (Entries 5-7). Without peroxide or acid, no etching occurred (Entries 8 & 9). It is surprising to find that there was no etching when no IPA was used (Entry 10), which indicates that every component is essential for successful TiN wet etching. Replacing IPA with different organic solvents such as toluene or DMSO, no etching occurred (Entry 11), while using other alcohols such as ethanol and 1-butanol always achieved total etching of TiN (Entries 12-16). One more experiment was done to confirm the role the alcohol played. After 2h pre-reaction time of F3 acid, t-BPB and IPA, 20 ml of toluene was added in the system. Total TiN etching was done in 6h (Entry 17). Studies of different reaction conditions prove that alcohol is a critical component for the etchant to work effectively.

In order to further investigate the function of alcohols in organic wet etching of TiN, ^{13}C NMR was used to characterize the species produced during the pre-reaction time. Fig. 5.9 (a-c) shows the ^{13}C NMR spectra of the original F3-acid, t-BPB and IPA. Fig. 5.9 (d) shows the spectrum of the mixture after 2 h reaction time at 65^{o}C. Two new peaks appeared in the solution spectrum compared to those of the initial reactants, i.e. peaks at 21.05 and 73.73 ppm. A slight shift of the carbonyl group (attributed to

Table 5.3. Listed results of TiN wet etching under different reaction conditions with different acids, peroxides and solvents.

Entry	Acid	Peroxide	Solvent	Etch Rate
1	F1	t-BPA	IPA	1.56 nm/h
2	F3	t-BPA	IPA	1.33 nm/min
3	F6	t-BPA	IPA	25 nm/24h*
4	F9	t-BPA	IPA	25 nm/24h*
5	F3	-	-	0
6	F6	-	IPA	0
7	F9	-	IPA	0
8	F3	-	IPA	0
9	-	t-BPB	IPA	0
10	F3	t-BPA	-	0
11	F3	t-BPA	DMF Toluene Ethyl Acetate DMSO F-IPA	0
12	F3	t-BPA	EtOH	25 nm/3h*
13	F3	t-BPB	IPA	25 nm/1h*
14	F3	t-BPB	1-Butanol	25 nm/1h*
15	F3	t-BPB	1-Heptanol	25 nm/7h*
16	F3	t-BPB	1-Decanol	25 nm/7h*
17	F3	t-BPB	IPA/Toluene	25 nm/6h*

* Exact etching rate has not been measured.

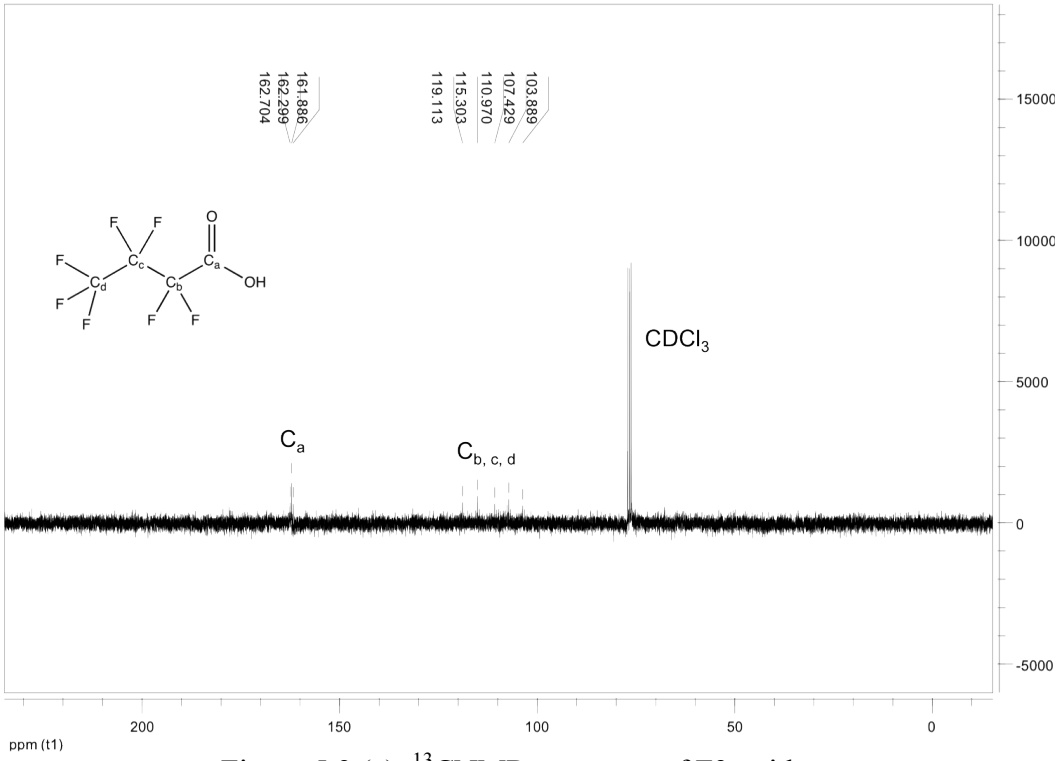

Figure 5.9 (a). ^{13}CNMR spectrum of F3-acid.

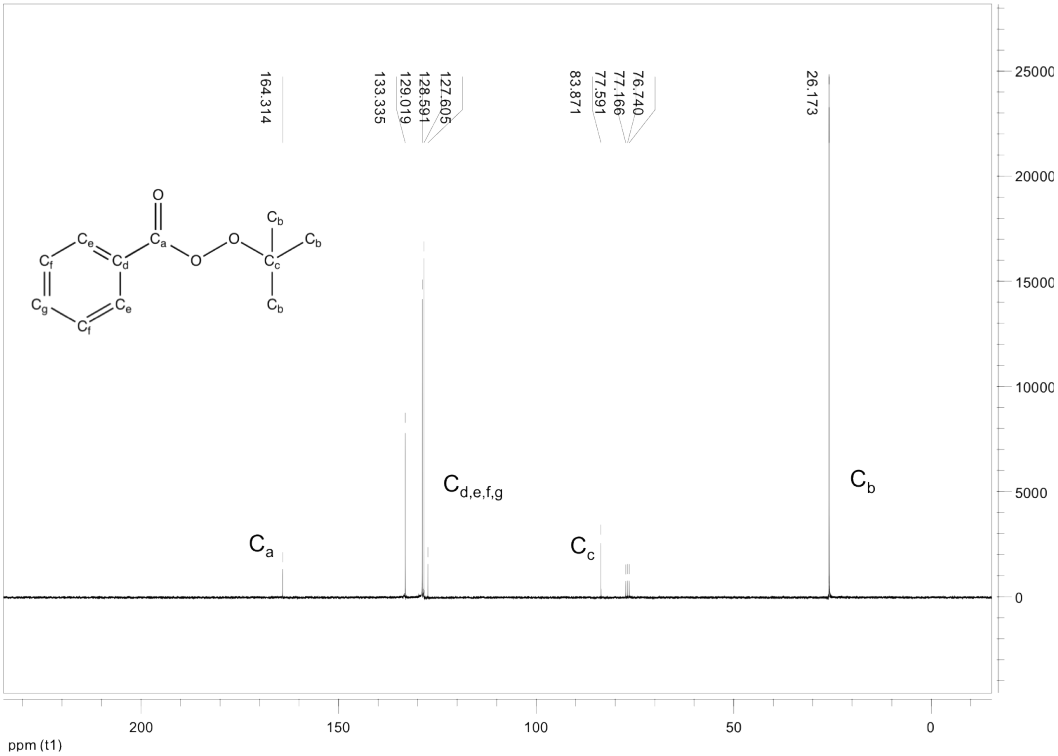

Figure 5.9 (b). ^{13}CNMR spectrum of t-BPB.

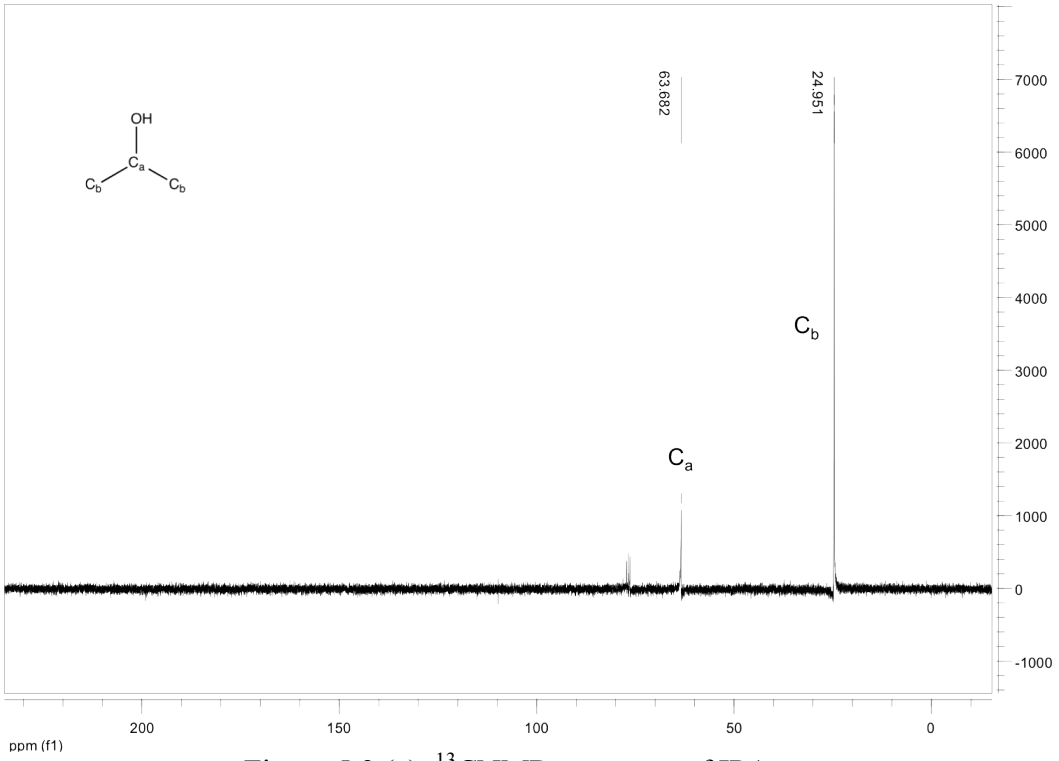

Figure 5.9 (c). ^{13}CNMR spectrum of IPA.

Figure 5.9 (d). ^{13}CNMR spectrum of mixture after 2 h reaction time.

F3 acid) from 162 ppm to 160 ppm could also be observed. To clarify these two new peaks, every possible combination of two of the three reactants was used under the same reaction conditions. Fig. 5.10 (a) shows the ^{13}CNMR spectrum of F3 acid with t-BPB. Although several new peaks appeared, none matches the new peaks in Fig. 5.9 (d). Fig. 5.10 (b) shows a spectrum of IPA with t-BPB. No new peaks were found, indicating no reaction between the alcohol and peroxide. Fig. 5.10 (c) shows the spectrum of F3 acid with IPA. Two new peaks at 20.93 ppm and 73.65 ppm and the shift of the C=O group of the F3 acid appeared, consistent with what is observed in Fig. 5.9 (d). Comparing Figs. 5.10 (a) to (c) provides a clearer vision o the origin of the two new peaks after the reaction of the three components (Fig. 5.10 (d)). The ^{13}CNMR spectra obviously indicate no reaction between IPA and t-BPB, while there is a reaction between F3 acid and t-BPB and between F3 acid and IPA. However, upon mixing three reactants, only reaction between F3 acid and IPA occurs. It is also interesting to find from Entry 10 in Table 5.3 that there was no etching without the alcohol. Experimental observations show that the solution remained clear after pre-reaction when all the components were used, while a dark solution was formed when only acid and peroxide were used (Fig. (5.11)). Drastic reactions between acid and peroxide are not unusual, which will consume both of the reactants quickly before TiN is etched away. When alcohol is added, the reaction between acid and peroxide is inhibited. It is theorized that alcohol is behaving as a stabilizer of the entire system by reacting with the acid. Since F3 acid is a strong acid, it is assumed that this stabilization effect was achieved through a self-catalysis esterification reaction between F3-acid and IPA as shown in Scheme 5.4 (a). The two new peaks belong to

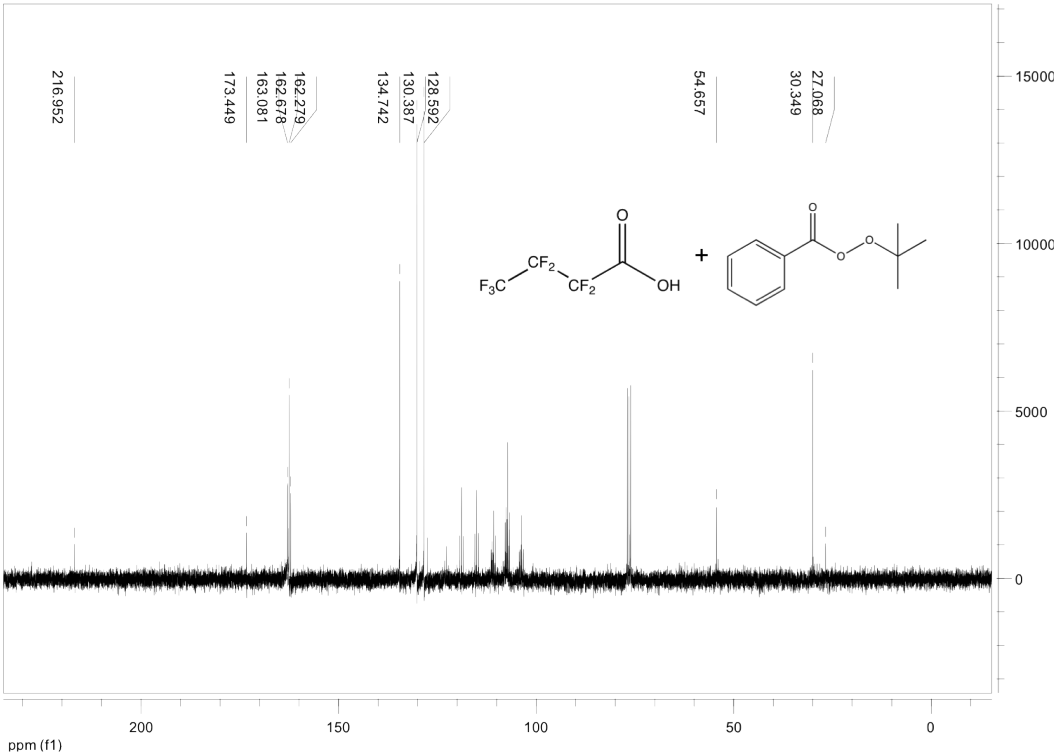

Figure 5.10 (a). ^{13}CNMR spectrum of reaction between F3-acid and t-BPB.

Figure 5.10 (b). ^{13}CNMR spectrum of reaction between IPA and t-BPB.

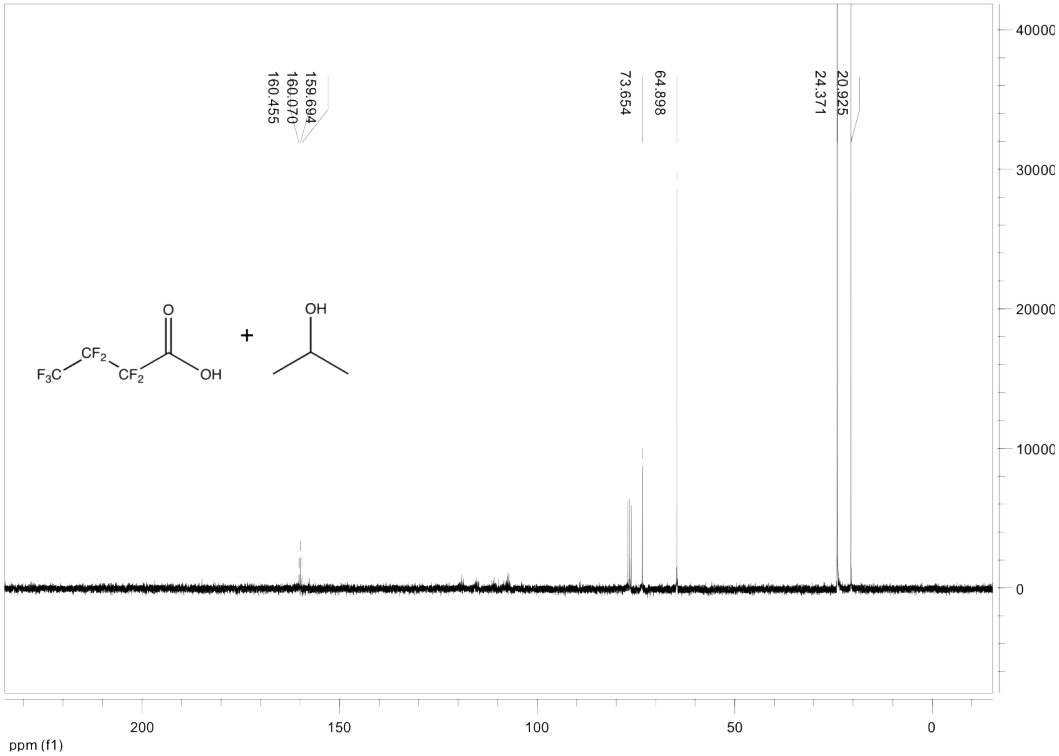

Figure 5.10 (c). ^{13}CNMR spectrum of reaction between F3-acid and t-IPA.

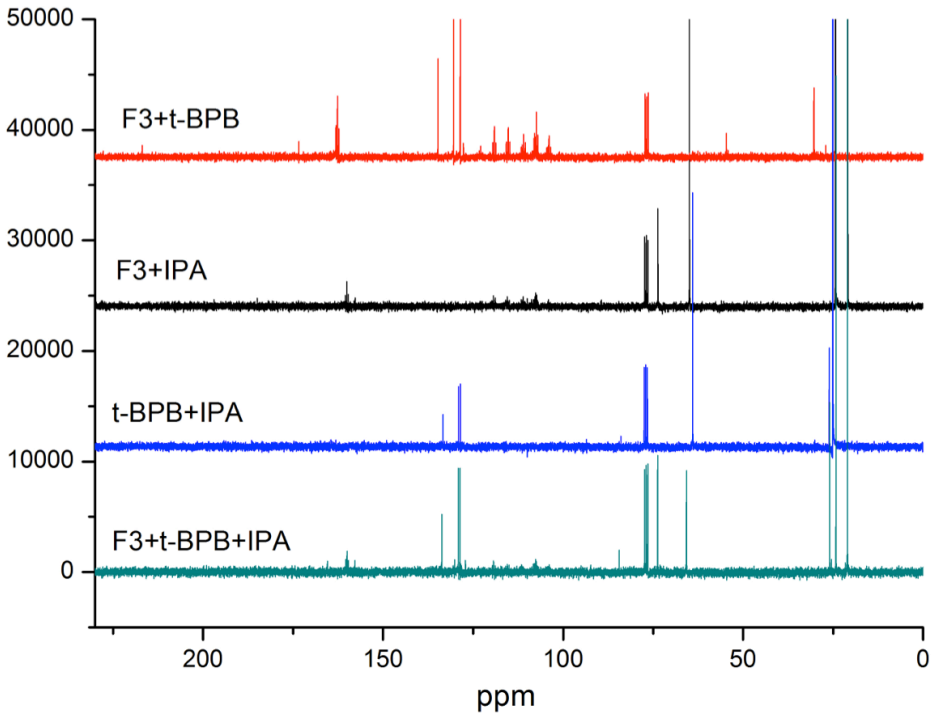

Figure 5.9 (d). Compiled ^{13}CNMR spectra of reaction between F3-acid, t-BPB and IPA.

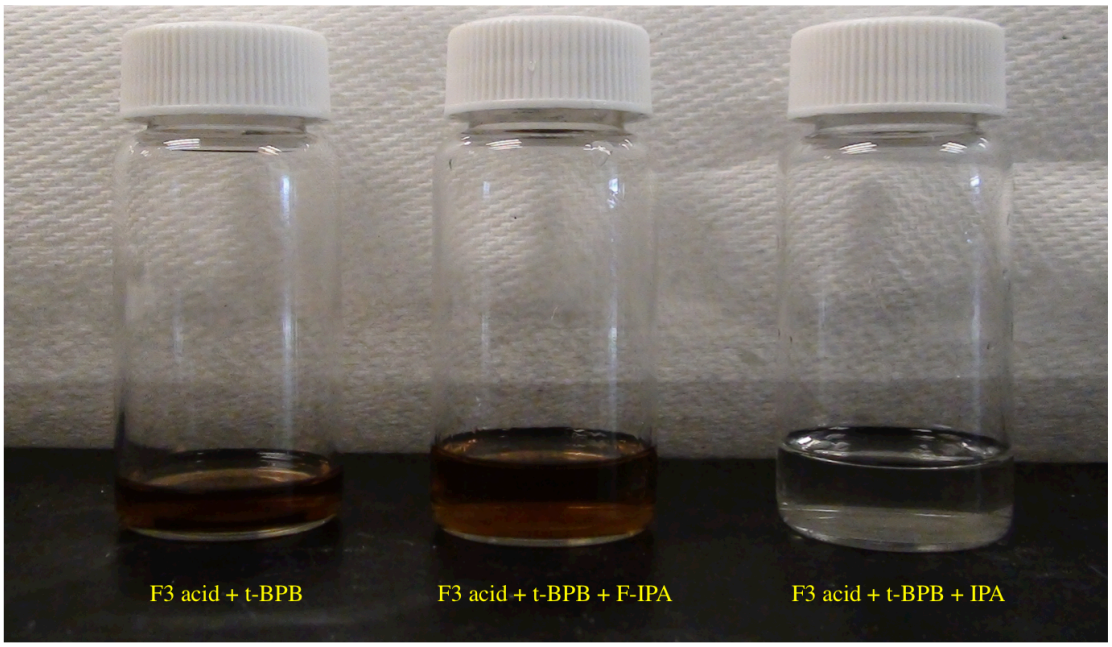

Figure 5.11. Experimental observation of mixing different components. Reaction condition: 2 h at 65 ^{o}C.

the primary and tertiary carbons adjacent to the newly formed ester group.

To verify this assumption, 1,1,1,3,3,3-Hexafluoro-2-propanol (F-IPA) was used to replace IPA. The same reactions were conducted under the same conditions. From Fig. 5.12, it is apparent that no reactions occurred between F3 acid and F-IPA. Since the reactivity of esterification between carboxylic acids and alcohols under acid catalysis depends on the nucleophilicity of the oxygen atom from the alcohols, it is reasonable that F-IPA, which has the more electron withdrawing - CF_3 - groups, is much less reactive than IPA. Instead, reaction between F3 acid and t-BPB occurred, which is consistent with the 'no-etching' results of Entry 11 in Table 5.3.

^{13}C NMR analysis shows that esterification reaction between F3 acid and IPA is the key element in stabilizing the strong acid-peroxide system, which will further facilitate the successful etching of TiN in the organic environment. The ester formed may serve as a reservoir of F-acid, releasing it gradually during the etching process, retarding the reactions between the acid and peroxide. Moreover, the water formed in the esterification reaction may also help to prevent the hydrophilic acid from reacting directly with the hydrophobic peroxide. Detailed studies are needed to clarify the real functions of each component in the system and the mechanism of TiN etching as well.

Selective etching of TiN over SiO_2, PolySi and Si_3N_4 is shown in Table 5.4. Etching was done with F3 acid, t-BPB and IPA at 65^oC for 1h. It was found that this system only worked for TiN. No etching of SiO_2, PolySi or Si_3N_4 was observed, indicating good selectivity of TiN etching.

Dry etching of TiN in $scCO_2$ was then attempted using similar reactants and

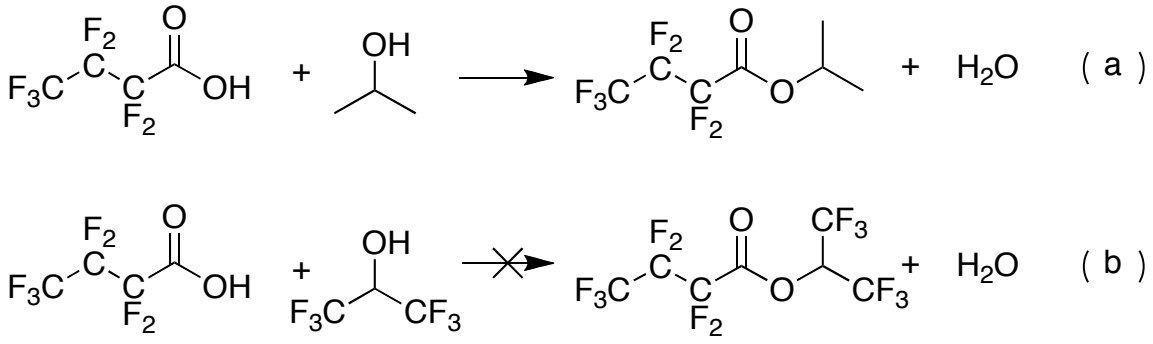

Scheme 5.4. Stabilization mechanism of alcohols. (a) Esterification reaction between F3 acid and IPA. (b) No reaction can occur between F3 acid and F-IPA.

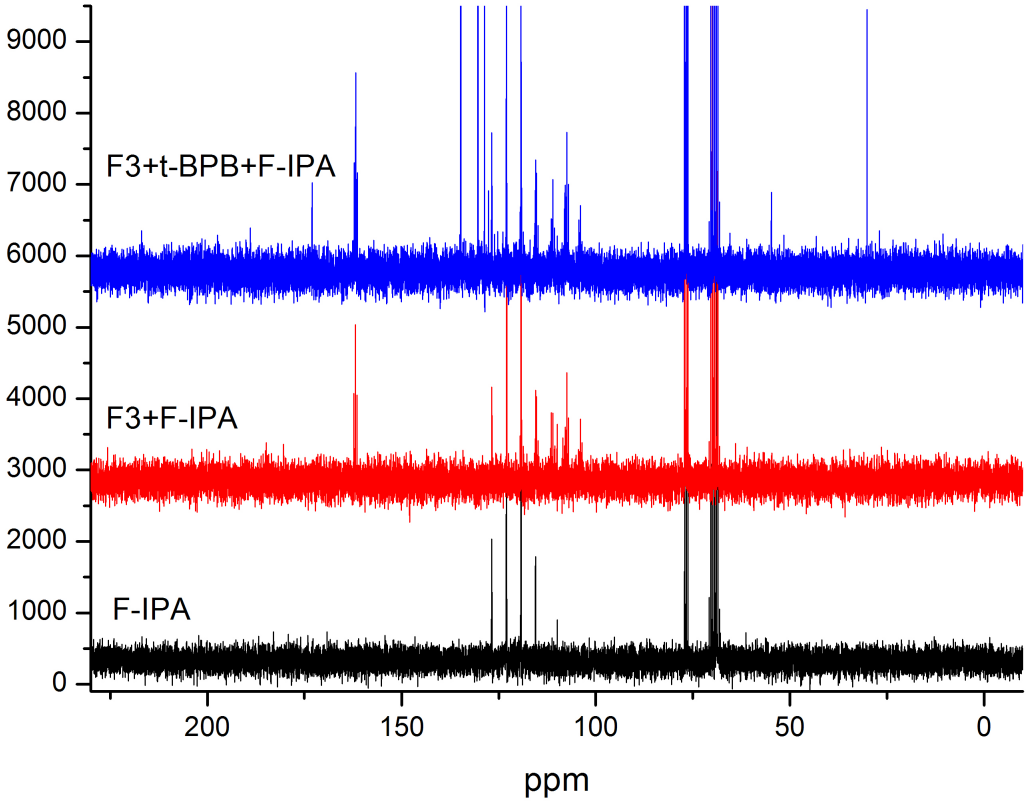

Figure 5.12. Compiled ^{13}CNMR spectra of reaction between F3-acid, t-BPB and F-IPA.

Table 5.4. Selective etching of TiN.

	ΔT (nm)
TiN	23
Si_3N_4	0
PolySi	0
SiO_2	0

reaction conditions. Table 5.5 shows the results of TiN dry etching. Although most of the processes did not work as effectively as in organic solvents, one sample showed a promising result. By using 1-decanol as the stabilizer, partial etching of TiN was achieved. As can be seen in Fig. 5.13, the thickness of dark spots on the wafer treated in $scCO_2$ is about 21 nm. Compared with the virgin wafer which has a thickness about 24 nm, 3 nm of TiN (or TiO_2) was etched away after 1 hour processing time. Possible reasons for the inhomogeneous and ineffective etching in $scCO_2$ are that leaking of $scCO_2$ from the chamber might result in quick loss of alcohol, or $scCO_2$ might have facilitated the reaction between F3 acid and peroxide, destroying the stability of the working system. Noticing that 1-decanol has longer aliphatic chains than isopropanol and 1-butanol, it is assumed that alcohols with higher viscosity and lower volatility should be applied in the dry etching process. More detailed optimization experiments need to be done for a complete and successful dry etching of TiN by $scCO_2$ processing.

5.4 Conclusion

By using co-solvents and additives, dry cleaning of the post-etch wafer in $scCO_2$ was successfully achieved. Fundamental studies show that changing the processing conditions such as the amount of co-solvent and additive, processing time and operating pressure, could affect the results of wafer cleaning. The best working condition was found to be using a small amount of both additives and co-solvents with a relatively low working pressure and short processing time.

Etching of TiN was successfully achieved in organic solvents, especially alkyl

Table 5.5. Drying etching of TiN in $scCO_2$ with different acids, peroxides, alcohols and processing time.

Entry	Acid	Peroxide	Solvent	$scCO_2$ processing time /h	Etch Rate
1	F1	-	-	4h	0
2	F3	t-BPA	IPA	4h	0
3	F6	t-BPB	Ethanol	4h	0
4	F9	t-BPB	1-butanol	4h	0
5	F3	t-BPB	1-heptanol	4h	0
6	F6	t-BPB	1-decanol	1h	3 nm / h

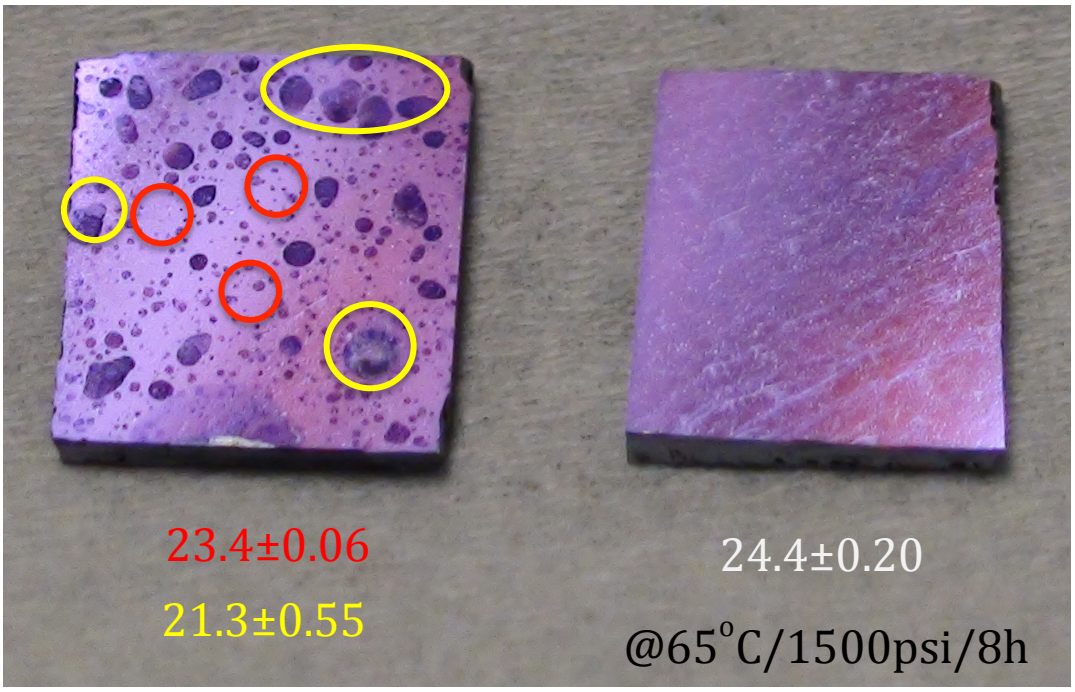

Figure 5.13. TiN dry etching in $scCO_2$ with F3 acid, t-BPB and 1-decanol. Left: wafer after processing; Right: virgin wafer.

alcohols. Detailed studies using ^{13}C NMR measurements of the reactants show that alcohols were serving not only as solvents, but stabilizers as well, preventing the reaction between strong acid and peroxide. Selective etching results show that this unique system was specifically suited for TiN etching. Although etching in $scCO_2$ was not as effective, some promising results still indicate potential applications of $scCO_2$ in TiN dry etching processes.

5.5 Acknowledgements

The authors is grateful to Samsung Co. Ltd. for financial support, to the Cornell-KAUST research center, the Nanobiotechnology Center (NBTC) and Cornell Center for Materials Research (CCMR) for use of their facilities. The author is also grateful to Dr. Yisheng Xu for wafer characterizations and Dr. Hyosan Lee from Samsung Company for technical support.

REFERENCES

(1) Romang, A.H.; Watkins, J. J. *Chem. Rev.* **2010**, *110*, 459.

(2) Tanaka, M.; Rastogi, A.; Toepperwein, G. N.; Riggleman, R. A.; Felix, N. M.; Pablo, J. J.; Ober, C. K. *Chem. Mater.* **2009**, *21*, 3125.

(3) Tomohiro, K.; Hoto, N.; Kawata, H.; Hirai, Y. *J. Photopolym. Sci. Tec.* **2011**, *24*, 71.

(4) Ramanathan, M.; Tseng, Y.-C.; Ariga, K.; Darling, S. B. *J. Mater. Chem. C* **2013**, *1*, 2080.

(5) Johnston, D. E.; Lu, M.; Black, C. T. *J. Micro/Nanolith. MEMS MOEMS* **2012**, *11*, 031306.

(6) Chini, S. F.; Amirfazli, A. *J. Micro/Nanolith. MEMS MOEMS* **2012**, *11*, 033003.

(7) Del Campo. A.; Arzt, E. . *Chem. Rev.* **2008**, *108*, 911.

(8) Tarutani, S.; Tsubaki, H.; Takizawa, H.; Goto, T. *J. Photopolym. Sci. Tec.* **2012**, *25*, 597.

(9) Cao, H.; de Pablo, J.; Nealey, P. Proceedings of the 44th International Conference on Electron, Ion, and Photon Beam Technology and Nanofabrication, 29 May–2 June 2000, Palm Springs, CA.

(10) Weibel G.L.; Ober C. K. *Microelectron. Eng.* **2003**, *65*, 145.

(11) Namatsu, H; Yamazaki, K; Kurihara, K. *Microelectron. Eng.* **1999**, *46*, 129.

(12) Jones, C. A.; Zweber, A.; DeYoung, J. P.; McClain, J. B.; Carbonell, R. DeSimone, J. M. *Crit. Rev. Solid State* **2004**, *29*, 97.

(13) Goldfarb, D. L.; de Pablo, J. J.; Nealey, P. F.; Simons, J. P.; Moreau, W. M.; Angelopoulos, M. *J. Vac. Sci. Technol. B* **2000**, *18*, 3313.

(14) Zweber, A. E.; Wager, M.; DeYoung, J.; Carbonell, R. G. *Langmuir* **2009**, *25*, 6176.

(15) Ventosa, C.; Rebiscoul, D.; Perrut, V.; Ivanova, V.; Renault, O.; Passemard, G. *Microelectron. Eng.* **2008**, *85*, 1629.

(16) Ota, K.; Tsutsumi, A. *J. Mech. Design.* **2008**, *2*, 619.

(17) Bessel. C. A.; Denison, G. M.; DeSimone, J. M.; DeYoung, J.; Gross, S.; Schauer, C. K.; Visintin, P. M. *J. Am. Chem. Soc.* **2003**, *125*, 4980.

(18) Jones, C. A.; Yang, D. X.; Irene, E. A.; Gross, S. M.; Wagner, M.; DeYoung, J.; DeSimone, J. M. *Chem. Mater.* **2003**, *15*, 2867.

(19) Li, Y. X.; Yang, D. X.; Jones, C. A.; DeSimone, J. M.; Irene, E. A. *J. Vac. Sci. Technol. B* **2007**, *25*, 1139.

(20) Wittmer, M.; Studer, B.; Melchior, H. *J. Appl. Phys.* **1981**, *52*, 5722.

(21) Gupta, S.; Song, J.-S.; Ramachandran, V. *Semiconduct. Int.* **1989**, *12*, 80.

(22) Kanamori, S.; Matzumoto, T. *Thin Solid Films* **1983**, *110*, 205.

(23) Liu, Y.; Kijima, S.; Sugimata, E.; Masahara, M.; Endo, K.; Matsukawa, T.; Ishii, K.; Sakamoto, K.; Sekigawa, T.; Yamauchi, H.; Takanashi, Y.; Suzuki E. *IEEE T. Nanotechnol.* **2006**, *5*, 723.

(24) Fillot, F.; Morel, T.; Minoret, S.; Matko, I.; Maitrejean S.; Guillaumot, B.; Chenevier, B.; Billon T. *Microelectron. Eng.* **2005**, *82*, 248.

(25) Kerber A.; Cartier E. A. *IEEE T. Device. Mat. Re.* **2009**, *9*, 147.

(26) Hellriegel, R.; Albert, M.; Hintz, B.; Winzig, H.; Bartha, J. W. *Microelectron. Eng.* **2007**, *84*, 37.

(27) Vitale, S. A.; Kedzierski, J.; Keast, C. L. *J. Vac. Sci. Technol. B* **2009**, *27*, 2472.

(28) Verhaverbeke, S.; Parker, J. W. *Mat. Res. Soc. Symp. Proc.* **1997**, *477*, 447.

APPENDIX:

CHARACTERIZATION OF POLYVINYLPYRROLIDONE-COATED COPPER NANOPARTICLES FOR INKJET PRINTING

A.1 Introduction

Inkjet printing is common technology used to print text or images on papers or other transparent substrates, and it has been further developed as an innovative technique for a variety of scientific and industrial patterning applications. Due to its combination of properties such as precise control, low cost, and maskless writing, inkjet printing has been applied to 'direct write' strategies for construction of organic electronics, nanotechnology and tissue engineering with complex patterns.[1] Similar to the household inkjet printer, there are two working modes for inkjet printing, i.e. continuous-mode and drop-on-demand (DOD) mode. The latter is more often used in microelectronics fabrication due to its smaller drop size and higher placement accuracy. In a DOD mode, ink droplets are ejected from a reservoir through a nozzle by an acoustic pulse, which is generated either thermally or piezoelectronically. [2]

One of the most interesting and versatile applications of inkjet printing in microelectronics patterning is to deposit metal nanoparticles onto substrates to form printed nanowires. These nanoparticles are first prepared and stabilized in selected solutions, which are then directly deposited onto substrates through inkjet printing. After evaporation of the solvent and perhaps sintering at desired temperatures for some time, the particles can assemble into metal nanowires. Lee et al. [3] prepared a water-based conducting ink, composed of silver colloids with a diameter ~ 50 nm dispersed in a water and diethylene glycol co-solvent system. The 25 wt.% silver ink had a viscosity of ~ 7.4 cP and surface tension of 33.5 dyn cm^{-1} at 20 ◦C, which was successfully inkjet printed on ordinary glass substrates using a commercial Epson

inkjet printer. After sintering the inkjet deposited silver at 260 ◦C for 3min, the resulting circuitry exhibited a resistivity of 1.6×10^{-5} Ω-cm, which could serve as conducting pathways for electronic applications. Redinger et al. [4] used an all ink-jet-deposition process to deposit gold nanocrystals, creating conductive lines with sheet resistance as low as 23 mΩ per square. Optimal printing conditions were found for polyimide dielectric layers and films as thin as 340 nm, providing potential applications as spiral inductors, interconnect, and parallel plate capacitors. Kim et al. [5] synthesized copper nanoparticles through a facile chemical reduction of copper sulfate with sodium hypophosphite in ethylene glycol in the presence of a polymer surfactant, which was included to prevent aggregation and give dispersion stability to the resulting colloidal nanoparticles. The size of the copper nanoparticles could be controlled to between 30 and 65 nm, and the copper inks were inkjet printed onto polyimide substrates to form metallic copper traces with low electrical resistivities (≥3.6 $\mu\Omega$•cm, or about twice the resistivity of bulk copper).

In order to gain good control over the size and shape of an ejected droplet, the chemical and physical properties of an ink composition, such as the solute and solvent materials, are of key importance. For example, the mechanics of drop formation in DOD printing is directly related to the viscosity, density and surface tension of the ink solution. Factors such as the size of the nanoparticles, the molecular weight of the stabilizer polymer matrices and aggregation state of the particles can significantly influence the print processes and fine structures of the final metal wires. In this chapter, we use a variety of characterization techniques to study the relationship between the

material properties and the printability of the ink solution provided by Intrinsiq Materials Inc. (Farnborough, Hampshire, United Kingdom). This work represents activity that was part of a JumpStart project sponsored by CCMR.

A.2 Experimental

A.2.1 Materials

Polyvinylpyrrolidone (PVP) coated copper nanoparticles were provided by Intrinsiq Materials Inc. (Farnborough, Hampshire, United Kingdom). Different batches were prepared through an *in-situ* plasma synthetic procedure followed by a series of washing steps. Polyvinylpyrrolidone (Mw~40,000 g/mol) was purchased from Sigma Aldrich (St. Louis, MO). Isopropanol (IPA) (histological grade) was purchased from Fisher Scientific (Pittsburgh, PA).

A.2.2 Preparation of Particle Dispersion Solution

1 mg of nanoparticles were dissolved in 20 mL of IPA, which was then sonicated for 30 min. After sonication, the solution was filtered through a syringe filter with 0.45 μm PTFE membrane. The as-prepared dark brown solution was used for characterizations.

A.2.3 Characterizations

XPS experiments were carried out on a Surface Science Instruments (SSI) model SSX-100. Attenuated total reflectance-Fourier transform infrared spectroscopy (ATR-FTIR) experiments were carried out on a Nicolet iZ-10 instrument equipped with a

diamond ATR crystal. Thermogravimetric analysis (TGA) was done on an RT Instrument model Exstar SII TG/DTA 6200. Dynamic light scattering (DLS) measurements were carried out on Malvern Zeta Sizer model Nano-ZS. Ultraviolet–visible spectroscopy (UV-vis) was done on a Molecular Devices model Spectramax M2. Gel permeation chromatography (GPC) experiments were done on a Waters Ambient-Temperature GPC, using dimethylformamide as eluent and polystyrene as standard.

A.3 Results and Discussion

Different batches of copper nanoparticles stabilized in polyvinylpyrrolidone (PVP) were synthesized and used for inkjet printing of copper wires by Intrinsiq. In order to investigate the interactions between copper cores and PVP matrices, several characterization methods were used. Figure A.1 shows the ATR-FTIR spectra of pure PVP and one batch of the nanoparticles (Sample 5323). The specific peak at 1657 cm^{-1} was attributed to the amide carbonyl groups from the side chains of the polymer. However, no distinct difference could be observed between the ATR-FTIR spectra of the as-prepared nanoparticles and the pure polymer, indicating very weak complexation between Cu and PVP. Figure A.2 shows a typical XPS spectrum of the sample. Peaks at the binding energy of 121 eV, 394 eV, 527 eV, 924 eV, belonging to Cu 3s, N 1s, O1s and Cu 2p orbitals, were observed, proving the hybrid composite structure of the nanoparticles. Specific binding energy peak positions were tabulated in Table A.1. It is evident that there was no change of the binding energy of oxygen

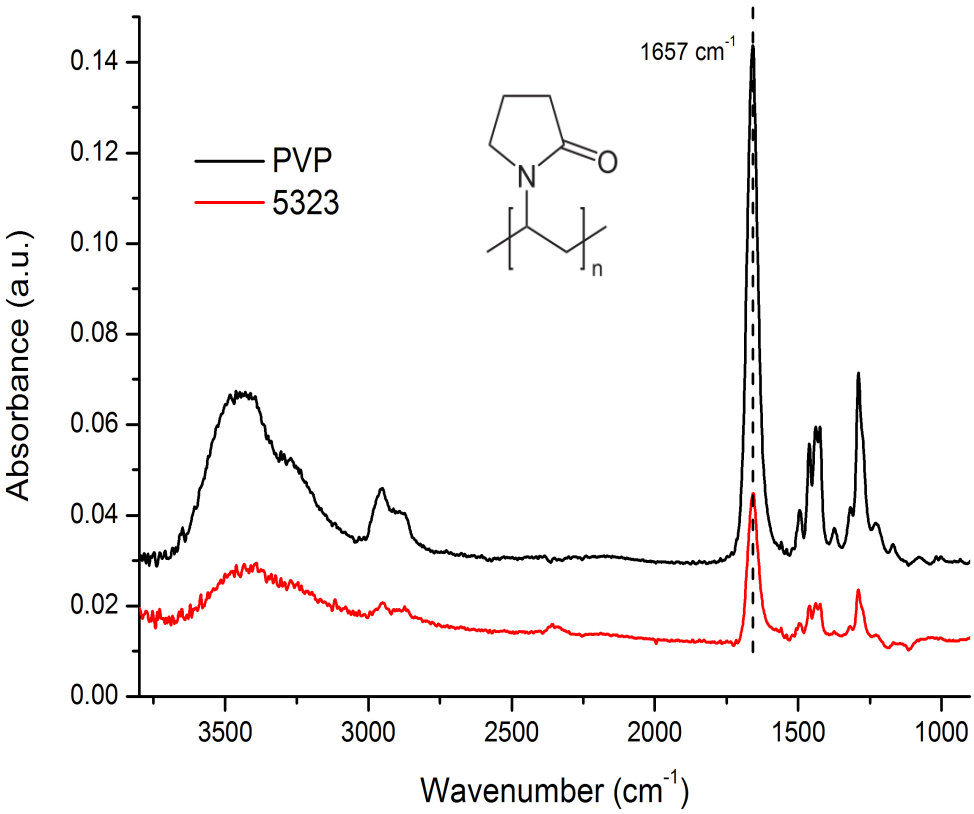

Figure A.1. ATR-FTIR spectra of pure PVP and nanoparticles. Typical peaks of PVP can be observed.

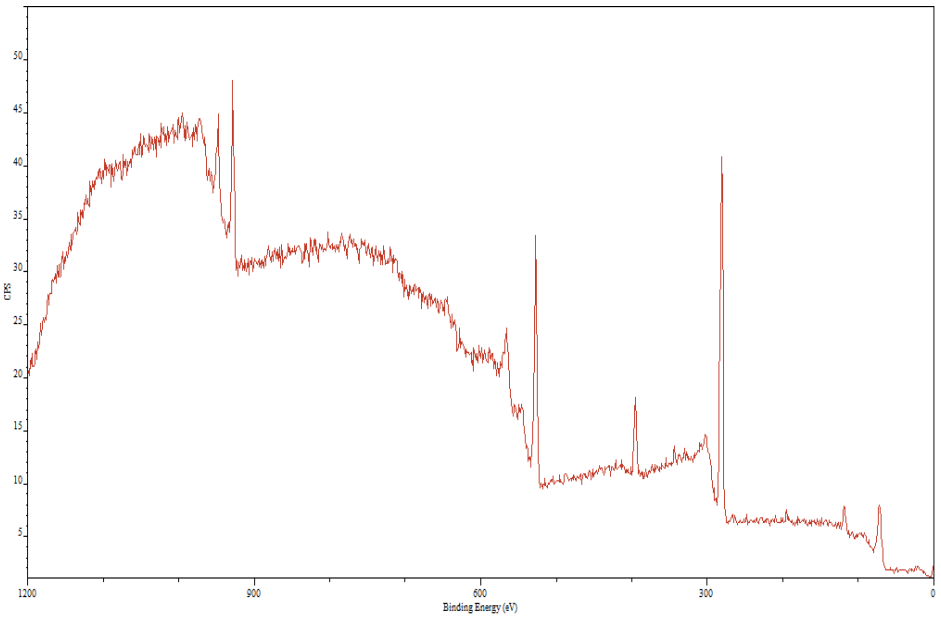

Figure A.2. Typical XPS spectrum of the nanoparticle. Specific peaks of Cu and PVP are detected.

Table A.1. Specific XPS peaks of PVP, Cu and selected nanoparticle samples.

Sample	O 1s	N 1s	Cu 3s
PVP	527	394	-
Cu	-	-	121
5257	527	395	118
5258	527	396	117

atoms on PVP before and after incorporation of Cu particles, while the slight shift of nitrogen and copper peaks indicated possible chemical interactions between the copper and nitrogen. Figure A.3 shows the UV-vis spectra of the nanoparticles compared to the pure PVP control. Three distinct peaks appeared: two intense peaks around 230 and 580 nm were attributed to the absorption of copper particles, while the weak peak around 330 nm resulted from the weak interactions between Cu and PVP. [6] Results of the UV-vis spectra were inconsistent with those of the ATR-FTIR spectra and XPS analysis, showing weak intramolecular interactions of the Cu-PVP nanoparticles.

Dynamic light scattering (DLS) measurements were used to investigate the particle behavior in solution. According to the information provided by Intrinsiq, the diameter of the particle is about 50 nm in the dry state. However, the DLS results (Figure A.4) reveal a typical particle size of ~ 150 nm in diameter, indicating severe aggregation of particles in solution. Moreover, sizes of the aggregates were not identical for different sample batches (Table A.2). Sample-5323 had the largest hydrodynamic diameter about 165 nm; sample-5257, 5290, 5309 had similar sizes around 150 nm; sample-5258 had a reduced size of 138 nm, while sample-5338 had the smallest diameter of 101 nm. The difference between the largest and smallest particle cluster is about 60 nm, which show completely different degrees of aggregation among different samples. It is worth noting that particle solutons used for DLS measurements were all clear dispersions, while large sediments and precipitations of particles could be observed before the filtration.

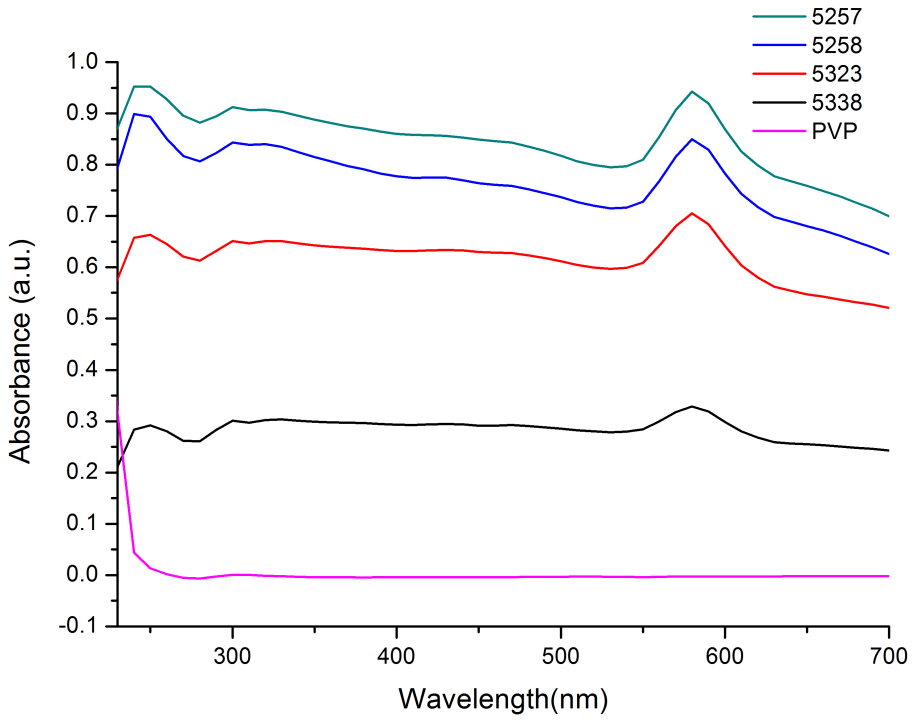

Figure A.3. UV-vis spectra of PVP and different batches of nanoparticle dispersion solutions.

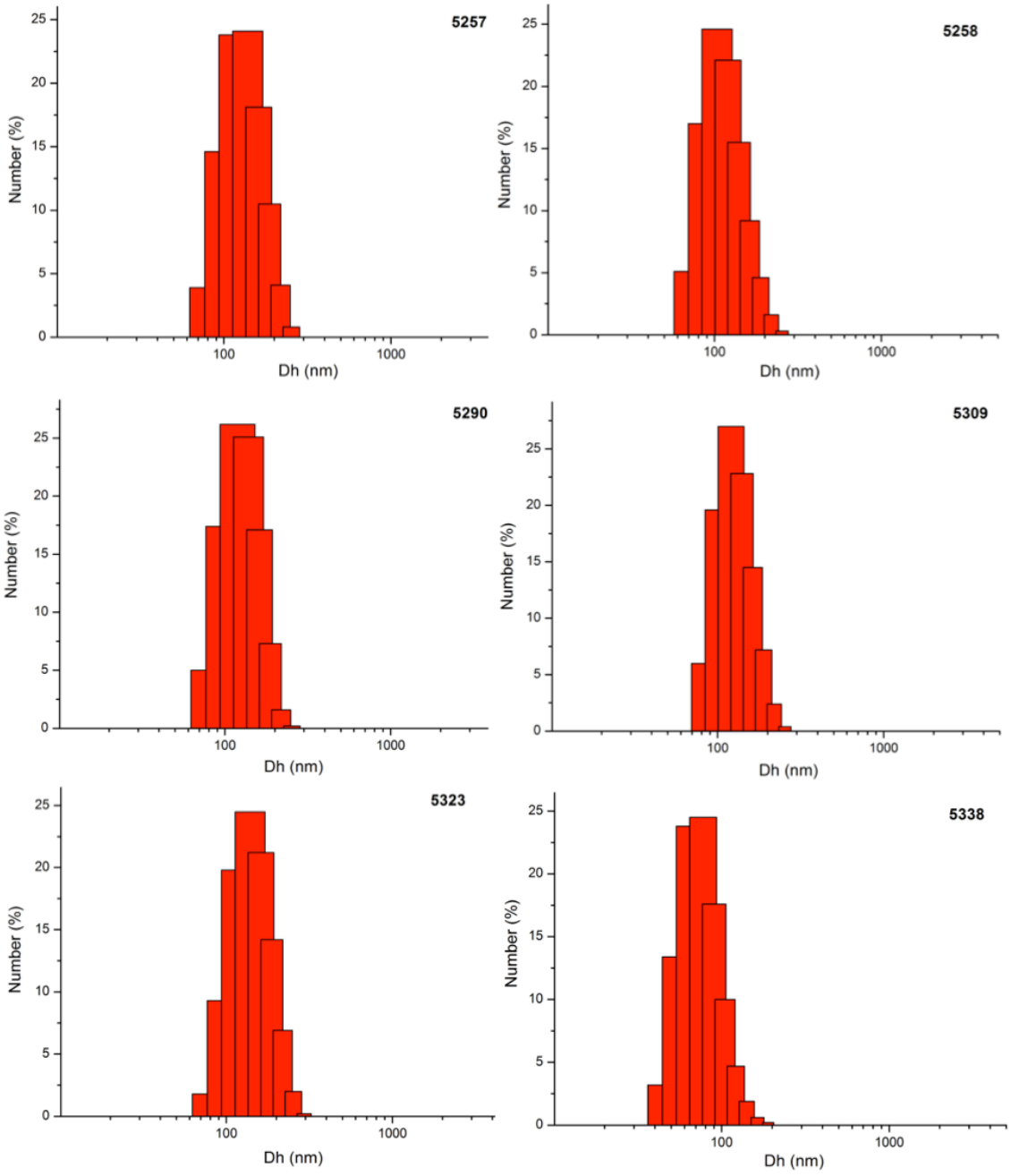

Figure A.4. DLS measurements of different batches of nanoparticle dispersion solutions.

Table A.2. Hydrodynamic particle size of different batches of nanoparticle dispersion solutions.

.

Sample	Number Average Particle Size (nm)	PDI
5257	157.0	0.175
5258	138.3	0.01
5290	152.7	0.102
5309	149.6	0.132
5323	165.5	0.14
5338	101.6	0.038

Thermogravimetric analysis (TGA) was used to characterize the mass compositions of the particles. Figure A.5 (a) shows the compiled TGA curves of the raw solid particles. All curves showed significant mass loss at around 450 ºC, which was due to the decomposition of the PVP polymers. It is obvious that PVP content varied in different sample batches. As has been mentioned before, dissolution of particles in IPA resulted in the formation of precipitates. Therefore, a more accurate estimation of the real content of PVP in the hybrid composites was made by filtering the large sediment through syringe filters to obtain clear dispersion solutions. The solutions were then evaporated and dried under vacuum to regain the solid particles for TGA measurements. Figure A.5 (b) consists of measured curves of the regained particles. A similar trend was observed to that of the raw particles, showing that the real content of PVP also varied for different sample batches. A quantification analysis is listed in Table A.3. As for the raw particles, sample 5309 only contained 9% of PVP, which increased to 20% after filtration. This huge increase was possibly due to the incomplete reaction for this batch, which resulted in a major component of unreacted copper in the sample. However, filtration of precipitates helped to remove large copper clusters, resulted in nanoparticles that could be dispersed and stabilized in IPA solutions. Sample 5323 and 5338 also showed increased amounts of PVP after filtration. No significant changes of PVP content were observed for sample 5257 and 5258. Finally, the weight percent of PVP in sample 5338 was much higher than those in other samples.

Figure A.6 shows that different amounts of PVP in the particles could lead to inconsistent viscosities of the samples, which would be a serious obstacle for universal

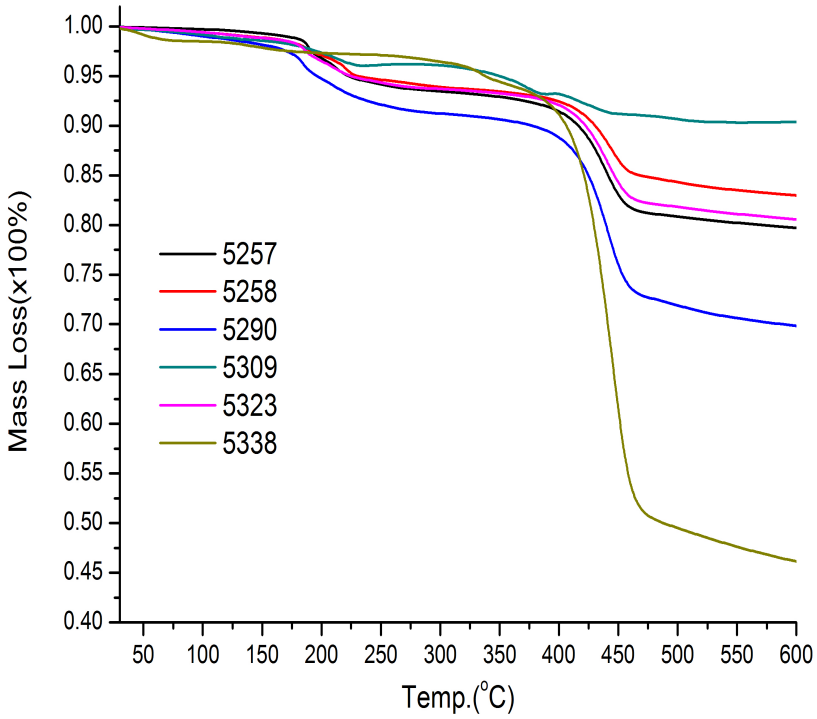

(a)

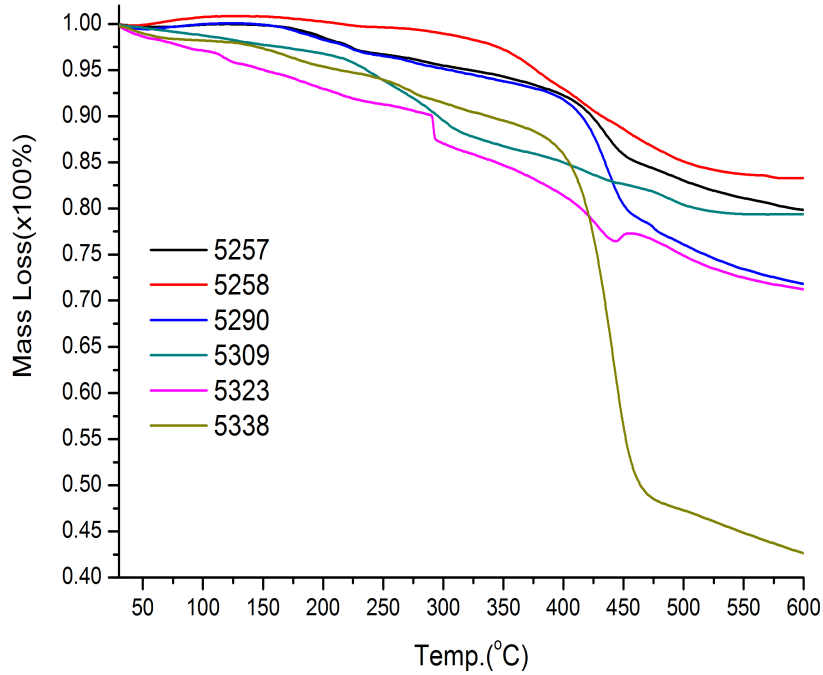

(b)

Figure A.5. TGA analysis of different batches of nanoparticle samples. (a): raw samples; (b): filtered samples.

Table A.3. PVP mass content in different sample batches.

Sample	Raw (%)	Regained (%)
5257	22	22
5258	18	15
5290	32	31
5309	9	20
5323	21	29
5338	58	64

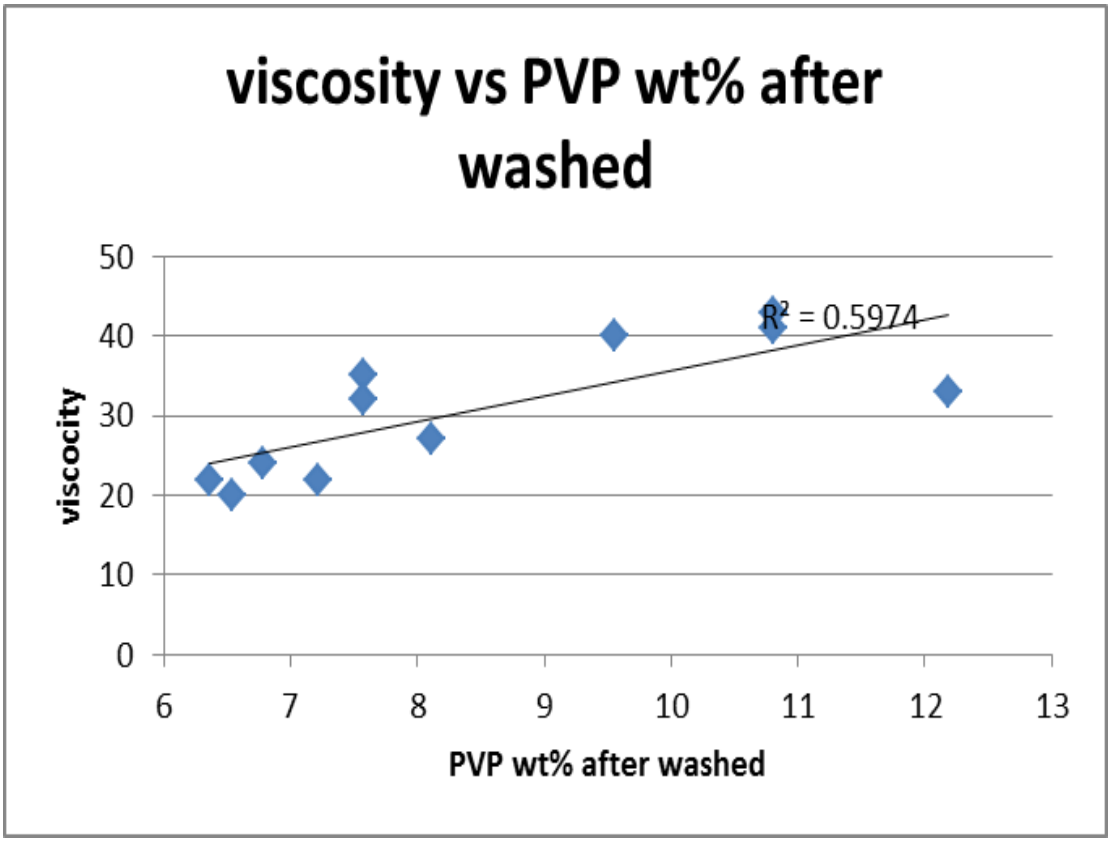

Figure A.6. Viscosity change with PVP content in the particles. (Data provided by Intrinsiq.)

inkjet printability and standard production operations. The effect of PVP content on the particle properties and behavior were then investigated in two different aspects. Intramolecular interactions between PVP matrices and embedded copper particles were first studied. PVP, due to its unique properties such as water solubility, high polarity, easy synthesis with fine-tuned molecular weight, and relatively high Tg, has been widely used as a capping agent in stabilizing, controlling and constructing metal nanoparticles and nanowires. Xia et al. [7] first reported the synthesis of monodispersed silver nanocubes in large quantities by reducing silver nitrate with ethylene glycol in the presence of PVP. It was suggested that the selective interaction between PVP and various crystallographic planes of silver could greatly reduce the growth rate along one facet direction and/or enhance the growth rate along the other direction. Teranishi et al. [8] obtained monodispersed Pd nanoparticles using a one-step reduction reaction of $[PdCl_4]^{2-}$ ions in alcohols with PVP as the protective polymer. The mean diameter of Pd nanoparticles could be controlled from 17 to 30 Å by changing the amount of PVP and the kind and/or the concentration of alcohol in the solvent. Other metals or metal oxides capped by PVP polymeric shells have also been prepared. [9-11] Although interactions between PVP and metal particles have been proved, they were, however, in our situation largely unaffected by the different PVP content in particles. As shown by XPS, ATR and UV-vis analysis, PVP complexed with Cu through weak nitrogen-copper interactions showed no significant difference between different sample batches. The weak but stable intramolecular interactions indicated possible fixed molar ratios between PVP ligand and Cu cores no matter how much PVP was used.

Effects of PVP content on intermolecular interactions were then explored. Particle sizes in dispersion solutions were measured and correlated with PVP content as is shown in Figure A.7. It is interesting to find that except for sample 5338, the particle size and PVP content showed a positive relationship as, in other words, particle size decreased along with a decrease in PVP content. The trend was not followed by sample 5338, of which the PVP content was much higher and the particle size was much smaller than other samples. As has been discussed above, DLS results showed that particle aggregations occurred in solution. It is therefore assumed that within a certain range of PVP content, in our case from 15% to 30%, the intermolecular interactions, i.e. the particle-particle interactions, were stronger than the particle-solvent interactions and were strongly dependent on the PVP content. The more PVP present in the particle, the stronger the intermolecular interactions and the larger the size of the aggregate. However, when the content of the PVP exceeded a critical threshold and became the main component of the material, the particle-particle interactions were weakened and the particle-solvent interactions became dominant, resulting in a better-dispersed solution and a sharp decrease of particle aggregation size. The correlation curves strongly suggested that the difference of PVP content could make a huge impact on aggregation behavior of the particles, especially in solutions.

Gel permeation chromatography (GPC) was used to further study the intrinsic properties of the PVP used for preparation of the nanoparticles. As shown in Figure A.8, the number average molecular weight (M_n) of the PVP was 17.4K g/mol, while the weight average molecular weight (M_w) was 35.2K g/mol. The polydispersity index

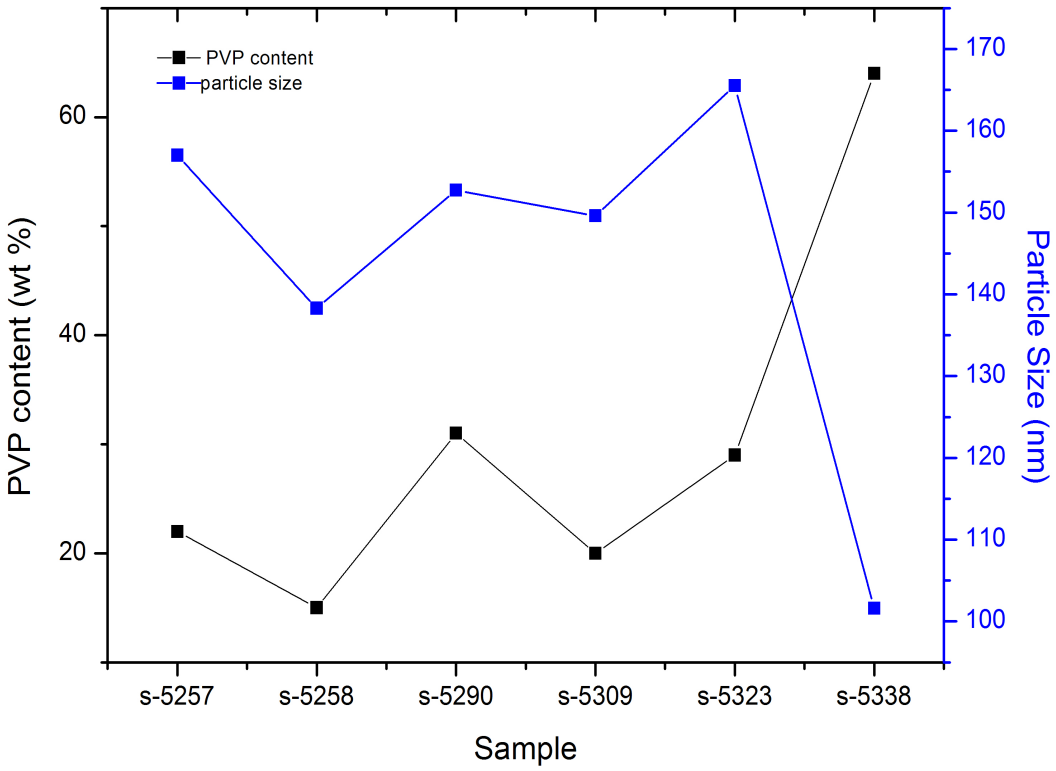

Figure A.7. Correlations of particle sizes with PVP content.

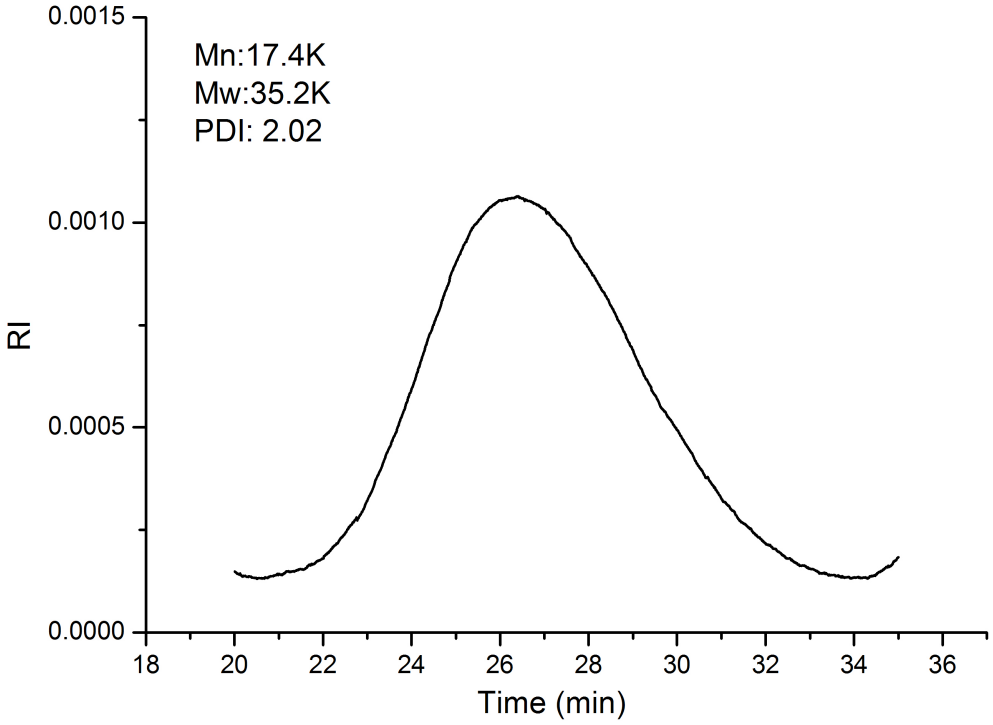

Figure A.8. GPC measurement of commercial PVP reagent.

of the polymer was therefore 2.02, indicating a relatively broad distribution of molecular weight of the commercial PVP. This inconsistency of molecular weight was a possible reason for the different PVP contents, considering the fixed molar ratios in the complex of PVP to copper. Moreover, it has been demonstrated in the literature that molecular weight of polymer additives can significantly affect the viscosity and printability of ink solutions. Schubert et al. [12] used a polystyrene/toluene solution as an inkjet printing model to study the spreading of the droplets. It was found that a variation of the polymer's molecular weight from 1.5 to 545K g/mol caused differences in the solution viscosity varying from 0.6 to 1.7 mPa•s and the Reynolds number decreased from 110 to 39. Further study from the same group showed that printability of polymer solutions decreases strongly with polymer molecular weight and concentrations, due to elastic stresses originating from elongational flow in the pipette nozzle. [13] Mun et al. [14] used poly(ethylene glycol) in glycerol/water as printing solution and investigated its viscoelastic jet stability. It was found that above M_w 300,000 g/mol, the break-up length increased and the elongational viscosity increased with elongation rate when M_w was above 100 000. According to these reports, molecular weight of the polymer component is one of the key factors controlling the viscoelastic properties of the ink solution. It is therefore reasonable to assume that the broad distribution of molecular weight of the PVP reagent, with a relative wide range of chain lengths, could not only result in different mass weight of PVP compositions, but different interactions among chain segments as well, which finally led to inconsistent viscosities among different sample batches.

A.4 Conclusion

A variety of characterization methods were used to study the Cu-PVP hybrid system as an inkjet printing solution. Viscosities were found to vary among different sample batches, which negatively affected the printability of the solution. XPS, UV-vis and ATR spectra showed little evidence of intramolecular interactions, while DLS and TGA indicated completely different particle sizes among each sample lot, which were also correlated with the PVP content. GPC results indicated that the broad distribution of molecular weight of the commercial PVP polymer used for particle preparation was possibly the cause of the different PVP content and inconsistent viscosities as well.

A.5 Acknowledgment

The author is grateful to the Intrinsiq Co. for financial support, to the CCMR coordinated JumpStart program and to both the Nanobiotechnology Center (NBTC) and KAUST-Cornell Center for use of their facilities. The author is also grateful to Dr. Christine Ouyang for XPS measurements and Dr. Michael Carmody from Intrinsiq Company for providing the samples.

REFERENCES

(1) Tekin, E.; Smith, P. J.; Schubert, U. S. *Soft Matter* **2008**, *4*, 703.

(2) Fromm, J. E. *IBM J. Res. Dev.* **1984**, *28*, 322.

(3) Lee, H.-H.; Chou, K.-S.; Huang, K.-C. *Nanotechnology* **2005**, *16*, 2436.

(4) Redinger, D. R.; Molesa, S.; Yin, S.; Farschi, R.; Subramanian, V. *IEEE Trans. Electron. Devices* **2004**, *51*, 1978.

(5) Lee, Y.; Choi, J.; Lee, K. J.; Stott, N. E.; Kim, D. *Nanotechnology* **2008**, *19*, 415604.

(6) Borodko, Y.; Lee, H. S.; Joo, S. H.; Zhang, Y.; Somorjai, G. *J. Phys. Chem. C* **2010,** *114,* 1117.

(7) Sun, Y. G.; Xia, Y. N. *Science* **2002**, *298*, 2176.

(8) Teranishi, T.; Miyake, M. *Chem. Mater.* **1998**, *10*, 594.

(9) Pastoriza-Santos, I.; Liz-Marzan, L. M. *Langmuir* **2002**, *18*, 2888.

(10) Graf, C. D.; Vossen, L. J.; Imhof, A.; van Blaaderen, A. *Langmuir* **2003**, *19*, 6693.

(11) Guo, Li.; Yang, S.; Yang, C.; Yu, P.; Wang, J.; Ge, W.; Wong, G. K. L. *Appl. Phys. Lett.* **2000**, *76*, 2901.

(12) Perelaer, J.; Smith, P. J.; van den Bosch, E.; van Grootel, S. S. C.; Ketelaars, P. H. J. M.; Schubert, U. S. *Macromol. Chem. Phys.* **2009**, *210*, 495.

(13) de Gans, B.-J.; Kazancioglu, E.; Meyer, W.; Schubert, U. S. *Macromol. Rapid Commun.* **2004**, *25*, 292.

(14) Mun, R. P.; Byars, J. A.; Boger, D. V. *J. Non-Newtonian Fluid Mech.* **1998**, *74*, 285.

CHAPTER SIX:

CONCLUSIONS AND PERSPECTIVES

Surface modification has played a key role in the preparation of materials with unique and desireable properties, e.g. anti-reflective coatings on glasses, anti-adhesion coatings on frying pans, etc. In order to obtain products with superior qualities and performance, proper modification methods and materials are necessary. Methods used for surface modification vary from spin/spray coating, vapor deposition to mechanical polishing, plasma/chemical etching etc. Materials applied for surface modification include almost all kinds of materials from polymer films, metal compounds to inorganic and organic particles etc. In order to improve selected surface properties on certain substrates, it is necessary to select and carefully design the modification methods and materials as well. Here in this thesis, several innovative applications of materials and methods for surface modification have been explored and discussed.

Biofouling has been a serious problem of polymeric membranes such as reverse osmosis (RO) membranes, which causes a decline of water flux and loss in the salt rejection properties of the membrane, thus increasing the energy cost and shortening the membrane lifetime. In order to suppress biofilm formation on membrane surfaces, polymer brushes with selected functional groups have been modified on the surface to improve the antifouling properties of the membrane. Poly(ethylene glycol) (PEG) and its derivatives, due to their high hydration forces, have been applied as fouling-resistant coatings. Zwitterionic structures, containing both positive and negative charges within one molecule, have also been applied to prevent initial, non-specific adhesion of microorganisms. A ‘layer by layer’ (LBL) mediated method was adopted to grow antifouling polymer brushes on a membrane surface without adversely affecting the membrane performance. Through electrostatic interactions, multiple

alternating layers of polycations and polyanions can be firmly coated onto different kinds of substrates. Since LBL films are assembled by physical intermolecular forces, the original membrane is not altered. While some of the polyelectrolytes do contain reactive chemical groups, e.g., polyallylamine hydrochloride (PAH), LBL films will generally not only protect the surface from being directly exposed to potential damage, but also help to amplify the number of reaction sites on the substrate. By taking advantage of the native negative charge of the polyamide surface, we first deposit a multilayer LBL film on the membrane and further modifications of the coated membrane surfaces are done by either a 'grafted to' or a 'grafted from' approach. Attached polymers consist of chains with either uncharged PEG side groups or charged zwitterionic groups. A variety of characterization methods such as attenuated total reflectance-Fourier transform infrared spectroscopy (ATR-FTIR) spectroscopy, X-ray photoelectron spectroscopy (XPS) and water contact angle measurements have been used to prove the successful coating of LBL films and the growth of polymer brushes as well. Membrane performance tests show no change of water flux and salt rejection ratio of the membrane after all the modification processes. Antifouling properties of the membrane have been characterized by both static protein adsorption and real-time cell attachment. Results show that the antifouling properties of the membrane have been improved. Further detailed analysis indicates that one type of antifouling coatings may work well against specific species of fouler, while the same coating may be completely vulnerable to other kinds of bio-foulants. Therefore, it is necessary to build up a more complex surface layer structure to perform against a

range of fouling species. One of the most interesting strategies is to construct a surface composed of more than one type of antifouling polymer.

Taking similar approaches as described in Chapter II, block copolymers with different compositions of different polymers, e.g. poly(ethylene glycol)-*b*-poly(sulfobetain), can be synthesized and grown on the membrane surface. The block copolymer layer contains both hydrophilic and zwitterionic segments and is expected to be effective against more kinds of bio-foulants. Further fundamental studies on the chemical and physical properties of the antifouling surface layer, e.g. the molecular weight of the polymer, the rheology of the film, etc., can help to understand details of the antifouling mechanism, which can further improve the antifouling properties of the membrane applied in a more complex biological environment.

Supercritical carbon dioxide ($scCO_2$), regarded as a 'greener' solvent compared to traditional hydrocarbon solvents, has been applied for enhanced oil recovery (EOR) in real oil fields for more than 30 years. The liquid character of $scCO_2$ facilitates oil dissolution and transport, while the gas-like properties enable enhanced diffusion behavior of $scCO_2$ into small porous fractures. Taking advantage of the unique properties of $scCO_2$, more than 50% of the oil stored underground can be recovered. Recently, the use of $scCO_2$ has also found application in enhanced coal bed methane (ECBM) production. Moreover, sequestration of carbon dioxide by storage in depleted oil reservoirs and gas shale is an efficient method to manage the "green house" effect.

One research interest is to develop subsurface mapping technologies to track the flow of $scCO_2$ underground for evaluation of EOR efficiency and CO_2 storage capacity.

One of the most attractive methods is to use a dual-tracer diffusion system, in which two tracers with at least one order of magnitude difference in response are dissolved and injected simultaneously into a diffusion cell. Diffusion behaviors of both tracers can then be predicted by selecting proper parameters and models according to the style of the flow cells. The tracers are required to be uniform, small (usually less than 50 nm for NP tracer) and easily detectable. Herein, a surface-initiated atom transfer radical polymerization (SI-ATRP) reaction was adopted to prepare $scCO_2$-philic nanoparticles. The particle is composed of an inorganic core (silicon dioxide or iron oxide) modified with a corona of fluoropolymers, which is covalently bonded on the core through the polymerization reaction. Incorporation of fluorescent labels in the polymer matrix helps to improve the detectability of the particles.

A variety of characterization methods such as thermogravimetric analysis, and dynamic light scattering measurements were used to characterize the properties of the as-synthesized nanoparticle. The particle contains a 60% wt of polymer corona and the diameter of particle dissolved in the solvent is less than 40 nm. The solution exhibits strong fluorescence at low particle concentrations and the intensity increase exhibits a linear relationship with concentration. Solubility tests in $scCO_2$ show good solubility of the as-prepared nanoparticles above the critical pressure and temperature. Moreover, the experimental results of the particle diffusion tests match well with the modeled predicative curves, indicating the nanoparticles can be applied as prospective tracers in the dual tracer mapping technology. Establishment of the synthetic procedure is expected to be further applied in the preparation of nanoparticles with other desired properties. For example, polymers with neutral charge such as poly (ethylene glycol)

can be modified onto the inorganic core to prepare non-sticky nanoparticles with zero surface charge, which can be applied as tracers in aqueous based systems. Fundamental studies such as controlling the molecular weight of the polymer corona and using various inorganic cores can help to fine tune the physical and chemical properties of the nanoparticle, e.g. particle size, particle detectability and solubility etc. The dual tracer system can be further applied in real field tests for practical oil recovery and CO_2 sequestration.

Supercritical CO_2 can also be applied for surface treatment in microelectronics processing. With the reduced dimensions of microelectronic devices, smaller and smaller features are required on the nanoscale level for high-resolution lithographic patterning. However, small features with high aspect ratios can easily collapse during post-patterning processes such as post-exposure development or post-etch cleaning, which is due to capillary forces caused by the high surface tensions of many of the liquids used in such processes. $scCO_2$, because of its low viscosity and zero surface tension, has emerged as an ideal candidate for microelectronics processing with minimum pattern collapse. Applications of $scCO_2$ in microelectronics processing include photoresist stripping, wafer cleaning, and metal etching while in this thesis, the last two applications were explored in detail. First, the removal of post-etch organic photoresist residue in the presence of co-solvents and additives in $scCO_2$ was investigated. Different co-solvents were used and quaternary ammonium salt was synthesized and applied as an additive. Various processing conditions were adopted to achieve the most effective cleaning procedure. Second, selective dry etching of

titanium nitride (TiN) in $scCO_2$ was developed. A novel formulation containing strong organic acids, strong organic peroxides and alcohol stabilizers were tested.

Detailed studies show that all of the three components are essential for successful TiN etching. Concentrations and volume ratios of the components can have significant impact on the etching processes. Using carbon nuclear magnetic resonance spectroscopy, it was confirmed that the esterification reaction between alcohols and acids is a key step to stabilize the entire system. The etchant solution worked efficiently for wet etching in organic solvents with a maximum etching rate of more than 1 nm/minute. Although dry etching in $scCO_2$ is not as efficient and homogeneous as wet etching, while promising results were obtained with an etching rate of 3 nm/hour. Further studies are expected to be focused on optimizing the dry etching processing conditions, e.g. adjusting the pressure and temperature, increasing the concentration of etchants etc., to achieve a more rapid etching rate and a more homogeneous etching process in $scCO_2$. It is also necessary to have a more fundamental and detailed study on the etching mechanism. Characterization methods such as liquid chromatography–mass spectrometry can be used to characterize the residue of the etching solution to provide a deeper understanding of the chemical species produced during the etching reactions.

In conclusion, it has been shown in this thesis that different methods and materials can be selected and applied to do surface modification on different substrates. Various applications such as antifouling coatings and mapping technologies for oil recovery etc. have been explored. It is believed and expected that further studies focused on

both fundamental mechanisms and practical research should be made to further develop new and innovative materials and methods for advanced surface modifications.